Stellingen

behorende bij het proefschrift van Hoyte C. Raven

1. In tegenstelling tot wat algemeen werd verwacht, zijn niet-lineaire effecten op het golfpatroon ook voor relatief slanke schepen belangrijk. De sterkste invloed ondervinden daarbij de divergerende componenten van het boeggolfsysteem.

2. Slow-ship linearisatie van het golfweerstandsprobleem behelst het opleggen van vrij oppervlak randvoorwaarden ter plaatse van het ongestoorde wateroppervlak, en het gebruik van de dubbel-model stroming als basis voor linearisatie. Het eerste veroorzaakt een te geringe boeggolfhoogte nabij de romp; het tweede een onvoldoende refractie-effect, en daardoor een fase-afwijking en te geringe amplitude van divergerende golven in het boeggolfsysteem.

3. Het gebruik van omstromingsberekeningen in het ontwerp ontleent zijn waarde aan het geven van inzicht in de stroming, ter ondersteuning en vergroting van onze kennis van de stromingsleer; niet aan het overbodig maken van die kennis.

4. Snelle vooruitgang in de numerieke scheepshydrodynamica kan worden geboekt door nieuwe methoden, direct nadat ze ontwikkeld zijn, daadwerkelijk in het scheepsontwerp te gaan toepassen.

5. De bijna volledige monopoliepositie van Wigley en Series 60 modellen als testgevallen in de internationale literatuur op het gebied van numerieke scheepshydrodynamica is een teken van een onvoldoende integratie van onderzoek en toepassing.

6. Een goed klimaat voor toegepaste research vereist enerzijds een nauw contact met de toepassingspraktijk, anderzijds voldoende afscherming; enerzijds duidelijke en pragmatische doelstellingen, anderzijds vrijheid om zijpaden in te slaan. De gedeeltelijke incompatibiliteit van deze randvoorwaarden maakt het organiseren van een toegepaste researchgroep tot een slecht gesteld probleem.

7. Alvorens wordt besloten tot het oprichten van een nieuw onderdeel van de krijgsmacht of de aanschaf van belangrijk nieuw materieel, dient de vraag beantwoord te worden waar en hoe hiermee geoefend zal kunnen worden, en dient voorzover relevant daarvoor een beleids - Milieu Effect Rapportage te worden uitgevoerd. De gang van zaken rond de Lucht Mobiele Brigade illustreert de noodzaak hiervan.

8. Het treffen van maatregelen tegen ongewenst autogebruik in Nederland wordt in ernstige mate belemmerd door het feit dat de meeste beleidsmakers behoren tot de groep mensen die de auto verreweg het meeste gebruikt; te weten, mannen tussen 20 en 59 jaar.

9. Tegenover de maatschappelijke kosten die het gevolg zijn van sportblessures staan grote maatschappelijke baten als gevolg van verhoogde creativiteit en produktiviteit door sportbeoefening.

10. Zeilen in een LASER is een effectieve manier van het beoefenen van experimenteel stromingsonderzoek. Het lereffect wordt verhoogd doordat, anders dan in de numerieke stromingsleer, een verkeerde conclusie nog wel eens een nat pak oplevert.
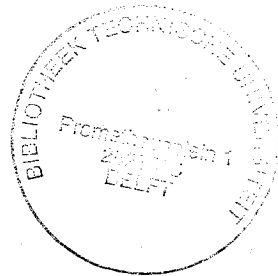
A solution method for the

nonlinear ship wave resistance

problem

Hoyte C. Raven

A solution method for the

nonlinear ship wave resistance

problem

door

Hoyte Christiaan RAVEN

scheepsbouwkundig ingenieur
geboren te Utrecht

Dit proefschrift is goedgekeurd door de promotor:
Prof. dr. ir. A.J. Hermans

Samenstelling promotiecommissie:

Rector Magnificus, voorzitter
Prof. dr. ir. A.J. Hermans,   Technische Universiteit Delft, promotor
Prof. dr. M.P. Tulin,   University of California at Santa Barbara, USA
Prof. dr. S.D. Sharma,   Gerhard Mercator Universität Duisburg, Duitsland
Prof. dr. ir. P.J. Zandbergen,   Universiteit Twente
Prof. dr. ir. L. van Wijngaarden,   Universiteit Twente
Prof. dr. ir. P. Wesseling,   Technische Universiteit Delft
Prof. dr. ir. J. Pinkster,   Technische Universiteit Delft

Contents

Nomenclature

C_p	Pressure coefficient, $p/(\frac{1}{2}\rho V_s^2 S)$
C_w	wave resistance coefficient, $R_w/(\frac{1}{2}\rho V_s^2 S)$
$\dot{E}$	energy flux (Section 4.5.2)
Fn	Froude number
Fn_Δ	Froude number based on panel length
Fn_{tr}	Froude number based on transom immersion, $U_\infty/\sqrt{-g\eta_{tr}}$
g	acceleration of gravity
G	Green's function
$H(x,z)$	wave elevation of base surface
h	water depth
k	wave number
k_0	fundamental wave number, g/U_∞^2
L, B, T	ship length between perpendiculars, beam and draft
l	curvilinear coordinate along free surface streamline
$\vec{n}$	normal vector
p	pressure
Rw_{pres}	wave resistance from hull pressure integration
Rw_0	the same, under still water line
Rw_{far}	wave resistance deduced from wave pattern far downstream
Rn	Reynolds number
S	wetted area of ship at rest
s	panel wave number, $k\Delta x/(2\pi)$
t	time
U_∞	undisturbed incoming velocity
V_s	ship speed
$\vec{v} = (u, v, w)$	velocity vector
x, y, z	coordinates, defined in Fig. 2.1
y_{fs}	distance of panels above wave surface
α	$y_{fs}/\Delta x$
γ	forward shift fraction of free surface collocation points
Δx	panel length
Δz_1	width of first panel strip on free surface, ahead of the hull
ϵ_k	residual error in kinematic free surface boundary condition
ϵ_d	residual error in dynamic free surface boundary condition
η	wave elevation
η'	wave height perturbation
η_r	double-body wave height

λ_0 fundamental (transverse) wave length

ν kinematic viscosity

σ source density

τ dimensionless wave frequency, $\tau = U_\infty \omega / g$

ϕ velocity potential

Φ base flow velocity potential

φ' perturbation potential

Ψ unsteady potential (Section 4.5.2)

ψ potential of perturbation of uniform flow (Section 4.5.2)

ω relaxation factor for wave height changes

Chapter 1

Introduction

1.1   The design of a ship's hull form

A ship in steady forward motion is subject to resistance forces of various kinds. The resistance at the desired service speed to a large extent determines the required engine power, and thereby the fuel consumption, one of the major factors influencing the transport economy of the ship. Minimisation of the resistance is, therefore, an important issue in ship design.

The resistance is mainly determined by hydrodynamic forces, which strongly depend on the shape of the hull. Optimising the hull form from the hydrodynamic point of view is a complicated problem; not only by the many constraints imposed by practical demands (main dimensions, deadweight, cargo capacity, building costs etc.) and by requirements on stability, behaviour in waves, manoeuvring and so on, but also by the influence of ambient conditions such as wind and sea, which may lead to a substantial increase of the required power compared to that needed in a calm sea. Minimum operational fuel costs would be achieved by designing the hull for best average performance over a range of conditions. This is, however, rarely feasible because of the current difficulty to quantify the effect of all parameters involved; and because of the more trivial reason of the severe time constraints that are the rule in practical ship design.

The usual simplification therefore is to separately consider the performance of the ship in still water and its behaviour in waves. Hydrodynamic optimisation of the hull form design for normal merchant ships primarily addresses the required power in a calm sea, which is a lower limit of the power in practical conditions; and the effect of the sea state generally is taken into account as a "wave added resistance". This procedure is supposed to lead to a reasonably close approach of the actual optimum performance in operational conditions, and besides, it matches the fact that the design requirements usually specify a minimum speed to be reached during trials in still water.

1.2   The role of wave resistance

The resistance of a ship in still water is therefore an issue of large practical importance. It consists of several contributions: a viscous resistance, associated with the generation of a boundary layer and wake; a wave resistance connected with the excitation of a wave pattern; air drag on hull and superstructure, in special cases spray drag, or induced resistance related to the generation of lift forces. Of course most of these contributions are interrelated in principle.

For most merchant ships the viscous resistance component is the largest. It is approximately quadratic in the ship's speed, and for well-designed ships increases gradually with the fullness of the hull form. Separation phenomena, however, may cause a sudden and drastic increase of the viscous drag.

Wave resistance in practical cases amounts to 10 to 60 % of the total resistance of a ship in still water. While at relatively low speeds the wave resistance is virtually zero, it increases very quickly at higher speeds, for fast displacement ships dominating the viscous resistance component. In addition it is very sensitive to the hull fullness and details of the hull form design, and is easily affected by relatively small design modifications. Besides its relative magnitude it is this property that makes wave resistance such an important aspect in ship hull form design. Consequently, the capability to predict the wave resistance for a given hull form, and to reduce it by hull form modifications derived from such predictions, is an important asset.

Conventionally, wave resistance was predicted and minimised with the aid of model tests. Towing the model at a correctly scaled speed produces a wave pattern that is geometrically similar with that at full scale and permits the wave resistance to be scaled up directly. Modifying the design to reduce its wavemaking required the eye of an experienced naval architect watching the model tests and judging the flow from its appearance at the surface — a difficult task involving intuition and experience rather than science. This empirical approach has been complemented by statistical analysis of experimental data, founded upon certain simple theories. The resulting semi-empirical methods generally yield useful predictions but they only take into account some main parameters of the design and give little support in optimising the hull form.

1.3   Dawson's method

The wave resistance problem lends itself quite well to an entirely theoretical treatment, an appropriate mathematical model for the wave generation and propagation being known. Since this model in its general form is too complicated to permit a direct solution by analytical means, the work of many hydrodynamicists and mathematicians during the last decades was focused on devising simplifications that would lead to a tractable mathematical problem and on the other hand would retain enough realism to be useful in practice. The main simplification required, and often motivated by certain assumptions on the hull shape or dimensions, was a linearisation of the

nonlinear boundary conditions to be imposed at the water surface. A whole series of linearised formulations has been proposed, applicable to thin ships, slender ships, flat ships, fast ships, etc. Almost none of these has been found to be sufficiently accurate for normal ships.

Stimulated by the increase of computer speed and the development of numerical methods, around 1976/1977 some researchers independently proposed closely related linearised theories claimed to be valid asymptotically for *slow* ships. One of these, the method proposed in 1977 by Charles Dawson [1], has been found to give fairly realistic results in general, and to be quite efficient and flexible. Since 1980 several authors have proposed further improvements. Dawson's method nowadays can be considered mature, it has been implemented in several different forms and is available at many institutes all over the world.

One member of this family is the code DAWSON developed by the author in 1986 — 1988, which has been used in practical ship design at the Maritime Research Institute Netherlands (MARIN) since 1986, and has meanwhile been applied to several hundreds of practical cases. The use of this method has caused a significant change in the design procedure of a ship's hull form at MARIN, which now is characterised by detailed pre-optimisation using the flow predictions, prior to any model test. Recent advanced techniques for visualising the computed flow permit to obtain detailed insight in the behaviour of the flow and its relation with the hull form, in a way not achievable in experiments. Thus the many wave pattern calculations have taught us a lot about wave making and have permitted a substantial further improvement of ship hull forms.

1.4   The development of a nonlinear method

Even so, several shortcomings of the predictions by linearised methods have come up. Quantitative wave resistance predictions have often been impossible. In general mainly the wave pattern around the forebody was useful, stern flows being poorly modelled. The predicted wave pattern displays systematic deviations, and certain important effects of the hull form are absent. All this makes the Dawson type of methods a tool requiring substantial experience in order to judge the quality of the results and to deduce recommendations for hull form modifications — there still is an appreciable amount of intuition and art involved.

In 1989 - 1990 the author has carried out a further investigation into the origin of the deviations of linearised predictions and into possibilities to improve the theoretical formulation [2]. Most of the shortcomings appeared to be closely linked to the linearisation itself and could not be simply removed by modifying that linearisation. In the meantime, two first methods to solve the complete, fully nonlinear problem had been developed elsewhere already. The publications concerned [3, 4] indicated the feasibility of discarding the linearisation altogether, but at the same time illustrated the difficulty of obtaining nonlinear solutions for anything but the simplest cases. Therefore, in 1990 it was decided to attempt to develop a new nonlinear method. It is this development and the resulting RAPID method that are the main subjects of this thesis.

1.5   Outline of this work

The next chapter first expounds the formulation of the wave resistance problem. To set the scene for the development of the nonlinear method we shall then discuss the formulation and properties of the linearised DAWSON method available at the start of the development. Chapter 4 describes the study mentioned above on the basics of the linearisation, as it has given indications on the best way to set up the nonlinear method and because it may be of interest in its own right. The derivation and development of the nonlinear RAPID method will then be dealt with. Chapter 5 discusses relevant earlier work and motivates the basic choices made, while Chapters 6 and 7 describe the details of the method and its properties. Chapter 8 adds another important feature, the treatment of the flow off an immersed transom stern. This has a few particulars that justify a separate discussion.

Some of the validations of the method by comparison with experimental data will then be discussed, and we shall study the magnitude and nature of nonlinear effects. Chapter 11 finally attempts to make up the balance, discussing to what extent the wave resistance problem can now be considered as solved and what are remaining problems and prospects for their solution.

Chapter 2

The wave resistance problem

This chapter describes what place the free surface potential flow problem takes in the description of the flow around a ship hull, and presents its mathematical statement.

2.1   Limitation of the problem

We restrict ourselves to the flow around a ship hull in still water. The water is assumed infinite in width but may have a restricted depth. The ship is supposed to move on a straight course with constant speed. In such a situation one can identify a number of different flow phenomena:

- a wave pattern generated by the ship

- a viscous boundary layer and wake field

- a screw race

- generally, some wave breaking

- sometimes, formation of spray

- in certain cases, lift effects on lifting components such as a keel, rudder, airfoil-shaped appendages or hydrofoils.

These phenomena are partly governed by different physical laws, have different time and length scales, and their theoretical prediction requires quite different mathematical models and computational approaches. Practical prediction methods therefore are based on a decomposition into

11

distinct mathematical problems covering one or more of these phenomena. In the present treatment of wave making we have to neglect some of the aspects listed, and it will be indicated below what consequences this will have in practical applications.

In the first place, propulsion effects are left out of account. Their modelling would be a problem quite distinct from that dealt with here, and a separate treatment of the situation corresponding to a resistance test (the ship being towed) generally is useful. Nevertheless, a class of simple representations of the propeller effect could well be incorporated in the method to be presented. The neglect of propulsion is likely to affect to some extent the prediction of stern waves, trim and sinkage.

Furthermore, wave breaking effects will have to be disregarded. The physical description of wave breaking is still incomplete, and no quantitative treatment of wave breaking is available for the problem considered. Fortunately it appears that for the majority of practical cases wave breaking, though almost always present, has relatively little effect on the overall flow behaviour.

For similar reasons spray will be neglected. Again, for most cases the neglect of spray will have no significant effect on the flow overall. The prime reason that some kind of simple modelling of the spray might once become useful is to resolve certain possible local anomalies at the intersection of the water surface with the hull.

Lift effects would provide little problem and actually are incorporated in the linearised DAWSON code described in the next chapter, but they are not included in the further development, nor in the RAPID code, for simplicity of presentation and because they are not essential for the main problem treated here. Related to this, the hull is supposed to be symmetrical and to move with zero leeway angle.

Finally, surface tension effects will be disregarded, being insignificant for full-scale ships.

2.2   Distinction of viscous and free-surface flow

After these simplifications the problem now consists of modelling the flow including just both main classes of phenomena that determine the flow around a ship hull: the generation of a wave pattern and the viscous boundary layer and wake. But also these are very different physical phenomena, taking place on quite disparate time and length scales and posing quite different demands on a numerical solution method. Prediction of viscous flow requires resolution of extremely small structures and very large velocity gradients near a wall, but viscous flow phenomena are generally confined to a relatively thin boundary layer and wake region. The nonlinearity of the governing equations forces us to use a field method discretising the entire threedimensional domain. The wave pattern on the other hand is a relatively large-scale phenomenon with length scales comparable to the ship dimensions, and requires a large flow domain to be modelled. The governing equations admit important simplifications and a solution by boundary integral type of approaches.

Consequently, a solution method for the combined problem of viscous flow with free surface, which would have to satisfy all these opposing requirements, in principle is less efficient and did not form a serious alternative at the moment that the work described in this thesis was undertaken. With present computer power it now just starts being feasible, although the most promising methods use a composite flow description (zonal approach) rather than directly tackling the combined problem of a viscous flow subject to free surface boundary conditions in a large domain (see e.g. [5, 6]).

While, therefore, the solution of the combined problem is not yet a quite practical approach, the concept of boundary layer theory enables us to separate the viscous problem and the free surface gravity wave problem. Provided that the Reynolds number

$$Rn = \frac{V_s L}{\nu}$$

is high enough, viscous effects are only felt in a thin boundary layer with a thickness δ. This boundary layer accommodates the adjustment of the velocity field to the no-slip condition on the wall. To leading order in δ the pressure inside the boundary layer is equal to that of the inviscid flow around the hull, and the inviscid flow in first approximation is unaffected by viscous effects. Therefore, to calculate the wave pattern generated by the ship all viscous effects will be disregarded: the inviscid flow around the bare hull will be calculated. In this way we shall obtain a flow prediction and wave pattern that are asymptotically correct for $Rn \rightarrow \infty$.

There is a close connection with the practical procedure in ship model testing. Here, too, a distinction is made between viscous flow and free surface flow, which satisfy different scaling rules. The model is tested at the same Froude number

$$Fn = \frac{V_s}{\sqrt{gL}}$$

as the ship, which according to inviscid flow theory makes the wave pattern geometrically similar and the wave resistance coefficient equal for model and full scale. Strictly speaking, the difference in Reynolds number between ship and model (usually, two orders of magnitude!) will cause a difference in the viscous flow effects, and thereby a difference in the wave pattern and wave resistance. But in the analysis of the experiments that difference is always disregarded, an approximation that has proven to be generally useful and fairly accurate.

The distinct treatment of wave making and viscous flow, although justified and generally accurate, means that the following "interactions" are disregarded:

- the boundary layer and wake "displacement effect" , most clearly present at the stern and usually reducing the stern wave height;

- certain flow regimes behind a transom stern, in particular the "dead water" type of flow;

- free-surface boundary layer effects.
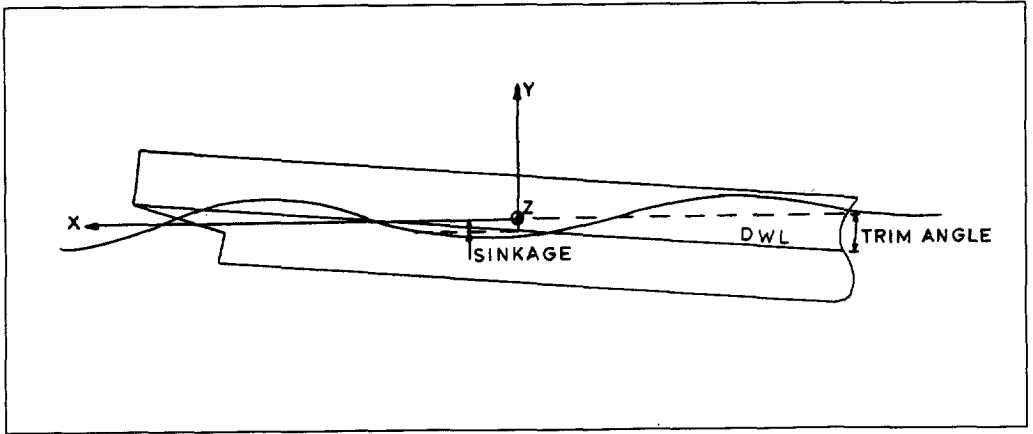
Figure 2.1: *Definition of the coordinate system*

Most viscous flow calculations in turn neglect the wavy shape of the free surface and disregard the effect of the wave pattern on the pressure and velocity boundary conditions.

2.3   The free-surface potential flow problem

Having confined the problem to that of an inviscid free surface flow around a ship hull, we shall now give its mathematical statement.

Coordinate system

The flow is described in an Eulerian sense. The coordinate system (Fig. 2.1) moves with the ship, having the same longitudinal speed as the hull, but does not follow its dynamic trim and sinkage. The origin is chosen at the centreplane of the ship at the midship section, at the level of the undisturbed waterplane. The x-axis is horizontal and points astern. The y-axis is positive upward, z is positive to port.

In this coordinate system the flow around the hull and the wave pattern are supposed to be steady. There is a uniform incoming flow in positive x-direction with velocity U_∞. All quantities are non-dimensionalised using a reference length L, usually the length of the ship between perpendiculars, and the reference speed U_∞ .

The free surface shape will be described as a single-valued function of the horizontal coordinates,

$y = \eta(x, z)$. This may seem rather restrictive as it excludes overtopping waves, but it will be argued later (Chapter 11) that this is not a restriction of much practical meaning.

Governing equations

In the absence of viscosity and wave breaking the irrotationality of the incoming flow is preserved, and a potential flow may be assumed, in which the velocity vector $\vec{v}$ is the gradient of a scalar potential:

$$\vec{v} = \nabla\phi \tag{2.1}$$

Incompressibility then leads to the Laplace equation

$$\nabla^2\phi = 0 \tag{2.2}$$

In addition we have the Bernoulli equation

$$p + \rho g y + \frac{1}{2}\rho\nabla\phi.\nabla\phi = C , \tag{2.3}$$

the constant C being equal throughout the domain.

Boundary conditions

kinematic hull boundary condition: On the wetted part of the hull a condition of tangential flow is to be satisfied:

$$\phi_n = 0, \tag{2.4}$$

where $\vec{n}$ is the unit normal vector on the hull, directed into the fluid domain.

dynamic hull boundary condition: An additional dynamic condition may be imposed, requiring equilibrium between the hydrodynamic and hydrostatic pressure forces on the wetted part of the hull and the ship's weight distribution. The resulting integral constraint primarily determines the dynamic trim and sinkage.

kinematic free surface condition: On the free surface the flow velocity must be tangential to that surface. Using the expression for the unit normal vector

$$\vec{n} = \frac{1}{\sqrt{1 + n_x^2 + n_z^2}}.(n_x \quad -1 \quad n_z)^T \tag{2.5}$$

we find

$$\phi_x\eta_x + \phi_z\eta_z - \phi_y = 0 \quad \text{at} \quad y = \eta(x, z) \tag{2.6}$$

dynamic free surface condition: The pressure, expressed in the velocities and wave elevation through Bernoulli's law, must be constant (atmospheric) at the free surface:

$$\frac{1}{2}Fn^2(1 - \phi_x^2 - \phi_y^2 - \phi_z^2) - \eta = 0 \quad \text{at} \quad y = \eta(x, z). \tag{2.7}$$

bottom boundary condition In most cases the depth of the water is assumed infinite, and the associated far-field condition is

$$\phi \to x \quad \text{for} \quad y \to -\infty. \tag{2.8}$$

For shallow water with depth h, instead a boundary condition is to be imposed on the bottom

$$\phi_n = 0 \quad \text{at} \quad y = -h/L \tag{2.9}$$

radiation condition: Some care is to be taken for the behaviour at infinity. Simply requiring decay of the disturbance with distance from the body is not appropriate. The desired solution is that which includes only the waves generated by the ship, which roughly speaking are found downstream of the bow. Upstream of the bow a non-wavy disturbance decaying as

$$\phi = x + \mathcal{O}(\frac{1}{\sqrt{x^2 + z^2}}) \quad \text{for} \quad x \to -\infty \tag{2.10}$$

is present. Downstream a wave-like behaviour must be admitted and at least for two-dimensional cases no decay may be enforced. The precise form of this "radiation condition" depends on the particular method to solve the problem.[1]

transom conditions: Besides these general conditions applying to all surface-piercing bodies, special conditions may be required to model the flow behaviour at the edge of a transom stern. We refer to Chapter 8 in this regard.

Possible solution approaches

The difficulty of this free-surface potential flow problem stems from the fact that boundary conditions are to be imposed on the free surface, the shape of which is still unknown; and that the boundary conditions are nonlinear, and the flow quantities depend in a nonlinear fashion on the location of the free surface. Solution methods for the fully nonlinear free surface-problem have only been proposed since about 1986. Before that time no complete solution of the problem in this form was feasible, and linearisation was the only viable alternative. Chapter 3 and 4 will pay some attention to such linearised methods and their performance in practical applications, as an introduction to the discussion of the nonlinear method forming the main subject of this thesis.

---

[1]The necessity of a radiation condition is, of course, connected to the fact that in a fully linearised formulation (such as thin-ship theory) any system of free waves may be superimposed on the actual solution. An infinite set of solutions exists, and the one to be singled out is that in which no wave energy is supplied otherwise than by the ship. This behaviour largely carries over to the nonlinear problem.

Chapter 3

Dawson's method

To illustrate the state of the art around 1989 and the principal starting point for the development of nonlinear methods, this chapter concisely introduces the linearised method proposed by Dawson and the extensions and improvements incorporated in the DAWSON code. We discuss its performance in practical applications and point out why better methods were desired.

3.1 Basic form

General approach

In Dawson's original paper [1], reference is made to the well-known Hess and Smith method [7] for computing the potential flow around a submerged body in an infinite fluid domain. This is a panel method, in which the body is covered with a large number (M, say) of quadrilateral source panels, each bearing an unknown constant source density. The velocity field then is the sum of the uniform incoming flow velocity and the velocity fields induced by all panels. In the centre of each panel a collocation point is chosen, where a boundary condition of zero normal velocity is imposed. These boundary conditions can be expressed in all M unknown source strengths, and together form a system of M equations in M unknowns. Solving this system and evaluating the velocities induced by the source strengths found we obtain the complete velocity field and, using Bernoulli's equation, the pressure field.

To apply the method of Hess and Smith to a surface-piercing body a treatment of the waterplane is necessary. The simplest approach is to neglect wavemaking altogether and to assume the water surface remains undisturbed. Computationally this is realised by reflecting the underwater part

of the hull in the still water plane, covering now both the hull and its mirror image with sources, and proceeding as before. The velocity field so calculated is symmetric with respect to the still water surface and is commonly denoted as *double-body flow*. It satisfies the kinematic but violates the dynamic boundary condition at the water surface; but it may be expected to approximate the actual flow in cases that the waves are small, i.e. at very low Froude numbers.

For non-negligible values of the Froude number one has to include the wavemaking, so free surface boundary conditions must be satisfied. Dawson proposed to cover also a part of the still water surface around the hull with source panels. The velocity field then is the sum of the incoming flow and the velocities induced by all panels, located on the hull, its mirror image and the panelled part of the free surface. In each free surface panel centre an appropriate free surface boundary condition is imposed, expressed in all unknown hull and free surface source strengths. With N free surface panels we now get a system of $M + N$ equations in $M + N$ unknowns. After solving this we can again compute the velocity and pressure field, and the wave elevation in each free surface panel center.

Free surface boundary condition

The exact free surface conditions (2.6) and (2.7) are nonlinear. Dawson linearised these by assuming the flow with waves to be a small perturbation of that without waves, the double-body flow. This assumption is likely to be valid for not too high Froude numbers, and consequently the resulting type of linearised theory is called *slow-ship theory*. The potential is decomposed into that of the double-body flow, Φ, and a perturbation φ'; and the wave elevation is decomposed into a part corresponding to the pressure in the double-body flow at the still water surface, η_r, and a perturbation η' :

$$\phi(x, y, z) = \Phi(x, y, z) + \varphi'(x, y, z) \tag{3.1}$$

$$\eta(x, z) = \eta_r(x, z) + \eta'(x, z) = \frac{1}{2}Fn^2(1 - \Phi_x^2 - \Phi_z^2) + \eta'(x, z) \tag{3.2}$$

with the assumptions that $\|\nabla \varphi'\| \ll 1$ and $\eta' \ll 1$. If the double-body flow has been computed first, both Φ and η_r are known.

Substituting this into the kinematic and dynamic boundary conditions and dropping terms of second or higher order in the perturbations we obtain boundary conditions that are linear in the unknowns φ' and η'. Next we use the dynamic boundary condition to eliminate η' from the kinematic condition and obtain a single, combined linear boundary condition expressed in derivatives of φ' and known quantities only.

This condition must in principle still be imposed at the unknown wave surface. But in Dawson's method it is simply imposed at the undisturbed free surface (i.e. φ' and Φ are evaluated at $y = 0$); a simplification introduced without further comment in [1]. In this way both basic difficulties of the full wave resistance problem, the nonlinearity and the free surface character, have been

eliminated. The derivation of the free surface condition will be discussed more extensively in the next chapter.

Dawson recasted the linearised free surface condition for the total potential into the following form:

$$(\Phi_l^2 \phi_l)_l + \frac{1}{Fn^2}\phi_y = 2\Phi_l^2\Phi_{ll} \tag{3.3}$$

where l is a curvilinear coordinate along the streamlines of the double-body flow on the undisturbed free surface. In addition to velocity components the free surface condition contains l*−derivatives* of velocities. Like the velocities themselves these could be expressed as the sum of the velocity derivatives induced by all source panels, but this would require the additional calculation of a complete matrix of induced velocity derivatives. Not only to avoid this but also for reasons to be given below, in Dawson's method these derivatives are expressed in the induced velocities by means of a finite difference scheme.

The absence of transverse derivatives in eq. (3.3) permits an elegant implementation. In Dawson's original method the free surface panels were arranged in strips aligned with the double-body flow on the undisturbed free surface. The desired l-derivatives are then found directly by finite differencing over the collocation points on successive panels within a strip.

The radiation condition

Up to this point the solution of the problem is still non-unique since the radiation condition has not been imposed yet, and solutions with waves upstream of the bow may still be found. But Dawson found that it is possible to enforce this condition indirectly by choosing a particular numerical method. Specifically, *upstream* differencing for the l-derivatives of the velocities in the free surface condition, together with the proper conditions at the upstream edge of the free surface domain, provides the right bias in the solution procedure suppressing any waves upstream of the bow. Although a variety of upstream difference schemes appeared to have this property, a particular 4-point scheme was selected based on the amount of numerical damping observed in the solution.

P.S. Jensen [8] ten years later pointed out that, if ϕ_{ll} is approximated by a two-point upstream difference scheme, the truncation error so introduced takes the same form as the so-called Rayleigh viscosity, a well-known artifice used in analytical methods to impose the radiation condition. Appropriate higher-order schemes may have a similar effect. This lends theoretical support to Dawson's treatment of the radiation condition.

Merits of Dawson's method

Dawson's method, which contained several original ideas, has initiated a sort of breakthrough in wave pattern calculation capabilities. His most important contributions were probably:

- The convincing demonstration of the use of simple Rankine sources to model surface waves. Such an approach had already been pioneered by Bai and Yeung [9] for zero-speed radiation and diffraction problems in frequency-domain formulation, and by Gadd [10] for the wave resistance problem. Essentially all earlier methods instead used Kelvin sources, which by definition generate a velocity field satisfying a Kelvin free surface condition; this eliminates the need for a free surface panelling. Consequently Rankine source methods require a much larger number of panels, but this disadvantage is largely offset by the far simpler arithmetic operations. Besides, the Rankine source approach provides much greater flexibility in imposing different free surface boundary conditions and dealing with various geometric configurations.

- The simple and generally effective way of imposing the radiation condition in a numerical method by means of an upstream difference scheme.

The method was originally proposed as an "engineering approach" containing several still unclarified points. But as its simplicity, flexibility and promising results attracted interest, much work has been done since to give it a stronger foundation and to find alternatives and improvements. Many different variations on Dawson's original theme are now in use all over the world, sharing the use of simple Rankine singularities but partly using alternative ways of linearising the free surface condition, satisfying the radiation condition, discretising the free surface and so on. No attempt will be made here to review the extensive literature on the subject. All this work, triggered by the remarkable paper of Dawson, has made this class of methods a mature tool of large use in practical ship design.

3.2   The DAWSON code

This section very briefly reviews some of the extensions and improvements of Dawson's method, used in MARIN's code DAWSON or otherwise relevant for the further discussion. This code is based on a prior development by the National Aerospace Laboratory NLR, a program named HYDROPAN [11], which contained a number of innovations compared to Dawson's method, and added a treatment of lift effects on foils based on the existing NLR PANEL method [12]. It was the starting point of my own work on Dawson's method beginning in 1986, which soon led to several changes and additions [13, 14]. The resulting drastically revised code was called DAWSON.

Numerical accuracy and stability

Dawson's method in its original form was known to have some less favourable numerical proper-
ties. An important contribution was made by Piers [15], who was able to explain and partly remove
these. He studied the accuracy and stability of the discretisation of the free surface, applying the
theory of discrete Fourier transforms to a two-dimensional free-surface flow with uniform-flow
linearisation.

For a twodimensional far field the errors incurred by discretising the free-surface singularity
distribution and those introduced by the difference scheme were derived and expressed as a
numerical dispersion (a wavelength error) and a numerical damping (an amplitude decay error).
In principle the constant-strength source distribution introduces errors of $\mathcal{O}(\Delta x)$ in the velocity
field, and as a matter of fact the numerical dispersion was found to be of that order even in the far
field, regardless of the difference scheme used. This explains the underestimation of wavelengths
already observed by Dawson [1] and often quite visible in predictions.

Piers proposed to cancel the leading order terms of the numerical dispersion for twodimensional
free waves by introducing a dispersion correction in the free surface condition. The correction is
a factor

$$(1 + \gamma_1 \frac{\Delta x}{Fn^2} + \gamma_1^2 \frac{\Delta x^2}{Fn^4})$$

multiplying the contribution of the free surface sources to the term

$$\Phi_l \frac{\partial}{\partial l}(\Phi_l \phi_l).$$

Numerical dispersion is thus reduced to $\mathcal{O}(\Delta x^3)$ for the model problem in the far field. This property
carries over to the corresponding Fourier modes in general 2D problems and to the transverse
wave components in a 3D problem. For other wave components, such as non-transverse waves
in 3D, the dispersion error is only partially cancelled. This dispersion correction has also been
adopted in DAWSON and proved valuable.

Another issue clarified by Piers was the fact that Dawson's method suffers from point-to-point os-
cillations in the free surface source strengths for relatively small panels (high "panel Froude num-
bers" $U_\infty/\sqrt{g\Delta x}$). The origin appeared to be an instability inherent in the use of constant-strength
source panels and finite differencing for the velocity derivatives. A free surface distribution of
normal dipoles, on the other hand, was claimed to be stable at all panel Froude numbers.[1]

On the other hand, a pure dipole distribution on the free surface was found to lead to a structure
of the matrix precluding the use of an iterative matrix solver. From a first inspection a combi-
ned source/dipole distribution with $\mu = -Fn^2\sigma$ on each free surface panel seemed to give best
prospects for a successful iteration, and this was used in HYDROPAN. Actually, an effective iterative
solver for the free surface part of the matrix could not be found though.

---

[1] However, this statement is only true if also the dipole-induced longitudinal velocity $u = 1/2\mu_x$ is calculated using a
backward difference scheme; a central scheme would produce a similar instability for high panel Froude numbers.

However, I later found that the, supposedly arbitrary, ratio of source and dipole strength had an unacceptably strong influence on the results [14]. A probable cause was detected in the derivation of the panel method, in which the integral over ϕ and ϕ_n resulting from Green's identity is transformed into an integral over singularity strengths. In this step, potential fields satisfying the Laplace equation are assumed in the virtual domains above the still water surface and inside the double hull. The choice of singularities in HYDROPAN however implies nonexistence of such potential fields and is, therefore, fundamentally wrong.[2] Therefore the entire dipole distribution was dispensed with and in DAWSON I returned to the use of a pure source distribution.

This reintroduced the risk of wiggles in the source strength, which, however, only are significant for strong disturbances at high panel Froude numbers. Further analysis led to the idea to shift the collocation points slightly upstream relative to the panel centres [13], which eliminates the zero of the discrete Fourier transform for this mode. This I found to be a very effective device to smooth the oscillations; but it introduces some additional first-order numerical dispersion and second-order numerical damping and is, therefore only used when really necessary.

These conclusions on the accuracy and stability have later been confirmed and considerably extended by Sclavounos and Nakos [16], who proposed a systematic and general methodology to determine the stability, numerical damping and dispersion of this class of numerical methods. With this approach they studied a variety of orders of singularity distributions, integral equations, and difference schemes.[3] As an alternative for Dawson's method they developed a new method based on quadratic spline basis functions for the source distribution and analytical velocity derivatives. That method itself is accurate and free of numerical damping. But at a later stage numerical filtering appeared necessary [17], reintroducing an effect not unlike that of the original numerical damping in Dawson's method.

Other modifications

Besides those mentioned above, the DAWSON code contains several other changes made to improve the accuracy, efficiency and range of application. Ref. [13] gives more details.

- The use of an upstream difference scheme in the free surface condition in Dawson's method is usually sufficient to enforce the radiation condition. But, in particular for high Froude numbers, waves upstream of the bow were sometimes found, incidentally resulting in completely unrealistic solutions. Shifting the collocation points slightly upstream relative to the panel centres, for the free surface panels ahead of the bow only, appeared to be extremely effective to remove this problem. Since in that region the free surface is basically flat, this local shift does not introduce any significant numerical damping.

---

[2] This nonexistence only appears for surface-piercing bodies and thus could stay unnoticed in the model study by Piers.
[3] In Chapter 6 we shall use this technique to study the discretisation proposed for our nonlinear method.

- The generation of a streamline grid on the undisturbed free surface is an awkward and time-consuming procedure allowing little control of the panel distribution. Therefore a simple, algebraically generated waterline-fitted free surface grid was used instead. Since panel strips thus are no longer aligned with the double-body flow, the l−derivatives must be composed from stripwise derivatives found by backward differencing, and transverse derivatives approximated by central difference schemes.

- Dawson's form of the linearised free surface condition was shown to be incorrectly derived. In the derivation the general expression

$$\Phi_x F_x + \Phi_z F_z = \Phi_l F_l,$$

which is valid provided F is a scalar and l is along the gradient of Φ, was applied with F a contravariant velocity component in a curvilinear system, viz. ϕ_l. Although the resulting error generally is small, in DAWSON we use the correct expression instead.

- Two alternative expressions for the wave resistance were derived using Lagally's theorem, and also a more accurate pressure integration over the hull was implemented. All expressions were compared in practice and showed a very similar dependence on panel density. None appeared to be significantly more accurate except for lifting surfaces.

- The code was extended to cases with immersed transom sterns. Additional panel strips aft of the transom are added in such cases, and a special form of the free surface condition is used in points adjacent to the transom. Moreover the DAWSON code was extended for dealing with a variety of other configurations and practical problems.

- Many other changes have been made to enhance the efficiency of the calculations. The code has been migrated to the larger and faster computers coming available, the solver has been implemented anew and parts of the code have been vectorised. While originally the calculations were carried out on a Cyber 175 mainframe that could cope with no more than 875 free surface panels and required calculation times up to one hour, we currently run DAWSON on the Dutch National Supercomputing facility, the CRAY C98, and panel numbers up to 6000 ask just a few minutes. Calculation times have been reduced by a factor of about 180 in the meantime (and 450 compared to HYDROPAN).

3.3   Properties of Dawson's method

Dawson's method, with the modifications mentioned above and as implemented in the code DAWSON, has been used very intensively in commercial ship design work at MARIN since 1986. Only since 1995 its role has been taken over by the nonlinear RAPID code. From the experience gained in all these applications, the following procedure to analyse the results of a calculation has been established.

The judgement on the quality of the design from a wave resistance point of view is *not* based on the predicted wave resistance but on the entire flow field. The wave pattern is inspected first,

indicating which wave components are dominant for the case considered. We then examine the hull pressure distribution and flow direction to identify which hull form aspects are primarily responsible for those components. The understanding of the flow so obtained indicates how the hull form design is to be modified in order to reduce the wavemaking. Once these modifications have been made and the code has been run for the new variation, the comparison between both designs is again not based on the predicted resistances but on the relative magnitude of the waves excited and their directions.

With this procedure, which minimises the influence of the weak points of the method, and which considers the calculations as a support of human understanding of fluid dynamics rather than as an absolute prediction of the resistance, Dawson's method has turned out to be an outstanding tool for ship design. Nevertheless, a number of important shortcomings have been identified:

1. In the predicted wave profiles along the hull, the bow wave crest is systematically too low for all linearised methods. Some examples will be shown later. Moreover, the predicted stern waves are often much higher and rather unrealistic; a deviation which may only partly be attributed to viscous effects.

2. Diverging wave components from the bow are often far underestimated. Wave crests are often somewhat more transverse than they should.

3. The predicted wave resistance is in most cases unreliable. The general trend is that fair resistance predictions can be obtained for slender ships at relatively high Froude numbers, such as frigates and sailing yachts [18], but not for most merchant vessels. Small changes in the stern area in particular can lead to large and unrealistic changes in the predicted resistance. For slow, full formed ships at low speed the predicted wave resistance is even generally *negative*, as will be discussed in the next chapter. Even the difference in predicted resistance between two design variations cannot always be trusted. On the other hand, a difference in the predicted wave *pattern* as a rule correctly indicates which design is better. This motivates why in the analysis the predicted resistance is not used.

4. The instability typical of Dawson's discretisation still is there. If, in an attempt to increase the numerical accuracy, very small panels are used (e.g. less than 2.5 % of the transverse wave length), oscillations in the free surface source strength and velocity field may turn up.

5. For ships with a bulbous bow just beneath the still water surface, irregularities in the predicted bow wave system are sometimes found which preclude any useful analysis. If the bulbous bow even pierces the still water surface (but becomes totally submerged at speed), the linearisation essentially cuts off the bulb at the still waterline and cannot predict the actual flow behaviour.

6. Also all other aspects of the hull form above the still waterline are disregarded. One of the striking examples is a transom stern at a distance above the still water surface, the most common type of stern for merchant vessels. In a linearised method, the same vessel is not supposed to have a transom stern and without further precautions a wrong type of flow would be predicted.

Some of these shortcomings are, of course, fundamental to linearised methods. Of some others, in particular the errors in the wave pattern and the resistance, the cause was not as evident. A study has, therefore, been carried out in 1989 — 1990 to investigate possibilities to improve upon the method within the framework of linearised methods. This study is discussed in the next chapter. As those conclusions that have directed the development of the nonlinear method are listed at the beginning of Chapter 5, Chapter 4 could be skipped by those less interested in the backgrounds of linearised methods.

Chapter 4

Adequacy of linearised free surface conditions

This chapter discusses some different linearisations of the free surface boundary conditions and pays attention to their consistency. We compare the accuracy of a few alternatives by considering the differences in predicted wave resistance and wave pattern; by checking the validity of the assumptions underlying the various theories; and by evaluating the higher-order terms disregarded in the linearisation. An explanation is given for the occurrence of negative resistance predictions in slow-ship theory. All this further motivates the development of a fully nonlinear method and provides indications how it should be set up. Much of this study has been published before in [2].

4.1 Uniform-flow linearisation

The simplest kind of linearisation is that with respect to a uniform flow. This supposes that at the free surface the entire disturbance caused by the presence of the ship is small. The total potential is decomposed as

$$\phi(x, y, z) = x + \varphi'(x, y, z) \tag{4.1}$$

where the perturbation potential φ' is of $\mathcal{O}(\epsilon)$, $\epsilon \ll 1$. Substituting this into the dynamic free surface condition results in

$$\eta = -Fn^2 \varphi'_x \tag{4.2}$$

to first order in ϵ. This shows that also the wave steepness (wave amplitude divided by wave length) is small of $\mathcal{O}(\epsilon)$. The kinematic boundary condition now yields:

$$Fn^2\phi_{xx} + \phi_y = 0 \tag{4.3}$$

or an identical condition for φ' . This is the well-known *Kelvin free surface condition*. It is consistent to impose it at the undisturbed free surface $y = 0$ instead of at the true wave surface, as is easily checked.

4.2   Slow-ship linearisation

A more refined linearisation assumes that the flow with waves is a small perturbation of the flow passing around the hull and having a flat water surface, the double-body flow. The latter is a good approximation for vanishing Froude number, and an appropriate perturbation parameter for the linearisation is Fn^2 . The potential is decomposed as:

$$\phi(x, y, z) = \Phi(x, y, z) + \varphi'(x, y, z) \tag{4.4}$$

where $\nabla\Phi$ is the double-body flow velocity and we assume that the perturbation velocity $\nabla\varphi' = \mathcal{O}(Fn^2) \ll 1$ at the free surface.

The dynamic free surface condition now yields

$$\eta = \eta_r + \eta' = \frac{1}{2}Fn^2(1 - \nabla\Phi.\nabla\Phi) - \frac{1}{2}Fn^2(2\nabla\Phi.\nabla\varphi' + \nabla\varphi'.\nabla\varphi') \tag{4.5}$$

which we substitute into the kinematic free surface condition to find the following *exact* combined free surface condition:

$$\begin{aligned}
\Phi_y + \varphi'_y = \quad &-\frac{1}{2}Fn^2\nabla\Phi.\nabla(\nabla\Phi.\nabla\Phi) - \frac{1}{2}Fn^2\nabla\varphi'.\nabla(\nabla\Phi.\nabla\Phi) + \\
&- Fn^2\nabla\Phi.\nabla(\nabla\Phi.\nabla\varphi') - Fn^2\nabla\varphi'.\nabla(\nabla\Phi.\nabla\varphi') + \\
&-\frac{1}{2}Fn^2\nabla\Phi.\nabla(\nabla\varphi'.\nabla\varphi') - \frac{1}{2}Fn^2\nabla\varphi'.\nabla(\nabla\varphi'.\nabla\varphi')
\end{aligned} \tag{4.6}$$

to be satisfied at $y = \eta$. [1] The last three terms are nonlinear, and linearisation now starts. At this point, different assumptions on the order of the terms have been made by different authors.

---

[1] It is to be noted here that, while the original expression for the kinematic condition contains η_x and η_z only, this new expression in ϕ contains y-derivatives as well. These two expressions are in agreement however, since with

$$\eta(x, z) = F(x, \eta, z)$$

the derivatives are written as

$$\frac{\partial\eta}{\partial x} = (\frac{dF}{dx})_{y=\eta(x,z)} = \frac{\partial F}{\partial x} + \eta_x\frac{\partial F}{\partial y}.$$

Using the kinematic condition we obtain the expression as given here.

Baba et al. [19, 20], Newman [21]

Around 1974 — 1976 several authors derived a slow-ship boundary condition following ideas put forward by Ogilvie [22] in his study of wave making by a 2D submerged body. Probably the first to implement this in a practical method were Baba and Takekuma [19]. A clear discussion of the order of different terms is given in Newman [21].

We expect that the perturbation will have a wave-like character in addition to non-wavy components. The dimensional wavenumber must be proportional to Fn^{-2}. Each differentiation of the perturbation potential φ' then reduces its order by a factor Fn^2. This increases the relative importance of higher derivative terms. Starting from the assumption that

$$\nabla \varphi' = \mathcal{O}(Fn^2)$$

we find the following orders for the six terms at the right hand side of equation (4.6):

$$\mathcal{O}(Fn^2) \ , \ \mathcal{O}(Fn^4) \ , \ \mathcal{O}(Fn^2) \ , \ \mathcal{O}(Fn^4) \ , \ \mathcal{O}(Fn^4) \ , \ \mathcal{O}(Fn^6).$$

The fourth and fifth term, which are of $\mathcal{O}(Fn^4)$, are nonlinear in φ', and a linear free surface condition is only obtained if they are omitted. Consistency then requires that the equation is truncated after the $\mathcal{O}(Fn^2)$ terms and only the first and third term at the right hand side are retained.

This linearised free surface condition is to be satisfied on the linearised free surface. The dynamic free surface condition yields, however,

$$\eta = \eta_r + \mathcal{O}(Fn^4), \tag{4.7}$$

so the boundary condition may equally be imposed at the surface $y = \eta_r$, the transfer adding only more 4th-order terms which must be neglected for consistency. The resulting free surface condition contains double-body velocities at $y = \eta_r$, which usually are expressed in those at $y = 0$ using a Taylor expansion. Because of the symmetry of the double-body flow and since $\eta_r = \mathcal{O}(Fn^2)$, the only change is that Φ_y is replaced by $\eta_r \Phi_{yy}$.

On the other hand, subject to the assumptions made above the perturbation potential may *not* be expanded from $y = 0$ towards $y = \eta_r$. The order reduction by differentiation of φ'-terms makes all terms in the Taylor expansion for φ' of the same order in Fn^2 and there is no justification to truncate the expansion at any point. The final free surface condition thus becomes:

$$Fn^2(\Phi_x^2 \varphi'_{xx} + 2\Phi_x \Phi_z \varphi'_{xz} + \Phi_z^2 \varphi'_{zz}) + \varphi'_y = (\Phi_x \eta_r)_x + (\Phi_z \eta_r)_z \ , \tag{4.8}$$

and is to be imposed at $y = \eta_r(x, z)$ although the double-body velocities are those at $y = 0$.

Eggers [23]

Another form of the free surface condition has been derived by Eggers. He shows that the procedure outlined above, which gives rise to the neglect of the terms containing first derivatives of φ' (such as the second term in (4.6)) suppresses the amplitude variation of the waves in the near field caused by the gradients of η_r. To avoid this he does not take into account any order reduction by differentiation. Again supposing that $\nabla\varphi' = \mathcal{O}(Fn^2)$ the six terms at the right hand side of equation(4.6) then are:

$$\mathcal{O}(Fn^2) \ , \ \mathcal{O}(Fn^4) \ , \ \mathcal{O}(Fn^4) \ , \ \mathcal{O}(Fn^6) \ , \ \mathcal{O}(Fn^6) \ , \ \mathcal{O}(Fn^8).$$

Now the last three terms, which are nonlinear, are of $\mathcal{O}(Fn^6)$ or higher. The first three terms constitute a linear free surface condition that consistently includes all terms up to $\mathcal{O}(Fn^4)$. Compared to equation (4.8) the second term, a single additional term containing first derivatives of the perturbation potential, is included. Therefore Eggers's condition is more complete, but it remains true that in principle higher derivatives of at least the wavelike part of φ' may be of the same order in Fn^2, possibly making this condition inconsistent.

With some further simplifications and expansion of the double-body flow in terms of that at the still water surface the free surface condition becomes:

$$Fn^2(\Phi_x^2\varphi'_{xx} + 2\Phi_x\Phi_z\varphi'_{xz} + \Phi_z^2\varphi'_{zz}) - 2\varphi'_x\eta_{rx} - 2\varphi'_z\eta_{rz} + \varphi'_y +$$
$$-Fn^2\Phi_{yy}(\Phi_x\varphi'_x + \Phi_z\varphi'_z) = (\Phi_x\eta_r)_x + (\Phi_z\eta_r)_z \qquad (4.9)$$

to be satisfied on $y = \eta_r(x, z)$. It is noted here that the last term at the left hand side was omitted in [23] but incorporated in [24].

The next step is to transfer the entire boundary condition from $y = \eta_r$ towards $y = 0$. This is possible because now also the perturbation potential admits expansion from $y = 0$: No order reduction due to differentiation being taken into account, the Taylor expansions can be truncated such that only terms up to $\mathcal{O}(Fn^4)$ enter. The final free surface condition to be satisfied on the still water surface thus becomes:

$$(Fn^2\Phi_x^2 - \eta_r)\varphi'_{xx} + 2Fn^2\Phi_x\Phi_z\varphi'_{xz} + (Fn^2\Phi_z^2 - \eta_r)\varphi'_{zz} - 2\varphi'_x\eta_{rx} - 2\varphi'_z\eta_{rz} + \varphi'_y +$$
$$-Fn^2\Phi_{yy}(\Phi_x\varphi'_x + \Phi_z\varphi'_z) = (\Phi_x\eta_r)_x + (\Phi_z\eta_r)_z \text{ at } y = 0. \qquad (4.10)$$

In [23] the properties of this slow-ship free surface condition (without the last term at the left) are analysed and local dispersion relations are derived. This analysis attaches much significance to the coefficients of the second derivatives of the perturbation potential, and based on their relative magnitude distinguishes elliptic, parabolic and hyperbolic domains on the undisturbed free surface. A relation is then sought with experimental observations of the flow around a full ship

bow. Although some interesting results are obtained, it must be kept in mind that the coefficients have been determined from a truncated Taylor expansion of somewhat disputable validity; without that expansion the free surface condition is of parabolic type everywhere (e.g. equations (4.8), (4.9)).

Brandsma and Hermans [25]

In a further study of the slow-ship linearisation Brandsma and Hermans take a position intermediate between the two previous alternatives. Like Eggers they do not consistently apply order reduction by differentiation because it obliges to drop the first derivative terms. Not only these are subsequently demonstrated to have an appreciable effect, but also their omission is expected to cause nonuniformities in the problems defining the perturbation potential to higher orders. Consequently they obtain a free surface condition to be satisfied at $y = \eta_r$ equal to that of Eggers, (4.9).

However, the next step, transfer towards $y = 0$, is not made. As we pointed out above, truncating the associated Taylor expansions cannot be truly justified if one admits a wavelike perturbation; but also these authors have objections against precisely that change in character of the free surface condition pointed out by Eggers [23]. In particular in the free surface condition (4.10) the coefficient of φ'_{xx} vanishes where $\Phi_x^2 = 1/3$, $\Phi_z = 0$, while it does not in (4.9). This could result in singular behaviour at an otherwise arbitrary free surface point at some distance ahead of the bow of a ship. Brandsma and Hermans considered this an undesirable artefact of the boundary condition transfer, which they therefore avoided.

In an analytical study they show that, for a two-dimensional flow past a submerged circular cylinder, the first derivative terms present in their (and Eggers's) free surface condition have a very strong effect on the result, yielding a wave resistance an order of magnitude higher than obtained with condition (4.8). This does show that the first derivative terms are not negligible, but of course does not resolve the consistency questions.

Nakos [26]

In his thesis Nakos rederives the slow-ship boundary condition based on the assumption that the perturbation potential and its derivatives are of $\mathcal{O}(\delta F n^2)$, where δ is a hull slenderness parameter not further defined. The questions of order reduction and the truncation of Taylor expansions are not touched upon. It appears that the final condition to be satisfied at $y = 0$ is basically identical to that of Eggers, including the term $-F n^2 \Phi_{yy}(\Phi_x \varphi'_x + \Phi_z \varphi'_z)$ but without the term $-\eta_r(\varphi'_{xx} + \varphi'_{zz})$. The latter omission cannot be justified from the basic assumptions made, since it is of equal order as, for instance, the term $\varphi'_x \eta_{rx}$ that is included indeed.

The interesting conclusion from Nakos's derivation is that slow-ship conditions are not just

applicable to slow ships, but also may be supposed to be theoretically valid for slender ships at higher speed.

Dawson [1]

Although Dawson's free surface condition definitely falls in the same category of slow-ship linearisations, he gives little theoretical justification and makes no reference to any formal assumption on the order of different terms, possible order reduction by differentiation or truncation of Taylor series. His free surface condition reads:

$$Fn^2(\Phi_x^2\varphi_{xx}' + 2\Phi_x\Phi_z\varphi_{xz}' + \Phi_z^2\varphi_{zz}') - 2\varphi_x'\eta_{rx} - 2\varphi_z'\eta_{rz} + \varphi_y' = \Phi_x\eta_{rx} + \Phi_z\eta_{rz} \tag{4.11}$$

at $y = 0$. This condition thus includes the first order terms expected to be important, but misses the transfer terms

$$-\eta_r(\varphi_{xx}' + \varphi_{zz}' + \Phi_{xx} + \Phi_{zz}) - Fn^2\Phi_{yy}(\Phi_x\varphi_x' + \Phi_z\varphi_z') = \eta_r(\varphi_{yy}' + \Phi_{yy}) + \eta'\Phi_{yy}$$

The importance of these will be examined later.

4.3   Solution methods

The two classes of linearised theories conventionally have been solved using entirely different methods. For mathematical problems defined by the Laplace equation, the Kelvin condition on $y = 0$ and the radiation condition, a Green function can be derived, generally called the Kelvin or Havelock source potential. The solution of the wave resistance problem linearised in this way thus can be composed by using distributions of Kelvin sources, their strengths adjusted such that the flow satisfies the hull boundary condition.

The basic assumption in a Kelvin linearisation, that the ship causes only a small perturbation of a uniform flow, can only be valid if the ship is slender in some sense. Based on such slenderness assumptions also the hull boundary condition could be linearised, leading to e.g. thin-ship, flat-ship and slender-ship methods. However, *none* of these has proven to be practically useful except for special cases like the extremely slender demihulls of catamarans.

In the sixties a next step was made by including the hull boundary condition in its exact form (i.e. the Neumann condition (2.4) for the potential, imposed on the true hull surface) but still using the Kelvin free surface boundary condition. Such *Neumann-Kelvin methods* used a distribution of Kelvin sources over the hull surface. With the computers available at that time, the added complexity of having to solve a system of equations for the source strengths forced people to use quite small panel numbers, leading to numerically inaccurate results. Thus the actual validity of Neumann-Kelvin theory did not become clear until many years later.

Unlike the Kelvin condition, slow-ship conditions have spatially varying coefficients. The integral over the free surface occurring in the boundary integral statement of the problem cannot, therefore, simply be eliminated by a proper choice of the Green function, and various alternative methods have been proposed.

Baba et al. [19, 20] use an analytical approach to solve the problem defined by their free surface condition. The evaluation of the resulting expression is made only asymptotically for $Fn \rightarrow 0$, which is more restrictive than other methods. To impose the free surface condition on the surface $y = \eta_r$ without resorting to Taylor expansions they apply a coordinate transformation making the double-body wave surface the new coordinate surface. The same transformation in principle should also be applied to the body shape. But to leading order the perturbation potential does not occur in the hull boundary condition, so for low Fn the body transformation may be disregarded.

Besides, the transformation introduces additional terms into the Laplace equation. Also these are of higher order and are simply disregarded. Brandsma and Hermans [25] use a similar approach, and for a 2D submerged cylinder they show that as a matter of fact the additional terms in the Laplace equation have little effect on the downstream wave amplitude and wave resistance.

The most practical solution procedure probably is that due to Dawson, described in the previous chapter. It is based on numerical rather than analytical evaluation, and consequently is more flexible than previous methods. This flexibility in principle permits to impose the free surface condition on the surface $y = \eta_r$ if desired, by distributing panels over that surface rather than the still water surface. This would remove some of the theoretical objections against the use of Taylor expansions for the perturbation potential. However, disadvantages would be:

- the rather doubtful definition of the double-body flow velocities in points above the still water surface;

- the geometric complications of determining the intersection of the double-body wave surface with the hull, and adapting the hull panelling to this intersection;

- the need to repanel the hull and the double body wave surface for each speed, and the consequent recalculation of all induced velocities;

These complications, and the fair results of Dawson's method in its original form, have made virtually all followers to impose a free surface condition on the still water surface. I am not aware of any further study of the effect of this simplification on the results.

4.4   Comparison of linearised formulations

From the previous discussion it appears that the validity of both main classes of linearised formulations can be questioned. For Neumann-Kelvin methods the basic assumption that the entire

perturbation caused by the hull is small, is obviously violated for hull forms of usual proportions. Treating the hull boundary condition exactly but linearising the free surface boundary condition with respect to a uniform flow basically is inconsistent and leads to certain conflicts at the waterline where both boundaries meet. The slow-ship formulations however, though intuitively appearing to be more realistic, are subject to doubts on the appropriate formulation, the validity of the transfer of the boundary condition using Taylor expansions, and the basic question whether they actually are asymptotically correct for vanishing Froude number. There is little evidence as to which of the forms mentioned above is correct or behaves best, virtually all practical calculation methods simply adopting Dawson's free surface condition.

As theoretical considerations did not answer the question which linearisation is better, in 1989-1990 I have studied their accuracy in practical applications. I thus hoped to be able to improve the formulation and to resolve some of the shortcomings of the DAWSON code listed in Section 3.3. Surprisingly little information appeared to be available. A main source, and possibly the one that had encouraged many people to adopt Dawson's method and free surface condition, was the First Workshop on Ship Wave Resistance Calculations held in 1979 [27]. Dawson's predictions presented here were consistent and in reasonable agreement with the experimental values. On the other hand, the results of various Neumann-Kelvin methods showed an extreme scatter, solutions of the same mathematical problem differing by up to a factor of 2 in the predicted wave resistance!

Obviously, large numerical errors must have been present in those calculations, prohibiting an assessment of the relative merits of different free surface conditions. Comparing predictions by Neumann-Kelvin and slow-ship methods requires much care for the numerical accuracy, because the entirely different solution methods generally used involve numerical errors of a different nature. For a fairer comparison we shall therefore apply the *same* numerical method to both classes of free surface conditions. Instead of using Kelvin sources, we shall solve the Neumann-Kelvin problem here using Rankine sources on the hull and a part of the free surface; and implement the velocity derivative φ'_{xx} by a difference scheme. The Neumann-Kelvin solution thus is obtained from the same DAWSON code by simply replacing the double-body flow in the free surface condition by a uniform flow. Due to the very similar implementations the numerical errors in the slow-ship and Neumann-Kelvin solutions most likely will now be of quite comparable magnitude; and using the current experience on the required discretisation we can make sure that these errors have little influence on the predictions.

An exception may be the immediate vicinity of the bow and stern stagnation points. Singular behaviour there may, for very small free surface panel size, cause large numerical errors that might be different for both formulations and thus might obscure the actual validity of the free surface conditions. It is also imaginable that these singularities would be handled differently by a method based on Kelvin sources. Thus the numerical comparisons we are going to make merely tell us how important the double-body flow contribution to the free surface condition is for *practical* discretisations; and panel refinement studies show to which extent our conclusions depend on panel density.

The linearisations studied are the Neumann-Kelvin formulation and the slow-ship conditions
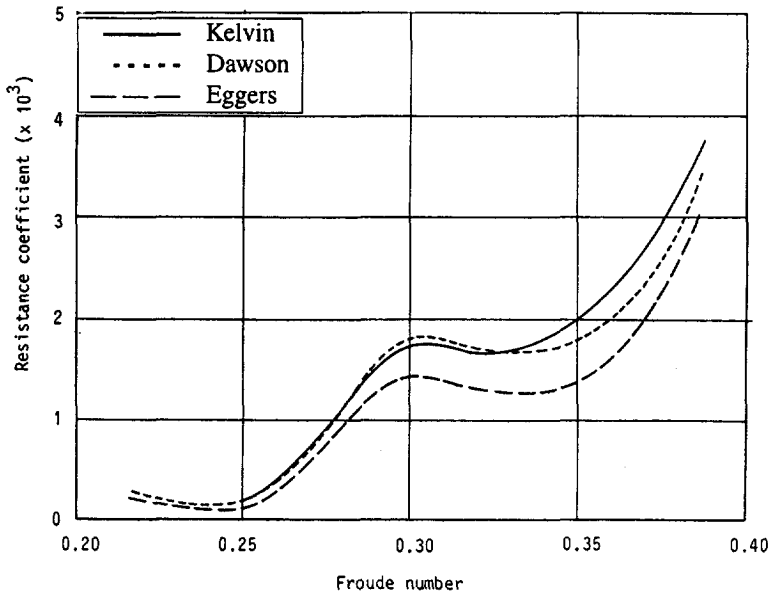
Figure 4.1: *Predicted wave resistance curves for Series 60 model, using different linearisations*

proposed by Dawson and Eggers [23] (equation 4.10 but without the last term at the left hand side). For Eggers's condition this study, as published in [2], apparently meant the first test in practical applications. A few evaluations of the condition proposed by Nakos [26] have been made as well. The comparison of different formulations will be carried out on three levels. First, predicted wave resistances and wave patterns are compared. Secondly we check the validity of some of the assumptions underlying the linearisations. The third level is an evaluation of the higher-order contributions to the free surface condition that have been dropped in the linearisation.

4.4.1   Predicted wave resistance and wave pattern

The wave resistance values used are those found by integration of the pressure (from the Bernoulli equation without linearisation) over the part of the hull under the still waterline. No waterline integral is taken into account for reasons to be discussed later.

The main findings of a number of comparisons are:

- Differences between wave resistances found using the Kelvin condition or Dawson's slow-ship condition are negligible for slender vessels like the Wigley hull, gradually increase with hull fullness, but remain fairly small for practical ship forms with a block coefficient up to 0.60 — 0.70. At least for the Series 60 $C_B = 0.60$ model Eggers's condition predicts
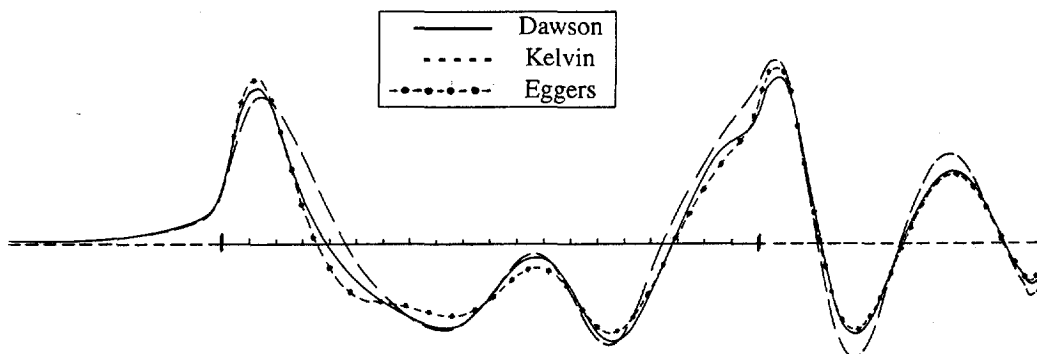
Figure 4.2: *Wave profile along the hull; Series 60 model, Fn = 0.25 .*

a lower wave resistance over the entire speed range (Fig. 4.1).[2] Experimental data are too scattered to really indicate which one is better.

- The wave profiles along the hull are quite similar for all methods. All linearised predictions are known to underestimate the bow wave height. Both slow-ship methods typically predict a more pointed bow wave shape than Neumann-Kelvin theory but only little increase in bow wave height, and they shift the aft slope of the bow wave to a more forward position. These effects are slightly stronger in Eggers's condition than in Dawson's. An example is Fig. 4.2.

- The differences in wave pattern between various free surface conditions are larger at some distance from the hull, where significant phase differences occur for the bow wave system but usually not for other parts of the wave pattern.

- As opposed to the above, for full hull forms (e.g. with a block coefficient above 0.80) drastic differences in predicted resistance occur at low speed. For example, for a tanker, $C_B = 0.82$ at $Fn = 0.18$ the Neumann-Kelvin resistance exceeds the experimental value by a factor of 4, while Dawson's slow-ship condition here predicts a *negative* resistance! An even lower value is predicted using Eggers's free surface condition.

- For the same example the wave patterns and profiles are shown in Fig. 4.3 and 4.4. Along the hull again both slow-ship conditions cause just a forward shift of the bow wave. Away from the hull the Kelvin condition yields larger wave amplitudes but a pattern similar to that of DAWSON, and definitely no indication of the drastic difference in resistance. The pattern predicted with Eggers's condition for this particular case displays a conspicuous Kelvin wedge apparently starting at the forward shoulder rather than at the bow, with only tiny bow waves outside.

---

[2]The results shown are those without dispersion correction factor in the free surface condition and are, therefore, not the best possible
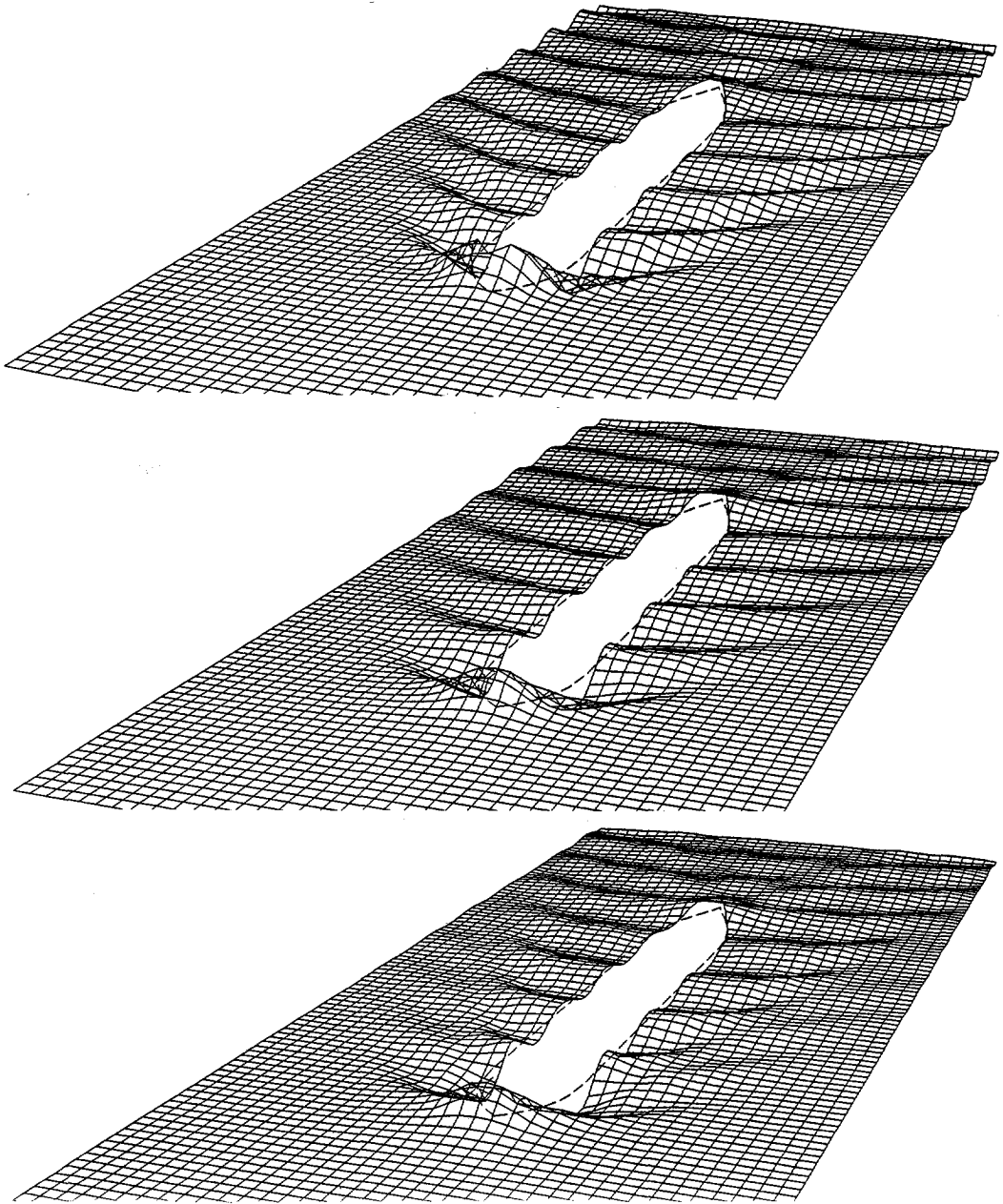
Figure 4.3: *Wave patterns for tanker model at Fn = 0.18 , using Kelvin condition (top) or Dawson's (middle) and Eggers's (bottom) slow-ship conditions. Wave heights are 5 times magnified.*
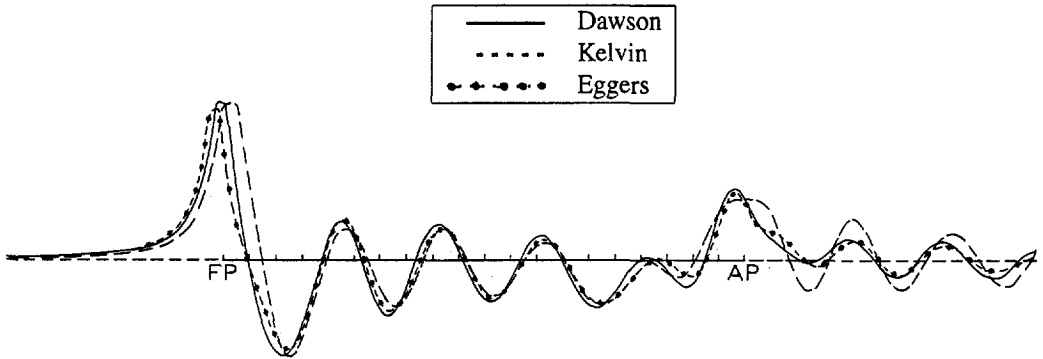
Figure 4.4: *Wave profiles along the hull; tanker model, Fn* = 0.18 .

- In general therefore we find that for moderately slender ships the double-body flow effect is of rather modest importance; at least for usual panel densities on the free surface and hull (but this conclusion was found not to depend strongly on the panel density). This seems to imply that the general preference for the slow-ship condition is not truly justified for these cases; an accurately evaluated Neumann-Kelvin formulation can give results of comparable validity.
  For full ships at low speed on the other hand, the Neumann-Kelvin prediction is far too high but the slow-ship theory resistance prediction is negative and thus equally useless. The latter paradoxical result is further studied in Section 4.5.

Some more examples of differences between linearised predictions will be presented in Chapter 10.

4.4.2   Validity of linearisation assumptions

The second stage of our inspection of the validity of linearisations is a direct check of the basic assumptions made. For the Kelvin condition, the assumption that at the free surface all deviations from a uniform flow are small is in any case obviously violated near the bow stagnation point, where the perturbation is of $\mathcal{O}(1)$. Also, a large waterline entrance angle requires a transverse velocity component of the same order as the incoming flow velocity. Nevertheless, except in the vicinity of stagnation points all components of $\nabla \varphi'$ generally are below 0.2 for relatively slender vessels of practical dimensions. This suggests that, except for the bow area, the Kelvin condition may well be acceptably accurate for a large class of vessels.

Slow ship theory assumes that the actual flow is close to the double-body flow. Dawson's free surface condition

$$\phi_y = \nabla\phi.\nabla\eta \approx \nabla\Phi.\nabla\eta + \nabla\varphi'.\nabla\eta_r = \text{term1} + \text{term2} , \qquad (4.12)$$
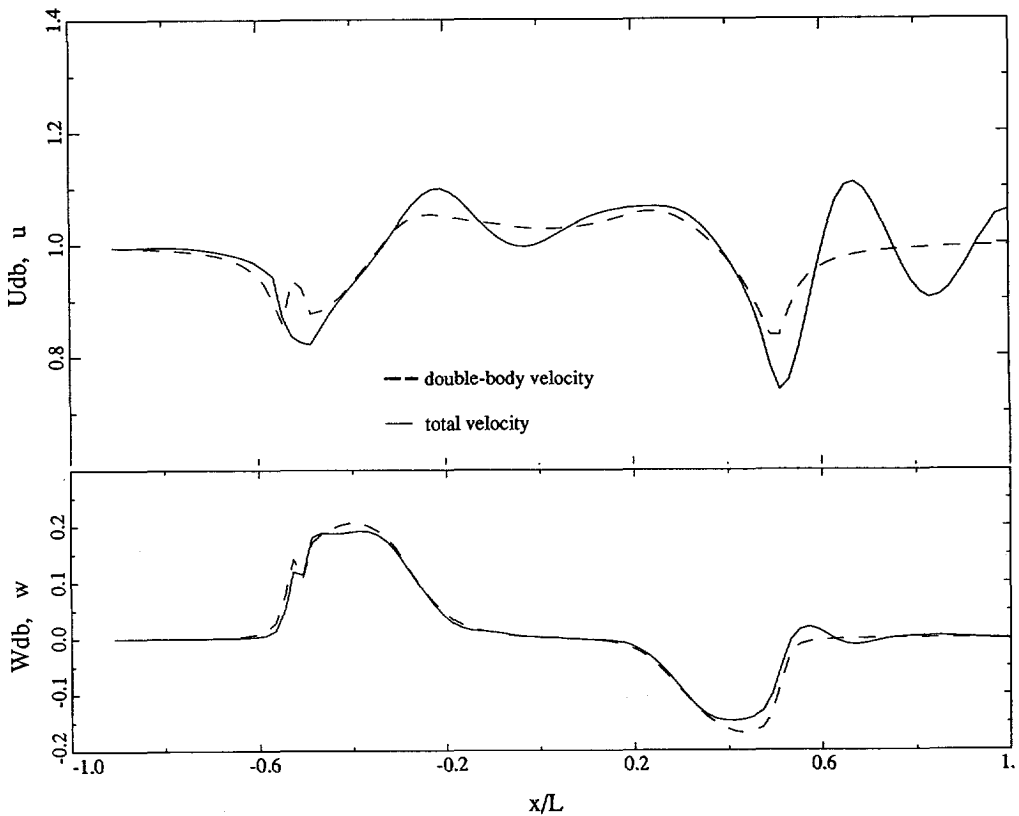
Figure 4.5: *Double-body and total velocities along the waterline; container feeder vessel,* $C_B =$
0.69 , *Fn* = 0.2373 .

neglects a term $\nabla\varphi'.\nabla\eta'$ and several transfer terms. Approximate validity therefore at least
requires that $\nabla\phi \approx \nabla\Phi$ or $\nabla\eta \approx \nabla\eta_r$.

As Fig. 4.5 illustrates[3], the first condition, $\nabla\phi \approx \nabla\Phi$, seems reasonable: In most cases at least the
transverse velocity $\phi_z \approx \Phi_z$, since both are determined by the waterline angle (The improvement
obtained by using $\phi_x \approx \Phi_x$ rather than $\phi_x \approx 1$ often is less clear.) This generally makes the first
term of the slow-ship expression more accurate than the equivalent term in the Kelvin condition,
$\vec{U}_\infty.\nabla\eta$.

The second term, however, only improves the result if η and η_r are well correlated. In particular
for rather slender ships at moderate speed this is not the case, the bow and stern wave lagging
behind the double-body wave and making η_{r_x} and η_x of opposite sign along a considerable part of

---

[3]The notable irregularity in the double-body flow near the bow is due to the presence of a bulbous bow close to the
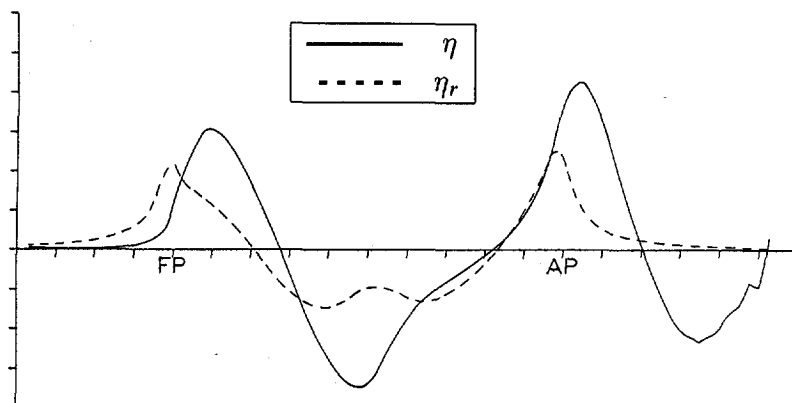still water surface

Figure 4.6: *Double-body and total wave height; Series 60 model, Fn = 0.35* .

the bow and stern waves. Fig. 4.6 illustrates this.

Therefore, while theoretically we found that the slow-ship linearisation might as well be applicable to slender ships at higher speed (page 32), in practice its advantage compared to Neumann-Kelvin theory is partially lost because of the increasing phase shift and the decreasing significance of double-body flow for increasing speed. The only region where double-body flow almost always is a valid approximation is directly upstream of the bow. This may explain the fact that the bow-wave system in slow-ship theory generally is somewhat more realistic.

Turning now to full-block ships at low speed, in Fig. 4.7 we compare the calculated longitudinal velocities near the bow of a tanker at *Fn* = 0.126. For both the Neumann-Kelvin and the Dawson result the longitudinal velocity is very close to that of the double-body flow, being entirely dominated by the hull boundary condition. But the corresponding wave elevations are very different: The slow-ship condition takes the double-body flow exactly into account and linearises in the small deviation only, but the Neumann-Kelvin method linearises the entire deviation from a uniform flow, resulting in a 50 % larger bow wave height. The vertical velocity must match the wave slope and therefore is also very different for the two methods, and so is the wave excitation at the bow. Not surprisingly, for slow ships slow-ship methods are definitely superior, notwithstanding the negative resistance they predict.

In addition to the assumptions concerning the flow at the free surface, a few other approximations are inherent in the linearisations. The transfer of the boundary condition from the actual wave surface towards the still water surface, with or without Taylor expansions, is only justified if higher vertical derivatives of the flow field are relatively small. But large vertical derivatives may be induced by the hull form, e.g. a bulbous bow just beneath the water surface. In principle a large curvature of the hull surface close to the waterline, a rather common feature in practice, violates the linearisation assumptions. The same is true for sloping sections at the waterline, which cause
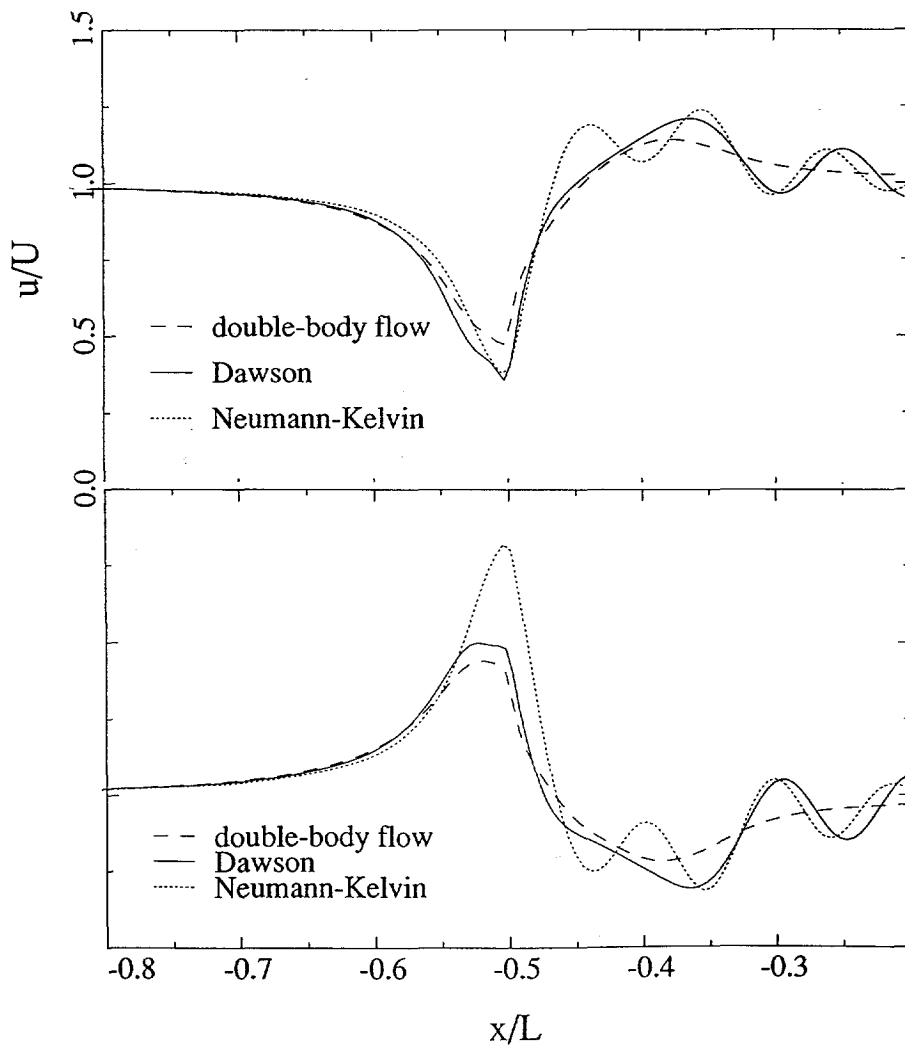
Figure 4.7: *Longitudinal velocities (top) and wave heights (bottom), near the bow of a tanker,*
Fn = 0.126 .

large gradients in the double-body flow field.

Moreover, all linearisations disregard the effect of the precise intersection of the free surface with
the hull. If the sections have a large slope near the waterline, the shape of the actual waterline may
be considerably different from that of the still water line. The most striking example of this is the
common pram-type stern with a transom above the still waterline. The still waterline then is quite
blunt, and gives rise to a very high stern wave in a linearised calculation. But this stern wave can
never be there since it would penetrate the overhanging stern. In reality the flow stays attached to

the hull, detaches from the edge of the transom in most cases, and leads to a large change in the waterline geometry and flow character not felt by a linearised method.

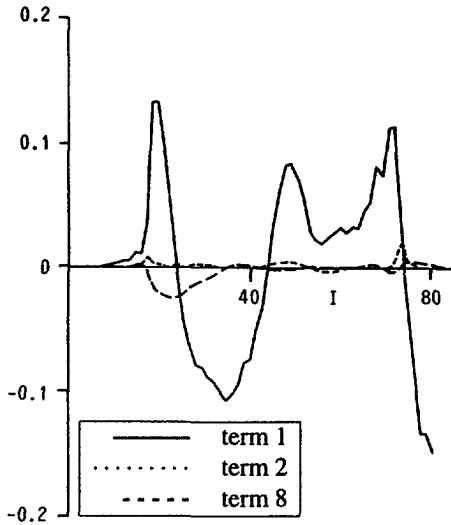## 4.4.3   Deviations from exact free surface conditions

Higher-order terms

Figure 4.8: *Relative importance of linear terms in Dawson's free surface condition; Series 60 at Fn = 0.35*

The third stage of the study of the linearisation accuracy is a numerical evaluation of the terms neglected in the linearisation. For this purpose the Kelvin and slow-ship free surface conditions have been expanded to higher order. For slow-ship theory Eggers's order assumptions have here been followed.

The higher-order terms are derived and classified in Appendix A. A distinction is made between the linear terms 1, 2 and 8; the higher-order transfer terms, and the remaining higher-order terms. Term 2 only occurs in slow-ship conditions. Term 8 approximates the transfer effect on the vertical velocity component. It is included in Eggers's free surface condition (4.10) but not in Dawson's. Most higher-order terms are nonlinear and could only be computed from a velocity field calculated first with the linearised method considered, thus providing an 'a posteriori' indication of the validity of the result itself. Where necessary, derivatives have been evaluated from velocities in free surface collocation points using finite differences.

Obviously several of the higher-order terms depend on η_r and must be negligible at larger distances from the hull. To keep the analysis manageable, I have only evaluated the higher-order terms for free surface collocation points along the waterline and centreline. Again the Series 60 parent hull and a tanker have been considered. All terms are contributions to the vertical velocity, and in the figures below they are compared with either the vertical velocity itself or the dominant contribution to it (term 1). The abscissa in all figures is the panel number along the longitudinal strip of free surface panels along the hull and the centreline; panel lengths are uniform. The bow is at the left, the stern at the right in all figures.

We first consider the *linear* terms (Figs 4.8, 4.9). In Dawson's free surface condition in general only term 1 is significant. Term 2 only gives a modest contribution at bow and stern, but, as
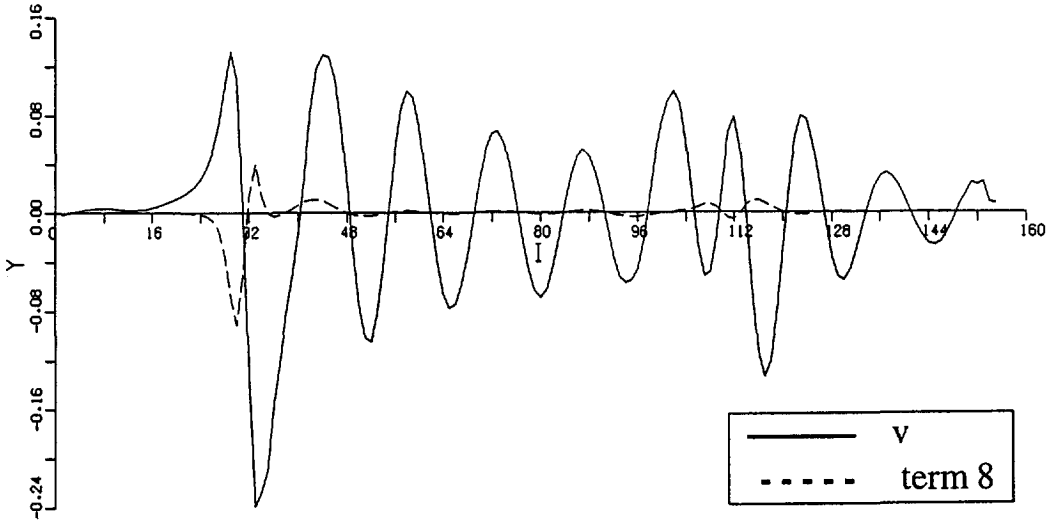
Figure 4.9: *Relative importance of linear terms in Dawson's free surface condition; tanker at Fn = 0.18*

anticipated, due to the considerable phase shift between η and η_r this contribution often is of the wrong sign. The linear transfer term 8, which is neglected in Dawson's condition but included in that of Eggers, is generally of substantial magnitude and is mostly concentrated at the bow. For the Series 60 hull at Fn=0.35 its maximum contribution is about 20% , but for the tanker model at *Fn* = 0.18 at the bow it even amounts to 70% of the local vertical velocity (Fig. 4.9)!

For the Series 60 at *Fn* = 0.22 the sum of the *leading-order neglected terms* (a measure of the error in the linearised free-surface condition) was found to be fairly small for all methods, confirming that both Kelvin and slow-ship linearisation are adequate. For higher speeds the higher order terms were contaminated by point-to-point oscillations, most likely connected with the fundamental instability of the constant-source discretisation mentioned on page 21, and such cases will be addressed later.

For the tanker the Neumann-Kelvin solution has a large error at the bow (Fig. 4.10), and Kelvin linearisation appears to be not applicable here. But the results suggest that for both slow-ship conditions the neglected terms are of moderate magnitude. Because it includes the large term 8, Eggers's condition here seems to be more accurate that that of Dawson. Strangely enough this is not reflected in a better wave resistance estimate, as we have seen before.

In several cases it was found that near the hull the higher-order terms are dominated by the transfer terms, in particular at higher speeds: The effect of imposing the boundary condition at the correct
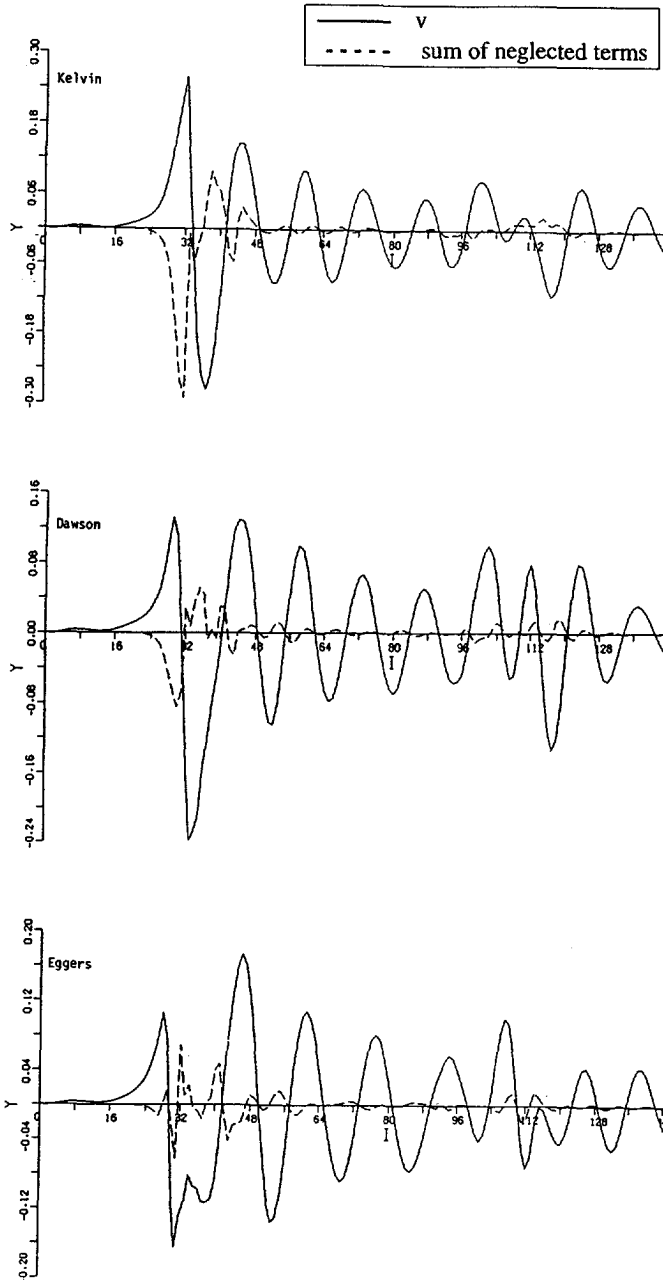
Figure 4.10: *Sum of terms neglected in free surface conditions; terms 3 to 6 for Kelvin and Eggers, terms 3 to 8 for Dawson. Tanker model, Fn = 0.18 .*

location is often more important than to include all squares and cross-products, at least close to the hull.

At least for the more severely nonlinear cases the perturbation expansions do not converge too well, as testified by considerable differences between consistent and inconsistent formulations of some of the higher-order contributions. Another fact learnt from this exercise is the appearance of double and triple wave numbers in the higher-order terms (e.g. Fig. 4.10) as could be anticipated from the theory.

Although this study has been illuminating in certain respects, in retrospect I think it is rather restricted:

- The magnitude of the neglected terms does not precisely indicate how the solution would change if they would be taken into account, so it can only be used in a comparative sense.

- In general Φ_x is singular at the bow stagnation point. Because $\Phi_x\eta_{r_x}$ generally is less singular, the terms included in the free surface condition (and so the solution) seem to be less affected. But higher derivatives of the double-body flow amplify the singular behaviour, and near the stagnation point some of the higher-order terms blow up. Transverse refinement of the free surface panelling in fact amplified the peaks in the higher-order terms somewhat, although it did not yet alter the qualitative behaviour and the comparison between linearisations here.

- The leading-order neglected terms have different expressions for the Kelvin free surface condition and the slow-ship condition, making a comparison based on their magnitude somewhat incomplete.

- The oscillatory character of higher derivatives in the present discretisation sometimes made a comparison of the magnitude of errors unsafe.

It is to be noted that an analysis not suffering from these shortcomings will be carried out in Chapter 10, making use of the nonlinear method now available.

Direct evaluation at the free surface

Some of these drawbacks are removed by directly evaluating the remaining errors in the free surface conditions at the calculated wave surface. In the standard DAWSON code this is impossible: at all points where a positive wave elevation is predicted, the wave surface is at the "wrong" side of the free surface singularities and the velocities cannot be computed. This difficulty could be overcome by using a new *raised-panel* method that had just become available in the course of the development of the nonlinear RAPID code. This imposes the same linearised free surface conditions in the collocation points on the still water surface, but uses source panels at a distance
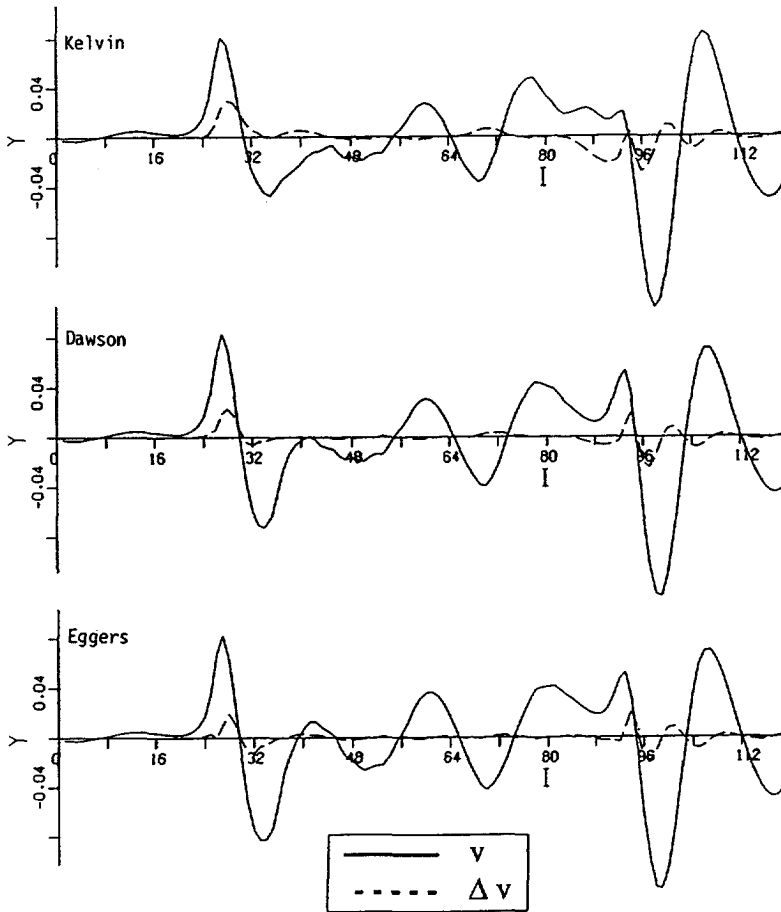
Figure 4.11: *Error in kinematic condition at predicted free surface. Series 60, Fn = 0.22 .*

above that surface. If we solve the linearised problem in this way it is an easy matter to compute the velocities generated by the same source distribution in points on the calculated wave surface.

These often appeared to be significantly different from the velocities on the undisturbed free surface, in particular the vertical component. This stresses the importance of the transfer effect. For the tangential velocities the transfer terms from Taylor expansions often represent these differences fairly well; but the difference in vertical velocity is not well represented by term 8. This again makes a basic assumption made in the linearisation doubtful.

By using the velocities evaluated at the wave surface, we can now compute the errors in the exact kinematic and dynamic free surface boundary conditions: a residual vertical velocity through the
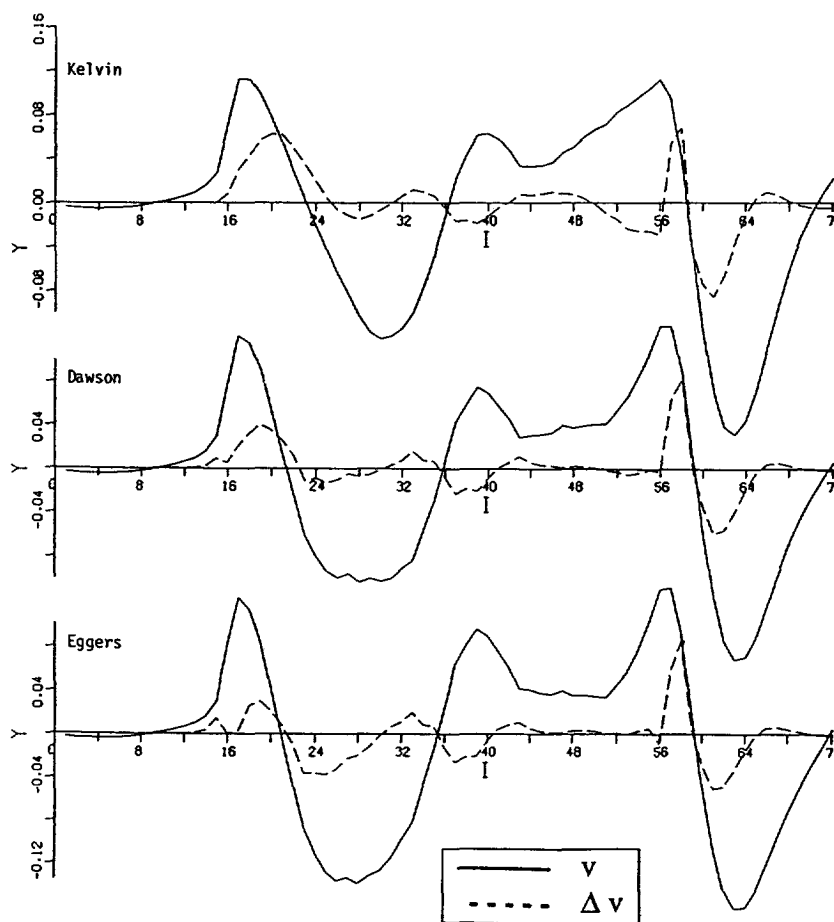
Figure 4.12: *Error in kinematic condition at predicted free surface. Series 60, Fn = 0.35 .*

calculated free surface, and a deviation from the atmospheric pressure. In all cases considered the latter error was small and provided few surprises, being in good agreement with the quantity $\eta^* - \eta_0$ defined in Appendix A, i.e. the higher-order contributions to the wave height. In the following we shall only consider the errors in the kinematic condition. The error distributions so obtained are much smoother and the conclusions drawn are clearer but similar to those from the previous approach.

For the Series 60 model, at low speed all linearisations lead to rather small errors (Fig. 4.11). At $Fn = 0.35$ the advantage of the slow-ship conditions is more pronounced, the error at the bow being 55 % of the vertical velocity for Kelvin and 30 % for Dawson (Fig. 4.12). Eggers's free surface condition is slightly better at both speeds. It is remarkable that all linearised methods

here give such large errors, notwithstanding the generally plausible predictions.

For the tanker the errors in the kinematic condition have a large peak at the bow, followed by relatively insignificant wavy errors with twice the fundamental wave number (Fig. 4.13). With the discretisation applied the height of the peak is $0.15U_\infty$ if Dawson's condition is used, and is even $0.33U_\infty$ for the Kelvin condition; both exceed the vertical velocity itself! Therefore again Dawson's method is found to be better than a Neumann-Kelvin method for full hull forms; although it also contains large errors.

With Eggers's condition on the other hand, the error has large positive and negative spikes slightly ahead of the bow, of $+0.178U_\infty$ and $-0.192U_\infty$. This was found to be caused by a local excessive transfer effect on ϕ_y and, even more, ϕ_x . If Eggers's condition is used, for this case there are extreme differences between the velocities evaluated directly at the free surface, and those on $y = 0$, even if transfer terms are added to the latter (Fig. 4.14). It is confusing that the attempt to incorporate part of the transfer effect, by including term 8, has precisely the opposite effect: The error in

$$\phi_y - \text{term8} \equiv \phi_y + \Phi_{yy}\eta + \varphi'_{yy}\eta_r$$

in the Eggers-solution is larger than the error in ϕ_y (without any transfer correction) in the Dawson-solution.

The explanation of this weird behaviour lies in a property of the free surface condition (4.10) noted before. The coefficient of φ'_{xx} changes sign for $\Phi_x = \sqrt{\frac{1}{3}} = 0.577$, at an otherwise arbitrary point on the free surface ahead of the bow. In the present case this happens quite close to the collocation points where the spikes are found. The ensuing change in character of the free surface condition is bound to cause some sort of singular behaviour. In those points the term containing φ'_{xx} hardly contributes to the free surface condition, and as a result an excessive value of $\varphi'_{xx} = -\varphi'_{yy} - \varphi'_{zz}$ is not controlled. Now

$$(\phi_y)_{y=\eta} - (\phi_y)_{y=0} = -\text{term8} + \eta'\varphi'_{yy} + \frac{1}{2}\eta^2\varphi'_{yyy} + ...$$

$$(\phi_x)_{y=\eta} - (\phi_x)_{y=0} = \eta\varphi'_{xy} + \frac{1}{2}\eta^2\phi_{xyy} + ...$$

showing that if φ'_{yy} blows up, higher-order contributions to the transfer blow up. Exactly the consistent inclusion of leading-order transfer effects increases neglected higher order contributions to the transfer, to the extent of invalidating the free surface condition and making Eggers's condition perform worse than Dawson's. This feature, which was already anticipated by Brandsma and Hermans [25] obviously could only be detected by the direct evaluation at the calculated free surface.

This most likely explains the unrealistic results obtained with Eggers's free surface condition for full hull forms. It supports the objections made in [25] against the change in character of the free surface condition, which follows from Taylor expansions that tend to diverge if the coefficient of φ'_{xx} vanishes. It is unfortunate that this form of the slow-ship condition, which seems to be more
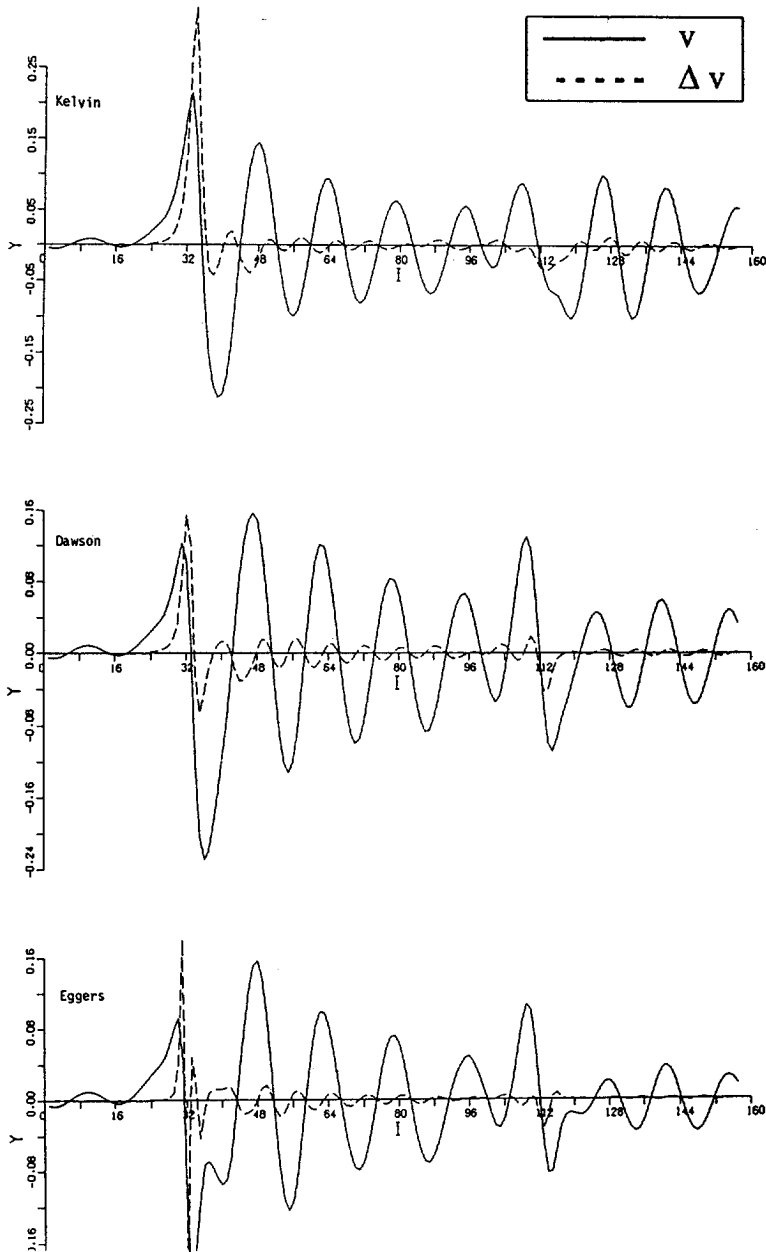
Figure 4.13: *Error in kinematic condition at predicted free surface. Tanker model, Fn = 0.18 .*
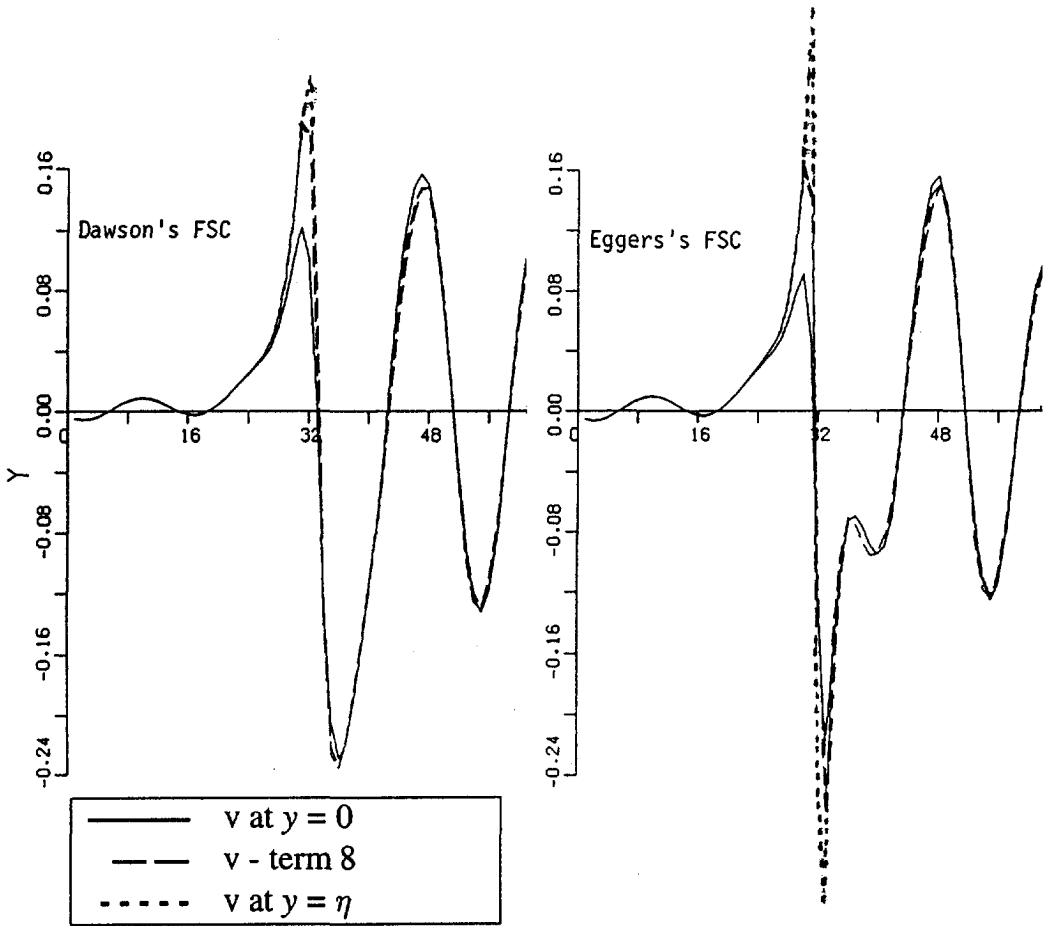
Figure 4.14: *Vertical velocities at undisturbed and actual free surface, near the bow of a tanker,*
Fn = 0.18 . *Left: Dawson; right: Eggers.*

consistent and perhaps slightly more accurate in other cases, fails so badly for full hull forms,
and perhaps for other cases as well if, in the discretisation used, there happens to be a collocation
point close to the location where $\Phi_x^2 = \frac{1}{3}$, $\Phi_z = 0$.

number of hull panels per side	545	1090	1415
zero-Fn pressure integral	.00071	.00042	.00020
wave resist. pressure integration	-.00082	-.00068	-.00067
wave resist. Lagally integr. over FS	-.00054	-.00048	-.00047
wave resist. Lagally integr. over hull	-.00068	-.00054	-.00052

Table 4.1: *Calculated resistance for tanker model, using Dawson's free surface condition; influence of hull panel density. Resistance calculated by integration of the pressure up to the still waterline, corrected for zero-Fn pressure.*

| free surface condition	Kelvin	Dawson	Eggers
wave resist. pressure integration	.00270	-.00068	-.00158
wave resist. Lagally integr. over FS	.00282	-.00048	-.00146
wave resist. Lagally integr. over hull	.00288	-.00054	-.00156
waterline integral	.00062	.00054	.00015

Table 4.2: *Calculated resistance for tanker model; influence of free surface condition; 1090 hull panels. The waterline integrals (4.20) have not been added to the resistances.*

4.5 The paradox of negative wave resistance

4.5.1 General

Although it was thus found that large errors in the free surface conditions occur for full hull forms, the fact that Dawson's method usually predicts a *negative* wave resistance for full hull forms at low speed still is a puzzling result asking for clarification. This fact was well-known but up to 1990 had hardly been given any public attention. It used to be attributed to insufficient resolution of the large pressure gradients on the hull, and poor numerical conditioning of the pressure integration. To check this hypothesis I have repeated the calculations for the same tanker model at $Fn = 0.18$, consecutively using 545, 1090 and 1415 panels on one half of the hull, most of them concentrated in the bow area. Table 4.1 shows the resulting resistance values.

As has been discussed in [13], the accuracy of the pressure integration is appreciably improved by integrating not c_p but $c_p - (c_p)_{Fn=0}$ over the hull, a quantity which is small according to the slow-ship assumptions and which generally has a much smoother distribution than c_p itself. This means that the pressure integral is corrected by simply subtracting the corresponding integral for $Fn = 0$, which theoretically is zero due to d'Alemberts paradox. The values in Table 4.1 are those after this correction.

We see that as a matter of fact the zero-Froude number pressure integral decreases upon panel refinement but is rather large even with the finest panelling. But the wave resistance itself is much less affected. This confirms that the corrected integration is relatively accurate for the two finer panellings here. Similarly, increasing the free surface panel density does not give substantial changes in the predicted wave resistance. Upon panel refinement, *for both slow-ship conditions the wave resistance obviously converges to a negative value.* On the other hand, the Neumann-Kelvin method predicts a very large resistance (Table 4.2).

The wave patterns according to different methods, already shown in Fig. 4.3, look physically plausible and do not indicate the huge differences in resistance between different linearisations. In all cases a realistic system of waves following the ship is predicted. The associated wave energy ought to have been supplied by the ship; but a negative value of the wave resistance means that the hull rather *extracts* energy from the flow and is, therefore, paradoxical.
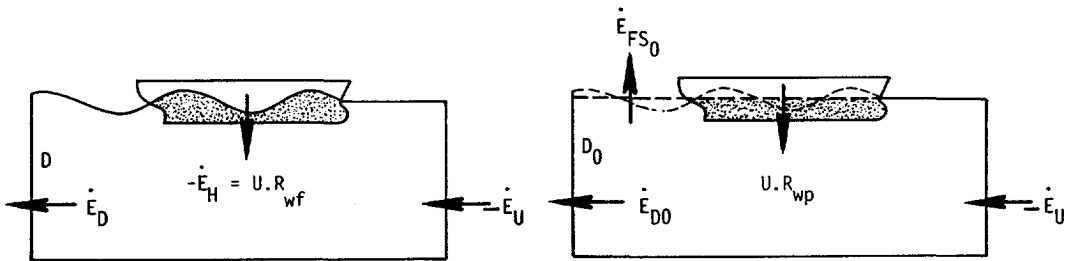
Figure 4.15: *Control volumes for energy balance. Left: exact case; right: linearised case.*

4.5.2   Energy balance

The exact case

To investigate what source of wave energy can be present other than the ship we consider the energy balance for a control volume surrounding the hull and moving with the hull (Fig. 4.15). As derived in [28] the general expression for the energy flux through a surface, in a stationary (earth-fixed) frame of reference, expressed in a general unsteady potential Ψ, is:

$$\dot{E} = -\int\int \{\rho\Psi_t(\Psi_n - V_n) - p.V_n\}dS \qquad (4.13)$$

where V_n is the velocity of the surface itself in the normal direction, and the energy flux is defined positive in the sense consistent with that of the normal. Dimensional quantities are used here. For

a steady flow the unsteady potential Ψ is related to the steady potential in an Eulerian description by $\Psi_t = U_\infty \psi'_x$, where $\nabla \psi'$ is the disturbance of the uniform flow.

The energy fluxes directed out of the control volume now are:
through the wetted part of the hull surface, $\mathcal{H}$:

$$\dot{E}_{\mathcal{H}} = -U_\infty \iint\limits_{\mathcal{H}} p.n_x.dS = -U_\infty.Rw_{pres}$$

(where $\vec{n}$ is the *inward* normal on the hull);
through the upstream plane $\mathcal{U}$:

$$\dot{E}_{\mathcal{U}} = -U_\infty \iint\limits_{\mathcal{U}} \rho gy dS$$

through the downstream plane $\mathcal{D}$:

$$\dot{E}_{\mathcal{D}} = +U_\infty \iint\limits_{\mathcal{D}} \rho gy dS - \frac{1}{2}\rho U_\infty \iint\limits_{\mathcal{D}} (\psi'^2_x - \psi'^2_y - \psi'^2_z)dS$$

where the lateral and upstream boundaries (but not the downstream plane) have been assumed to recede to infinity. *No energy flux is present through the true free surface*, since the pressure is equal to zero and $\Psi_n = V_n$ if the exact free surface conditions are satisfied.

Conservation of energy requires that the sum of all fluxes is zero, which yields:

$$Rw_{pres} = Rw_{far} \equiv \frac{1}{2}\rho \iint\limits_{\mathcal{D}} (-\psi'^2_x + \psi'^2_y + \psi'^2_z)dS + \frac{1}{2}\rho g \int\limits_{l_D} \eta^2 dz \,, \qquad (4.14)$$

in which the second term is a line integral along the intersection l_D of the downstream plane $\mathcal{D}$ with the free surface.

This well-known result has been derived without making any simplification of the boundary conditions and is valid for *the exact potential flow problem*. It shows that the wave resistance may just as well be determined from pressure integration over the hull or from the disturbance at any distance aft of the hull. Consequently Rw_{far} is independent of the position of the aft plane, in agreement with the fact that there is a constant horizontal transport of wave energy. Far downstream a system of free harmonic waves is present, and by substituting the associated potential we find that *the wave resistance is positive definite*.

The linearised case

Since in our linearised calculation the wave pattern far downstream seems realistic, it is natural to assume that the expression for Rw_{far} , applied to that pattern, will again produce a positive result.

Must not then also Rw_{pres} be positive again? The answer is: yes, asymptotically for $Fn \to 0$, provided that a consistent free surface condition has been imposed.

To see this we consider a control volume bounded by the *calculated* wave surface. There now is a non-zero energy flux through that surface, connected with deviations from the exact free surface boundary conditions, i.e. with the sum of the terms neglected in the linearisation as studied in Section 4.4.3. According to equation (4.13) this flux is, in terms of nondimensional quantities:

$$\dot{E}_{\mathcal{FS}} = -\rho g L^3 U_\infty Fn^2 \iint\limits_{\mathcal{FS}} (\psi'_x \Delta v_n - \frac{1}{2}\Delta c_p \eta_x)dS \qquad (4.15)$$

where Δv_n is the remaining normal velocity through the calculated free surface, Δc_p the dimensionless remaining pressure at that surface. The energy balance now reads:

$$Rw_{pres} = Rw_{far} + \dot{E}_{\mathcal{FS}}/U_\infty , \qquad (4.16)$$

where Rw_{far} is as defined in equation (4.14). Consequently *the far-field and pressure integral resistance are now different*, and the latter may loose its positive-definiteness dependent on the distributions of Δv_n and Δc_p over the free surface.

For the case considered the fluxes have been numerically evaluated using the raised-panel method mentioned on page 46. The resulting resistance contributions were found to be quite large, and to bring the predicted Rw_{far} of the three linearised methods much closer together than the Rw_{pres}−values. Although the evaluation was numerically inaccurate, the negative resistances seemed to be mostly removed in this way. The largest total flux was found for Neumann-Kelvin, but the largest local flux occurred again at the singular point ahead of the bow in Eggers's method.

Elimination of the free surface energy flux requires exact satisfaction of the nonlinear free surface conditions. Theoretically, the best that can be achieved in a linearised method is reduction of the resistance difference to a higher order in the perturbation parameter than the resistance itself. For a Kelvin free surface condition the resistance is $\mathcal{O}(\epsilon^2)$, the deviations from the exact free surface conditions are $\mathcal{O}(\epsilon^2)$ and the flux is $\mathcal{O}(\epsilon^3)$. Consequently, the far-field and pressure integral resistance differ by a higher-order quantity and become equal for $\epsilon \to 0$.

In slow-ship theory the resistance is usually assumed to be $\mathcal{O}(Fn^6)$ or even $\mathcal{O}(Fn^8)$. Eggers's free surface condition consistently takes into account all terms up to $\mathcal{O}(Fn^4)$. Therefore Δc_p and Δv_n are $\mathcal{O}(Fn^6)$ and the flux (4.15) is $\mathcal{O}(Fn^8)$: again the far-field and pressure resistance are probably equal to leading order. The omission of all transfer terms in Dawson's condition on the other hand introduces a difference of $\mathcal{O}(Fn^4)$!

The basic assumptions of Baba et al (see Section 4.2), the order reduction by differentiation of φ', force to truncate the free surface condition after the terms of $\mathcal{O}(Fn^2)$, making the integrand in (4.15) of $\mathcal{O}(Fn^4)$ and the energy flux of $\mathcal{O}(Fn^6)$, while according to this theory $Rw = \mathcal{O}(Fn^8)$, and a similar inconsistency occurs.

We thus conclude that for the Kelvin condition and for Eggers's condition asymptotic agreement of

the pressure and far-field resistance may be expected, but not for the other conditions mentioned. One may, however, object that the control volume considered is only appropriate for a linearised calculation using raised panels. In a more familiar implementation source panels are on the still water surface, which partly is inside the control volume just considered. It then is more fundamentally correct to consider a control volume with the $y = 0$ plane, denoted as $\mathcal{F}S_0$ here, as its upper boundary (Fig. 4.15). The part of the hull surface bounding the control volume now is that under the still water line, $\mathcal{H}_0$. The resistance found from pressure integration over that surface, the value commonly used in a linearised calculation, is called Rw_0 here. Also the downstream plane $\mathcal{D}_0$ now only consists of the part $y < 0$. Consequently the first term of $\dot{E}_{\mathcal{D}_0}$ exactly cancels $\dot{E}_\mathcal{U}$ and no line integral is found. An energy flux through the undisturbed free surface is present, according to the general expression (4.13):

$$\dot{E}_{FS_0} = -U_\infty \iint\limits_{FS_0} \rho\psi'_x\psi'_y dS \tag{4.17}$$

Energy conservation now demands that

$$Rw_0 = \frac{1}{2}\rho \iint\limits_{\mathcal{D}_0} (-\psi'^2_x + \psi'^2_y + \psi'^2_z)dS - \iint\limits_{FS_0} \rho\psi'_x\psi'_y dS \tag{4.18}$$

We first inspect this expression for a Neumann-Kelvin method. Substituting the Kelvin condition we find:

$$-\iint\limits_{FS_0} \rho\psi'_x\psi'_y dS = -\iint\limits_{FS_0} \rho(-g\frac{\eta}{U_\infty})U_\infty\eta_x dS = +\rho g \iint \eta\eta_x dS = \frac{1}{2}\rho g \int\limits_{l_D} \eta^2 dz + \frac{1}{2}\rho g \oint\limits_{WL} \eta^2 n_x dl ,$$

$\vec{n}$ being the inward normal on the waterline, and we obtain:

$$Rw_0 = \frac{1}{2}\rho \iint\limits_{\mathcal{D}_0} (-\psi'^2_x + \psi'^2_y + \psi'^2_z)dS + \frac{1}{2}\rho g \int\limits_{l_D} \eta^2 dz + \frac{1}{2}\rho g \oint\limits_{WL} \eta^2 n_x dl \tag{4.19}$$

Comparing this with (4.14) we see that this is almost identical to the expression for the exact case, except that:

- The downstream integral is over $\mathcal{D}_0$ rather than $\mathcal{D}$. But the resulting difference in the integral is of $\mathcal{O}(\epsilon^3)$ and therefore vanishes asymptotically;

- An additional integral along the waterline of the hull is found. Its appearance is not unexpected, since it seems rational to correct Rw_0 for the integration up to the actual waterline, to account for the difference $\mathcal{H} - \mathcal{H}_0$. But we would then obtain

$$Rw_{pres} = Rw_0 + \frac{1}{2}\rho g \oint\limits_{WL} \eta^2 n_x dl \tag{4.20}$$

so the correction would have exactly the opposite sign! This has been called "Gadd's paradoxon" and is dealt with in [29]. In general terms it can be attributed to the inconsistency of imposing the hull condition exactly but at the free surface assuming small perturbations of a uniform flow; for a "thin ship" with $n_x = \mathcal{O}(\epsilon)$ the waterline integral is of $\mathcal{O}(\epsilon^3)$ and vanishes asymptotically.[4]

Apart from this waterline integral, again we conclude that if the Kelvin condition is imposed Rw_0 and Rw_{far} are equal to leading order.

For slow-ship theory a similar consideration is less straightforward. Eggers [23] derives that the only form of the free surface condition resulting in leading-order equality of the far-field and pressure integral resistance is the one proposed by him (equation (4.10); the last term at the left hand side is erroneously lost). This derivation relies on the same basic assumptions on the order of terms and ignores any order reduction by differentiation. Dawson's free surface condition would then result in a leading-order difference of both resistance evaluations. Therefore generally the conclusions are the same as those drawn from the previous momentum balance.

4.5.3 Summary

Consideration of the energy balance for the *exact* potential flow problem has confirmed that the resistance from pressure integration over the hull is equal to that derived from the disturbance far behind the ship and is positive definite. In a *linearised* calculation this identity is lost because the residual errors in the free surface conditions cause an energy flux through the calculated wave surface. However, for a Kelvin condition we have found that this flux is of higher order, and consequently the difference between the far-field resistance and pressure integral is of higher order. The hull pressure integration then also will be positive at least for sufficiently small waves.

For the slow-ship condition used by Baba et al the resistance difference is actually of lower order in Fn than the resistance itself, and none of the properties of the far-field resistance apply to the resistance found from pressure integration over the hull. The same is true for Dawson's free surface condition. Consequently, even if a realistic system of waves is present behind the ship and Rw_{far} therefore is positive, Rw_{pres} will be different and might be negative: Part of the wave energy is not supplied through the hull surface but through the free surface in the near-field, governed by the double-body flow nonuniformity. Since the resulting waves need not have the proper relation with a hull pressure distribution they may happen to propel the ship.

The slow-ship condition derived by Eggers does lead to equality of both resistances save for terms of $\mathcal{O}(Fn^8)$, subject to his assumptions on the order of terms. Nevertheless, the fact that the

---

[4]In slow-ship theory the same waterline integral displays another puzzling inconsistency: For $Fn \to 0$ it approaches $\frac{1}{2}\rho g \oint_{WL} \eta_r^2 n_x dl$ and is of $\mathcal{O}(Fn^4)$ in general; while the wave resistance itself should be of $\mathcal{O}(Fn^6)$! This fact, apparently not noted before, may explain why in practice the waterline integral is found to reduce the accuracy of the resistance estimate at low speeds.

higher-order contributions to the free surface conditions, and similarly to the energy flux, locally may become so important with this particular boundary condition (page 48) appears to cause a large overall energy flux and still to lead to a negative pressure integral resistance.

At least for blunt hull forms at low speed the resistance found from the disturbance far behind the ship may well be realistic while that from pressure integration is not. The latter could then simply be ignored. The most practical way to evaluate (4.14) is by applying one of the formula's used in wave pattern analysis methods, in particular by performing a transverse cut analysis. The transverse cuts should be located far enough from the hull to be outside the region where the double-body flow is significantly nonuniform, because there the free surface energy flux still may contribute; but on the other hand, as argued in [2] it should be far enough from the downstream edge of the free surface domain to avoid any influence of the downstream truncation. Also the spurious decay of the wave pattern caused by numerical damping may obscure the result. Success with this approach, at least for slender vessels, has been obtained by Sclavounos and Nakos [17]. I have never attempted it in DAWSON.

Of course, even if the negative resistance predictions are circumvented in this way, the difference with the near-field resistance and the related inaccuracies in the near-field flow pattern remain a fundamental shortcoming. We conclude that no obvious satisfactory method appears to be there to eliminate the occurrence of negative resistances in slow-ship methods without leaving the concept of linearisation.

4.6 Conclusions

Principal conclusions from these studies are:

- All linearised free surface conditions considered here appear to contain inconsistencies in certain respects. For the Neumann-Kelvin problem there is the basic conflict between the treatment of hull and free surface boundary conditions, and the resulting "Gadd's paradoxon". For slow-ship theory there has been much debate on the proper formulation, in particular on the necessity of supposing order reduction for differentiation of the perturbation potential; and additional inconsistencies arise in the waterline integral and the calculation of the resistance.

- Besides restrictions on the type of flow, there are also restrictions on the hull form for linearised methods. Large curvatures or large section slopes at the waterline in principle invalidate the linearisation.

- The predictions by different linearised methods are quite similar for practical ship forms with a block coefficient up to 0.60 —0.70. On the other hand, for full ships at low speed there are large differences in the predicted resistances, but none of them is useful.

- For slender ships at higher speeds all linearised methods appear to make substantial errors in the exact free surface conditions, even in cases for which plausible predictions are obtained. Slow-ship conditions seem to be marginally more accurate than the Kelvin condition. For full, slow ships very large errors are made in the free surface conditions, Kelvin being distinctly the worst.

- While the resistance found from the disturbance far behind the ship is positive definite, that found from pressure integration over the hull in a linearised method may differ by a higher-order quantity related to an energy flux through the wave surface. For certain slow-ship conditions the difference may even be of leading order. In extreme cases this may lead to a negative resistance found from pressure integration, a phenomenon that cannot be eliminated without leaving the concept of linearisation.

- No promising possibilities for improvement were found within the framework of a linearised approach. Overall Dawson's formulation appears to be a fairly reliable choice for most practical hull forms. The more consistent formulation of Eggers is somewhat more accurate for slender ships but leads to problems for blunt hull forms.

All of the problems mentioned here in principle can be removed by imposing nonlinear boundary conditions on the free surface, and therefore ask for the development of a fully nonlinear method.

Chapter 5

Basic decisions on the formulation of the method

After defining the requirements that a nonlinear method should satisfy, we survey relevant earlier literature and motivate the choices made with regard to the basic solution approach.

5.1 Requirements for the nonlinear method

The studies discussed in the previous chapter have repeatedly indicated that the predictions by currently used linearised methods, while being qualitatively realistic in most cases, contain considerable errors. Moreover, in particular slow-ship conditions are full of inconsistencies and internal contradictions, making it hard to assess their theoretical validity. There are no obvious prospects for improving the linearisations so as to eliminate these drawbacks or the practical shortcomings identified in Section 3.3.

These considerations led to the decision to attempt to develop a solution method for the fully nonlinear steady free-surface potential flow problem. In choosing its basic setup the findings of the last chapter have been quite helpful. In particular:

- Of the higher-order terms neglected in linearised methods, the terms representing the transfer of the boundary condition from the actual to the undisturbed free surface are important and sometimes dominant; in particular if nonlinear effects are large. So to include the principal nonlinear effects *the free surface condition must be imposed on the actual free surface, not*

on any approximation of it. Of course all other nonlinear contributions must be included as well.

- The importance of the transfer effect indicates that it is desirable to include this effect as implicitly as possible in an iterative solution procedure. But *this should not be achieved by the use of Taylor expansions,* since it was found that these sometimes converge rather poorly, in particular in certain critical cases such as near a bluff bow; and because they introduce higher-order derivatives that are better avoided.

- Since several higher-order contributions have a wavenumber two or three times as high as the main wave component, *a nonlinear calculation must have a better numerical accuracy and use a finer discretisation* in order to properly resolve these nonlinear effects.

- In particular it is mandatory that a nonlinear method is insensitive to the point-to-point oscillations found in Dawson's method for high panel densities.

- It was found that, with the discretisation used in DAWSON, higher-order derivatives found from difference schemes are oscillatory due to this same slight numerical instability. Moreover, the consistency of higher derivatives is doubtful if a first-order singularity method is used. Therefore *the nonlinear free surface condition should rather avoid the higher derivatives of the potential responsible for these oscillations, or be based on a superior numerical method.*

- A drawback of linearised methods noticed before is the neglect of the precise intersection of the free surface and the hull, specifically for flat stern shapes or hulls with large curvature near the waterline. *The nonlinear method should accurately take into account the actual shape of the intersection; and the hull boundary condition should be imposed on the actual wetted surface of the hull.*

In addition the following requirements were posed, based on other experiences with the DAWSON code or based on the practice of using wave pattern calculations at MARIN:

- The method should model the flow off an immersed transom stern without meeting the inconsistencies inherent in linearised methods for this application.

- Of primary importance is an accurate prediction of the flow and wave pattern in all respects, as these direct the optimisation of ship hull forms. The accuracy of the resistance prediction is of somewhat later concern, although it is desired that trends and variations are well represented.

- The code must be robust and stable enough for routine application; and the computation cost and turnaround time for a calculation must fit within the tight budget and time schedule of practical ship design projects.

5.2 Literature survey

5.2.1 Steady methods

Prior to the start of the present development around 1990, a number of papers had appeared on, mostly tentative, methods to solve the steady nonlinear wave resistance problem for general 3D cases. All of these were based on an iterative approach. We shall briefly consider the most relevant of these, leaving out of account a few special methods for specific classes of nonlinear problems, such as for 2D submerged bodies, bottom bumps etc.

One of the earliest relevant attempts was made by **Gadd** [10] and published in 1975, even preceding Dawson's paper! He imposed free surface conditions containing first-order transfer terms (from Taylor expansions) at the still water plane, thus inherently assuming small wave elevations; but other nonlinear terms were included completely. Both free surface boundary conditions were combined and solved iteratively to incorporate the nonlinearity. His method was very original for that time, using distributions of Rankine sources over the hull and the still water surface and several numerical tricks to improve stability and accuracy. But the hardware then available forced to use excessively coarse discretisations and the results could not be any better than those of later slow-ship linearised methods. Moreover, the method does not satisfy any of the requirements listed in the last section.

Another tentative method to deal with nonlinear free surface problems was proposed by **Korving and Hermans** in 1977 [30]. They initially only considered the problem of waves excited by a bottom bump in a 2D case, but in a cooperation between Delft University of Technology and MARIN the method was extended to handle 3D surface-piercing bodies [31]. The method consisted of an alternating application of a Laplace problem solver and a free surface correction. In the Laplace problem, Neumann boundary conditions were imposed on the hull, the bottom, and the free surface found in the last iteration. The solution was obtained by a hybrid method based on subdividing the domain by a few horizontal planes; representing the distribution of the potential between those planes by cubic splines; and solving for the spline coefficients by a 2D Finite Element method in the planes. The free surface correction step computed a perturbation of this potential field and free surface shape, the distribution of which was represented by polynomials over elements on the free surface. Linearising in the perturbations, assuming a simple vertical distribution of the perturbation potential and solving for the perturbations by downstream marching appeared to produce a solution with waves only downstream of the object, as desired. The complete cycle converged rather slowly for a Series 60 case, and produced results with a large amount of numerical dispersion. Also here, hardware restrictions led to poor numerical accuracy. But at the same time it is not clear whether a finer discretisation would not in fact have inhibited convergence of the iteration. In a later application to a push-barge train in shallow water [32] (admittedly a very difficult problem!), wave amplitudes tended to double in each iteration. The development has not been pursued after 1982 for lack of prospect.

A nonlinear method based on Dawson's ideas has been published by **Daube and Dulieu** in 1981 [33]. The exact combined free surface condition is cast in a form containing derivatives along free surface streamlines only. This in itself does not involve any approximation, but in the numerical evaluation these streamlines are simply approximated by the streamlines of the double-body flow. Other nonlinear effects seem to be included and upon convergence the free surface condition is imposed on the actual free surface. Although basically inconsistent, in retrospect this method seems a good compromise as it models the most important nonlinear effects. But the results shown in [33] differed very little from Dawson's linearised results. The paper does not specify convergence properties, number of iterations or other numerical details. Somewhat surprisingly, nothing more has been heard of this code, until quite recently it turned up again under the name ODYSSEY.

Maruo and Ogiwara [34] proposed a method theoretically more or less equivalent to that of Gadd, a panel method imposing an incomplete nonlinear free surface boundary condition on the plane $y = 0$. The transfer of the boundary conditions is accomplished by Taylor expansions, so again the most important nonlinearities are improperly represented. The resulting condition is similar to the slow-ship condition, with some additional terms expressed in the results of the previous iteration. Consequently the method, like that of Gadd, still inherently assumes certain perturbation expansions and does not solve the exact problem. Moreover it did not converge at bow and stern unless the nonlinear contributions were artificially reduced.

A somewhat related method was presented by **Musker** [35] in 1988. Also he uses Taylor expansions, to first order in the wave elevation, for transferring the free surface condition towards the still water surface. A quadratic, incomplete form of the free surface condition containing derivatives along double-body streamlines only is imposed. Flat source panels are used at a small distance *above* the still water surface, in order to permit analytical evaluation of velocity derivatives while using constant source-density panels; this feature will be addressed later. The solution is obtained by a Newton iteration process, which is original but costly. In [36] it is mentioned that panel refinement on the free surface inhibited convergence, making it impossible to obtain numerically accurate results. The method seems to have been slightly further developed since, and is being used infrequently [37].

One of the first attempts to impose a *complete* nonlinear free surface condition in a 3D flow was made by **Xia** at Chalmers University, marking the start of a development continuing until recently. In his thesis [38] from 1986 he describes some tests with prototype iterative methods in which the free surface conditions are linearised by assuming small changes relative to the solution of the previous iteration, and imposed at the wave surface found in the previous iteration. Like in Dawson's method the velocity derivatives in the free surface conditions are approximated by an upstream finite difference scheme. In the first attempt Xia used flat constant-strength source panels, which between iterations moved up and down to follow the evolution of the free surface but which stayed horizontal. This does not seem to be a sound approach, as the free panel edges inside the actual fluid domain might cause trouble. Convergence could only be obtained for cases with small nonlinearity.

An alternative method with source panels in a fixed horizontal plane at a distance above the wave surface converged in all cases considered and indicated at least qualitatively correct nonlinear effects, but it was rejected because of an undue dependence of the solution on the distance of the panels above the still water surface. This dependence most likely was caused by the fact that the free surface panels almost touched the wave surface at some points and were rather far off at others, besides other numerical effects, and could have been avoided.

This development was continued by **Ni** [3], who followed a similar iteration process but simply put the free surface panels on the instantaneous wave surface. His free surface conditions contain transfer terms, as these were supposed to improve the convergence (while having no effect at all on the final solution). According to Ni the use of higher-order source panels (in this case parabolic panels carrying a linear source density) is essential to realise a convergent procedure; a remark which probably only applies to the particular numerical modelling used.

The results shown by Ni were generally poor, often even worse than can be obtained with a linearised method. Bow wave heights in most cases were far too small, large numerical damping was visible, and for the HSVA tanker model test case the length of transverse waves was about 20 % too large. Moreover the convergence of the iterative solution was incomplete and appeared to depend in an unpredictable manner on numerical details; e.g. no convergence could be obtained if a four point rather than three point difference scheme was used; dropping the transfer terms prevented convergence unless a double model was used, etc.

The next step in this development was the thesis by **K.J. Kim** [39]. He basically reprogrammed the method of Ni, adding only some details, but showed more favourable results, in particular for a Wigley hull at $Fn = 0.31$. However, the results for a practical RoRo ship with bulbous bow were not significantly better than those of a linearised method. While no cases of divergence are reported, the necessity of improving convergence for more complicated cases is mentioned.

Y.-H. Kim and Lucas [40] several years later came up with a very similar method, finding it necessary to add explicit artificial damping in the free surface boundary condition in order to obtain convergence. But this damping directly affects the final solution, and is, therefore, not acceptable.

An important parallel development, also initiated around 1986, was that at Institut für Schiffbau in Hamburg, Germany, by **Jensen** et al [4, 41, 42, 43]. This is a most original method, based on the use of simple point sources at a distance above the wave surface. The free surface boundary condition imposed in each iteration includes transfer terms. The velocity derivatives are not approximated by a finite-difference scheme but computed analytically; this eliminates most of the numerical damping but reintroduces the problem of imposing the radiation condition. This, however, appears to be adequately satisfied if the free surface sources are shifted back over one source spacing relative to the collocation points. A remarkably small number of free surface collocation points was often used, sometimes just 7 per transverse wave length. This choice seems to be based on inspection of only the predicted wave resistance for some cases, and on some calculations for submerged bodies; but it is clear that such discretisations let most nonlinear

effects (typified by higher wavenumbers) unresolved.

While the method is full of clever ideas, the results initially shown [4] were far from convincing. The hull wave profiles for the Wigley parabolic hull were nothing better than for a linearised method, with in particular some 40 to 50 % underestimation of the bow wave height. Results for the Series 60 hull were somewhat better. For a tanker model no convergence could be achieved, and for other cases also nonconvergence was reported if the collocation points were brought closer to the waterline. Thus this paper largely confirmed that important convergence difficulties were the rule in nonlinear solutions for the steady wave resistance problem, and that no distinct improvement compared to linearised predictions had been obtained yet around 1989.

5.2.2   Transient methods

Besides these developments on iterative solution methods of the steady problem there have been several attempts to solve a corresponding nonlinear *unsteady* problem. Rather than giving a complete review of the extensive literature on such methods we confine ourselves to just a few papers that are related to the present work or in which applications to steady forward-speed cases have been shown. In the latter case an equivalent time-dependent problem is formulated, usually by starting from rest, accelerating the model to the desired speed and continuing the calculation until a steady state has been reached. Time stepping thus replaces iteration.

The unsteady kinematic and dynamic free surface boundary conditions in nondimensional form, shown for reference here, are:

$$\eta_t + \phi_x\eta_x + \phi_z\eta_z - \phi_y = 0 \tag{5.1}$$

$$-Fn^2\phi_t + \frac{1}{2}Fn^2(1 - \phi_x^2 - \phi_y^2 - \phi_z^2) - \eta = 0, \tag{5.2}$$

both to be imposed at $y = \eta(x, z, t)$. Virtually all methods in this class apply a basic solution scheme originally due to Longuet-Higgins and Cokelet [44]. In each time step first the instantaneous velocity field is used to integrate the kinematic condition in time, providing the change of the wave elevation in the current time step; and the dynamic free surface condition is integrated to find the new potential at that free surface. Next, the Laplace equation is solved under the new free surface, with that free surface potential as a Dirichlet boundary condition, to find the velocity field at the new time level. Then the whole cycle restarts for the next step.

This time-stepping scheme is quite natural, leads to simple boundary conditions for the Laplace equation and is well amenable to theoretical analysis. Care is needed in the selection of the time-stepping scheme, to avoid too stringent stability limits for the time step. Also, care must be taken in the specification of the movement of free surface collocation points. Lagrangian points are sometimes chosen (as in the original method of Longuet-Higgins and Cokelet), which simplifies the formulation but is not quite suitable for forward-speed problems; or points that only move up and down with the free surface elevation, or any combination of these options (the so-called Mixed Eulerian-Lagrangian method).

An early development in this class was that by **Coleman, Haussling and Van Eseltine** at DTRC [45, 46]. Its typical feature was the use of a finite-difference approach to solve the Laplace equation. This requires the generation of a full three-dimensional grid in the domain outside the hull. For the nonlinear time-dependent problem this grid must evolve with the solution and must be adapted to the instantaneous free surface at every time step. An elegant solution has been found by mapping the physical domain onto a fixed rectangular computational domain with a Cartesian grid. The backtransformation of the latter defines a curvilinear boundary-fitted grid in the physical domain. The mapping is defined by Poisson equations for 2D cases, and algebraically in 3D applications.

At each time step the free surface conditions are advanced in time. This provides the new free surface shape and potential which serve as boundary conditions for the mapping equations and the transformed Laplace equation, respectively. With implicit time-stepping all these equations form a fully coupled system which at each time step is solved simultaneously in the computational domain using an SOR iteration procedure.

Applications have been shown to semi-infinite ship hulls (afterbodies), to calculate the evolution of the flow past the transom. Good results were obtained in general, and computation times were moderate. It is most surprising that this beautiful and promising development apparently has not been pursued. Using modern numerical algorithms it should be possible to make it substantially more efficient. However, the finite-difference approach has a number of drawbacks which we shall discuss later in this chapter; perhaps these, or difficulties encountered in the extension to the flow about a forebody, have prohibited further development.

Another interesting method has been developed by **Beck, Schultz and Cao** at Michigan University, starting around 1988 [47, 48, 49]. This is a Boundary Integral Method, with as its main feature the use of point sources at a distance above the free surface and inside the body, instead of source panels on the boundaries. The code has been applied to several unsteady problems at zero forward speed, such as added mass and damping calculations, showing its flexibility and reasonable accuracy. Steady forward speed problems present a few other difficulties. One of these is that a Lagrangian movement of the nodes at the free surface, a choice which simplifies the implementation of the free surface conditions, leads to nodes penetrating the hull surface and bunching up near stagnation points. This is overcome by prescribing the node movement such that they pass around the hull.

In [49] a preliminary application to a Wigley hull starting from rest is shown. The results indicate that even for this simple case the ship must have travelled for at least 4 ship lengths before the flow has become reasonably steady, at $Fn = 0.25$. In particular, of all the unsteady wave components excited at start-up, the so-called $\tau = \frac{1}{4}$ component, a wave which group velocity just matches the speed of the ship, causes slowly decaying oscillations in the results that substantially increase the required simulation time. Similar experiences have been mentioned by others [50]. Consequently, several hundreds of time steps must be made, and computation times mentioned are of the order of hours on a CRAY YMP.

In particular with the recent popularity of time-domain methods for seakeeping calculations, many other developments on unsteady nonlinear free surface potential flow problems have been published. Most of them are mainly directed at the calculation of ship motions, often without forward speed. Since these are less connected with the present subject they will not be discussed here.

5.2.3   Summary

From this literature review the following picture of the state of the art around 1989 — 1990 emerges. All iterative methods for the steady nonlinear problem had important convergence difficulties in all but the simplest cases; convergence obviously is the central issue in setting up such a method. It is noteworthy that the convergence often has been found to depend on small details of the numerical method and discretisation and on the precise formulation of the free surface condition.

The results published generally were not in significantly better agreement with experimental data than those of accurately solved linearised methods, perhaps due to insufficient resolution; but finer discretisations frequently caused divergence. Obviously, the nonlinear methods available at that time indeed eliminated linearisation errors but introduced errors of comparable magnitude in the discretisation and numerics.

The existing transient solution methods on the other hand seemed quite promising, and remaining problems perhaps were more tangible because of the close relation with a physical evolution process. But progress in these methods was slow, and applications to steady cases could be expected to remain quite costly.

Therefore, at the start of the present development of a nonlinear method to solve the wave resistance problem, the few relevant earlier publications did not really stimulate such a venture. Since that time, however, for some methods the numerical difficulties have largely been overcome: Both for the method of Jensen, Söding and Bertram (the present code SHALLO) and for the code developed by Ni, Kim and Larsson (SHIPFLOW) several improvements have been made since, and these days both are being used in practice.

5.3   Steady iterative or time-dependent?

The first decision to be taken is, whether a steady iterative or a time-dependent solution method is to be developed. A potential advantage of the latter is its applicability to truly unsteady free surface problems: the calculation of ship motions in a seaway, with or without forward speed; (inviscid) mooring forces on a ship or construction in waves and current, and added resistance of a ship in waves. All of these are essentially determined by a nonlinear free surface potential flow problem

subject to unsteady boundary conditions similar to (5.1), (5.2).

Linearisations valid for small wave and ship motion amplitudes permit to uncouple diffraction and radiation problems and to decompose the radiation problem into motions in the six degrees of freedom. The resulting uncoupled problems can then be solved in the frequency domain, e.g. using Greens functions that inherently satisfy a linearised free surface condition. But if a greater accuracy and applicability is desired, also for these unsteady problems the step towards a fully or partly nonlinear method is to be made, and the complete problem of the coupled motions of a ship with or without forward speed in incoming waves must be solved in the time domain. A method of the class reviewed in Section 5.2.2 above is then required; and as we have seen this could also be used to compute the steady wave pattern of a ship.

The question thus posed itself whether a unified method able to solve both steady and unsteady problems would not be a better objective of our development. But a tradeoff is to be made between efficiency and generality. Separate methods for different classes of problems usually will be more efficient. Since at the time of taking this decision, in 1989, the practical demand for a fully nonlinear treatment of diffraction and radiation problems was not yet obvious, and because the development of an *efficient* nonlinear method for the steady problem without further compromises already seemed hard enough, the decision was taken to focus on the latter problem.

Therefore the choice between an iterative or a time-dependent solution procedure has been based on the expected chance of success and efficiency for *steady* applications. From this point of view,

Advantages of the time-dependent approach are:

- The natural formulation of the time-stepping procedure, and its relation with a physical evolution process. The success of this scheme, at least in applications without forward speed, has often been demonstrated. However, straightforward application for substantial forward speed may encounter difficulties [51].

- The resulting free surface boundary condition for the Laplace problem is of Dirichlet type, and its properties are well known. If a Boundary Integral Method is used, by a proper choice of the singularity type and integral equation the problem can simply be cast in the form of a Fredholm equation of the second kind, and relatively simple iterative methods for solving the resulting set of equations may be successful.

- In cases for which no steady potential flow solution exists, e.g. if wave breaking is essential, a time-dependent solution method most likely will indicate so.

Disadvantages of the time-dependent approach are:

- The large number of time steps required before a steady solution is reached: published numbers range from 200 to 1200. Of course this depends on the initial conditions prescribed;

probably the usual way of starting from rest and accelerating the model to its final speed is inefficient if only the steady solution is of interest. Also, when time accuracy is sacrificed a speedup may be possible, if the stability of the time integration permits. Anyway the calculation time needed is expected to be a disadvantage.

- Connected to this, the difficulty with the $\tau = \frac{1}{4}$ component, mentioned above. The wave energy in this component stays near the hull and produces oscillating contributions to the forces, decaying as $1/t$ [49] and considerably delaying the approach to steady state.

- The necessity of specifying open-boundary conditions. In the unsteady problem, at start up waves with all lengths and velocities can be generated, including those moving faster than the ship itself. Such waves must be allowed to leave the domain through the outer boundaries without too much reflection, since otherwise they will spoil the solution and delay the convergence to a steady state. But, in particular for 3D nonlinear problems, no satisfactory non-reflective boundary conditions for are known.

- In some cases wave breaking may physically just be a transient phenomenon occurring for a certain start-up history. As wave breaking is likely to terminate the calculation it would prohibit to reach a steady state. This might require substantial experimentation with start-up procedures.

As opposed to this, the **advantages of steady iterative methods are**:

- The number of iterations does not depend (obviously) on any physical evolution process, and may be much smaller than the number of time steps in a transient approach — provided that an effective formulation of the iterative procedure can be found.

- If the dimensions of the computational domain are properly selected, far-field conditions are immaterial, except those at the upstream boundary. In the steady approach all waves satisfy the steady dispersion relation and are thus contained inside an approximate "Kelvin wedge". Reflections only occur at the lateral and downstream boundaries of the calculation domain and need not have a significant effect on the flow near the ship hull.

Disadvantages of steady iterative methods are:

- The convergence is troublesome according to most previous publications. But there is much freedom in the formulation of the iterative procedure, so better methods might be found.

- For most formulations of the free surface boundary conditions the resulting system of equations does not lend itself quite well to a simple iterative solution.

- As opposed to time-dependent methods, a radiation condition must now be imposed, which prevents the occurrence of steady waves ahead of the ship. However, the experience on ways to enforce the radiation condition in numerical methods for the linearised problem will hopefully be applicable.

Based on these considerations I anticipated that nonlinear time-dependent methods would not become suitable for routine application in a near future; an expectation that now, 6 years later, has largely been confirmed. Therefore I decided to try *to set up an iterative method for solving the steady wave resistance problem.*

5.4   The free-surface condition

With this choice our method will consist of solving a series of Laplace problems alternated with an update of the boundary conditions and boundary locations. The convergence of the iterative process, of such crucial importance for the success of a steady method, strongly depends on the formulation of the free surface conditions imposed in each iteration and of the free surface updates. Two free surface conditions are available, the kinematic and the dynamic condition, equations (2.6) and (2.7). Both contain the velocities and wave elevations at the free surface as unknowns. Only one condition can be imposed upon the solution of the Laplace equation in each iteration; another condition must then be used to establish the relation between successive iterations, i.e. the boundary updates. Three options can now be distinguished.

The first option would be to impose the *kinematic* boundary condition upon the solution of the Laplace equation: the potential is then calculated in a domain bounded by the current guess of the free surface shape, and on that free surface the normal velocity is set to zero, a Neumann condition that is easily implemented. The velocities thus found are substituted into the dynamic condition which provides an explicit expression for a new free surface elevation, and a new iteration can be started. Although this may seem a fairly obvious formulation of the iterative process, it is well known that straightforward application will produce a solution without a trailing wave pattern. The only way to get the desired solution is, not to use simply the dynamic condition but to apply special, somewhat far-fetched prescriptions to deduce a new free surface from the calculated potential, e.g. [52, 31]. For 3D cases this is a difficult technique and no successes have been shown.

The second possibility is just the other way round: impose the *dynamic* condition upon the solution of the Laplace equation in each iteration, and use the kinematic condition to update the free surface. In principle this is possible by rewriting the dynamic condition as an expression for ϕ_x and integrating it over x to find a new value of the potential at the free surface. This is subsequently imposed as a Dirichlet boundary condition for the Laplace equation. The resulting velocity field is substituted in the kinematic condition and integrated over x to find a new free surface shape. This procedure effectively is a steady analogy of the Longuet-Higgins & Cokelet scheme. An example of a method attempting this approach, applied to a 3D surface pressure distribution, is [53]. One may suppose this rather cumbersome procedure to suffer from error accumulation in the integrations over x.

In both approaches the two free surface conditions are uncoupled. But the kinematic and dynamic condition *together* determine the wavelike behaviour, so the correct physical behaviour must

be obtained by iteratively incorporating the interplay between them; a hard job for an iteration process. The third and final possibility eliminates this weak point by imposing a *combination* of both free surface conditions in the solution of the Laplace equation, and to use one of the conditions to update the free surface. Substituting the expression for η from the dynamic condition into the kinematic condition we obtain an expression in the gradient of the potential only. This condition is basically Kelvin-like, and even more resembles slow-ship free surface conditions; so it already includes the wavelike behaviour and much of the physics. Therefore, the iterative procedure based on such a combined condition is more "implicit" than the two previous possibilities and most likely will have better convergence properties. A possible drawback is the form of the combined free surface condition, which in a Boundary Integral Method leads to a set of equations less amenable to iterative solution. This formulation seemed most promising and has been selected. The precise derivation will be shown in Chapter 7.

5.5   The Laplace solver

The next important decision to be taken is on the method to solve the Laplace equation for the velocity potential. The most common choice is a Boundary Integral or Panel Method, but Finite-Difference, Finite-Element or Finite-Volume methods may also be used. Such field methods may have the advantage that they are more easily extended to the solution of viscous flow equations, and perhaps to any (future) treatment of wave breaking. However, disadvantages are:

- For each iteration a three-dimensional grid must be generated (or adapted) fully automatically, conforming to the hull and the instantaneous shape of the free surface. This may be a time-consuming and error-prone step.

- The topology of this grid is not always clear, in particular near the hull/free surface intersection: at most locations this is a more or less perpendicular intersection, and mapping of the hull and the free surface to different coordinate planes is an obvious choice; but e.g. at a transom stern there is a tangential connection between both planes, and large local grid skewness is unavoidable. Something similar goes for the hull/centreplane intersection, notably at the bow.

- The treatment of outer boundaries is much less straightforward than in Boundary Integral Methods.

- Most likely the computational effort will be substantially larger.

An often mentioned drawback of field methods is the large number of unknowns and the resulting memory requirements. But this is not necessarily correct. Suppose that for a three-dimensional case the number of cells or panels in each direction is $\mathcal{O}(N)$. For a Boundary Integral Method the number of panels then is $\mathcal{O}(N^2)$. The matrix is full, so the number of matrix elements to be computed and stored is $\mathcal{O}(N^4)$. Solution of the system by Gauss elimination will require $\mathcal{O}(N^6)$

operations, a usual iterative method $\mathcal{O}(N^4)$. But special solvers exist [54] that should be able to solve the problem in $\mathcal{O}(N^2)$ operations.

For a Finite-Volume Method for the same case, the number of unknowns is $\mathcal{O}(N^3)$. The matrix is banded, and the number of nonzero elements to be computed and stored is $\mathcal{O}(N^3)$, which at least asymptotically is *less* than for the Boundary Integral Method! The number of operations required to solve the system of equations by a standard iterative procedure would be $\mathcal{O}(N^6)$, but using optimal multigrid techniques could be reduced to $\mathcal{O}(N^3)$.

What this argument demonstrates is that the preference for Boundary Integral Methods is not as obvious as commonly assumed. But of course the two classes of techniques are not as easily comparable as this, since they have a different relation between the discretisation density and the (order of) accuracy. It may well be that a field method in practice requires a finer discretisation than a Boundary Integral Method to achieve equal accuracy. Current evidence (e.g. [55]) indicates that the actual computational effort for solving a practical problem is one or two orders of magnitude larger for the field methods. The disadvantages of field methods listed above, and the fact that components of a Panel Method were already available, made me decide to select a Boundary Integral or Panel method as the basis of our method.

5.6   The integral equation

There are many ways of casting the boundary value problem for the Laplace equation into the form of a boundary integral equation. The choice of the particular formulation has consequences for the uniqueness of the singularity distribution for given boundary conditions, for the possibility of applying an iterative matrix solver to the resulting set of algebraic equations, and for the accuracy of the discretised solution.

The basis of Boundary Integral Methods is the expression obtained by applying Green's second identity to the potential in the fluid domain and a Green's function. For the latter we choose

$$G(\vec{\xi}; \vec{x}) \equiv -\frac{1}{|\vec{x} - \vec{\xi}|} .$$

We then find

$$4\pi T\phi(\vec{x}) = \int\int [\frac{\partial\phi}{\partial n_\xi}(\vec{\xi}).G(\vec{\xi}; \vec{x}) - \phi(\vec{\xi}).\frac{\partial G}{\partial n_\xi}(\vec{\xi}; \vec{x})]dS_\xi \qquad (5.3)$$

and a corresponding equation for $\nabla\phi$. The integral is to be taken in a principal value sense, and is over a closed boundary consisting of the wetted part of the ship hull, the free surface and a boundary at infinity. The contribution of the latter vanishes if ϕ is the potential of a perturbation of the free stream. For points in the interior of the domain $T = 1$, for points on a smooth part of the boundary $T = 1/2$, and outside the domain $T = 0$.
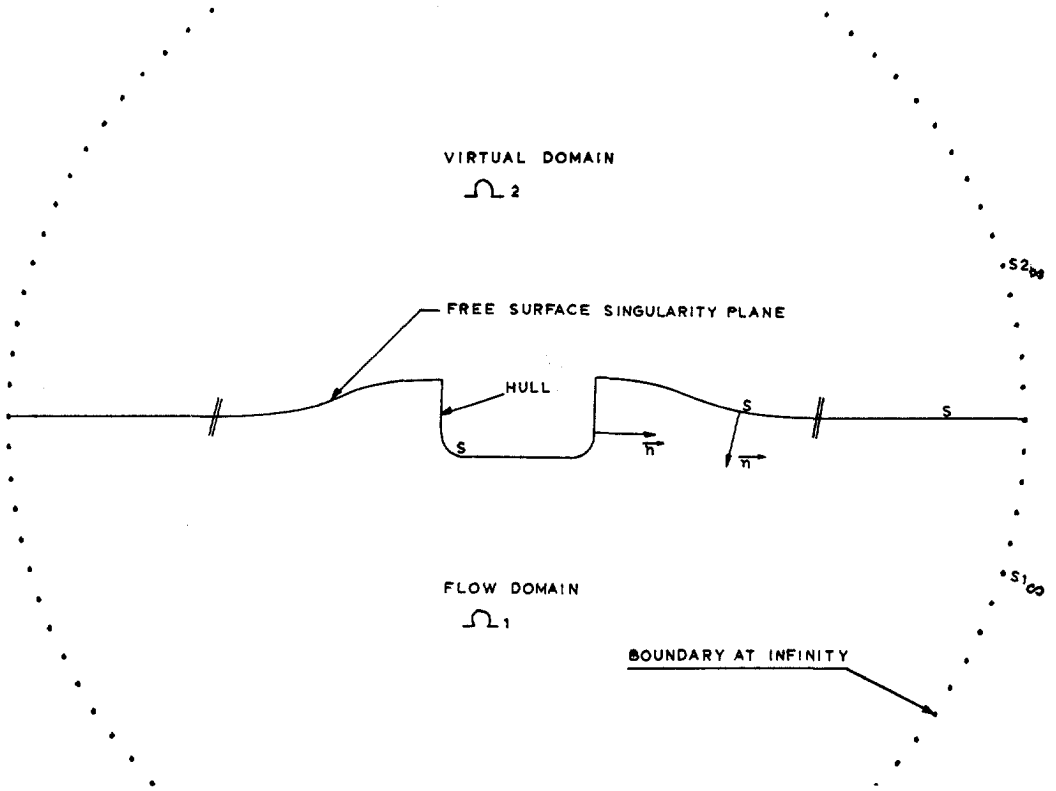
Figure 5.1: *Decomposition of space used in derivation of source method*

The integral equations to be solved are obtained by substituting the boundary conditions, which prescribe either ϕ or ϕ_n or any combination of both. The boundaries are then discretised into panels on which certain modes of the unknowns are assumed. Collocation leads to a set of algebraic equations for the potential or its normal derivative in discrete points at the boundaries. The contributions of all panels to ϕ and ϕ_n in all collocation points must be determined; if there are N panels, the number of influence coefficients to be computed is $2N^2$. Once the equations have been solved we need the velocity distribution on the boundaries. This can be obtained by numerically differentiating the potential, but this is not a very accurate process; in particular for the hull surface, where the topology of the panelling is relatively free and differencing over segment boundaries is cumbersome. The alternative is to compute a further $3N^2$ influence coefficients to evaluate the induced velocities directly.

One of the alternatives for this "Green's identity form" is a source-only formulation. We suppose a virtual domain Ω_2 above the free surface (or any other surface where singularities will be located, as will appear later) and inside the hull, as sketched in Fig. 5.1. In this domain a potential field

ϕ_2 is assumed. Applying Greens theorem to the true and the virtual domain yields:

$$4\pi T\phi_1 = \int\int_S [\phi_{1_n}.G - \phi_1.G_n]dS + \int\int_{S_{1\infty}} [\phi_{1_n}.G - \phi_1.G_n]dS \tag{5.4}$$

$$4\pi(1 - T)\phi_2 = \int\int_S [-\phi_{2_n}.G + \phi_2.G_n]dS + \int\int_{S_{2\infty}} [\phi_{2_n}.G - \phi_2.G_n]dS , \tag{5.5}$$

where in the integrand of the first term in the second equation we have changed the sign because $\vec{n}$ is an *outward* normal for Ω_2 as indicated in Fig. 5.1. The T-factor has here been redefined as: $T = 1$ for a point in the interior of Ω_1, $T = 0$ for a point in the interior of Ω_2, $T = 1/2$ for a point on a smooth part of the interface S. Adding both equations the second terms at the right together yield the potential field corresponding with the undisturbed flow, $\phi_\infty(\vec{x})$ (or zero, if ϕ is defined as a perturbation upon that potential), and we obtain:

$$4\pi T\phi_1(\vec{x}) + 4\pi(1 - T)\phi_2(\vec{x}) = 4\pi\phi_\infty(\vec{x}) + \int\int_S [(\phi_{1_n} - \phi_{2_n}).G + (\phi_1 - \phi_2).G_n]dS . \tag{5.6}$$

We now fix the solution in Ω_2 by demanding that the potential is equal on both sides of the surface S, which is a valid boundary condition for ϕ_2. Only a contribution from the jump in normal velocity $\sigma = \phi_{1_n} - \phi_{2_n}$ remains, which is the source strength on S. A similar procedure is followed for the integral equation for the velocity $\nabla\phi$. The final expressions for the potential and the velocity thus become:

$$4\pi\phi_1(\vec{x}) = 4\pi\phi_\infty + \int\int_S \sigma(\vec{\xi})G(\vec{\xi};\vec{x})dS_\xi \tag{5.7}$$

$$4\pi\nabla\phi_1(\vec{x}) = 4\pi\nabla\phi_\infty(\vec{x}) + 4\pi(1 - T)\sigma(\vec{x})\vec{n} + \int\int_S \sigma(\vec{\xi})\nabla_{\vec{x}}G(\vec{\xi};\vec{x})dS_\xi \tag{5.8}$$

Here $T = 1$ for a point in the interior of Ω_1, and $T = \frac{1}{2}$ for points on the boundary S.

In our problem all boundary conditions will be expressed in velocities, and the potential itself plays no role (contrary to most unsteady formulations). Hence equation (5.8) must be used. To compute all velocity components the required number of influence coefficients is now $3N^2$, which is more than for the Greens identity formulation (5.3). But this is more than offset by the advantage that the velocities can be computed directly once the source strengths have been found.

A choice between the Green's identity form and a source-only form (or any alternative) is now to be made. For familiar types of boundary conditions the properties of these methods are well known and discussed at length elsewhere, e.g. [56]. In our problem, a Neumann condition is imposed on the hull. Both the potential equation (5.3) for the Green's identity formulation, and the gradient equation (5.8) in the source-only formulation lead to a Fredholm equation of the second kind; after discretisation the resulting systems of equations are well-conditioned and generally can be

solved iteratively. A known advantage of first order source methods is that for external flows about convex bodies a relatively high accuracy is obtained, but this does not seem really decisive.

The free surface boundary condition however is less suited to the use of a source-only method. Like linearised conditions our free surface condition will have a form

$$\alpha \phi_s + \phi_n = \beta \tag{5.9}$$

containing both normal velocity and tangential velocity contributions. Here the first term includes the contributions from the upstream difference scheme for ϕ_{ss}, so α is a vector. A pure tangential velocity boundary condition would lead to a Fredholm integral equation of the first kind. The normal velocity contribution in our free surface condition is beneficial in a source method and introduces relatively large diagonal entries in the matrix. Even so, at least for relatively dense panellings the tangential velocity terms tend to dominate, and consequently the system of equations is less well conditioned. Moreover, a source-only formulation may suffer from point-to-point oscillations in the solution as found in Dawson's method (see page 21).

Applying a Green's identity formulation to the same free surface condition we would have to express all tangential derivatives, ϕ_s and ϕ_{ss}, in the surface potentials using difference schemes. The result would be a Robin type of boundary condition, which we could use subsequently to eliminate ϕ_n from equation (5.3) to arrive at an integral equation of the second kind for the surface potential. A possible disadvantage of this approach is the more important role of difference schemes.

Summarising, using a Green's identity formulation could have an advantage with regard to the matrix conditioning and the use of iterative solution methods, but would require a larger number of influence coefficients to be computed unless the velocities would be found from numerical differentiation; and it would probably require much experimentation because of the lack of experience with the unusual implementation of the free surface boundary condition. Setting up a source-only method on the other hand will be a much smaller step, and most of the experience gathered with Dawson's method will be applicable. Attention is needed for the susceptibility to wiggles in the solution; but as will appear in the next chapter, this problem will be eliminated along the way.

While for the present application not all the advantages and disadvantages of different forms of the integral equation could already be foreseen, I decided to use the source-only form, and I could thus use the DAWSON code as a useful vehicle for testing and composing the nonlinear code.

Chapter 6

Analysis of raised-singularity methods

This chapter motivates the choice for a "raised-panel" method. Some of the practical advantages of such an approach and a few preliminary experiences with its application are considered. Then a theoretical study is carried out of the numerical dispersion and damping and the stability of the method proposed.

6.1 Why a raised-singularity method?

In a conventional source panel method the boundaries of the flow domain are covered with a source distribution discretised into panels; and a set of collocation points is chosen, usually the panel centroids, where the boundary conditions are imposed.

For our nonlinear problem this procedure has some important drawbacks. In the first place, in each iteration of the solution procedure a new approximation of the free surface shape is computed. The free surface panelling would then have to be adapted to the new free surface, and the hull panelling to the new waterline. From one iteration to another essentially all source panel sizes, positions and attitudes, and all collocation point positions, may change. This requires many geometric manipulations and may have a destabilising effect on the convergence of the iterative process (which, as previous publications indicated, is quite sensitive to numerical details).

Another drawback appeared to be in the implementation of the "transfer effect", the effect on the free surface condition of the difference between the velocities at the new and the previous free surface. In the last chapter we have recommended that this effect be modelled as implicitly

as possible in the iteration scheme, because of its importance.[1] In anticipation of the discussion in the next chapter, our iterative procedure will consist of solving a series of Laplace problems with a linearised free surface condition, alternated with updating the free surface shape. Suppose that at some iteration k we have an approximation of the free surface, $\eta^{(k-1)}$, found in the preceding iteration; and a base flow field $\nabla\Phi^{(k)}(x, \eta^{(k-1)}, z)$ at that surface. We linearise the free surface condition with respect to that base flow, impose it in collocation points at $y = \eta^{(k-1)}$, and compute new velocities $\nabla\phi^{(k)}(x, \eta^{(k-1)}, z)$ in those points. The dynamic condition then provides a new wave elevation $\eta^{(k)}$.

For the next iteration we have to derive a base flow field $\Phi^{(k+1)}(x, \eta^{(k)}, z)$ on this new surface $y = \eta^{(k)}$. But the velocity field that we have just computed is only defined in the domain below the free surface panels, and therefore only extends to $y = \eta^{(k-1)}$. Where $\eta^{(k)} > \eta^{(k-1)}$ the new base flow field cannot be calculated — except by using Taylor expansions which we want to avoid.

One of the two most important previous nonlinear methods, that by Ni [3], in fact does apply such Taylor expansions, both in the calculation of the new base flow field and in the free surface condition imposed. On the other hand, Jensen [4] simply assumes

$$\nabla\Phi^{(k+1)}(x, \eta^{(k)}, z) = \nabla\phi^{(k)}(x, \eta^{(k-1)}, z),$$

so he transfers the velocity field from $y = \eta^{(k-1)}$ towards $y = \eta^{(k)}$ without any correction. But he subsequently *does* include transfer terms from Taylor expansions in the free surface condition; this actually is inconsistent because these terms address precisely the same effect. Although these choices do not influence the converged result, both procedures seem undesirable in view of our previous findings on the importance of transfer and the unreliability of Taylor expansions. An alternative is therefore sought.

Such an alternative presents itself if we realise that it is not necessary that the singularities generating the flow are on the boundaries of the domain. It is allowed to position them *outside* the domain under certain conditions, provided that the collocation points (where the boundary conditions are to be satisfied) remain on the true boundary. For our particular application *we shall put the sources or source panels at some distance above the free surface. The collocation points are put on the instantaneous free surface, approximately under the panel centres.* This is what we shall call a *raised-panel method* in the following. On the other hand, the treatment of the hull is conventional, with panels on the hull surface and collocation points in their centres. The hull panelling is extended to the intersection with the free surface singularity plane. The panel layout is sketched in Fig. 6.1.

This method has several advantages for the solution of the nonlinear wave resistance problem:

- Since basically the distance from the panels to the free surface is arbitrary within certain limits, it is no longer necessary to adapt the source panels to the new free surface in

---

[1] While this actually referred to transfer over a distance η, the same will apply for transfer over $\eta^{(k)} - \eta^{(k-1)}$ in the initial iterations of a nonlinear method.
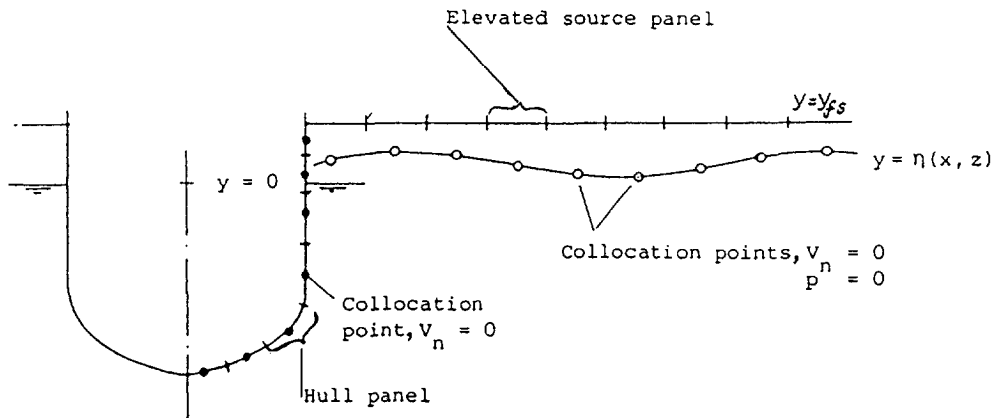
Figure 6.1: *Hull and free surface panel layout for raised-panel method.*

each iteration. In most cases the changes of the wave elevation in an iteration are easily accommodated within the space between the panels and the free surface. The source panels are then kept at a fixed position and we only have to move the free surface collocation points up or down to the new approximation of the free surface. This is much simpler and more stable.

- The velocity field found at a certain stage is defined in the domain under the *source panels* and therefore now extends above the free surface. This eliminates the difficulty with the transfer of the base flow just explained. In iteration (k) we compute the velocities in the collocation points, $\nabla \phi(x, \eta^{(k-1)}, z)$, substitute these into the dynamic condition and find a new free surface, $\eta^{(k)}$. After moving the collocation points to the new free surface, the velocity $\nabla \Phi^{(k+1)} = \nabla \phi^{(k)}(x, \eta^{(k)}, z)$ can be calculated straightaway from equation (5.8). This requires that the influence coefficients of all sources in these new points are computed; but these are needed anyway in the next iteration to set up the new system of equations. Thus, a correct evaluation of the new base flow only requires some additional matrix-vector multiplications. The significance of this recalculation of the base flow will be studied in Section 7.3.2.

- Due to the distance between the panels and the free surface, the velocity field induced in the fluid domain is much smoother than with a usual method.

- Because the free surface panels do not move in each iteration, the influence coefficients of free surface panels in hull collocation points do not change; this saves a small part of the calculation time.

- A possible additional benefit is the "desingularisation", which permits to use more ap-

proximate formulas instead of exact analytical expressions for computing the influence coefficients. This again might save some computing time.

6.2   Previous methods

Some general information on methods with such offset singularities was available in the literature. In most cases these papers concern simpler boundary conditions, of Dirichlet or Neumann type.

In the method of **Webster** [60] for calculating the potential flow around closed bodies in an infinite fluid domain, triangular panels with linear source density are located inside the hull, at a distance of less than half the panel edge length and half the local radius of curvature of the hull surface. The collocation points are chosen on the hull directly opposite to the panel corner points. The method generally is successful, but has difficulty in representing the flow at corners such as a ship bow [4].

Han and Olson [57] propose to choose not only the singularity strengths but also their positions as unknowns. The error in the boundary conditions is minimised with respect to all these unknowns, which even for a linear boundary condition gives rise to a nonlinear optimisation problem requiring iteration. The number of singularities is far smaller than the number of collocation points. In general these authors find that the sources move away from the boundary to large distances in the course of the solution process. This approach may lead to accurate solutions for smooth problems, but will not be quite well suited to less regular problems.

Schultz and Hong [58] propose a formulation for 2D internal potential problems based on Cauchy's law. One of the methods studied uses sources outside the boundary. In general they find a decreasing discretisation error for increasing distance from the boundary. But for boundaries with sharp corners a method with singularities outside the boundary was found to have somewhat larger errors than a standard approach. In [47] it is concluded from a numerical experiment that the distance of the panels to the free surface should be proportional to the panel length to some power less than one in order to obtain convergence for decreasing panel size. However, this is dimensionally incorrect, and seems to result from an improperly defined test problem.

Cao [48] also studies a "desingularised" method based on Green's identity rather than on a source method. In this case the boundary integral equation is (5.3), evaluated at points at a small distance outside the boundary ($T = 0$). The integration is over the boundary of the domain as usual, and the smoothness of the basis functions assumed there directly affects the smoothness of the velocity field in the domain. Consequently this approach does not benefit from the increased smoothness of velocity fields obtained for raised panels or point sources, and to achieve a similar accuracy the basis functions must be of a higher degree, making the method much more expensive than the raised point source approach.

Cao also indicates that the use of raised *source panels*, while being more accurate than point

sources for not too large distances to the boundary, does not admit larger distances because of deteriorating matrix conditioning. Therefore the point source method has been finally selected. It has subsequently been developed to solve 3D unsteady free surface problems by Beck, Schultz and Cao [47, 49] and was discussed already in Section 5.2.2.

There were also a few publications on raised-singularity methods specifically for the ship wave resistance problem. **Xia** [38] has experimented with a method using source panels at a distance above the free surface, but he soon gave up because of a significant (and then unexplained) dependence of the results on that distance (see page 63).

The method by **Jensen et al** [4, 43] discussed in Section 5.2.1 uses point sources in a fixed horizontal plane at a distance of 1 to 3 source spacings above the undisturbed free surface (according to the first publications). This distance is claimed to have only little influence on the results, but no theoretical study on the accuracy and order of this method has been performed.

Musker [35] used source panels at only about 15 % of the panel length above the still water surface, with the purpose to obtain an accurate representation of velocity gradients while using simple constant-strength source panels. In [36] the effect of numerical parameters is judged from their effect on the predicted resistance only. Doubling the panel elevation was found to cause a significant Fn-shift of the resistance curve.

It appears that for Dirichlet or Neumann conditions there was already some information on the use of offset singularities, and fairly detailed studies of the accuracy had been performed. But for the particular application considered here, with a boundary condition of quite different form, little theoretical information was available on the accuracy of the method, the effect of the distance of the singularities above the free surface, and restrictions on that distance.

6.3   Initial test calculations

To test the feasibility of the raised-singularity approach I have initially written a prototype code, in which constant-strength source panels were located in a plane at a fixed distance y_{fs} above the undisturbed free surface. On the undisturbed free surface the linear Kelvin condition was imposed, implemented using an upwind difference scheme like in Dawson's method. This code immediately produced quite acceptable results, fairly close to the results of a standard Neumann-Kelvin code and not too dependent on the panel elevation y_{fs}. However, two important indications were obtained [59].

Position of collocation points
In all but the simplest cases the source distribution severely oscillated. The vertical velocity induced at the free surface (which, contrary to that in a standard source method, is not simply proportional to the local source strength now) was less oscillatory. But the oscillations reduce the accuracy and were expected to give trouble in the convergence of the iterative procedure.

The occurrence of point-to-point oscillations is a known property of Dawson's method and has been discussed on page 21. It may be explained by the fact that constant-amplitude oscillations in the source strength do not induce any longitudinal velocity in the collocation points. Regardless of the difference scheme used the ϕ_{xx}—term in the Kelvin condition then is unaffected by the oscillations, and these will turn up for higher panel Froude numbers. Exactly the same holds for the initial raised-panel method, except that due to the distance between the panels and the collocation points the local contribution to ϕ_y is substantially weaker, and oscillations occur in almost all cases.
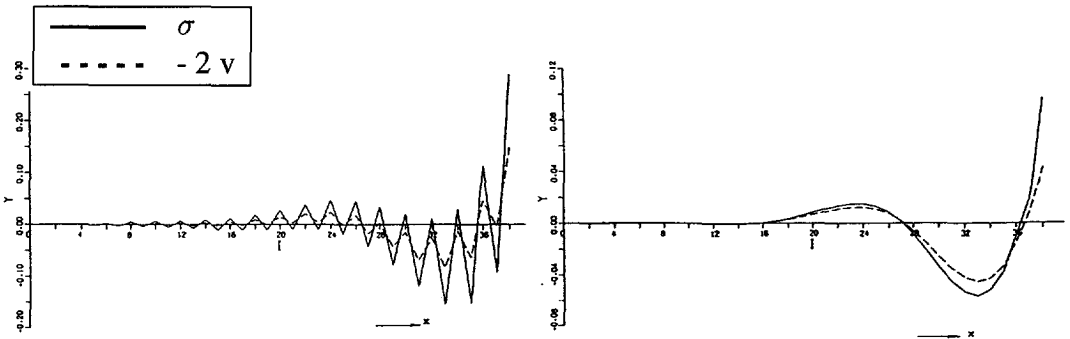
Figure 6.2: *Effect of forward shift of collocation points on the source strength and vertical velocity. Left: no shift. Right: collocation points shifted over half a panel length. (Vertical scales are different.)*

To eliminate these, a very effective trick that I found earlier for DAWSON could be used: we simply shift the collocation points forward by a small amount. This introduces a self-induced longitudinal velocity and suppresses oscillations completely, as Fig. 6.2 demonstrates. Contrary to DAWSON, in a raised-panel method the position of collocation points relative to the panels is relatively free and such a shift need not introduce significant errors; its precise effect will be studied in the next section.[2]

Dispersion differences
The second important finding from these initial calculations was the fact that at a distance from the hull significant phase differences occurred between the predictions of the standard method and those of the raised-panel code. Also the use of raised point sources rather than raised panels produces slight phase differences. Regardless of which results were in better agreement with experiments, these findings asked for clarification and thus gave rise to the study discussed in the next section.

---

[2]In DAWSON the errors introduced are due to the fact that, if the collocation point is on the panel but not in its centre, the self-induced longitudinal velocity is exactly taken into account but the self-induced normal velocity must be set to $-\frac{1}{2}\sigma$. With raised panels all self-induced velocity components are regular and can be exactly taken into account.

6.4   Accuracy Analysis

The accuracy aspect typical for our problem is the representation of surface waves, and we are going to study what errors occur in the prediction of the wave lengths (a numerical dispersion) and the wave amplitudes (due to numerical damping). The main error sources involved are the discretisation of the continuous free surface source distribution, and the difference scheme used for approximating the velocity derivatives occurring in the free surface condition. Besides, the truncation of the free surface distribution and the discretisation of the hull source distribution introduce errors, but these are less specific for the method considered here and will be left out of account.

In the past the free surface errors have already been analysed for the standard approach, most systematically by Sclavounos and Nakos [16]. We shall now apply their methodology (and notation) to the raised source panel method. We impose the linear Kelvin free surface condition, but analogous to Dawson's method we implement the ϕ_{xx} term by a difference scheme applied to ϕ_x, to make it representative of the combined free surface condition that we shall use for the nonlinear method (and that will be derived in Section 7.2). The analysis is restricted to 2D cases for simplicity.

6.4.1   The continuous case — a raised source distribution

For reference we first consider a *continuous* source distribution $\sigma(x)$ with infinite extension, at a constant distance y_{fs} above the undisturbed free surface. The velocity components induced at the still water plane $y = 0$ (perturbations of the uniform inflow) in a 2D case are:

$$\phi_x(x) = \frac{1}{2\pi} \int_{-\infty}^{+\infty} \frac{x - \xi}{(x - \xi)^2 + y_{fs}^2} \sigma(\xi) d\xi \tag{6.1}$$

$$\phi_y(x) = \frac{1}{2\pi} \int_{-\infty}^{+\infty} \frac{-y_{fs}}{(x - \xi)^2 + y_{fs}^2} \sigma(\xi) d\xi . \tag{6.2}$$

These expressions are substituted in the Kelvin condition

$$\phi_{xx} + k_0 \phi_y = RHS.$$

Since they only apply to the velocities induced by the free surface source distribution, all other disturbances (e.g. a submerged body generating waves) are accommodated in a right hand side that is supposed to be known. We thus obtain a boundary integral equation of the form:

$$\mathcal{W}_1 \sigma = RHS \tag{6.3}$$

The properties of the linear operator $\mathcal{W}_1$ are studied in Fourier space. The Fourier series repre-

sentation

$$\sigma(x) = \frac{1}{2\pi} \int\limits_{-\infty}^{+\infty} \tilde{\sigma}(k) e^{ikx} dk \tag{6.4}$$

is substituted into the boundary integral equation. The expressions (6.1, 6.2) are in convolution form,

$$\phi_x(x) = \int_{-\infty}^{\infty} \sigma(\xi) F(x - \xi) d\xi , \quad \phi_y(x) = \int_{-\infty}^{\infty} \sigma(\xi) G(x - \xi) d\xi , \tag{6.5}$$

in which

$$F(x) \equiv \frac{1}{2\pi} \frac{x}{x^2 + y_{fs}^2} , \qquad G(x) \equiv \frac{1}{2\pi} \frac{-y_{fs}}{x^2 + y_{fs}^2} . \tag{6.6}$$

Therefore we can apply the convolution theorem yielding:

$$\tilde{\phi}_x(k) = \tilde{\sigma}(k).\tilde{F}(k) \qquad \tilde{\phi}_y(k) = \tilde{\sigma}(k).\tilde{G}(k) \tag{6.7}$$

The Fourier transforms of the functions F and G are found by complex contour integration over a semicircle (below the abscissa for $k > 0$, above it for $k < 0$), and are:

$$\tilde{F}(k) = \frac{1}{2\pi} \int_{-\infty}^{+\infty} \frac{\xi e^{-ik\xi}}{\xi^2 + y_{fs}^2} d\xi = -\frac{1}{2} i e^{-|k|y_{fs}} .sign(k), \tag{6.8}$$

$$\tilde{G}(k) = \frac{1}{2\pi} \int_{-\infty}^{+\infty} \frac{-y_{fs} e^{-ik\xi}}{\xi^2 + y_{fs}^2} d\xi = -\frac{1}{2} e^{-|k|y_{fs}}. \tag{6.9}$$

The differentiation of ϕ_x introduces a factor $+ik$ in the Fourier transform. Altogether we find:

$$\tilde{\mathcal{W}}_1(k)\tilde{\sigma}(k) = R\tilde{H}S, \tag{6.10}$$

with

$$\tilde{\mathcal{W}}_1(k) = -\frac{1}{2} e^{-|k|y_{fs}}(|k| - k_0). \tag{6.11}$$

It appears that the difference with the operator for a source distribution *on* the still water surface is simply a factor $e^{-|k|y_{fs}}$: due to the distance of the source panels from the free surface they must have a larger strength than if they were on the free surface itself.

It is useful to cast the above results in a slightly different form. Our primary interest is the calculated velocity field, not the source strength. We use the expressions (6.7) to eliminate $\tilde{\sigma}(k)$ and find:

$$\tilde{\phi}_{xx}(k) + k_0\tilde{\phi}_y(k) = [ik\frac{\tilde{F}(k)}{\tilde{G}(k)} + k_0].\tilde{\phi}_y(k) = (k_0 - |k|)\tilde{\phi}_y(k) \equiv \tilde{\mathcal{W}}_v(k)\tilde{\phi}_y(k) \tag{6.12}$$

It follows that the solution for the vertical velocity in the continuous case is:

$$\phi_y(x) = \frac{1}{2\pi} \int_{-\infty}^{+\infty} \frac{R\tilde{H}S(k)}{\tilde{\mathcal{W}}_v} e^{ikx} dk . \tag{6.13}$$

The zero of the Fourier transform of the operator $\tilde{\mathcal{W}}_y$ determines the wavelike behaviour of the solution far downstream; this has the wavenumber $k = k_0$ as expected. The proper behaviour far upstream may be ensured by introduction of a Rayleigh viscosity.

6.4.2   The discrete case — raised source panels

We now consider the *discretised* problem. Constant-strength source panels of uniform size Δx are located in the plane $y = y_{fs} = \alpha \Delta x$. Panel j extends from $x = (j - \frac{1}{2})\Delta x$ to $x = (j + \frac{1}{2})\Delta x$. The collocation points are supposed to be shifted upstream over a distance $\gamma \Delta x$ relative to the panel centres, and are at the positions $(j - \gamma)\Delta x$.

The velocities induced in the collocation points by the source panels now become:

$$
\phi_x(x_m) = \frac{1}{2\pi} \int_{-\infty}^{+\infty} \sigma(\xi) \frac{(m-\gamma)\Delta x - \xi}{((m-\gamma)\Delta x - \xi)^2 + y_{fs}^2} d\xi = -\frac{1}{2\pi} \sum_{j=-\infty}^{+\infty} \sigma_j \int_{\chi=(m-\gamma-j+1/2)\Delta x}^{(m-\gamma-j-1/2)\Delta x} \frac{\chi d\chi}{\chi^2 + y_{fs}^2} =
$$

$$
= -\frac{1}{4\pi} \sum_{j=-\infty}^{+\infty} \sigma_j . ln \frac{(m-\gamma-j-1/2)^2 + \alpha^2}{(m-\gamma-j+1/2)^2 + \alpha^2} \tag{6.14}
$$

$$
\phi_y(x_m) = -\frac{y_{fs}}{2\pi} \int_{-\infty}^{+\infty} \sigma(\xi) \frac{d\xi}{((m-\gamma)\Delta x - \xi)^2 + y_{fs}^2} = \frac{y_{fs}}{2\pi} \sum_{j=-\infty}^{+\infty} \int_{\chi=(m-\gamma-j+1/2)\Delta x}^{(m-\gamma-j-1/2)\Delta x} \frac{d\chi}{\chi^2 + y_{fs}^2} =
$$

$$
= \frac{1}{2\pi} \sum_{j=-\infty}^{+\infty} \sigma_j . [arctan(\frac{m-\gamma-j-1/2}{\alpha}) - arctan(\frac{m-\gamma-j+1/2}{\alpha})] \tag{6.15}
$$

These expressions have the form

$$
\phi_{x_m} = \sum_{j=-\infty}^{+\infty} \sigma_j P(m-j), \qquad \phi_{y_m} = \sum_{j=-\infty}^{+\infty} \sigma_j Q(m-j), \tag{6.16}
$$

which is the discrete analogue of the forms (6.5). Similarly to the continuous case we now introduce the Discrete Fourier Transform, defined as:

$$
\hat{\sigma}(k) = \Delta x \sum_{j=-\infty}^{+\infty} \sigma_j e^{-ikj\Delta x}. \tag{6.17}
$$

Without loss of generality the discretised source distribution can now be written:

$$
\sigma_j = \frac{1}{2\pi} \int_{k=-\frac{\pi}{\Delta x}}^{+\frac{\pi}{\Delta x}} \hat{\sigma}(k) e^{ikj\Delta x} dk . \tag{6.18}
$$

With this definition of Discrete Fourier Transforms, a discrete convolution theorem holds:

$$\text{If}\quad a_m = \sum_{j=-\infty}^{+\infty} b_j.c_{m-j}\,,\quad\text{then}\quad \hat{a}(k) = \frac{1}{\Delta x}\hat{b}(k).\hat{c}(k)\,. \tag{6.19}$$

When we take Discrete Fourier Transforms of the induced velocities it is useful to take into account the fact that the collocation points are not at the same x-positions as the panel centres. We redefine

$$\hat{\phi}_x(k) \equiv \Delta x \sum_{m=-\infty}^{+\infty} e^{-ik(m-\gamma)\Delta x}\phi_{xm} \quad\Longleftrightarrow\quad \phi_{xm} = \frac{1}{2\pi}\int_{k=-\frac{\pi}{\Delta x}}^{+\frac{\pi}{\Delta x}} e^{ik(m-\gamma)\Delta x}\hat{\phi}_x(k)dk \tag{6.20}$$

Now we apply the discrete convolution theorem, modified for this shift factor, and find:

$$\hat{\phi}_x(k) = \frac{e^{ik\gamma\Delta x}}{\Delta x}\hat{P}(k)\hat{\sigma}(k)\,,\quad \hat{\phi}_y(k) = \frac{e^{ik\gamma\Delta x}}{\Delta x}\hat{Q}(k)\hat{\sigma}(k)\,. \tag{6.21}$$

$\hat{P}$ and $\hat{Q}$ are found from expressions (6.14) and (6.15):

$$\hat{P}(k\Delta x,\alpha,\gamma) = -\frac{\Delta x}{4\pi}\sum_{m=-\infty}^{+\infty} e^{-ikm\Delta x}ln\frac{(m-\gamma-1/2)^2+\alpha^2}{(m-\gamma+1/2)^2+\alpha^2} \tag{6.22}$$

$$\hat{Q}(k\Delta x,\alpha,\gamma) = \frac{\Delta x}{2\pi}\sum_{m=-\infty}^{+\infty} e^{-ikm\Delta x}[arctan\frac{m-\gamma-1/2}{\alpha} - arctan\frac{m-\gamma+1/2}{\alpha}]. \tag{6.23}$$

The next step is to introduce a difference scheme for ϕ_{xx}, represented by the general expression

$$\phi_{xxm} = \sum_{l=-\infty}^{+\infty} \phi_{xl}d_{m-l}, \tag{6.24}$$

where the d's are the coefficients of the difference scheme, nonzero only for some nearby collocation points. For instance, for a three-point upwind scheme,

$$\phi_{xxm} = d_0\phi_{xm} + d_1\phi_{xm-1} + d_2\phi_{xm-2}\,. \tag{6.25}$$

This expression again is in a "discrete convolution form". Consequently,

$$\hat{\phi}_{xx}(k) = \frac{\hat{\phi}_x(k).\hat{D}(k)}{\Delta x} = \hat{\phi}_x(k).(d_0 + d_1e^{-ik\Delta x} + d_2e^{-2ik\Delta x}) \tag{6.26}$$

for the same three-point upstream scheme.

We now take the Discrete Fourier Transform of the Kelvin boundary condition:

$$\phi_{xxm} + k_0\phi_{ym} = RHS_m\quad\text{for all }m\quad\Rightarrow\quad \hat{\phi}_{xx}(k) + k_0\hat{\phi}_y(k) = \hat{RHS}(k) \tag{6.27}$$

and collecting all expressions derived above we find:

$$\hat{W}_1(k)\hat{\sigma}(K) = R\hat{H}S(k),   \tag{6.28}$$

with

$$\hat{W}_1(k) = \frac{e^{ik\gamma\Delta x}}{\Delta x}(\frac{\hat{D}}{\Delta x}.\hat{P} + k_0\hat{Q}).   \tag{6.29}$$

To find the operator acting on ϕ_y , in analogy to the treatment of the continuous case we use (6.21) to eliminate $\hat{\sigma}(k)$ and find:

$$\hat{W}_v(k)\hat{\phi}_y(k) = R\hat{H}S(k)   \tag{6.30}$$

where

$$\hat{W}_v(k) = \frac{\hat{D}(k)}{\Delta x}.\frac{\hat{P}(k)}{\hat{Q}(k)} + k_0 .   \tag{6.31}$$

Exactly as is done in [26] we now use the aliasing theorem, which relates the Discrete Fourier Transform of discrete values of a continuous function to the Fourier Transform of the function itself:

$$R\hat{H}S(k) = \sum_{n=-\infty}^{+\infty} R\tilde{H}S(k + \frac{2\pi n}{\Delta x}) .   \tag{6.32}$$

It shows that the Discrete Fourier Transform of the forcing on a certain grid also contains contributions of higher-frequency components of the continuous forcing function. These themselves cannot be resolved but they alias to wavenumbers that are resolved. Inspection shows that the discrete operator is periodic,

$$\hat{W}_v(k) = \hat{W}_v(k + \frac{2\pi n}{\Delta x})   \tag{6.33}$$

Using this property and the aliasing theorem we derive:

$$\phi_{y_m} = \frac{1}{2\pi} \int_{k=-\pi/\Delta x}^{+\pi/\Delta x} \frac{R\hat{H}S(k)}{\hat{W}_v(k)} e^{ikm\Delta x}dk = \frac{1}{2\pi} \int_{-\infty}^{+\infty} \frac{R\tilde{H}S(k)}{\hat{W}_v(k)} e^{ikm\Delta x}dk   \tag{6.34}$$

which can be compared with the corresponding expression for the continuous case, (6.13).

The accuracy of the discretised method now follows from the difference between the Fourier transform of the continuous operator $\tilde{\mathcal{W}}_v(k)$ and the Discrete Fourier Transform of the operator for the discretised method, $\hat{W}_v$. This difference will be cast in the same form as done in [16] and [61] to permit a direct comparison with the results given there. Because of the symmetry properties of all operators we only have to consider positive k-values. Defining the nondimensional wave number

$$s \equiv \frac{k\Delta x}{2\pi}$$

and the panel Froude number

$$Fn_\Delta \equiv \frac{U_\infty}{\sqrt{g\Delta x}}$$
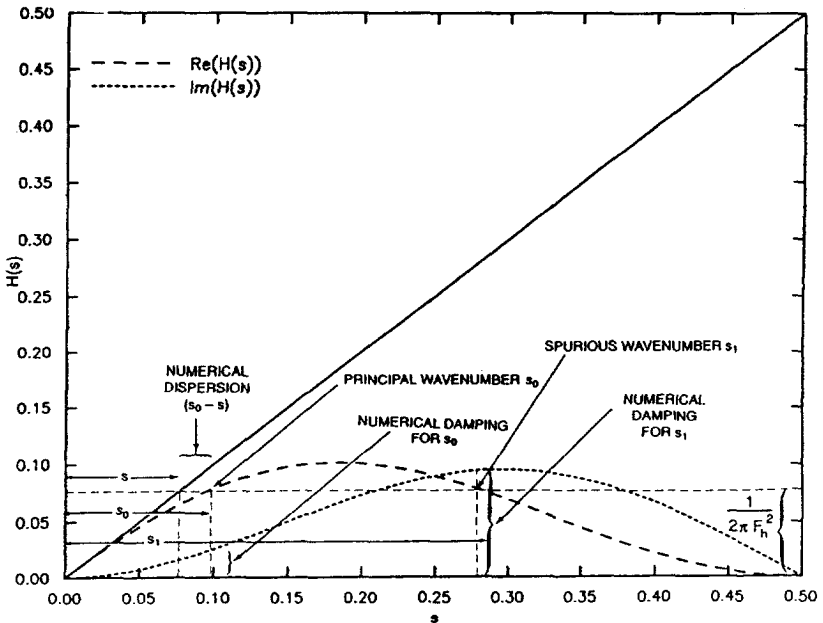
Figure 6.3: *Interpretation of graphs for Lh(s) (here denoted as H(s)).*

we find for the continuous operator:

$$\tilde{W}_v(k) = (k_0 - k) = k_0(1 - 2\pi F n_\Delta{}^2 s) . \tag{6.35}$$

Similarly we write the DFT of the discrete operator as:

$$\hat{W}_v = k_0(1 + \frac{\hat{D}\hat{P}}{k_0\hat{Q}\Delta x}) = k_0(1 - 2\pi F n_\Delta{}^2 Lh(s)) \tag{6.36}$$

where

$$Lh(s) = -\frac{1}{2\pi}\frac{\hat{D}\hat{P}}{\hat{Q}} = -is\frac{\hat{D}}{2\pi i s}\cdot\frac{\hat{P}}{\hat{Q}} \tag{6.37}$$

The operators relating the vertical velocity distribution on the free surface to the forcing now appear to differ by the deviation of the function $Lh(s)$ from s . Since the roots of the operators (6.35) and (6.36) are determined by the expression in brackets, this difference also determines the errors in the calculated wave components far downstream.

Expression (6.37) has been evaluated for a range of the parameters s, α and γ and various difference schemes. The Discrete Fourier Transforms $\hat{P}$ and $\hat{Q}$ involve infinite series that have been summed numerically. For $\hat{P}$ the asymptotic behaviour of the terms for m tending to infinity
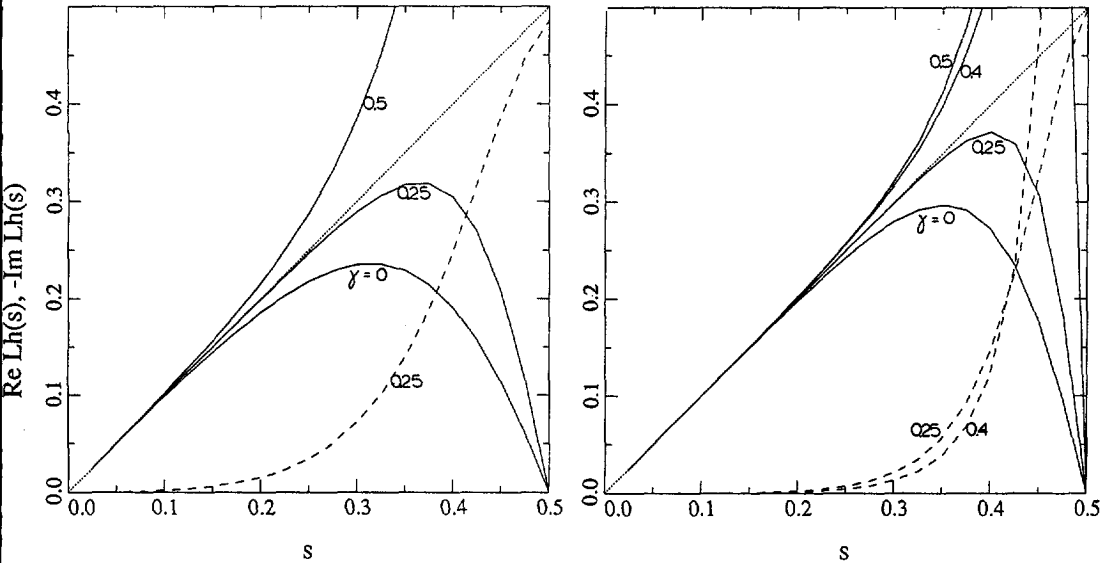
Figure 6.4: *Lh(s) for raised-panel method, for* $\alpha = 0.5$ *(left) and 1.0 (right), varying* γ.

was subtracted first to improve the convergence of the sum. With 20000 terms an accuracy of at least 6 digits was obtained.

The properties of the discretised method can now be inspected by making graphs of the real and imaginary parts of $Lh(s)$. The interpretation of these graphs is schematically illustrated in Fig. 6.3, copied with permission from [61]. $s = 0$ refers to an infinite number of panels per wavelength, while $s = 0.5$ means two panels per wavelength (as is the case for point-to-point oscillations). The principal far-field wave number found by the discretised method is determined by the intersection of $\mathcal{R}e(Lh)$ with a horizontal line with ordinate $1/(2\pi Fn_\Delta^2)$. The numerical damping is proportional to $-\mathcal{I}m(Lh)$ for that wave number. [3] Any secondary intersection away from the line $Lh(s) = s$ indicates a spurious wave number. In the following graphs, the full line indicates the real part $\mathcal{R}e(Lh)$, the dashed line $-\mathcal{I}m(Lh)$, unless indicated otherwise.

6.4.3   Results — Source discretisation effects alone

We first assume that no errors are introduced by the difference scheme, i.e. we set $\hat{D}(k) = ik\Delta x$.[4] Figure 6.4 shows the function $Lh(s)$ for the raised-panel method over the interval of interest, for varying γ (the forward shift of the collocation points relative to the panel centres), for $\alpha = 0.5$ and $\alpha = 1.0$ (the distance of the panels above the water surface, divided by the panel length). Fig. 6.5

---

[3]The minus sign differs from the notation in [16] due to the different definition of the Fourier transform.

[4]It is to be noted that the results below are not simply applicable to a method in which the velocity derivatives are computed analytically, because the kernel of the integral equation then is different.
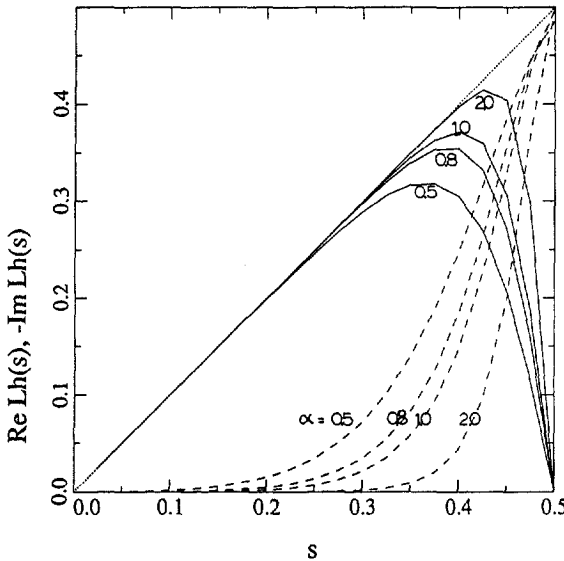
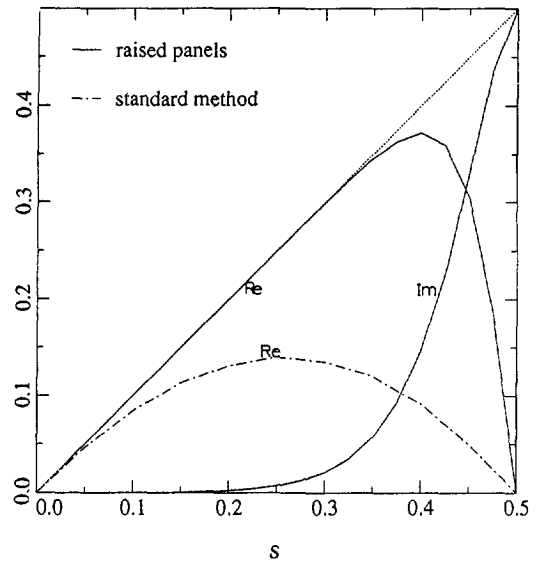Figure 6.5: *Lh(s) for raised-panel method*, $\gamma =$ 0.25 , *varying* α.

Figure 6.6: *Lh(s) for raised-panel method* ($\alpha =$ 1.0, $\gamma = 0.25$) *and conventional method*

shows the behaviour for $\gamma = 0.25$ and varying α. The following conclusions can be drawn:

- In almost all cases the function $\mathcal{R}e(Lh)$ only deviates from its counterpart for the continuous case, $Lh(s) = s$, at higher nondimensional wave numbers (coarse panellings). This indicates that the numerical dispersion is extremely small. For increasing α the function Lh follows the analytical line up to larger wave numbers, and the numerical dispersion is further reduced.

- *Numerical damping is present at higher wavenumbers.* For fixed forward shift $\gamma = 0.25$, increasing α reduces the damping; in particular it shifts the onset of significant damping towards higher wave numbers. For $\alpha > 1$ the function $Lh(s)$ thereby is almost exact up to $s \approx 0.25$ (i.e. only four panels per wave length!).

- Figure 6.4 shows that the forward shift fraction γ has a strong effect on Lh. The numerical dispersion for large s is affected to some extent, the best result being obtained for $\gamma \approx 0.25$ (at least for this value of α) ; the accuracy for $\gamma = 0$, $\alpha = 0.5$ is comparatively poor. In addition there is a very large effect on the numerical damping. For $0 < \gamma < 0.5$ the damping increases strongly towards $s = 0.5$, a favourable property suppressing any numerical oscillations related to a spurious root of the operator.

- Both $\gamma = 0$ and $\gamma = 0.5$ have zero numerical damping (as long as the difference scheme is not taken into account). For $\gamma = 0$ the spurious root at higher wave numbers thus will lead to oscillatory results as found before. For $\gamma = 0.5$ no spurious root is present and

smooth results would be obtained. Therefore, notwithstanding its slightly larger numerical dispersion, the absence of damping could make $\gamma = 0.5$ the best choice. This will, however, be reconsidered below in combination with the difference scheme.

Figure 6.6 compares $Lh(s)$ for our raised-panel method (for $\alpha = 1.0$, $\gamma = 0.25$) and for a conventional method with constant-strength source panels on the still water surface, both without taking into account the effect of a difference scheme. Obviously the standard method gives a large numerical dispersion far exceeding that of the raised-panel method. Table 6.1 compares the resulting wavenumber errors. The raised-panel method is virtually exact for panel elevations exceeding one panel size, having a numerical dispersion of only 0.03 % if 20 panels per wavelength are used.

	$\alpha = 0.5$	$\alpha = 1.0$	$\alpha = 1.5$	$\alpha = 2.0$	Standard	Corrected
$s = 0.05$	0.9937	0.9997	1.0000	1.0000	1.0744	1.0003
$s = 0.10$	0.9819	0.9986	0.9999	1.0000	1.1608	1.0026
$s = 0.15$	0.9611	0.9957	0.9996	1.0000	1.2623	1.0090

Table 6.1: *Wavenumber ratio k/k_0 for raised-panel and standard method; errors due to the difference scheme disregarded.*

In the conventional method considerable errors occur. As mentioned in Chapter 3, Piers [15] devised a correction for this large, first-order numerical dispersion, reducing it to third order for 2D far-field waves. As appears from the table the dispersion correction as a matter of fact makes the standard method almost as accurate as the raised-panel method. However, in 3D flows the dispersion correction factor is only of the right magnitude for transverse waves ($k = k_0$), and does not fully correct dispersion errors in other components. E.g. for components at an angle of 60°, the wave number error is 29 % with dispersion correction, and 38 % without, for $s = 0.05$. The raised-panel method, which does not require any explicit dispersion correction and so does not have such an explicit dependence on the wavenumber, therefore is much more attractive.[5]

6.4.4   Results — The difference scheme

The difference scheme introduces additional errors, which we shall first examine separately. Various schemes have been proposed in the past for this application, e.g. [61]; but most methods use the scheme proposed by Dawson. Fig. 6.7 shows the real and imaginary part of $\hat{D}/ik\Delta x$, the ratio of the DFT of the difference operator to the Fourier transform of the differentiation. The

---

[5]It is noted that for diverging waves some other changes occur as well in both methods. There is a different treatment of transverse and longitudinal derivatives in the free surface condition, wave crests are no longer aligned with panel edges, and panel widths usually differ from panel lengths. A full 3D analysis would be useful but complicated.
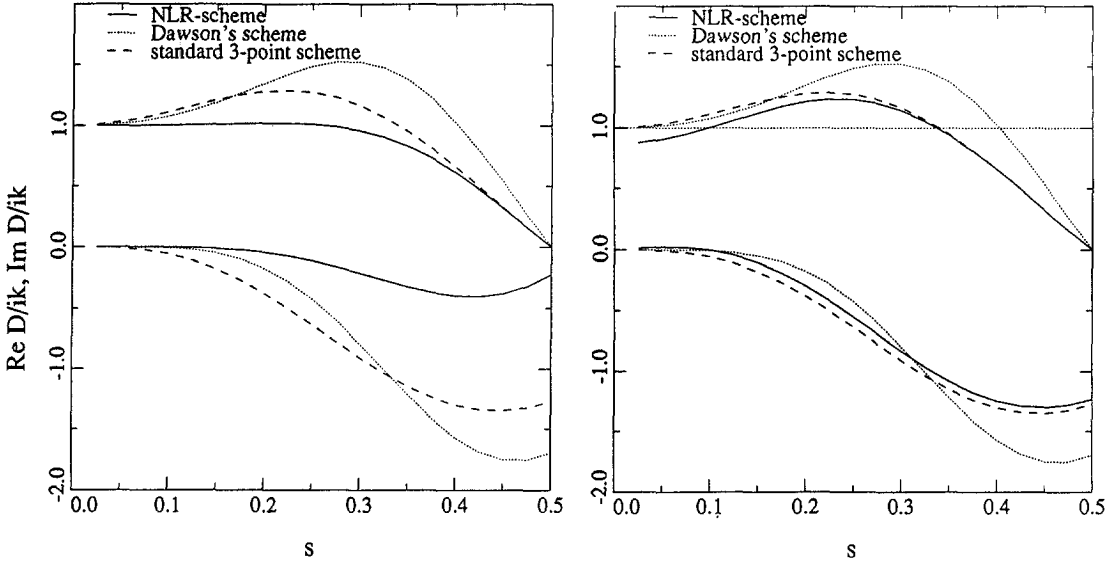
Figure 6.7: *Real and imaginary part of $\hat{D}/(ik\Delta x)$ for various difference schemes. Left: NLR-scheme for $k = k_0$; right: NLR-scheme for 10 panels per transverse wavelength.*

schemes considered here, all for uniform step size Δx , are the standard 3-point upwind scheme,

$$\frac{\partial f}{\partial x} \approx (1.5f_i - 2f_{i-1} + 0.5f_{i-2})/\Delta x; \tag{6.38}$$

Dawson's 4-point upwind scheme,

$$\frac{\partial f}{\partial x} \approx \frac{10f_i - 15f_{i-1} + 6f_{i-2} - f_{i-3}}{6\Delta x}; \tag{6.39}$$

and the particular three-point upwind difference scheme designed by the NLR that is used in DAWSON:

$$\frac{\partial f}{\partial x} \approx -\frac{1}{2Fn_\Delta^4}\frac{(f_i - f_{i-1})}{\Delta x} + (1 + \frac{1}{6Fn_\Delta^4})\frac{(1.5f_i - 2f_{i-1} + 0.5f_{i-2})}{\Delta x} \tag{6.40}$$

This is a combination of a two-point and a three-point scheme, weighted such as to reduce the numerical damping for 2D far-field waves to fourth order. The weighting is determined by $1/Fn_\Delta^4 = k_0^2\Delta x^2$, so the scheme is tuned to represent the principal component $k = k_0$.

The left part of this figure suggests superiority of the NLR-scheme, for which $\hat{D}/ik\Delta x$ is close to unity up to about $s = 0.25$; but this view is too optimistic. In calculating these values, in the expression for the NLR-scheme I replaced $1/Fn_\Delta^4$ by $k^2\Delta x^2$. This is a reasonable approximation in twodimensional cases, when the principal wavenumber dominates. Consequently the left part of Fig. 6.7 indicates the variation of numerical errors in the component $k = k_0$ for *varying panel density*, and shows that for 2D cases the use of the NLR-scheme permits to use larger panels than the other schemes; a property that is due to its built-in "adaptivity" to the principal wave number.

But in threedimensional cases the freedom in the wave direction means that all wavenumbers $k > k_0$ occur, and the approximation made is not permitted. In that case, Fn_Δ is fixed by the selected number of panels per transverse wave length, but the actual wavenumber of the waves to be resolved is unknown and variable. The adaptivity then does not work. The right part of Fig. 6.7 indicates the variation of the errors in the NLR-scheme for *varying wavenumbers*, for 10 panels per transverse wavelength. The behaviour is similar to that of the standard 3-point scheme, but the dispersion error is about zero for the principal component $k = k_0$, i.e. $s = k_0 \Delta x/(2\pi) = 1/(2\pi Fn_\Delta^2) = 0.1$. For 20 or more panels per transverse wave length the NLR-scheme essentially reduces to the standard 3-point upwind scheme.

We conclude that the NLR-scheme does not behave significantly better than the standard 3-point scheme in threedimensional cases with sufficient panel density. Compared to Dawson's scheme the order of the numerical dispersion and damping contributions is lower for fixed Fn_Δ but the values of both errors are smaller for coarse panellings. Therefore the NLR-scheme is useful but could, in particular if dense panellings are used as a rule, equally well be replaced by Dawson's scheme.
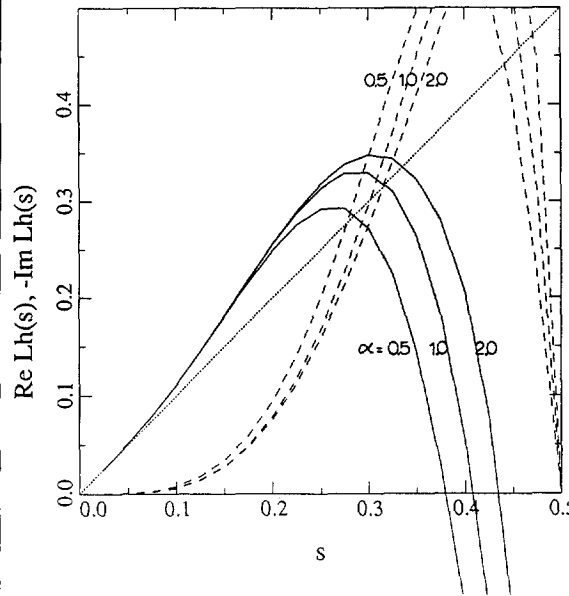
Figure 6.8: *Lh(s) for raised-panel method with standard 3-point scheme;* $\gamma = 0.25$, *varying* α.
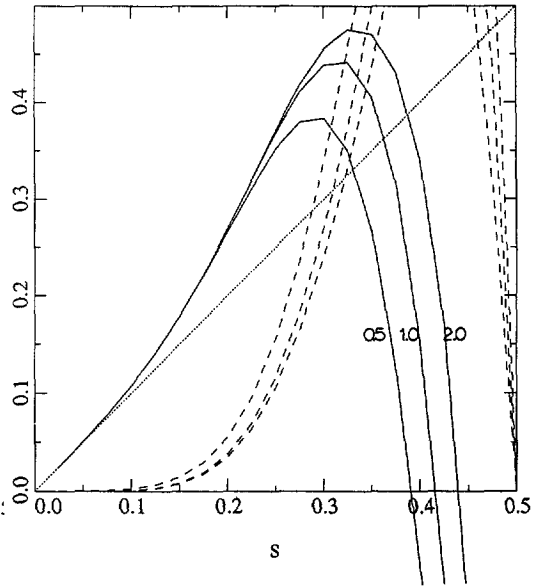
Figure 6.9: *Lh(s) for raised-panel method with Dawson's 4-point scheme;* $\gamma = 0.25$, *varying* α.

6.4.5   Results — Source discretisation and difference scheme

The numerical dispersion and damping for the complete operator is found by combining both contributions. This means that

$$\mathcal{R}e(Lh) = \mathcal{R}e(Lh_{an}).\mathcal{R}e(\frac{\hat{D}}{ik\Delta x}) - \mathcal{I}m(Lh_{an}).\mathcal{I}m(\frac{\hat{D}}{ik\Delta x}) \tag{6.41}$$

$$\mathcal{I}m(Lh) = \mathcal{I}m(Lh_{an}).\mathcal{R}e(\frac{\hat{D}}{ik\Delta x}) + \mathcal{R}e(Lh_{an}).\mathcal{I}m(\frac{\hat{D}}{ik\Delta x}), \tag{6.42}$$

where $Lh_{an}(k) \equiv -is\hat{P}(k)/\hat{Q}(k)$ is the operator found if the errors due to the difference scheme are disregarded (as considered in Section 6.4.3).

Figure 6.8 first represents $Lh(s)$ for the raised-panel method with $\gamma = 0.25$, using the standard three-point upwind scheme for ϕ_{xx}. Comparing this with Fig. 6.5 we see that both the dispersion and the damping are dominated by the errors in the difference scheme for low and moderate s. The difference scheme introduces a quite substantial numerical dispersion, causing a deformation of all lines of $\mathcal{R}eLh(s)$ which is unrelated to α . Its main origin is the deviation of the real part of $\hat{D}/ik\Delta x$ from unity. In addition a significant amount of damping is introduced, again mainly by the differencing. The large deviation from Fig. 6.5 for high s is understood from the fact that $Lh(s)/Lh_{an}(s)$ becomes purely imaginary for $s \to 0.5$; for this difference scheme $\hat{D}/(ik\Delta x) \to -4i/\pi$.

Figure 6.9 gives the corresponding result for the Dawson scheme, which significantly improves upon the 3-point scheme, in particular for the damping.

Figure 6.10 illustrates the effect of the forward shift γ . The difference scheme used here is the NLR-scheme, with a fixed Fn_Δ corresponding to 20 panels per transverse wavelength (which makes it almost identical to the standard 3-point upwind scheme). In general for $\gamma > 0$ there is a strong numerical damping for those high wave numbers that otherwise could lead to instability and are poorly represented anyway. The differencing now adds damping also for $\gamma = 0$, which, however, vanishes at $s = 0.5$. Also the real part vanishes here, and a spurious root exists: for $\Delta x \to 0$ point-to-point oscillations are sure to turn up.

For $\gamma = 0.25$ a spurious root is present at a somewhat lower wave number, but the numerical damping at that wavenumber is quite large so no oscillations are found. For $\gamma = 0.5$ the damping has a somewhat peculiar behaviour, strongly increasing for $s \to 0.5$. Since there is no spurious root here, there is no real need for this. The conclusion from this graph is that $\gamma = 0.25$ or $\gamma = 0.5$ will have largely equivalent properties in practice. However, $\gamma = 0.5$ later turned out to have a drawback for nonlinear calculations. In the course of the calculation the separation between panels and collocation points cannot always be precisely controlled, and it may locally become fairly small. If the points are positioned right under the (singular) panel edges this is more detrimental for accuracy and stability than if they are at a different position. Therefore *the final forward shift selected (and always used since) is 25 % of the local panel length, being more forgiving with respect to the vertical distance and resulting in complete suppression of oscillations.*
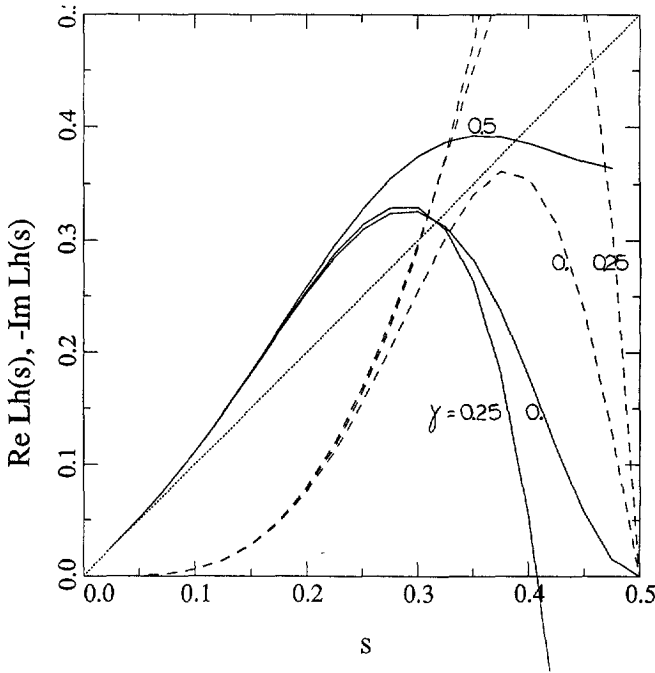
Figure 6.10: *Lh(s) for raised-panel method.* $\alpha = 1.0$, *varying* γ. *NLR-difference scheme with 20 panels per transverse wavelength.*

Fig. 6.11 compares our results for $\alpha = 1.0$, $\gamma = 0.25$ with those of a conventional method with constant-strength source panels on the free surface; both methods using Dawson's scheme. It is important to note that *the relevant part of these plots as far as accuracy is concerned, is the region* $s < 0.1$; for a usual choice of 30 panels per wavelength this covers all components with divergence angles $0 < \theta < 70°$. In this range, numerical damping is as small as with the conventional method, while a large added damping due to the source discretisation is observed above $s = 0.2$ (5 panels per wavelength). The raised-panel method has a significantly reduced numerical dispersion for fine panellings, as is also shown in Table 6.2. In particular, if we disregard the numerical dispersion due to the source discretisation for low s (and Section 6.4.3 indicates that this is justified), we may approximate the numerical dispersion by that caused by the differencing; this is of $\mathcal{O}(s^3)$ if Dawson's scheme is used.

This compares quite favourably with the conventional method, which has a large numerical dispersion of $\mathcal{O}(s)$! This is introduced by the source discretisation, and is only partially cancelled by an opposite, third-order dispersion caused by Dawson's difference scheme (compare Fig. 6.6 and 6.11). But this cancelling will be substantially less for non-transverse waves, since the upwind difference scheme only applies to the x-direction while the source discretisation applies to both directions. This makes the advantage of the raised panel method more pronounced.

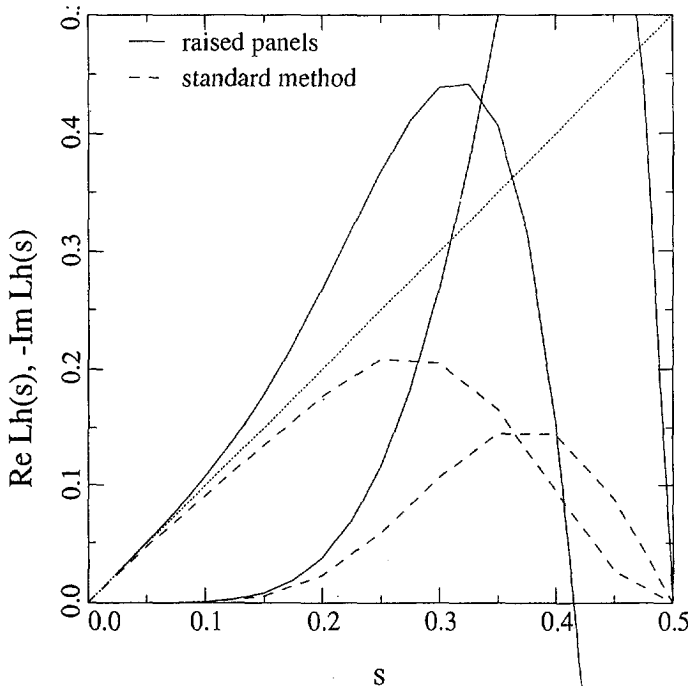The reasonable performance of Dawson's difference scheme in steady ship wave problems is

Figure 6.11: *Lh(s) for raised-panel method (α = 1.0, γ = 0.25), and conventional method; both using Dawson's difference scheme.*

panelling	conventional	raised	raised	raised
diff. scheme	Dawson	Dawson	NLR $20/\lambda_0$	optimised
$s = 0.025$	1.037	0.9959	0.9921	0.9978
$s = 0.05$	1.057	0.9830	0.9692	0.9900
$s = 0.10$	1.095	0.9282	0.8976	0.9443
$s = 0.15$	1.113	0.8394	0.8254	0.8466

Table 6.2: *Wavenumber ratio k/k_0 for conventional Dawson-type method, and for raised-panel method with various difference schemes. α = 1.0, γ = 0.25.*

related to this partial cancelling of the dispersion error introduced by a conventional source discretisation. But for a raised-panel method there is no such dispersion error, so there is little reason to select Dawson's scheme. The difference scheme should rather be optimised separately in order to minimise its errors. Fig. 6.12 shows an example of the results for a modified 4-point scheme designed to minimise the damping at low s while having acceptable numerical dispersion. Further improvement has obviously been obtained; the damping is virtually zero for
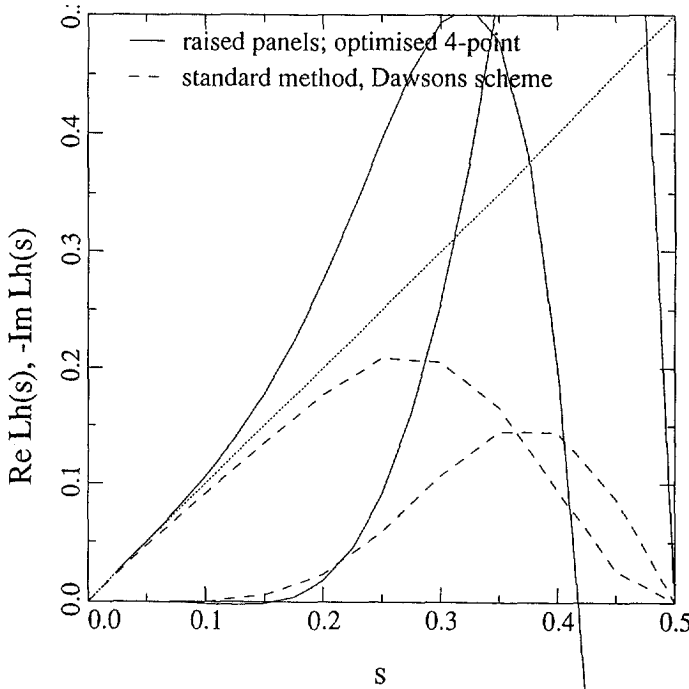
Figure 6.12: *Lh(s) for raised-panel method.* $\alpha = 1.0$, *varying* γ, *improved 4-point upwind scheme; and for conventional method with Dawson's scheme.*

$s < 0.15$ and the numerical dispersion has now been reduced to one-fifth at $s = 0.05$, one half at $s = 0.10$, compared with Dawson's method (Table 6.2). While up to now we have always used the NLR-scheme instead, this will soon be replaced.

6.4.6 Results — The source strengths

The operator $\hat{W}_1$ derived above is of some interest as well, since it relates the *source strength* to the forcing. Even more illustrative is the expression (6.21),

$$\frac{\hat{\sigma}(k)}{\hat{\phi}_y(k)} = \Delta x \frac{e^{-ik\gamma\Delta x}}{\hat{Q}(k)} \tag{6.43}$$

which indicates the amplitude and phase of the source distribution necessary to generate a certain vertical velocity distribution. It can be compared with its continuous counterpart,

$$\frac{\tilde{\sigma}(k)}{\tilde{\phi}_y(k)} = -2e^{ky_{fs}} = -2e^{\alpha s} \tag{6.44}$$

Fig. 6.13 makes this comparison. The ratio of the amplitude of the source strengths and induced
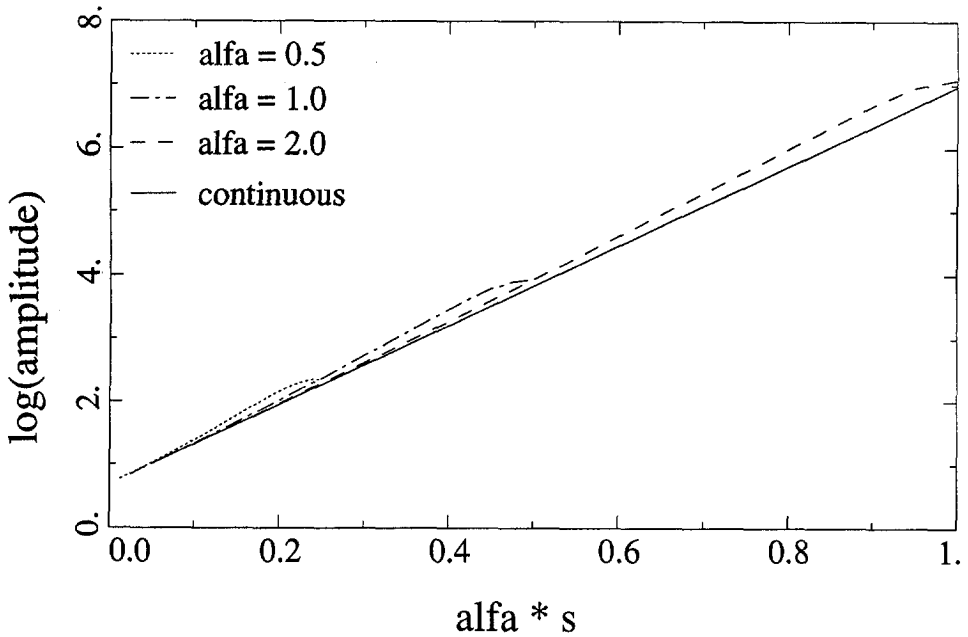
Figure 6.13: *Source strength amplitude for raised-panel method.* $\gamma = 0.25$.

vertical velocities (the modulus of the above expressions) is shown on a logarithmic scale, so the graph for the continuous case is a straight line. The amplitude for the discretised case (6.43) turns out to follow this behaviour quite closely. Different values of α have only a marginal effect on the source strengths for fixed $\alpha.s$. This means that the magnitude of the source strengths is not primarily determined by the ratio of the panel elevation to the panel length, but by the ratio of the panel elevation to the wave length that is to be resolved.

Besides a small effect of the discretisation on the amplitude, there is a more pronounced effect on the phase. In the continuous case the phase lag between the vertical velocity in the collocation points and the source strength is simply $2\pi\gamma s$, proportional to the forward shift. In the discretised case the phase lag is equal to this for $s = 0$ and $s = 0.5$ but is much reduced for intermediate wave numbers. Practical consequences of this are not clear however.

6.4.7   Raised point-source method

I have carried out a similar (but less complete) analysis for a raised point-source method [59]; paying attention to the effect of the source discretisation only, not to the difference scheme. For 2D problems this method appears to be as accurate as a raised-panel method, although for a somewhat larger elevation. But in a 3D point source method there is a further subdivision in transverse direction, into an array of point sources (having equal strength in our 2D analysis). This introduces additional errors in the induced velocities. The analysis then shows that the 3D

raised point-source method is substantially less accurate unless the aspect ratio of the 2D source array is kept close to unity. E,g. for $s = 0.05$ and $\Delta z/\Delta x = 2$, the wave length error is 2.5 % ; for $\Delta z/\Delta x = 3$, the error even amounts to 11.6 %. Since keeping the aspect ratio close to unity often requires a greater number of sources than otherwise needed and thus increases the calculation time, this is a disadvantage of the point-source approach. On the other hand, the simple induced velocity expressions and the possibility to use larger source elevations without compromising the conditioning of the matrix equation are advantages [48].
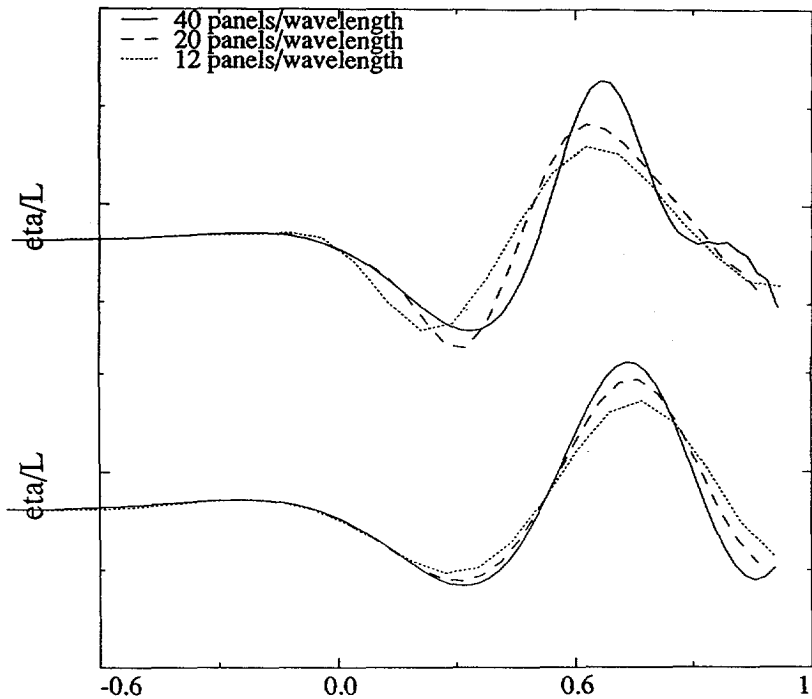
Figure 6.14: *Effect of panel length Δx on wave pattern. Conventional method, with dispersion correction (top), and raised-panel method (bottom). Wigley hull, Fn = 0.4 , at z/L = 0.35 .*

6.5 Numerical verification

The conclusions drawn from this 2D analysis have largely been confirmed by numerical experiments for 3D cases. The occurrence of oscillations for $\gamma = 0$ has already been illustrated in Fig. 6.2. The fact that $\gamma = 0.5$ and $\gamma = 0.25$ give closely corresponding results agrees with our experience. Also the fact that the numerical dispersion is small, is fully borne out by numerical experiments. Fig. 6.14 compares predictions by a conventional and a raised-panel code for the Neumann-Kelvin problem, for a Wigley hull at $Fn = 0.40$. Longitudinal cuts through the

wave pattern are shown as found with various panel densities. In the conventional method the dispersion correction factor has been used; but since the dominant bow waves are not transverse, this correction is insufficient and panel refinement still causes a significant aft shift of the wave system, most notably of the first wave trough. For the raised-panel code only a very small forward shift is observed, in agreement with the much smaller numerical dispersion which is of opposite sign. Moreover the convergence of the amplitude is better for the raised-panel code. It appears that upon panel refinement the predictions by both codes approach each other.
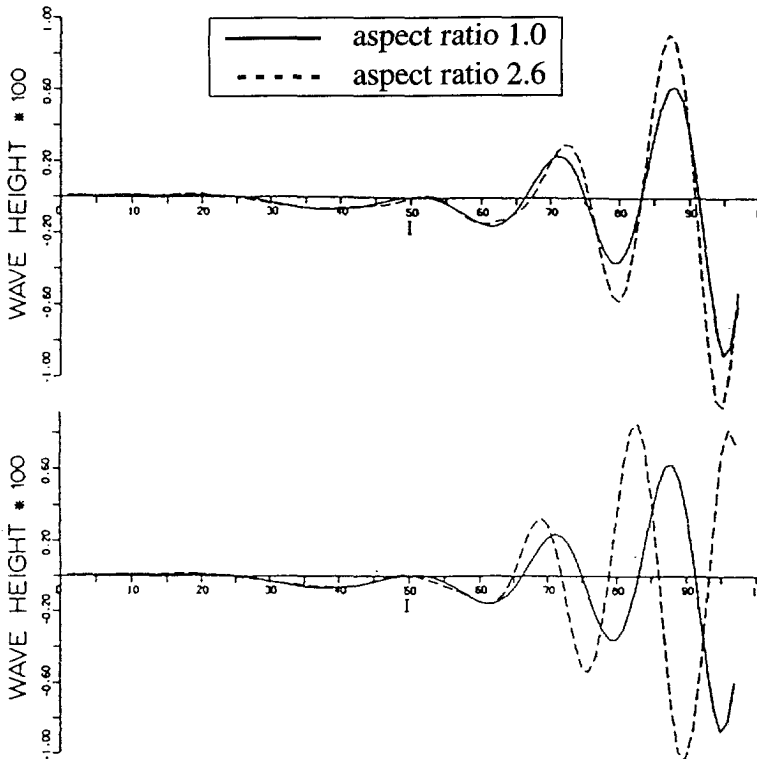
Figure 6.15: *Effect of source distribution aspect ratio on numerical dispersion. Strut-like hull, Fn = 0.25, wave cut at z/L = 0.46 . Raised source panels (top) and raised point sources(bottom).*

The effect of the aspect ratio of the source array or source panel distribution is shown in Fig. 6.15, which compares longitudinal cuts at a distance from the hull. The reduction of the aspect ratio from 2.6 to 1.0, here accomplished by increasing the number of free surface strips from 8 to 20, has no effect on the phase for the raised-panel method but a substantial effect for the raised point-source method, exactly as the analysis predicts.

The effect of the distance of the panels above the free surface, $\alpha \Delta x$, will be tested in Section 7.3.3, in connection with the fully nonlinear method.

6.6   Conclusions

We conclude from this accuracy analysis that

- For a constant-strength source panel method, using raised panels gives a drastic reduction of the numerical dispersion caused by the source discretisation.

- For correctly chosen parameters the discretisation of the source distribution introduces almost no errors for as little as 4 panels per wavelength.

- The use of a difference scheme introduces much larger errors. Nevertheless, with raised panels the numerical dispersion for usual panel densities remains much smaller than with a conventional method, being of third rather than first order in the panel size. Also in practical 3D calculations, a large accuracy and grid independence of the phases of waves are observed.

- The freedom in the position of the collocation points relative to the panels permits to modify the method's properties, in particular to add numerical damping at high grid wavenumbers.

- For the raised-panel method instability with respect to point-to-point oscillations only occurs for $\gamma = 0$ (no collocation point shift). For usual parameter values no oscillations occur.

- The use of the NLR-scheme seems attractive as it adapts to the number of panels per transverse wavelength so as to minimise the errors. But in 3-D cases it loses most of its advantages, and Dawson's scheme, or rather a scheme optimised for the raised-panel method, is preferable.

- The source strength amplitudes in a raised-panel method are larger than those in a conventional method, and almost exactly correspond with the amplitude of a continuous raised source distribution, being exponential in the ratio of panel elevation to wave length.

The favourable properties of the raised-source method, together with its practical advantages and simplicity, made me select this approach as the basis of the nonlinear method to be developed.

The analysis also tells us that the difference scheme is the dominant source of numerical errors, and a method using exact evaluation of velocity gradients induced by the panels might be more accurate; an analysis similar to that given here would be needed to confirm this. But the differencing has been found to be a practical way to enforce the radiation condition, and the added numerical damping it introduces may be beneficial for the stability and robustness. Therefore, and because at that stage of the development the effect of the difference scheme on the accuracy was not yet as clear as it is now, the decision was taken to use difference schemes in the implementation of the free surface condition in our nonlinear method.
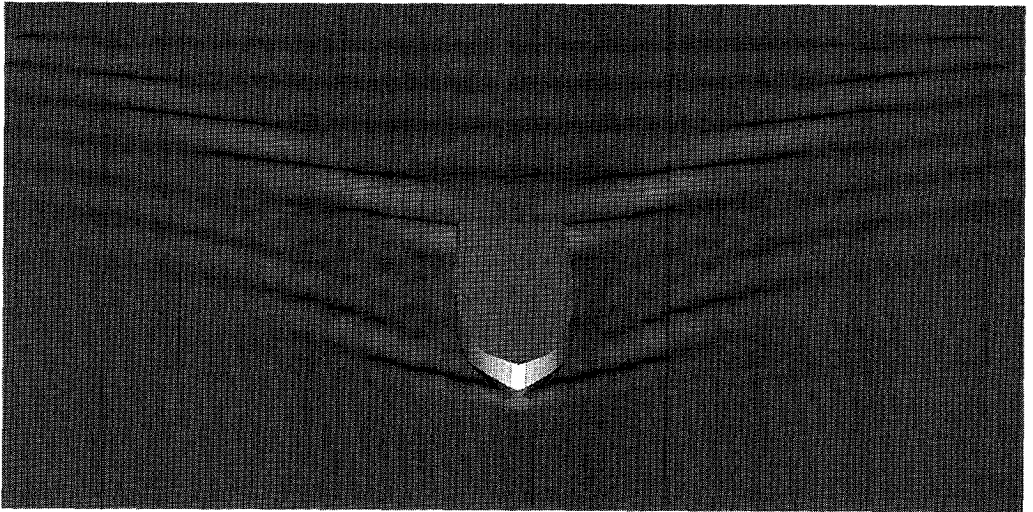
Figure 6.16: *Just to remind you of the problem we are solving...*

Chapter 7

The RAPID method

The basic components of the nonlinear method are now described, and its behaviour in practical applications is studied. A series of numerical experiments is discussed to establish the convergence properties, the accuracy and the sensitivity for numerical parameters.

7.1 General approach

Several basic decisions on the setup of the nonlinear method have been mentioned and motivated already in previous chapters. In particular, an iterative procedure will be used, consisting of a sequence of linear problems, defined such that convergence to the solution of the complete steady nonlinear problem is obtained; the Laplace problem in each iteration will be solved using constant-strength source panels located at a distance above the free surface; and the combined free surface condition is treated using an essentially DAWSON-like method, modelling derivatives of velocities by means of a difference scheme. For obvious reasons I have baptised this approach the "RAPID" (**RA**ised **P**anel **I**terative **D**awson) method.

The general course of the calculation is as follows:

1. Choose an initial approximation of the free surface, and an initial velocity distribution $\nabla \Phi$ on that surface.

2. Define a panel distribution on the hull, and a free surface panel distribution at a specified distance above the free surface. Choose collocation points on the approximate free surface, shifted forward relative to the panel centres in agreement with the findings of the last chapter.

3. In the free surface collocation points, impose a combined free surface condition, linearised in perturbations of the assumed velocity distribution and free surface. Impose the hull boundary condition in the hull collocation points. Solve the resulting set of linear equations for the source strengths.

4. Compute the velocity and pressure field. Calculate a new estimate of the wave elevation from the dynamic free surface condition. Determine the resistance, vertical force and trimming moment by integrating pressure forces over the hull.

5. Move the free surface collocation points to the new free surface. Adapt the estimated velocity field $\nabla\Phi$ to the new solution.

6. Ascertain that the distance from the new free surface collocation points to the free surface panel surface is within reasonable bounds everywhere; if not, adapt the free surface panels to the current estimate of the wave surface, and adapt the hull panelling accordingly, taking into account any (change of) dynamic trim and sinkage.

7. Calculate the residual errors in the nonlinear free surface conditions, i.e. the normal velocity through the free surface and the deviation from atmospheric pressure. If these exceed the specified tolerances, return to step 3.

The details of all these steps will now be described.

7.2   Description of the method

7.2.1   The panel layout

In the linearised code DAWSON a double body is used, defined by mirroring the underwater part of the hull in the still water plane. This is consistent with the use of double-body flow linearisation, reduces flow irregularities at the waterline caused by the edge of the hull panelling, and theoretically would reduce the effect of the truncation of the free surface domain. But the first argument does not apply to a nonlinear method, the second is meaningless for a raised-panel method, and the third was numerically found to be insignificant. For reasons of calculation efficiency and conditioning we therefore use a single hull in RAPID. The hull panelling is extended up to its intersection with the free surface panels. The basic panel layout has already been shown in Figure 6.1.

The discretisation of the source distributions is similar to that used in DAWSON. The hull is represented by flat quadrilateral panels with constant source density. These are located on the hull surface itself, to retain compatibility with DAWSON and to avoid problems at corners in the hull geometry. Also the free surface singularities are flat quadrilateral panels with constant source density, positioned at usually about 0.8 panel length above the free surface; a compromise between

the wish to reduce numerical dispersion and damping (by increasing α) and the necessity to retain a good conditioning of the system of algebraic equations. The free surface panelling is fitted around the waterline at the specified height, and is based on transverse lines and roughly longitudinal lines passing around the hull.

The velocities induced by source panels are calculated exactly for nearby points, or approximated by multipoles or point sources for more distant points, like in the method of Hess and Smith. By a proper implementation the calculation of induced velocities vectorises completely, in spite of the presence of this branch.

7.2.2   The free surface boundary condition

The free surface condition to be imposed in each iteration is derived as follows. The velocity and free surface elevation to be calculated are decomposed as:

$$\nabla\phi = \nabla\Phi + \nabla\varphi', \tag{7.1}$$

$$\eta = H + \eta', \tag{7.2}$$

where $H(x, z)$ is an assumed wave surface, $\nabla\Phi(x, H, z)$ a "base flow" velocity distribution on that surface, and $\nabla\varphi'$ and η' are (hopefully small) perturbations. The kinematic and dynamic boundary conditions, linearised in these perturbations, then read:

$$\Phi_x\eta_x + \Phi_z\eta_z + \varphi'_x H_x + \varphi'_z H_z - \Phi_y - \varphi'_y = 0 \tag{7.3}$$

$$\eta = \frac{1}{2}Fn^2(1 - \Phi_x^2 - \Phi_y^2 - \Phi_z^2 - 2\Phi_x\varphi'_x - 2\Phi_y\varphi'_y - 2\Phi_z\varphi'_z). \tag{7.4}$$

These equations actually are to be satisfied on the new (unknown) free surface $y = \eta$, but to allow a direct solution they must be transferred to the known surface $y = H$. Just as in slow-ship theory, consistency would require that a Taylor expansion in η' be used to incorporate this transfer. But Chapter 4 has indicated that for Dawson's method these Taylor terms tended to be most irregular and sometimes to give a poor approximation of the true transfer effect. Although the irregularity may be much reduced due the smoothness of the raised-panel method, I decided to leave out the transfer terms and to use the conditions in the form presented above. The ensuing formal inconsistency of the linearisation is, of course, meaningless for the converged result.

Next, the wave elevation η from the dynamic condition is substituted into the kinematic condition. One must be careful here, since η is a function of (x, z) alone, while the right hand side of the dynamic condition in principle is a function $F(x, y, z)$. Consequently,

$$\phi_x\eta_x + \phi_z\eta_z = (\phi_x F_x + \phi_x\eta_x F_y) + (\phi_z F_z + \phi_z\eta_z F_y) = \phi_x F_x + \phi_y F_y + \phi_z F_z \tag{7.5}$$

in which we have used the kinematic condition. However, in our implementation the partial derivatives of F are defined as differences between values in collocation points which are on the free surface, so the F_y-contribution is inherently taken into account.

The resulting combined condition then reads:

$$-\frac{1}{2}Fn^2(\Phi_x\frac{\partial}{\partial x} + \Phi_z\frac{\partial}{\partial z})[\Phi_x^2 + \Phi_y^2 + \Phi_z^2 + 2\Phi_x\varphi_x' + 2\Phi_y\varphi_y' + 2\Phi_z\varphi_z']+$$

$$+ \varphi_x'H_x + \varphi_z'H_z - \Phi_y - \varphi_y' = 0. \tag{7.6}$$

In the discretisation of this free surface condition the derivatives of the factor in square brackets, and those of H, are approximated by finite differences. Only the former play a role in the converged solution. The $x-$ and $z-$derivatives are composed from upwind schemes along the roughly longitudinal lines through collocation points, and mainly central schemes along transverse lines.

7.2.3   Other boundary conditions

The implementation of the boundary condition on the hull is obvious; a zero normal velocity in the panel centroids. For numerical reasons the same condition is imposed on the part of the hull between the wave surface and the free surface panels, in order to produce a smooth continuation of the velocity field across the still waterline.

The treatment of the radiation condition is similar to that in Dawson's method. Also in the nonlinear case the use of an upwind difference scheme, together with conditions imposed at the upstream end of the free surface domain, appear to introduce the proper bias in the numerical solution, and waves upstream of the bow are not observed.

No particular treatment is applied to the outer boundaries of the free surface domain. Outside of the free surface panels the perturbation velocity components all gradually fall to zero. While this edge is significantly "softer" than that in a method with non-raised panels (where the vertical velocity has a sharp cutoff at the edge), some reflections still are present. But if the lateral boundaries are chosen at such a distance that over the length of the domain the entire Kelvin wedge is included, reflections only occur at the downstream boundary. These do not reenter the domain and their effect is quite localised and harmless.

For calculating the flow and wave pattern in shallow water, an additional no-flux condition is imposed on the water bottom. Rather than covering this boundary by panels we reflect the entire configuration (hull and free surface) in the bottom. Since we use a single hull there is only a single mirror image, not an infinite series of images.

7.2.4   Initial solution

In the derivation of the free surface condition no specific relation has been assumed between the base flow and base surface. This provides complete freedom to select any initial flow field and free

surface shape. The choice has no influence on the final result provided that correct convergence criteria are imposed (and supposed that the solution is unique), but may well influence the number of iterations needed. The simplest approach is to start from a flat free surface and a uniform flow. The first iteration then produces the Neumann-Kelvin approximation. Alternatively one may start with a flat free surface with double-body velocity field; the first iteration then leads to an incomplete slow-ship free surface condition. One may even start from a result for a previous design variation, or for the same vessel at a different speed, draft, trim or water depth. A clever choice considerably reduces the number of iterations required; experience with running the code helps.

7.2.5   The matrix solver

It is well known that the system of equations obtained by imposing the combined free surface condition is poorly suited to iterative solution methods. Therefore in almost all methods for the steady problem a Gaussian elimination procedure is used, and this is what I initially used as well. For usual panel numbers this was by far the most time-consuming part of the solution process.

An iterative solver that is known for its robustness in a variety of applications is the GMRES algorithm. When applied to our system of equations this method fails to converge (at least, in significantly less than N operations), and a proper preconditioning is indispensable. The preconditioning I currently use is a partial Gaussian elimination procedure devised and kindly provided to me by Prof. H. Söding (Institut für Schiffbau, Hamburg, Germany) that just eliminates the larger contributions from the lower triangle of the matrix [62]. While for large panel numbers the speedup compared to Gaussian elimination is already quite appreciable, most likely more efficient preconditioners can be designed by exploiting the known structure of the matrix.

7.2.6   Update of wave surface and velocity field

After solving for the source strengths we can easily compute the velocity components in all collocation points. Substituting these into the dynamic free surface condition yields a new estimate of the wave elevation. The free surface collocation points are then moved (essentially vertically) towards the new free surface.

Repeated full application of these wave height updates, however, has been found to frequently lead to divergence. A slight amount of underrelaxation, only applied to the changes of the wave elevations, already cures this problem. In difficult cases underrelaxation is useful in the initial stage of the calculation but it does not always add enough to the stability to remove more serious convergence problems. Fortunately these are rare.

The velocities at the free surface found in iteration k are those in the current free surface collocation points, located at $y = H^{(k)}$. For the next iteration we need an estimate of the velocity field at

$y = H^{(k+1)}$. As discussed on page 77 this can simply and efficiently be computed in a raised-panel method. One may call also this treatment inconsistent, because it corrects for transfer effects that are disregarded in the free surface condition itself. But in any case it avoids the introduction of several higher-order derivative terms and Taylor expansions. To what extent it improves the convergence is examined in Section 7.3.2 below.

7.2.7   Convergence criteria

The formal independence of H and $\nabla\Phi$, the underrelaxation and the liberty in selecting an initial solution demand that care is taken in deciding when the nonlinear solution has been approximated sufficiently well. The free surface condition can be cast in the alternative form:

$$\varphi'_y - \varphi'_x H_x - \varphi'_z H_z + Fn^2(\Phi_x\frac{\partial}{\partial x} + \Phi_z\frac{\partial}{\partial z})(\Phi_x\varphi'_x + \Phi_y\varphi'_y + \Phi_z\varphi'_z) =$$

$$= -\epsilon_k + (\Phi_x\frac{\partial}{\partial x} + \Phi_z\frac{\partial}{\partial z})\epsilon_d = -\Phi_y + \Phi_x H_x^* + \Phi_z H_z^* , \tag{7.7}$$

where

$$\epsilon_k = \Phi_y - \Phi_x H_x - \Phi_z H_z, \tag{7.8}$$

$$\epsilon_d = \frac{1}{2}Fn^2(1 - \Phi_x^2 - \Phi_y^2 - \Phi_z^2) - H, \tag{7.9}$$

the residual errors in the kinematic and dynamic condition at the start of the iteration; and

$$H^* = \frac{1}{2}Fn^2(1 - \Phi_x^2 - \Phi_y^2 - \Phi_z^2), \tag{7.10}$$

the wave height corresponding to the new base flow velocities.

Owing to the recalculation of the base flow velocities, these correspond with a potential field satisfying the Laplace equation and are defined on the surface $y = H$. Consequently, if both residual errors vanish everywhere at the free surface, the base flow $\nabla\Phi$ and the base surface H are a valid solution of the nonlinear free surface conditions, and the iteration can be terminated. Equation (7.7) shows that then the perturbations must vanish as well.

In most other nonlinear methods the convergence criterion applied is that the change of the wave elevation between iterations falls below a certain tolerance. From equation (7.7) it can be checked that this is formally insufficient, and that, dependent on the details of a method, it may admit residual errors due to the fact that velocities are defined on a wrong surface or due to neglected terms of higher order in $\nabla\phi'$. Only if the norm of the wave elevation changes is less than the tolerance in *two* consecutive iterations, satisfaction of the boundary conditions is guaranteed.

In general we find that two conditions must be imposed to be sure of convergence. To get direct insight in the accuracy of the solution I have chosen to check convergence by computing both

residuals ϵ_k and ϵ_d and imposing a criterion on the maximum norm of both. Usually the conditions are:

$$\epsilon_k < 0.002U_\infty \quad \text{and} \quad \epsilon_d < 0.0025Fn^2. \tag{7.11}$$

This generally means that wave height changes in the final iterations are less than about $10^{-4}L$ everywhere in the domain.

7.2.8   Free surface panel adaptation

The accuracy analysis in Chapter 6 has shown that theoretically there is much freedom in the distance from the free surface panels to the wave surface. A useful minimum is about 0.5 panel length. The maximum distance is not dictated by these accuracy considerations but by the conditioning of the resulting set of equations. If a collocation point is at a distance of several panel lengths from the nearest free surface panel, the matrix tends to become singular. Deteriorating matrix conditioning in general starts causing trouble for distances of about 1.5 to 2 times the panel size.

If we use free surface panels in a fixed horizontal plane above the still water surface, this plane must be positioned higher than the highest wave elevations. These are bounded by the stagnation height $\eta_{max} = \frac{1}{2}Fn^2L$. For the usual panel size of about 3 to 5 % of the fundamental wave length $\lambda_0 = 2\pi Fn^2L$, the stagnation height amounts to 2.6 to 1.6 panel length. Raising the panels by at least this amount in order to keep clear of the highest wave crests is likely to cause trouble near wave troughs.

Therefore, some adaptation of the free surface panelling to the wave surface is needed to keep the distance within the desired bounds everywhere. The panels are repositioned to be approximately parallel to the current guess of the wave surface at the specified distance y_{fs}. But there is no need to apply the adaptation in every iteration, nor is it necessary to adapt the panels very carefully: an approximate adaptation once every few iterations usually suffices. Thus the raised-panel method retains its advantages of better stability and efficiency compared to methods using panels on the free surface itself, which require a *careful* adaptation in *every* iteration.

In order to maintain a closed boundary and to avoid numerical difficulties, adaptation of the free surface panels also requires adaptation of the upper hull panels such that they conform with the modified intersection. At the same time the attitude of the hull may be adapted to the latest estimates of the dynamic trim and sinkage, derived from the balance between the hydrostatic and hydrodynamic pressure forces on the hull and the ship's weight and centre of gravity. A routine has been written that carries out these geometric manipulations automatically, using a basic hull panel file, the latest geometry of the wave surface and a specified trim and sinkage. Fig. 7.1 shows a hull and free surface panelling as generated by the automatic adaptation.
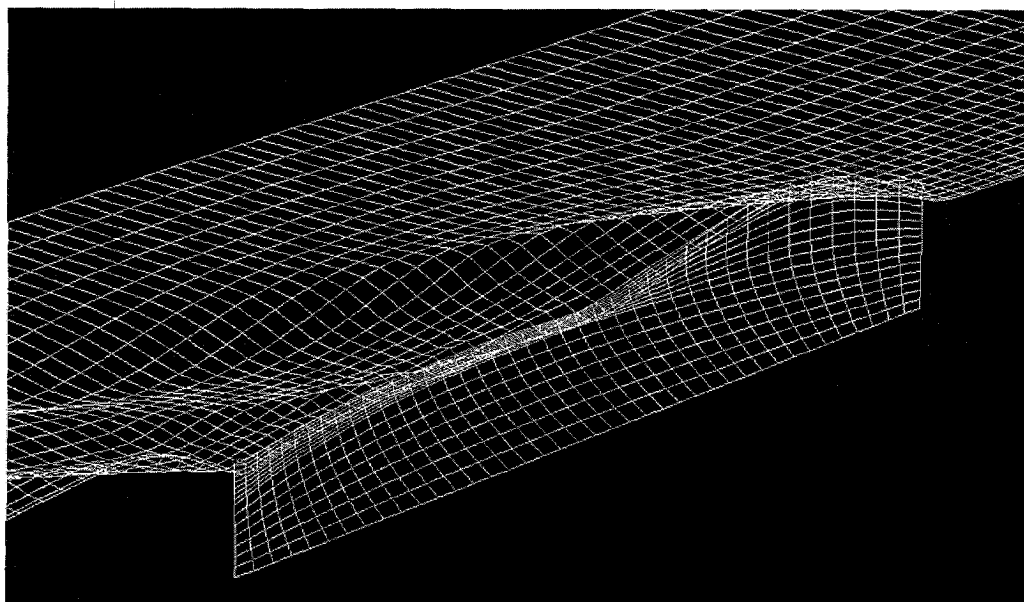
Figure 7.1: *Final hull and free surface panelling for a nonlinear calculation. (The free surface panelling is here shown projected onto the wave surface, with which it actually is parallel.)*

7.2.9   Resistance calculation

Once the converged solution has been obtained, or at any intermediate stage, the wave resistance can be computed by integrating the longitudinal component of the pressure force over the entire wetted part of the hull under the calculated wave profile.

In a linearised method the pressure forces are integrated over the area below the still waterline, as has been discussed on page 55. Since the hydrostatic pressure distribution then integrates to zero (except for a transom flow, see page 147) it suffices to integrate the hydrodynamic pressure contribution only. As opposed to this, in a nonlinear method we have to integrate over the area under the actual wave profile[1], so we must include the hydrostatic pressure and integrate the *total* pressure. But this may reduce the accuracy very much. For slow ships, for which the accuracy of the wave resistance calculation is a point of concern anyway, the hydrostatic pressure far exceeds the hydrodynamic pressure on most of the hull. The unavoidable small errors in the panel normals and centroids, and any areas of the hull uncovered by panels, lead to drastic inaccuracies in such cases.

---

[1] A waterline integral formally cannot be used since it depends on order assumptions that are inconsistent with the method.

For a specific case of a tanker at $Fn = 0.126$, integrating only the hydrostatic pressure over the area under the still waterline yielded a spurious longitudinal pressure force amounting to 0.0076 % of the displacement — a small error but meaning an inaccuracy of 70 % in the wave resistance. The total pressure acting on the first vertical strip of panels (with a width of less than 0.5 % of the ship length) contributed a longitudinal force of 32 times the *total* wave resistance! Only 11 % of this force was due to the hydrodynamic pressure; but still that was 4 times as much as the wave resistance of the entire hull. This illustrates that for slow ships extreme care is needed to compute a wave resistance by pressure integration.

Our current procedure is to integrate the total pressure up to the calculated wave profile, and to subtract the integral of the hydrostatic pressure force over the area under the still waterline (which ought to be zero). This is equivalent to integrating the hydrodynamic pressure over the area under the still waterline, and the total pressure over the area between the actual waterline and the still waterline. This often reduces the magnitude of the integrand very much and thus reduces the sensitivity of the result to inaccuracies. Nevertheless, further improvement is desired, as will appear below.

An alternative way to evaluate the wave resistance is to apply a wave pattern analysis approach to the calculated wave pattern. This will remove the difficulty of the poor conditioning of the pressure integration, but I expect that it will introduce some other problems, such as the limited number of data points in a transverse cut analysis and the possible dependence of the result on the position of a wave cut. Nevertheless the feasibility of this method has been demonstrated [63] and it definitely deserves to be attempted. This will be done in a near future.

7.2.10   Calculation times

# hull panels	# FS panels	total # panels	CPU sec/iteration
264	930	1194	2.2
1159	1647	2806	7.5
1832	3170	5002	30
1440	4518	5958	42

Table 7.1: *Required CPU time per iteration, for* RAPID *on a* CRAY *C98. Panel numbers are for one symmetric half.*

The code currently runs on a CRAY C98 supercomputer, vectorises well and reaches a computing speed of 400 to 730 Mflops on a single processor (which has a theoretical top performance of 1 Gflops). Owing to the use of the iterative equation solver, calculation times required for the entire sequence of iterations in practice are just 1.5 to 4 times as large as for a usual linearised code such as DAWSON (which still uses LU decomposition). Some timings are given in Table 7.1. For cases with poor conditioning the calculation time may occasionally be several times higher, as a
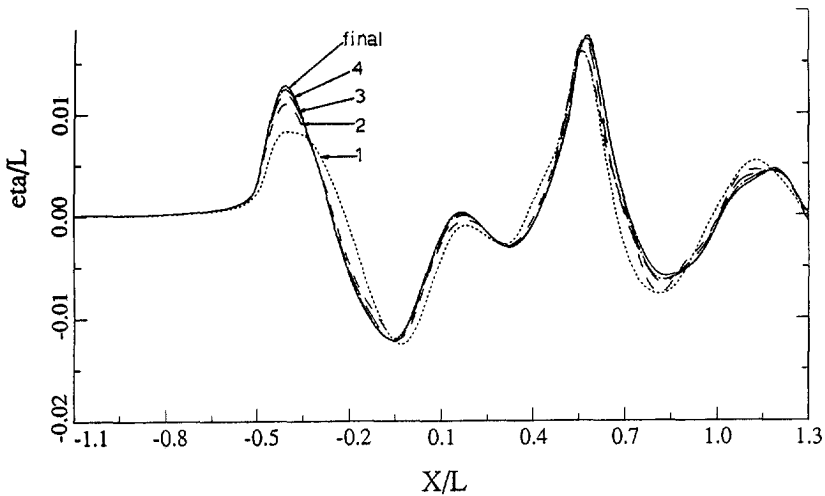
Figure 7.2: *Wave profile along the hull in successive iterations. Series 60 model, Fn = 0.316.*

result of slow convergence of the GMRES solver. Anyway neither the computing costs nor the turnaround time prohibit extensive use of the method in practical design projects.

7.3   Evaluation of numerical properties

We shall now consider some of the principal numerical properties of the method, and study the effect of numerical parameters.

7.3.1   Convergence of the iterative procedure

The first issue to be discussed is the convergence of the iterative procedure, of such crucial significance for the usefulness of the method. As the literature survey in Section 5.2 indicated, previous methods have been reported to meet substantial difficulties in several cases, in particular for full-formed ships such as tankers, or if fine free surface panellings are used near the hull. As opposed to this, the convergence of the present method has been found to be quite good and robust throughout. The great majority of practical cases, including full hull forms, provide no convergence problems. It is to be noted that *this desirable behaviour is obtained without any explicit smoothing, filtering or damping of any kind.* Some numerical damping is inherent in the use of the upstream difference scheme, but this plays only a minor role in this regard, since even for very fine panellings the iteration converges (although often less quickly).

The convergence criteria are usually met after 5 to 25 iterations (starting from uniform flow),

dependent on the difficulty of the case. On the basis of a visual inspection of the wave profile along the hull the calculations would probably be terminated much earlier in most cases.

Fig. 7.2 illustrates how the hull wave profile evolves in the course of the iteration. The convergence is monotonous at most locations, and already after about 4 iterations the wave profile is very close to the final solution here.
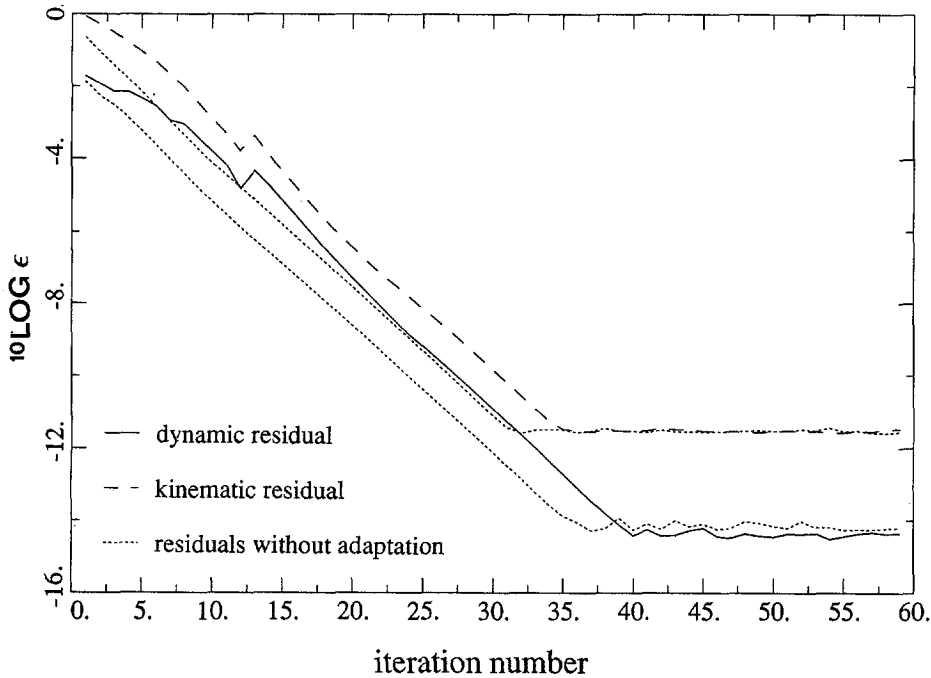
Figure 7.3: *Convergence history. Maximum norms of kinematic and dynamic residuals on the free surface. Relaxation factor $\omega = 0.7$.*

Fig. 7.3 plots the maximum residual errors occurring at the free surface in consecutive iterations on a logarithmic scale. After the initial iterations the convergence rate is constant, and the residuals decrease fairly quickly until a minimum level determined by machine accuracy is reached. If no free surface panel adaptation is applied the convergence appears to be slightly faster for this simple case; the figure shows that the free surface panel adaptations at iterations 4, 8 and 13 temporarily delay the convergence as a result of e.g. the geometric changes. But for most cases one simply does not have a choice: without adaptation of the free surface panelling from time to time, wave crests would soon reach the panels and the calculation would blow up. That a raised-panel method makes it unnecessary to carry out this adaptation in every iteration may be one of the explanations for its robustness.

Underrelaxation·may help convergence in the initial stage but is of little meaning thereafter. The fact that the convergence of the free surface shape generally seems to be monotonic suggests that one should rather apply *over*relaxation. But for a simple Wigley hull case, all values of ω different from 1.0 quite substantially delay the convergence; for ω = 0.6, 0.8, 1.0 and 1.2, the number of iterations required to reach machine accuracy is 35, 23, 16 and 28, respectively. In general, a high value of ω reduces the stability in critical cases, and even ω = 1.0 may lead to a slow divergence in later stages. Therefore we generally keep ω < 0.9.

In the large range of practical applications run during the last few years (about 90 different hull forms per year since 1994) the following convergence problems have occasionally occurred:

- Sudden divergence in the initial stages of the iteration. This is usually due to initial conditions too remote from the final solution. This class of difficulties is in most cases simply obviated by choosing a clever route towards the final result, temporarily modifying the draft, trim, speed etc.

- Difficulties in reducing the residual errors below a certain level, at a later stage of the iteration process. In some cases this may eventually lead to growth of the residuals or sudden divergence. This usually occurs at points along a steep wave slope or crest, at some distance away from the hull. A hypothesis (but not more than that) is that locally a potential flow solution, without energy dissipation by wave breaking, does not exist. This class of convergence problems generally is quite hard to solve, unless by using a coarser free surface grid (which means that accuracy is sacrificed).

7.3.2   Effect of base flow recalculation

As mentioned before, following each iteration a new base flow is computed by evaluating the last velocity field at the new collocation point positions. The idea behind this is to incorporate the transfer effect on the velocity field at least after the iteration, rather than to simply shift the velocity field towards the new free surface location. The importance of the transfer effect as identified before suggests that this will improve the base flow estimate and thus speed up the convergence.

To check whether this base flow recalculation helps, a method without it has been tested as well for some cases. In this approach the free surface velocities $\nabla\phi^{(k-1)}$, actually valid in the collocation points at $y = H^{(k-1)}$, are simply supposed to be valid at the new base surface $y = H^{(k)}$. Rather surprisingly, in some tests with this method the maximum residual errors in the free surface conditions in corresponding iterations were much lower but the maximum wave height changes turned out to be almost identical to that of the normal method, and the convergence rate as well. This raises the questions what causes this drastic change of the residuals and why the resulting wave height change does not show a similarly drastic decrease.

The effect of recalculation is of leading order in the velocity change in an iteration. E.g. for the term $\Phi_x\eta_x$, recalculation prior to iteration k effectively adds a term like $\Phi_{xy}.\Delta\eta^{(k-1)}.\eta_x$. In practice

the effect appears to be significant mainly at the bow and stern wave crests where large velocity gradients are present.

To see how these base flow velocity changes affect the result of the iteration we reconsider equations (7.7) — (7.9). Suppose that no base flow recalculation is applied, and that the relaxation factor $\omega = 1$. Iteration $(k - 1)$ solves the problem subject to linearised boundary conditions. The new wave height is found from the nonlinear dynamic free surface condition. The free surface velocities found are simply transferred towards the new free surface without a change, so the new base flow still satisfies the dynamic condition identically: ϵ_d is zero. The velocities have been computed such that they satisfy a linearised kinematic free surface condition, so the residual errors ϵ_k only consist of contributions that are $\mathcal{O}(\nabla\varphi')^2$. Therefore the calculated residuals are relatively small. But if, instead, the base flow is recomputed, the added transfer contributions of $\mathcal{O}(\nabla\varphi')$ enter the residuals, leading to an *apparent* increase of the maximum residual errors. This does not, however, indicate a poorer accuracy of the intermediate result.

The larger residuals make the *RHS* of eq. (7.7) larger, and one would expect a completely different convergence history for both methods. But it appears that the difference in $\nabla\Phi$ between both methods is corrected immediately by a difference in $\nabla\varphi'$ such that both methods give again a very similar result. This may be explained from the stability of the method for base flow disturbances, a prerequisite for a successful iteration. Suppose that a small perturbation $\Delta\Phi_x = \delta e^{ikx}$ is added to the base flow. If we assume that the resulting change $\varphi'_x = \mu e^{ikx}$, we can derive from equation (7.7) that $\mu = \delta(1 + \mathcal{O}(\delta))$, so the perturbation is cancelled immediately save for higher order terms. Therefore the effect of recalculation on the convergence history will be small anyway.

Given the similar convergence histories, the usefulness of recalculation of the base flow is indicated by $\nabla\varphi'$: the smaller this is, the smaller the linearisation errors. The $\mathcal{L}_2$-norms of the components of $\nabla\phi^{(k)} - \nabla\Phi^{(k)}$ and $\nabla\phi^{(k)} - \nabla\phi^{(k-1)}$ have been evaluated for a range of cases. The results were fairly inconclusive, and even from this point of view the advantage of base flow recalculation was not decisive.

A tentative explanation of this finding follows from some further reflection on the basis of the methods. The method with recalculation rests on the implicit assumption that the linearised free surface condition imposed in a certain iteration results in an approximately correct *velocity and potential field in space*, but that the collocation points where the free surface velocities are found are not at the correct position. Correspondingly, the result would be improved by re-evaluating the flow field at the wave elevation found. This new base flow is a valid potential flow generated by the source distribution of the previous iteration, and a further change of the source strengths is directly related to the change of the velocity field $\nabla\varphi'$. But since the iterative procedure is not formulated as a relaxation for the source strengths this does not seem to have any particular advantage.

On the other hand, in the method without recalculation we implicitly suppose that *the free surface velocities* found in the collocation points are approximately correct, and an improved guess is obtained by applying a vertical shearing transformation ($y' = y + \Delta\eta(x, z)$) to the velocity

field. This introduces errors in the Laplace equation: the new base flow field strictly is not an incompressible potential flow. But as the method is formulated in terms of the total potential rather than in a Delta-form, this is of little concern.

The inconclusive results indicate that neither of the two possible assumptions is consistently valid. Therefore the expected advantage of recalculation has not really materialised, and the recalculation may just as well be discarded from the point of view of convergence speed. Its effect on robustness is still an open question.
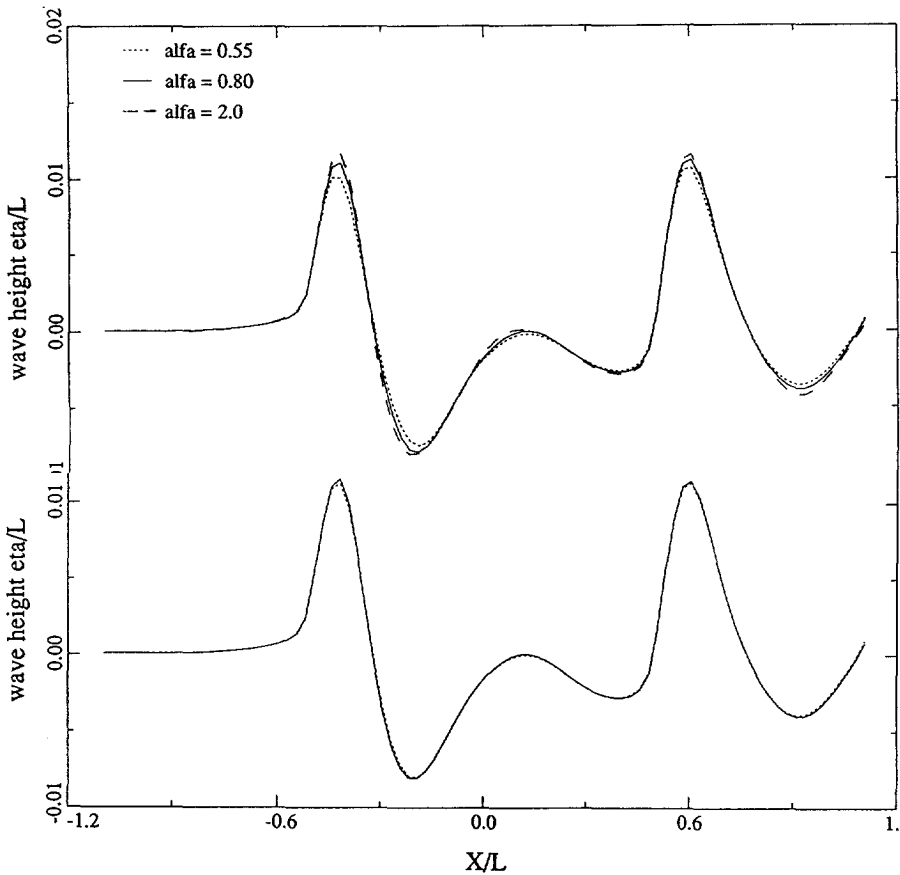
Figure 7.4: *Effect of panel elevation on hull wave profile. Wigley hull, Fn = 0.316 ; without (top) and with (bottom) free surface panel adaptation.*
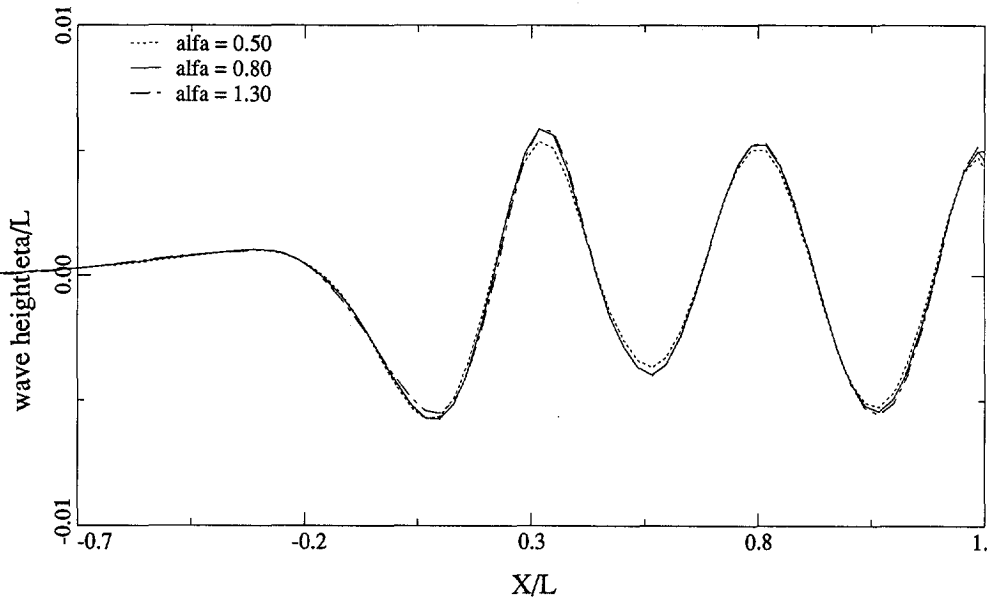
Figure 7.5: *Effect of panel elevation on longitudinal cut at z/L = 0.2723 . Series 60 model, Fn = 0.316 , 10 * 79 free surface panels.*

7.3.3   Effect of panel elevation

As mentioned before there is some liberty in selecting the parameter y_{fs}, or the nondimensional parameter $\alpha = y_{fs}/\Delta x$, for the raised-panel approach. Regardless of the discretisation an upper bound is dictated by the limit on the analytical continuation of the potential field outside the fluid domain. For the discretised system a corresponding limit is imposed by the increase of the condition number of the matrix, reducing the accuracy with which the system of equations is solved and perhaps causing trouble in the iterative solution. On the other hand, the accuracy and stability analysis in Chapter 6, pertinent to 2D linearised cases, indicates that increasing α may slightly improve the accuracy by reducing the numerical damping. The best choice is determined by the trade-off between these effects.

Several numerical experiments have been carried out to determine what effect α has in 3D nonlinear cases. Fig. 7.4 shows the effect on the hull wave profile for the simple Wigley model at $Fn = 0.316$, using a 12 by 87 free surface panelling (25 panels per fundamental wavelength). The maximum wave height found at the bow then is about $0.5\Delta x$. Consequently, if no free surface adaptation is applied the smallest α for which a computation can be made is around 0.55. The resulting wave profiles for $\alpha = 0.8$ and $\alpha = 2.0$ appear to be in fair agreement, but that for $\alpha = 0.55$, with panels almost touching the wave crests, slightly deviates.

The lower half of the figure demonstrates the beneficial influence of the free surface panel adaptation. In the converged situation the free surface panels now are at an approximately constant

distance $\alpha\Delta x$ from the wave surface. Not only α can be further reduced below 0.55 without any problem, but also the dependence of the wave profile on α is much reduced: the results for $\alpha = 0.55$ to 2.0 now coincide. In all subsequent calculations, free surface panel adaptation has been applied.

Fig. 7.5 shows a longitudinal wave cut at a distance from the hull, for the Series 60 $C_B = 0.60$ model at $Fn = 0.316$. The results for $\alpha = 0.80$ and $\alpha = 1.30$ are identical, that for $\alpha = 0.5$ shows a very small reduction of the wave amplitudes at a distance from the hull, probably due to the larger numerical damping.
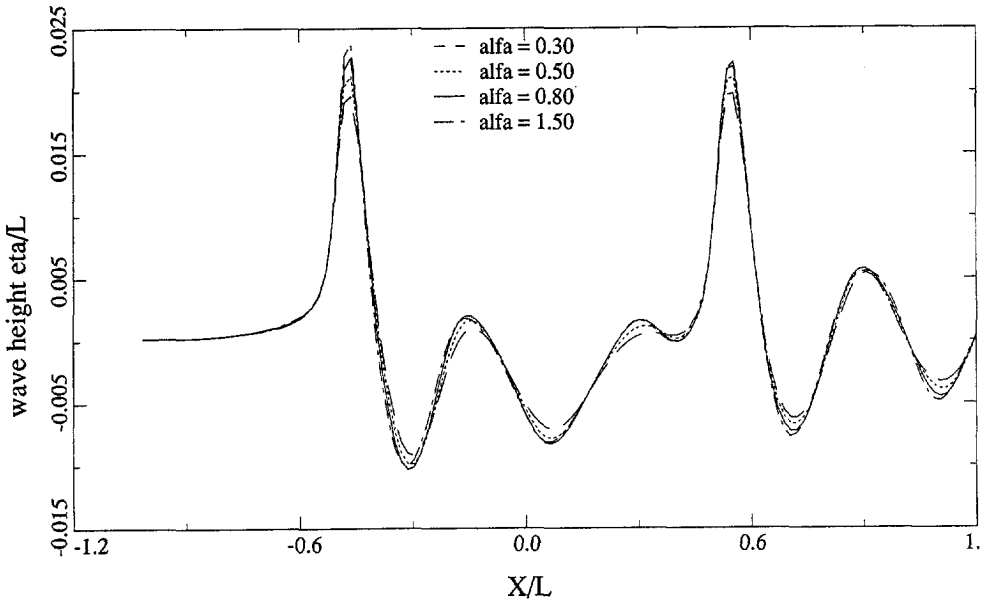
Figure 7.6: *Effect of panel elevation on hull wave profile. Parabolic hull, L/B = 4 , Fn = 0.25 .*

Next we consider a more strongly nonlinear case, a hull with parabolic waterlines, fore and aft symmetric, and rectangular (wall-sided) sections, with $L/B = 4$, $L/T = 20$. The waves produced at $Fn = 0.25$ are markedly nonlinear. The free surface panelling has 12 strips of 124 panels, 24 panels per fundamental wavelength. Varying α from 0.5 to 1.3 has very little effect on the hull wave profile (Fig. 7.6), except that the bow wave height tends to increase slightly with α. The result for $\alpha = 0.3$ has a somewhat reduced amplitude and some phase lag.

However, the wave cuts at greater transverse distances indicate a stronger effect (Fig. 7.7). $\alpha = 0.3$ and 0.5 both give a reduced wave amplitude. The results for $\alpha = 0.8$ and $\alpha = 1.3$ are in fair agreement except for some deviations at $z/L = 0.3$. Upon closer inspection these largely consist of a superimposed shorter wave component with a length of about half the fundamental wavelength, which is of numerical origin. There is also a discernible short wave just preceding the bow wave.
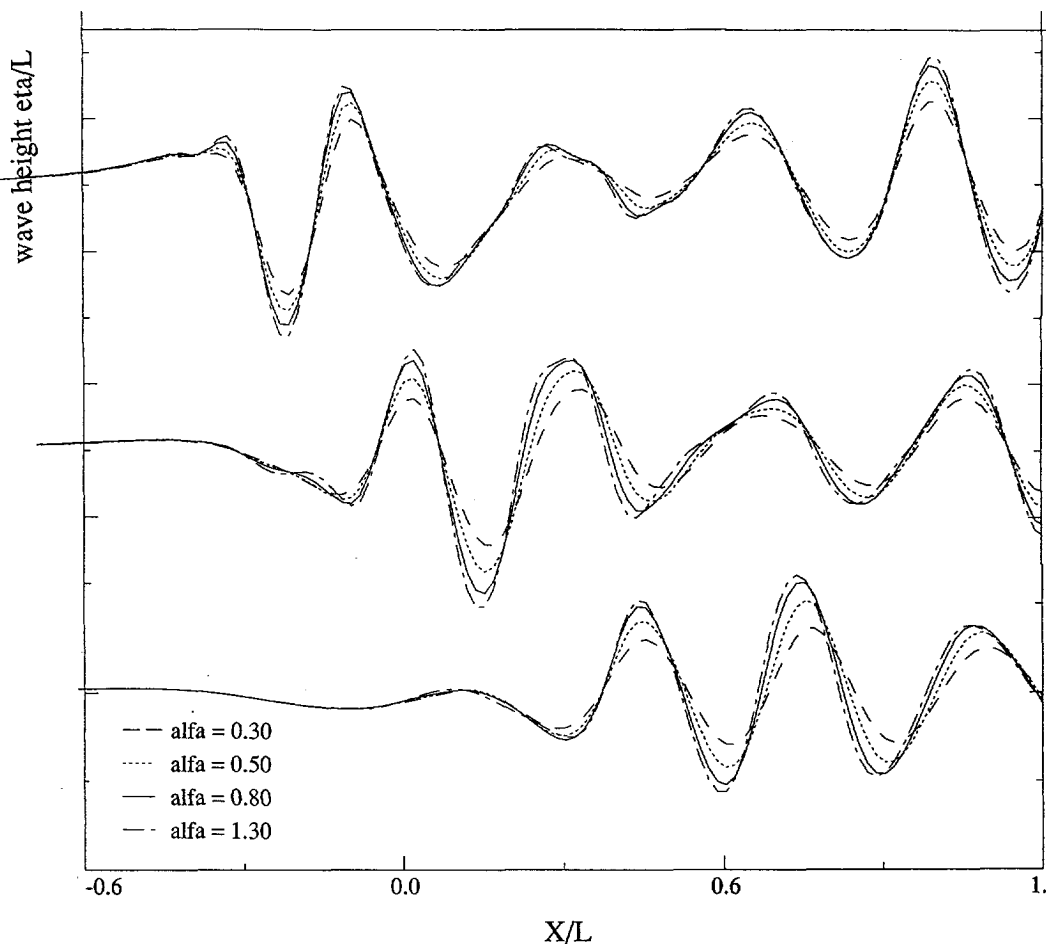
Figure 7.7: *Effect of panel elevation on wave pattern. Parabolic hull, L/B = 4 , Fn = 0.25 . Longitudinal cuts at z/L = 0.2, 0.3 and 0.45.*

What precisely its explanation is, is not yet known; but the reduced numerical damping together with the rather poor conditioning for large α apparently may lead to such spurious short waves in strongly nonlinear cases. In Section 6.4.6 we have seen that the source strength amplitude is determined by the panel elevation divided by the wavelength, rather than by α . This indicates that difficulties with matrix conditioning for increasing α will occur first for diverging waves, and maybe this is what we observe here. The resulting deviations do not occur too frequently and are fairly gentle and rather easily controlled; nevertheless the underlying slight instability is a point asking for improvement.

In all cases dealt with here the effect of variations of α (within the limits mentioned) on the resistance is fairly small, causing differences of a few percent. In other cases a greater sensitivity of the resistance has been detected.

The conclusions from these and other numerical tests are that:

- There is very little effect of α on the hull wave profile and on the resistance, for $0.5 < \alpha < 1.3$; There is some more effect on the waves away from the hull, in particular for strongly nonlinear and diverging waves;

- A value of $\alpha \approx 0.8$ gives accurate results and a good numerical stability in the great majority of applications; small variations of α around this value have no significant effect on the results;

- Experience tells that for α greater than about 1.3 (to some extent depending on the panel aspect ratio) numerical difficulties may arise due to a poorer conditioning of the algebraic equations, deteriorating convergence of the iterative procedure, or the occurrence of gentle short waves or transverse oscillations of numerical origin.

- For comparing in detail the wave patterns of different ships, a similar free surface panelling and the same value of α should preferably be used.

7.3.4   Effect of free surface panel density

model	Fn	Grid nr.	# FS strips	# panels/strip	$\lambda_0/\Delta x$	$\Delta z_1/L$
Wigley	0.316	I	14	84	25	0.0178
		II	17	136	40	0.0123
		III	24	169	50	0.0057
Parabolic $L/B = 4$	0.25	I	10	66	12	0.0157
		II	10	134	24	0.0157
		III	10	267	48	0.0157
		IV	15	134	24	0.0078
		V	21	134	24	0.0039
Series 60	0.316	I	10	79	20	0.0439
		II	10	157	40	0.0439
		III	20	79	20	0.0122
		IV	17	203	56	0.0172

Table 7.2: *Panel numbers and sizes used in study of panel density influence. Numbers are for one symmetric half. Δz_1 is the width of the free surface panels adjacent to the centreline; the strip width expansion ratio is 1.1 in all cases.*

Chapter 6 has theoretically analysed the effects of the free surface panel density on the accuracy of the results for a 2D linearised case. The true effects in real 3D nonlinear applications, and the effects of the transverse panel distribution, have been checked by test calculations on different grids, the densities of which are given in Table 7.2.
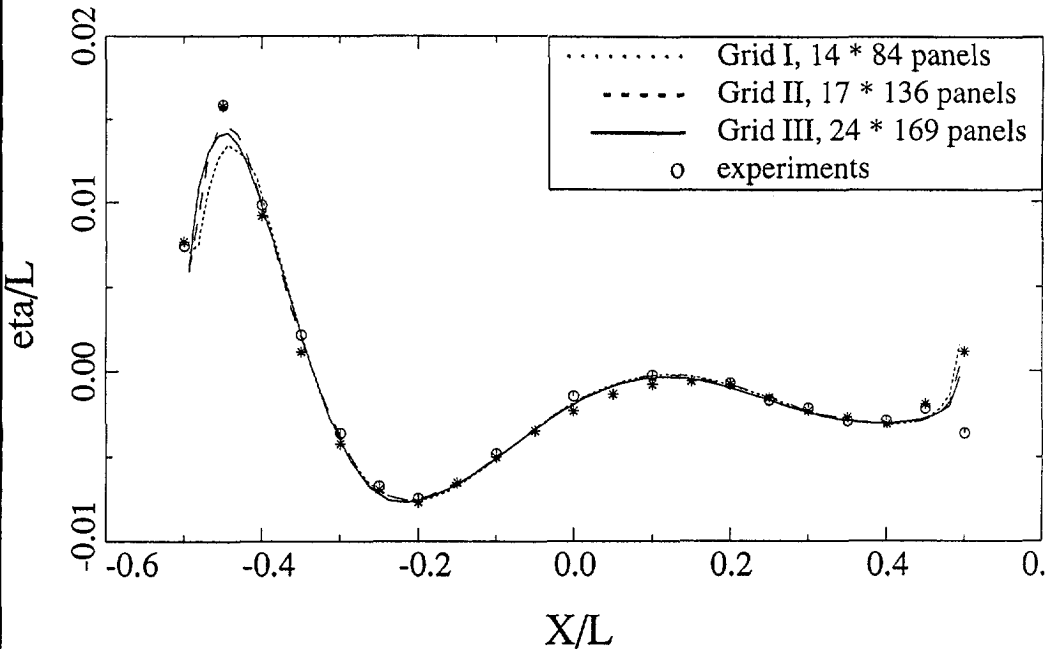
Figure 7.8: *Wave profile for Wigley hull at Fn = 0.316 , calculated with various free surface panellings, and experimental profile.*

The first test case again is the Wigley hull at *Fn* = 0.316. The hull panelling consists of 48 strips of 17 panels on each symmetric half. The three free surface panellings are all of equal extent and represent a simultaneous transverse and longitudinal refinement. As Fig. 7.8 shows, the wave profiles along the hull converge excellently, the three grids giving almost identical results in complete agreement with experimental data from the ITTC Cooperative Experimental Program, except for a slight underestimation of the bow wave height. It is noteworthy that the bow wave height does not continuously increase with panel refinement, but only is somewhat more sensitive to the local free surface panelling than other parts of the wave pattern.

Away from the hull a slightly larger grid dependence is observed. The longitudinal wave cuts in Fig. 7.9 show that the short wave disturbance found at *x/L* = 0.55 is insufficiently resolved by the coarsest grid and has some phase and amplitude differences even on the finest grids. The cause of this is that in a ship wave pattern diverging waves are present with wavelengths tending to zero, and complete grid independence will in principle never be achieved. Fortunately these very short wave components are meaningless for the resistance.

A significantly more critical case is the wall-sided parabolic hull with *L/B* = 4 at *Fn* = 0.25 , as introduced in the last section. Grids II, IV and V (Table 7.2) form a transverse refinement series in which the distance of the first row of collocation points to the waterline is twice reduced by one half. Fig. 7.10 compares the hull wave profiles. There is some deviation for the coarsest grid,
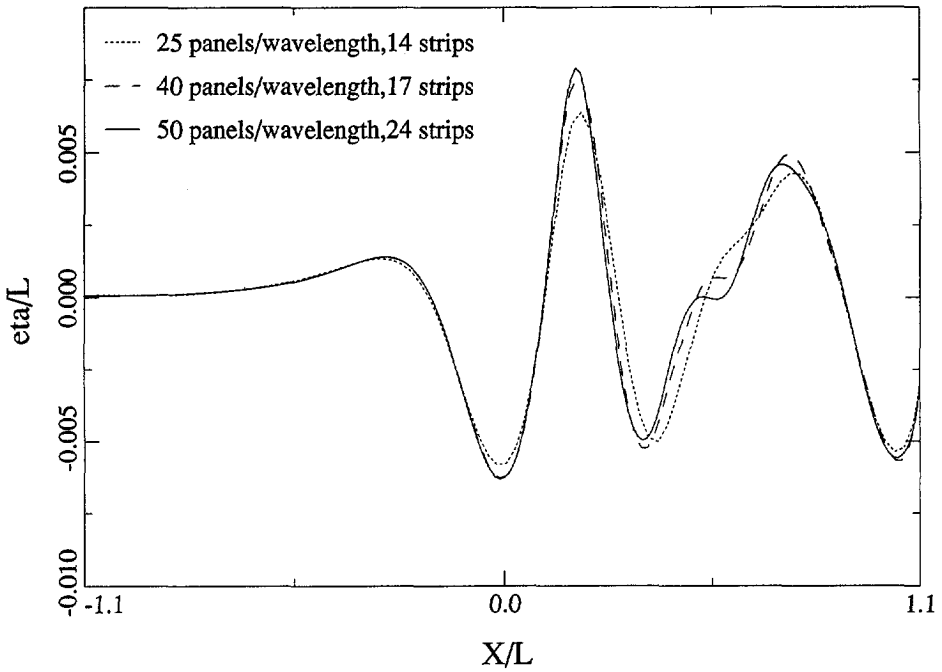
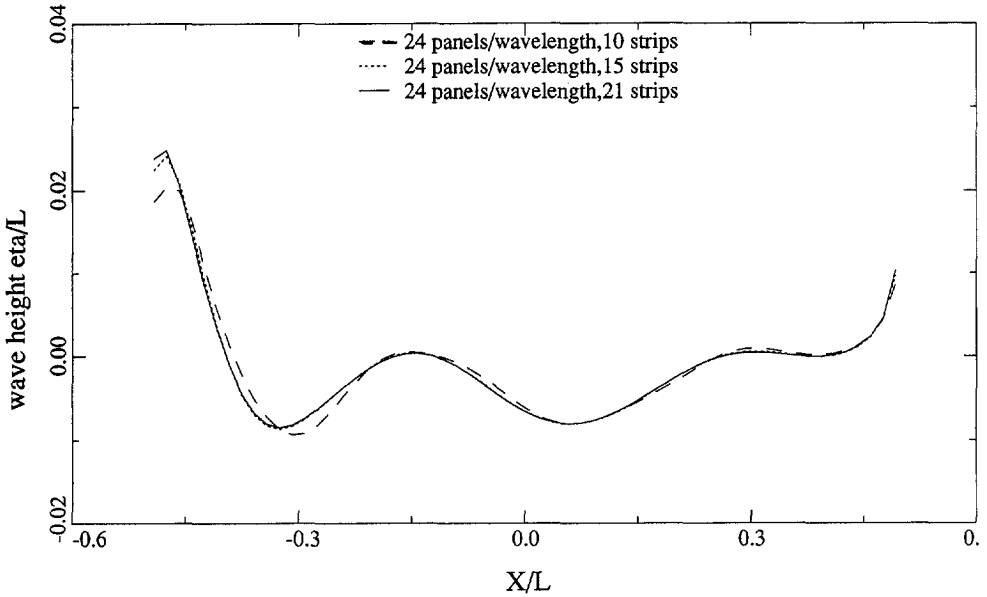Figure 7.9: *Longitudinal cut at z/L = 0.2 for Wigley hull with various free surface panellings.*

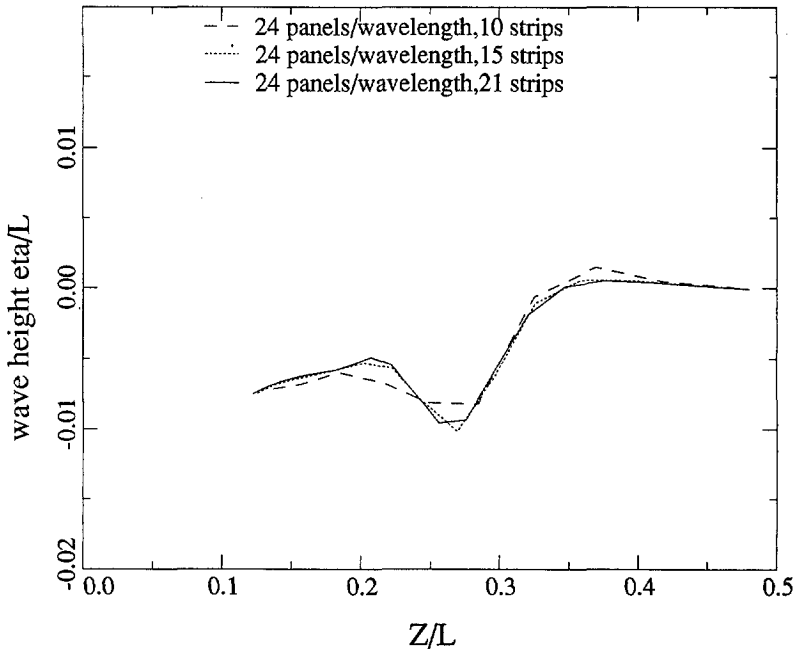Figure 7.10: *Calculated hull wave profiles for parabolic model with L/B = 4, with transverse panel refinement.*

Figure 7.11: *Calculated transverse wave cut at x/L = 0.1 , for parabolic model with L/B = 4, with transverse panel refinement.*

with a small underestimation of the bow wave crest and a slight phase lag; but the results for Grids IV and V are in complete agreement. There is again no indication at all of singular behaviour at the bow wave crest. Fig. 7.11 shows a transverse cut at $x/L = 0.1$ and provides no surprises; it appears that in this case 10 panel strips are insufficient to capture the details of the wave pattern. Predicted resistances on these grids differed by no more than 2 %.

An interesting finding from this study is that this very good convergence with transverse refinement is only obtained provided that α is kept constant, i.e. if the free surface panel elevation is scaled with the panel length and not with its width or the square root of its area. The latter in this case would require a reduction of y_{fs} with transverse refinement, resulting in a less systematic convergence of the result.[2] On the other hand, for the conditioning of the resulting system of equations the panel width is also important, and keeping y_{fs} constant while strongly reducing the panel widths will eventually cause numerical difficulties.

Grids I, II and III (Table 7.2) represent a longitudinal refinement series. We observe a reasonable convergence of the hull wave profiles (Fig. 7.12) for $x < -0.2$, with very little effect on the bow wave shape. Further aft however, the result on the finest grid deviates by the appearance of a slight disturbance with a wavelength (measured longitudinally) of about $\frac{1}{4}\lambda_0$ (where λ_0 is the transverse

---

[2]It is noted that most cases are less sensitive to y_{fs} than this particular one, and the requirement on y_{fs} is less strict.
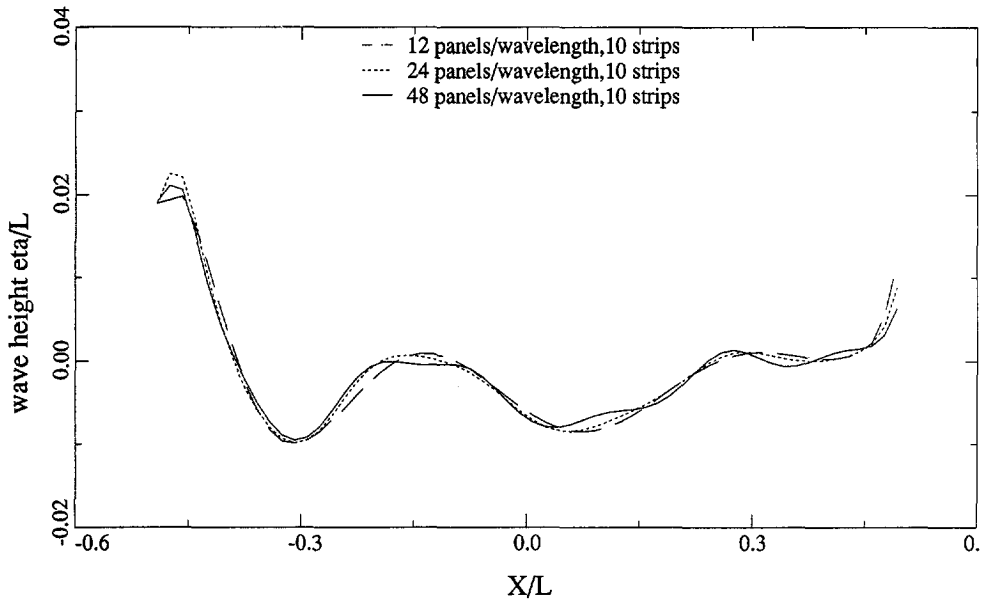
Figure 7.12: *Calculated hull wave profiles for parabolic model with L/B = 4, with longitudinal panel refinement.*

wavelength). The question arises whether this is a real physical phenomenon unresolved on all but the finest grid, or an instability turning up when the longitudinal step size is reduced and the associated numerical damping becomes insufficient. This question will be addressed below.

The longitudinal wave cuts at $z/L = 0.3$ (Fig. 7.13) illustrate that grid I is far too coarse, the result being affected by numerical damping and dispersion. The two fine grids give results in close agreement, except for a slight deviation at $x/L = 0.4$. This seems to correspond with the short-wavelength perturbation in the hull wave profile, suggesting the presence of a diverging wave progressing at an angle of around $75°$. This agrees with the dispersion relation for a wavelength $\lambda = \frac{1}{4}\lambda_0$ as observed at the waterline. This suggests that the perturbation is a physical effect rather than an instability.

The predicted resistance increased by 28 % when going from Grid I to Grid II, and a further 5.6 % from Grid II to Grid III. This illustrates how sensitive the resistance is for grid density.

The third example of a panel refinement study is the Series 60 $C_B = 0.60$ hull at $Fn = 0.316$. Grids I, II and III vary the density in longitudinal and transverse direction, Grid IV is an attempt to achieve optimum accuracy for given panel number. Fig. 7.14 shows some transverse cuts at various $x-$positions for the different grids. Also in this case transverse refinement has rather little effect except for a better resolution of transverse features. Longitudinal refinement however introduces some local irregularities that move outward and aft, quite similar to what happens for the previous case, and again the question arises whether this is an instability or a realistic wave component.
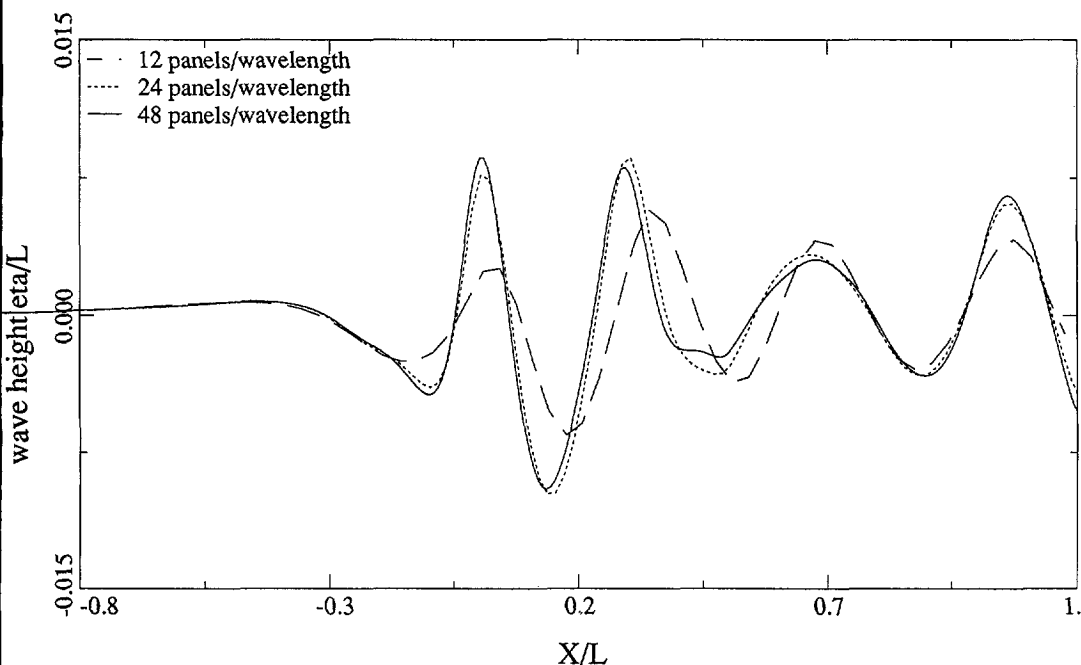
Figure 7.13: *Longitudinal cut at z/L = 0.3 for parabolic model with L/B = 4, with longitudinal panel refinement.*

For this case extensive experimental data are available [64] which permit to answer this question. The comparison with the data in Fig. 7.14 shows that this wave pattern "irregularity" is present in the physical experiment at exactly the same positions (such as $z/L = 0.22$ in the first cut, $z/L = 0.27$ and 0.33 in the second). Only the finest grid is able to reproduce these features. We conclude that in this case, and probably in the previous one as well, the change introduced by longitudinal panel refinement is not a symptom of numerical instability but is the eventual resolution of sharply diverging waves that are present in the actual wave pattern.

A longitudinal cut is shown in Fig. 7.15. Again transverse refinement (10 to 20 strips) makes little difference, while longitudinal refinement causes some increase of the wave amplitude remote from the hull due to the reduction of numerical damping, and eventually introduces some short wave components missing in the results on coarser grids. This short wave is at the right position but still has some distortion due to the marginal resolution.

The predicted resistance shows again a significant sensitivity to grid density. Longitudinal refinement here caused total variations of 8 %, transverse refinement up to 13 %. For this case a final test has been made to assess the effect of the hull panelling on the predictions. Refining it from 24 * 25 to 56 * 16 panels here causes no change whatsoever in the wave pattern, but a substantial change (12 % increase) of the wave resistance found from pressure integration over the hull. The dependence on the hull panelling thus is either caused by inaccuracies in the pressure integration
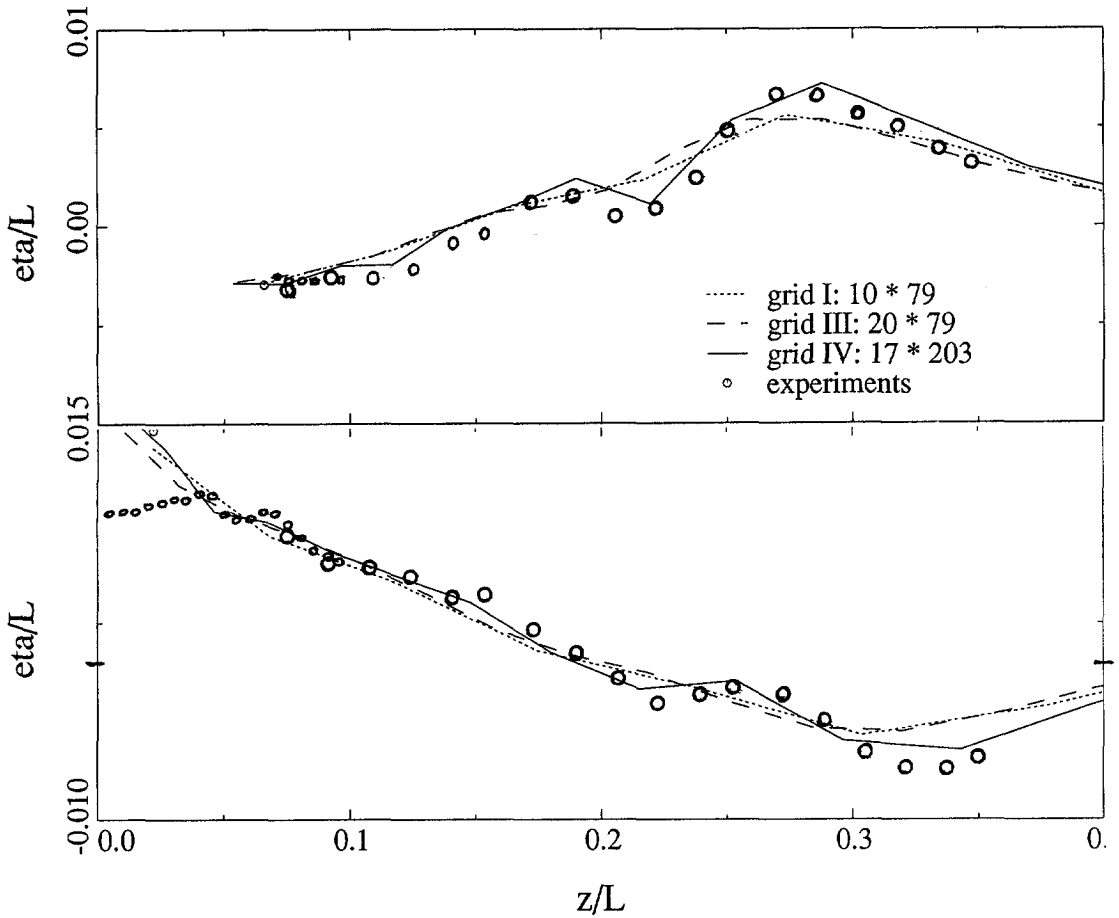
Figure 7.14: *Calculated and experimental transverse wave cuts for Series 60. x/L = 0.35 (top) and 0.60 (bottom).*

itself or by pressure changes that do not affect the wave pattern.

The conclusions from these numerical experiments are:

- In general a very good convergence of the wave pattern predictions with free surface panel refinement occurs; in this respect the method is superior to usual linearised methods with panels on the free surface.

- The panel length has a larger effect than its width, most likely due to its connection with the numerical damping introduced by the longitudinal difference scheme; certain short wave components may only be found on quite fine panellings.
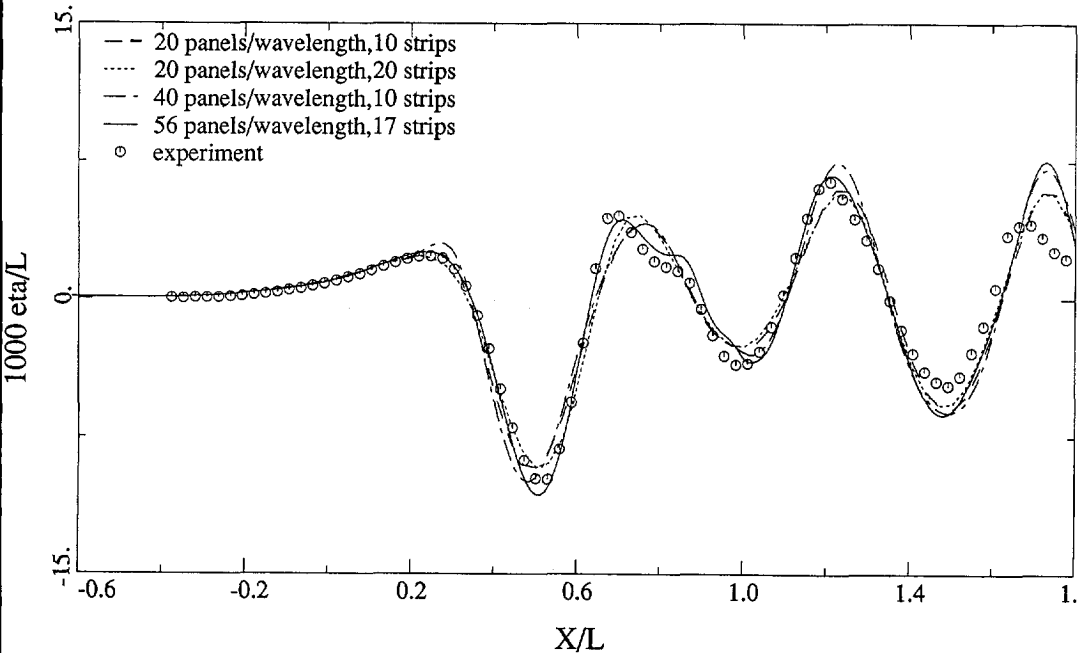
Figure 7.15: *Calculated and experimental wave cut at z/L = 0.1903 for Series 60 model at Fn = 0.316.*

- To obtain best grid-independence it is important to scale the panel elevation with the panel length rather than with its width or area.

- Panel refinement in the range tested here gives no indication of any singular behaviour of the solution near the bow.

- For accuracy of the predicted wave pattern, recommended minimum panel numbers are: 20 to 30 per fundamental wave length, and 10 to 15 strips over the usual domain width of half a ship length.

- The variations of the wave resistance with free surface panel density are significant. The good convergence of the wave pattern suggests that a better accuracy must be achievable.

- Requirements on the hull panelling come from the need to accurately resolve the hull pressure distribution and streamline direction and to obtain a good wave resistance, rather than from its effect on the predicted wave pattern.
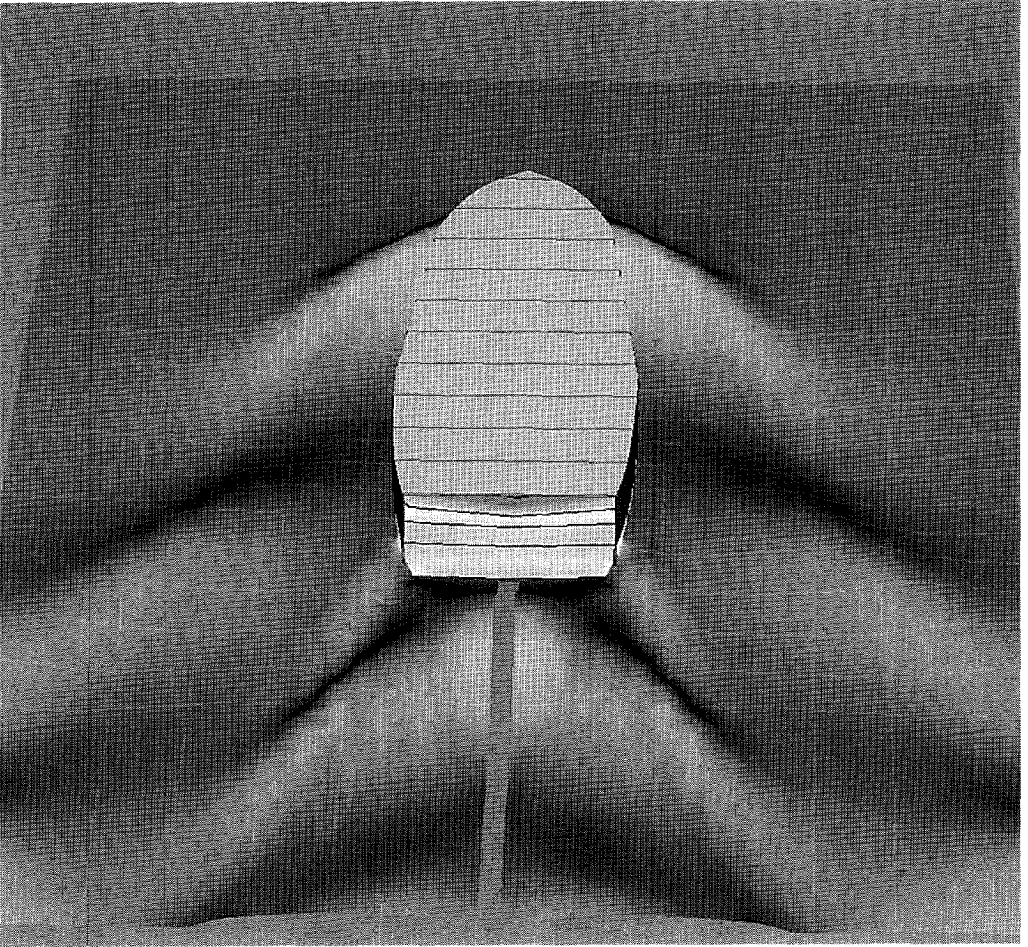
Figure 7.16: *The steep wave pattern of a harbour tug, as calculated by* RAPID

Chapter 8

Modelling the flow around transom sterns

The flow phenomena occurring for transom sterns, their mathematical modelling and numerical implementation are discussed. The accuracy of the numerical treatment chosen is studied.

The method as described in the previous chapter is adequate for ships with a cusped or rounded stern, but is not complete for the great majority of modern ships which have a transom stern, a truncated afterbody form ending in a flat transverse plate. For such stern shapes the free surface and flow often detach from the sharp lower edge of the transom, a behaviour that must be explicitly taken int account in the mathematical model.

The flow around the afterbody and off the transom plays an important role in the generation of stern waves. Linearised codes give rather poor indications on how to minimise these waves, since the modelling of transom flows is basically inconsistent with the linearisation assumptions and thereby incomplete. Therefore up to now this aspect had to be left out of account in practical design studies. But stern waves often represent a large part of the wave resistance, and for a nonlinear method the capability to handle transom flows therefore is of primary importance.

The present chapter discusses the physical phenomena playing a role in transom flows, studies possible mathematical models and their implementation, and describes a numerical validation of the aspects involved. Further validation by comparison with experimental data is provided in Chapter 9.
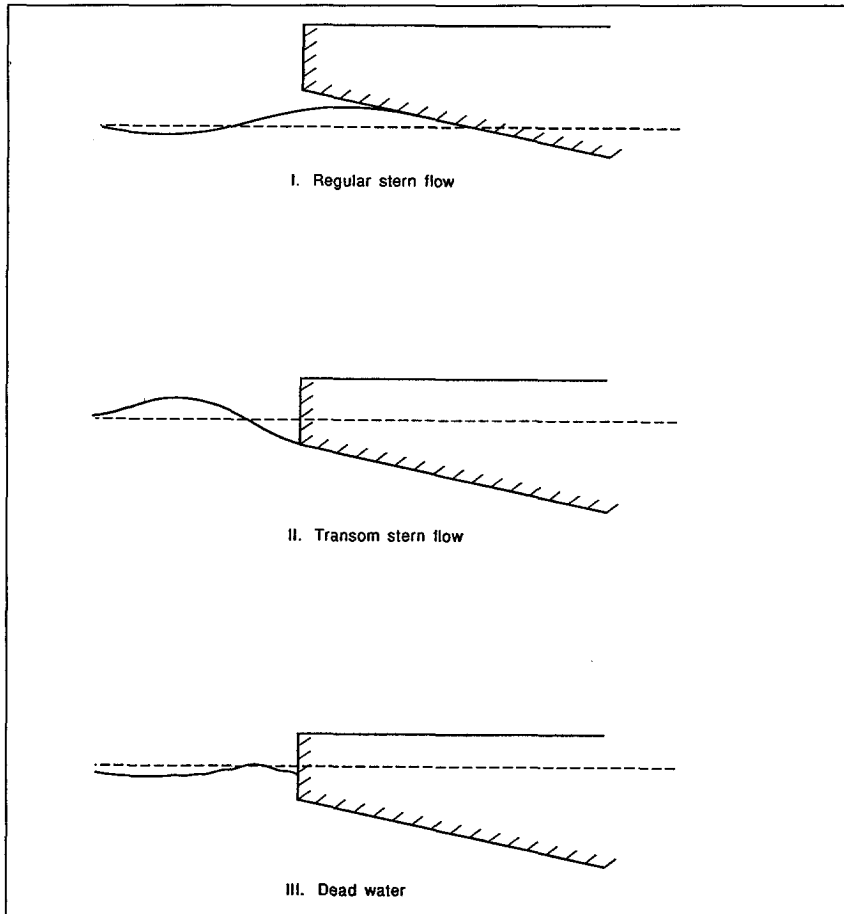
Figure 8.1: *Side views of possible flow regimes occurring at a transom stern.*

8.1   Physical Phenomena

For ships having a transom stern, three flow regimes may be distinguished, as sketched in Fig. 8.1:

1. The "regular" type of flow, which is similar to the flow past a cruiser stern. The lower edge of the transom is above the free surface and plays no role in the flow behaviour.

2. The "transom flow", as occurring for immersed transoms at a sufficiently high speed. The flow and free surface leave the hull along the lower edge of the transom. The transom itself remains dry.

3. The "dead water" type of flow, occurring for deeply immersed transoms at low speed. Behind the transom a region of separated, turbulent flow occurs, where the fluid essentially moves with the hull rather than with the ambient flow.

Which flow type actually occurs depends on the hull geometry and ship speed. Of course combinations of these flow regimes occur, with different types prevailing at different lateral positions.

Regular flow
Let us first consider what happens if the transom is at a relatively large distance above the undisturbed free surface. In potential flow, dependent on the hull form the last part of the actual waterline may be either a streamline that passes through the rear stagnation point, or the locus of points where streamlines leave the hull and continue on the free surface. At such a smooth detachment of the free surface from the hull, both the hull boundary condition and the two free surface boundary conditions must be satisfied.

The kinematic free surface condition and hull boundary condition together demand that the flow leaves the hull tangentially, unless the detachment is in a stagnation point. The dynamic free surface condition tells that the total pressure is zero (or rather, atmospheric) at the detachment point. Moreover, on the wetted part of the hull surface the pressure evidently must be positive. The latter requirement, and the condition that the flow does not immediately penetrate the hull aft of the detachment point, mean that also the *curvature* of the streamlines and free surface at detachment must be continuous and equal to that of the wall.

Although the detachment point is on the hull, an extra boundary condition (zero pressure) is to be satisfied there, so an additional degree of freedom must be present. This is the location of detachment. Suppose that we increase the draft of the vessel, or that the stern wave height increases because of e.g. an increasing ship speed. The location of the detachment point then adjusts to maintain a zero total pressure at detachment, most likely by moving aft.

Transom flow
If the detachment point shifts aft, at some moment it reaches the transom edge, and the flow regime changes into a transom flow. At the transom edge still the hull boundary condition and both free surface conditions are to be satisfied. Since a discontinuous vertical velocity is excluded here, again the two kinematic conditions tell that the slope of the free surface streamlines at detachment is equal to that of the hull streamlines. But the freedom in the location of the detachment point is lost, and the question poses itself how the dynamic free surface boundary condition (zero pressure) can still be satisfied at the transom edge.

However, an important difference with the smooth detachment case is that the curvature of the streamlines at detachment is no longer fixed: at the transom edge the hull curvature is infinite, there is no chance that the free surface penetrates the hull after detachment, and consequently the curvature of the streamlines is free. This is the degree of freedom permitting satisfaction of the dynamic boundary condition.

To make the total pressure zero the hydrodynamic pressure must cancel the hydrostatic pressure:

$$Cp_{dyn} = -Cp_{stat} = \frac{\rho g \eta_{tr}}{1/2 \rho U_\infty^2} = -2/Fn_{tr}^2 \qquad (8.1)$$

where $-\eta_{tr}$ is the depth of the transom edge below the still water level and $Fn_{tr} \equiv U_\infty/\sqrt{-g\eta_t r}$ is the Froude number based on that depth. For a transom edge below the still water level the hydrostatic pressure is positive, the hydrodynamic pressure must be negative, which in most cases is achieved by an upward curvature of the flow immediately aft of the transom edge, resulting in a more or less marked "rooster tail". For a transom high above the still water level a positive hydrodynamic pressure is required, and the wave surface curves downward upon leaving the transom edge. But if the transom height is too large, the pressure may fall below atmospheric pressure already at some point ahead of the transom edge, and the free surface detaches earlier, leading to a regular flow.

Since mathematically the sudden transition from a hull boundary condition to a free surface condition at a sharp corner may well introduce some kind of singularity, the precise behaviour at the transom edge is something to be further examined.

Dead-water flow
For a further increasing transom depth or for decreasing speed the required hydrodynamic pressure coefficient at the transom edge increases in absolute value, and the upward curvature of the streamlines must increase. A very steep forward face of the wave aft of the transom results, eventually giving rise to a spilling breaker following the transom at a short distance. At still lower speed or greater draught this closes upon the transom and forms a dead-water zone, in which viscous flow separation occurs at the transom edge. The streamline curvature is moderate, nevertheless the pressure in the dead-water area is relatively low due to viscous head loss.

The reverse sequence of phenomena, the transition from a dead-water flow to transom flow, is of interest as well. For increasing speed the water level depression connected with the low pressure behind the transom will eventually make the dead-water region disappear; a transition entirely determined by viscous effects, not by wave breaking (that seems to govern the transition from transom flow to dead water flow). Although this suggests that the reverse transition might occur at a different speed, in reality the unsteadiness in wave breaking and turbulent flow will probably remove such a "hysteresis".

The transitions between the various flow regimes are practically relevant, as a dead-water region is to be avoided, and a transom that is at a too high position as well. Expression (8.1) tells that the transom Froude number Fn_{tr} is an important nondimensional parameter determining what flow type will occur; according to a rule-of-thumb [65], transition from dead-water flow to transom flow often occurs at $Fn_{tr} \approx 4 - 5$. But the shape of the transom and afterbody, and the wave system generated by the entire hull, are important as well and can make this rule entirely useless. In addition, in several cases the viscous boundary layer along the hull affects the flow off the transom, most likely favouring the dead-water type of flow.

It is evident that a dead-water flow regime cannot be modelled in inviscid flow unless by crude ad-hoc assumptions; and that there is no obvious way to determine whether or not a certain flow will give rise to dead water or to a transom flow. Only the regular and transom flow can be appropriately represented in a potential flow method.

Below, after a critical examination of some previous proposals for transom flow modelling, I shall motivate the choice made in RAPID, and discuss its implementation and a numerical examination of its validity.

8.2   Literature survey

Some analytical studies on the details of the flow off transom sterns have been published, and we shall consider these first in order to identify requirements for a numerical modelling.

Vanden-Broeck [66]
considers the flow off the transom stern of a 2D semi-infinite body with a flat bottom. The nonlinear solution is obtained by a semi-analytic approach. It is demonstrated that in inviscid flow there are two distinct flow patterns in this case: one with the flow rising along the transom up to a rear stagnation point, another with the flow detaching from the transom edge. The latter appears to exist only for $Fn_{tr} > 2.23$; the former is the only possible one for lower speeds but it becomes physically unrealistic at higher speeds.

Schmidt [67]
solves the problem of the flow off a twodimensional semi-infinite afterbody with a more general shape, applying a flat-ship linearisation. Both a smooth detachment (regular flow) and detachment from a sharp corner (transom flow) are considered. The expressions derived for the pressure on the hull and the wave elevation in the vicinity of the detachment point are :

$$p(x) = \rho U_\infty^2 C_2 |x|^{1/2} + \mathcal{O}(x^{3/2}) \quad , \quad x \uparrow 0 \tag{8.2}$$

$$\eta(x) = \eta_{tr} + \eta_x(0).x + \frac{2}{3} C_2 x^{3/2} + \mathcal{O}(x)^2 \quad , \quad x \downarrow 0, \tag{8.3}$$

where $x = 0$ is in the detachment point and x is positive aft.

For a smooth detachment $C_2 \geq 0$ because the pressure must be positive on the entire wetted part of the hull; but $C_2 > 0$ would lead to a solution in which the free surface penetrates the hull immediately. Therefore, $C_2 = 0$, a condition which determines the location of the detachment point. It follows that in 2D flow at a smooth detachment $p_x = 0$, and that the curvature of the streamlines is equal to that of the hull, in agreement with our physical description above.

For a transom flow, C_2 generally is nonzero, and a mildly singular behaviour at the transom results. The wave slope is

$$\eta_x(x) = \eta_x(0) + C_2 x^{1/2} + \mathcal{O}(x) , \tag{8.4}$$

so the free surface leaves the bottom of the hull tangentially but its curvature tends to infinity at the detachment point. Similarly the pressure derivative p_x on the hull has a square-root singularity at the transom edge.

Tulin and Hsu [68]

A paper often cited in the context of modelling transom stern flows is that of Tulin and Hsu [68], which deals with high-speed displacement hulls with transom sterns. The method proposed extends the 1957 paper by Tulin [69] on the planing of slender surfaces at high speed. The hull is supposed to be slender, which permits to approximate the 3D potential flow by the solution of a sequence of 2D Laplace problems in transverse planes. In the high-speed limit the appropriate linearised free surface boundary condition is $\phi_x = 0$. On the major part of the free surface this is simply $\phi = 0$, for which an implementation using an inverse mirror image of the 2D potential field above the still water surface presents itself.

In a flat-ship linearisation appropriate to planing surfaces, the flow can then be modelled using a vorticity distribution on the waterplane of the hull and becomes analogous to *slender wing theory*, a simplified treatment of the flow about wings with very low aspect ratio; see e.g. [70]. For high-speed displacement hulls Tulin and Hsu do not make a flat-ship approximation, and must take into account the hull boundary condition on the sides of the hull. A particular aspect of their theory, again inspired by slender-wing theory, is that a specified transverse velocity is required on the free surface in the "rear shadow" of the hull aft of the section of maximum waterline beam, in order to model the smooth flow along the waterline of the afterbody required by the hull boundary condition. The use of the inverse mirror image above the still water surface translates this transverse velocity boundary condition into a given vorticity distribution on the relevant part of the free surface, which extends aft with constant strength. An additional hull vorticity distribution is used to cancel the resulting normal velocity on the hull. Aft of the transom both vorticity distributions are retained. The resistance obviously is connected with this vorticity, the only trace the ship leaves at infinite Froude number, and it tends to a nonzero limit for $Fn \rightarrow \infty$ unless the waterline slope at the transom is zero. The comparisons with experimental data do not permit verification of this curious result, or of the dependence on the waterline slope in general.

The paper points out the analogy of this treatment of the flow past the afterbody, with the way a Kutta condition is imposed in slender-wing theory. In that case usually the assumption is made that no lift is generated on the part of the foil aft of the location of maximum span. This requires that the potential and transverse velocity field generated at the section with maximum span is retained for all stations downstream — which is achieved by keeping the same boundary vorticity. For flat foils this velocity field satisfies the boundary condition on the aft part of the foil, being parallel to the camberplane; and there is no pressure jump across the foil, because all longitudinal gradients vanish, making the pressure equal to zero. Thus in slender-wing theory a sort of Kutta condition is satisfied, albeit one that is insensitive to the geometry of the trailing edge. As opposed to this, in the method of Tulin and Hsu [68] longitudinal gradients do not vanish aft of the location of maximum waterline beam, because of the effect of the hull boundary condition and hull source distribution. But they do vanish aft of the transom where the flow in transverse planes is determined by the shed vorticity only. Therefore the pressure in general is nonzero along the afterbody, and jumps

to zero at the transom edge. The sudden disappearance of the hull source distribution also causes a discontinuity in the transverse velocities and a non-tangential flow off the transom edge.

It can be concluded that the method does not strictly model a condition of smooth flow off the transom edge, and the geometry of the transom has only a quite indirect effect on the flow. This approximation may be justified for $Fn \rightarrow \infty$, but does not provide any further insight into the *details* of the flow off transom sterns, which are of importance at finite Fn. This is at variance with earlier statements by others [72], in which in particular the role of vorticity in the "Kutta condition" modelling has been misunderstood.

Linearised methods, standard approach
We shall now consider previous implementations of transom flows in practical calculation methods. Almost all of these address linearised free surface conditions. It is noteworthy that they consistently meet conceptual difficulties in the linearisation of the free surface conditions just behind the transom, in prescribing tangential flow and zero pressure at the detachment point, in determining the double-body flow for a non-closed body with open transom, and in calculating the resistance. In DAWSON a model has been implemented that works fairly well for a class of transom flows but is subject to the same objections. Most other linearised methods seem to follow a similar approach, although the precise forms of the conditions imposed at the transom edge and their implementation vary.

The principle of implementing transom flow conditions in a linearised Rankine source method is, to add a special free surface panel segment behind the transom; and to impose modified free surface boundary conditions in the first collocation points behind the transom, obtained by using known values at the transom edge, rather than unknown values in an upstream free surface collocation point. Different, largely equivalent ways of arriving at these known values are used, all based on the requirement that the free surface detaches from the transom edge, leading to a prescribed velocity magnitude there; and that the flow must be tangential, and approximately aligned with the double-body flow or longitudinal direction. Representative for this conventional approach in linearised methods is the paper by Cheng [71]. A basically similar modelling is advocated by Nakos and Sclavounos [17], who state that, while the condition of zero pressure at the transom edge is not explicitly enforced, their experience, and that of many others, indicates that it is well satisfied in practical calculations. Information on the accuracy of the predicted flow off the transom is hardly available for these methods.

Reed and Telste [72, 73]
proposed somewhat different treatments. In [72] they invoke the analogy of a condition of smooth flow off the transom edge with a Kutta condition at an airfoil trailing edge. Based on this analogy they claim that trailing vorticity is an important aspect in transom flows, and motivate this by referring to the paper by Tulin and Hsu [68]. Our discussion of that paper above indicates that this argument is invalid, the vorticity being connected with the use of an inverse mirror image in the virtual domain above the free surface rather than with a physical phenomenon.

They propose two alternative approaches. The first one computes a distribution of Havelock sour-

ces on the hull from the usual Neumann-Kelvin problem, and then adds a hull dipole distribution plus a trailing dipole sheet starting at the transom edge, the strength of which is solved from the required longitudinal velocity at the transom edge. But the effect of the dipoles on the flow was found to be small in the cases considered, and the comparison with experimental data was poor.

The other method uses Rankine sources and dipoles on hull and free surface. Also the transom is covered with panels on which a condition of prescribed longitudinal velocity is imposed. The same condition is used as well in the difference scheme in the free surface condition, and to fix the trailing dipole strength. Evidently this threefold use of the same condition results in an almost singular matrix, and one of the three is to be dropped. The method finally selected happens to use only transom panels and no trailing dipole sheet, as opposed to the claimed physical significance of the latter.

Reference [73] presents a continuation of this work. While still the importance of trailing vorticity is stressed, the method actually used does not incorporate any trailing vorticity inside the flow domain. The method is of Greens identity type, so it uses surface potential and normal velocity as unknowns. The free surface section behind the transom now is a cylindrical surface extending aft from the transom edge, and linearisation of the free surface condition is carried out with respect to this surface. Again, the linearisation itself appears to be a major source of difficulties in the treatment of transom sterns. The results presented are significantly better than those in [72], but this is due to better numerics rather than to a better transom flow modelling.

Söding, Bertram and Jensen [74] model transom flows in their steady nonlinear method in a different way. Unlike most others they cover the transom with source panels. In the corresponding hull collocation points they impose a normal (longitudinal) velocity of a magnitude such that according to the dynamic condition the wave elevation matches the transom immersion. Since *no finite difference scheme is used in the method, the geometry of the free surface panelling is* relatively free, and no special transom strips are added. The approach seems rather crude and does not model any particular condition on the flow direction at the transom edge. How it performs in actual applications seems not to have been published.

Coleman and Haussling [45, 46]

have done important work on transom flows, addressing the unsteady problem of the transom flow for an impulsively started semi-infinite ship afterbody with constant or varying section. Their method has already been outlined in Section 5.2.2. Nonlinear transom flow problems are considered in [45] and [46]. Early flow detachment is catered for by checking whether the pressure remains positive on the wetted part of the hull and adjusting the latter if required. The method is quite complete and produces plausible results. For 2D cases remarkable agreement with the analytical results of Vanden-Broeck was obtained concerning the non-existence of transom flow for low Fn_{tr}. In those cases the time-dependent calculation was terminated upon the occurrence of vertical wave slopes, indicative of the onset of wave breaking.

It is to be noted that in none of the numerical methods described in this section any attention has been payed to the precise behaviour of the flow at the transom edge. E.g. the infinite streamline

curvature found by Schmidt is discretised away in Coleman's method by mapping the wetted part of the hull and the free surface onto the same coordinate plane. The square-root singularity in the pressure however is indicated by their numerical results (Fig. 5 of Ref. [45]).

8.3   Mathematical Modelling

From the literature survey there thus appears to be some confusion about the proper modelling of transom flows. In the first place, several difficulties are encountered in imposing transom conditions in linearised methods, in general terms explained by the fact that this basically is inconsistent with the linearisation. Linearisation assumes that the variation of the hull shape near the undisturbed waterline is small; i.e. a small curvature, and in slow-ship theory also a small slope of the sections and buttocks. Only then the exact position of the hull - free surface intersection has a negligible effect on the flow and linearisation is permitted. However, at a transom edge the hull curvature is infinite, and we want to have a *particular* hull - free surface intersection; an inconsistency causing recurring difficulties. Also the significance of double-body flow for a non-closed surface is quite doubtful, and using this flow as the basis for linearisation is rather objectionable. These difficulties are amplified by the fact that in many transom flows large nonlinear effects occur due to the large gradients and vertical velocities. Most of these difficulties and ambiguities disappear as soon as we adopt a fully nonlinear treatment of the boundary conditions.

Secondly, there appears to be disagreement on the possible role of trailing vorticity. Reed et al [72, 73] claim vorticity to be quite important but fail to demonstrate so; Tulin and Hsu [68] employ boundary vorticity distributions but in an entirely different context; and most other methods use only source distributions and produce equally plausible results. This has to be resolved before setting up a nonlinear treatment.

Main incentive to use vortex wakes has been the apparent overspecification of the problem caused by the unclear role of the dynamic condition at the transom edge; and the vague analogy of transom conditions with a Kutta condition for an airfoil, which also imposes an extra condition on the flow at a sharp corner. But an important distinction is that for a lifting body the circulation provides an additional degree of freedom, while for a surface-piercing transom stern hull no circulation can exist.

To illustrate this, let us consider twodimensional flows first. For an airfoil the flow domain is multiply connected, and the solution is not uniquely specified unless the circulation is prescribed through a Kutta condition. This fixes the direction in which the flow leaves the trailing edge and thus selects one solution from the infinite set.

But for the flow around a two-dimensional surface-piercing body the flow domain is bounded by the hull and the free surface which is attached to the transom edge. Therefore the domain is singly

connected, and there cannot be any unknown circulation around the body.[1]

Also, the so-called Kutta condition at the transom edge has a totally different meaning. Without that condition there is no infinite set of solutions satisfying all boundary conditions, but just two: the flow that moves up along the transom and leaves it at a stagnation point, and the flow that leaves the lower edge of the transom tangentially. There is no freedom in the direction of the flow at the transom edge, since any non-tangential flow off the edge would give a kink in the streamline and thus either a stagnation pressure or an infinite negative pressure at detachment, both violating the dynamic condition. Therefore, *the tangential flow off the transom edge is the only transom flow existing, the problem is completely posed and any additional Kutta condition is fundamentally superfluous.*

In a three-dimensional case the situation is similar. For a wing, spanwise vorticity is again present, continuing into trailing longitudinal vortices at the tips. But for the surface-piercing body there does not seem to be any reason why the three-dimensionality would suddenly introduce spanwise vorticity which is not there in 2D; consequently there is no longitudinal vorticity generated in this way either. Moreover, *if* trailing longitudinal vorticity would be generated, this would start at the transom edge, i.e. on the free surface, so it would remain on the free surface; on the boundary of the fluid domain therefore. There is no cut in the domain, no additional degree of freedom, and the boundary vorticity has no physical effect on the flow field in the domain at all.

Therefore, in my opinion the use of a trailing vortex wake for transom flows, although perhaps numerically helpful in some models, cannot be given any *physical* meaning, and vortex or dipole distributions *inside* the fluid domain are fundamentally wrong in this case. I have selected an implementation using source distributions alone.

The next important question is what the precise behaviour at the transom edge will be. As pointed out above, little attention has been given to this in previous methods. But there are two indications that care may be needed. One comes from free streamline theory, as applied to e.g. the cavity or wake flow behind a flat plate at large incidence. Although the neglect of gravity may well affect some of the conclusions, free-streamline theory tells that the flow leaves the edge tangentially, but with infinite curvature. The other indication is the paper by Schmidt [67] discussed above, which for the flat-ship linearised problem comes to very similar conclusions. Although the details may be a consequence of the necessary simplifications and linearisation, both theories suggest that a more or less singular behaviour at the edge may result.

---

[1] Adding a virtual domain above the free surface is of mathematical rather than physical meaning and does not affect the uniqueness of the potential in the real fluid domain.
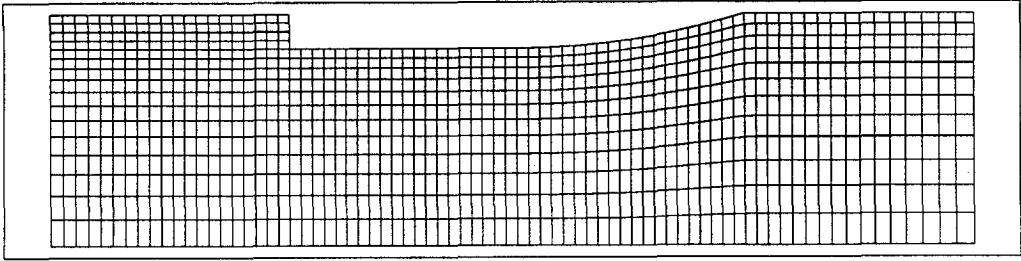
Figure 8.2: *Example of free surface panelling for transom stern hull*

8.4   Implementation

We shall now discuss the implementation of transom conditions in the nonlinear method. This has largely been patterned after the method used already for several years in the DAWSON code but avoids many of the inconsistencies inherent in linearisation of transom flows.

In the hull panelling the transom is left open. The free surface panel distribution is matched to the transom stern by the addition of a few extra strips of panels aft of the transom (Fig. 8.2). One might think of imposing transom conditions in points right at the transom edge; but with the usual constant-strength source panels on the hull the velocity field is singular here in the discretised formulation. Therefore transom conditions are to be imposed in the first row of collocation points aft of the transom, and are to be based on velocities in collocation points rather than on velocities at the transom edge itself.

The free surface condition to be imposed in these first points aft of the transom requires a special treatment. The kinematic condition contains the term η_x. For all other free surface points this is expressed in the wave elevations η in the point considered and in a few upstream points by a difference scheme. These η's are then expressed in the velocities by means of the dynamic condition. In this process any arbitrary pressure added to the dynamic condition drops out; in other words, the combined form actually means that in a free surface collocation point the velocity must be parallel to the *isobar surface* passing through that point, but the pressure corresponding to that isobar surface is eliminated. The wave elevation is only retrieved afterwards from the dynamic free surface condition.

This approach cannot and should not be applied for the first points aft of the transom. The velocities at the transom edge may not be used, as mentioned above, nor those in the last hull collocation points since these do not correspond with a wave height. In addition the elimination of the pressure would make it impossible to impose any condition on the wave elevation at or near the transom itself within each iteration, and the free surface would most likely start somewhere at the transom face.

Therefore I impose a modified condition that the velocity must be directed along a (curved) line from the transom edge (x_{tr}, η_{tr}, z) to the wave surface at the position of the first collocation point, $(x_{tr} + \Delta x, \eta, z)$. Two alternatives have been tried:

- The behaviour according to Schmidt [67], (8.3), which yields for the wave slope at a distance Δx aft of the transom edge:

$$\eta_x = \frac{3}{2}(\eta - \eta_{tr})/\Delta x - \frac{1}{2}(\frac{\partial y}{\partial x})_{hull}, \qquad (8.5)$$

in which η_{tr} and $(\partial y/\partial x)_{hull}$ are the height of the transom edge above the still water level and the buttock slope at the transom, at the corresponding distance z off the centreline;

- A simple Taylor expansion in the transom edge point:

$$\eta_x = 2(\eta - \eta_{tr})/\Delta x - (\frac{\partial y}{\partial x})_{hull}. \qquad (8.6)$$

The former has been derived from a flat-ship linearisation and is, therefore, not necessarily appropriate here. The second formulation is more generally applicable to regular behaviour aft of the transom edge.

This simple modification applies to the first points of the free surface strips aft of the transom. For the second points, in the free surface condition the same three-point difference scheme is used as everywhere else. This involves again the transom edge height. For all downstream points no modification is needed. Exactly the same treatment is applied in the determination of the slope of the base surface in each iteration, H_x.

We have seen earlier that mathematically two valid solutions of the problem exist: a stagnation point flow and a transom flow. The treatment outlined here guarantees that some kind of transom flow is obtained. The free surface streamline computed comes from the transom edge to within the discrete approximation used, and upon panel refinement the solution converges towards a tangential flow off the transom edge. Otherwise there would be a kink in the streamline at the transom edge, which would cause a pressure peak; the imposed zero pressure in the first free surface point excludes this for vanishing panel size.

In principle the zero-pressure condition at the transom edge is not imposed directly, and the question might arise whether any residual pressure, connected with an erroneous streamline curvature, could be there. In our numerical validations this possibility will be indirectly checked by comparing the two above expressions for η_x, which for given η differ in the terms determining that curvature. But anyhow $p = 0$ in all collocation points on the free surface streamlines that originate from the transom edge. Panel refinement then may be supposed to force also the pressure at the transom edge towards zero, any fixed residual pressure otherwise requiring a pressure gradient of $\mathcal{O}(1/\Delta x)$ along the first part of the free surface streamline.

In any case our implementation formally is as accurate as one may expect from a discretised method. How appropriate it is in practice for finite panel sizes can only be deduced by numerical experimentation. This will be performed in the next section.

Although basically the nonlinear treatment of the transom conditions is similar to the linearised treatment in DAWSON, it is a significant advantage that the nonlinear terms and transfer terms are fully included. These can be very large, in particular for low transom depth Froude numbers, when large vertical velocities and large free surface curvature occur near the transom. Moreover, since the nonlinear method imposes the exact free surface boundary conditions, we can be more confident that the physical mechanisms governing the transom flow are fully included.

8.5 Results

The implementation chosen leads to an excellent convergence of the iterative procedure. As the transom edge is a fixed point in the result, very large errors in the dynamic and kinematic boundary conditions are found initially if one starts from a flat free surface. But the fact that this point is fixed also appears to stabilize the results locally, and convergence usually presents no problem at all.

The possibly weakly singular behaviour of the solution at the transom edge in a 3D nonlinear case forces to carry out careful grid refinement studies. In addition, the importance of the assumptions made on the flow behaviour at the edge will be studied.

8.5.1 Longitudinal grid refinement

For the panel refinement study the test case (Fig. 8.5) is a mathematical hull form with $B/L = 0.15$, $T/L = 0.05$, rectangular sections with a rounded bilge; parabolic waterlines in the forebody; an afterbody that is prismatic up to $x = 0.25$ L, and has an upward bottom slope of $9.1°$ aft of this point. The Froude number is 0.40 and the transom immersion 0.01 L. Consequently $Fn_{tr} = 4.0$, which in reality may be just sufficient to make the flow clear the transom and thus produces the steepest wave. In this study, 4 free surface panel strips aft of the transom, and 10 next to the hull, were present on each side of the symmetry plane.

The general appearance of the wave pattern is displayed in Fig. 8.3. Fig. 8.4 is a close-up of the transom area, illustrating the rooster tail and the sharp diverging waves originating near the corners of the transom. Fig. 8.6 shows the predicted free surface shape and vertical velocity aft of the transom on the line of collocation points closest to the centreline, for hull and free surface panel lengths of 0.05 L, 0.025 L and 0.0125 L respectively. The heavy line in the left figure represents the location of the transom edge and the slope of the hull bottom. The marker in the right figure indicates the vertical velocity at the edge as found from dynamic condition and buttock slope.
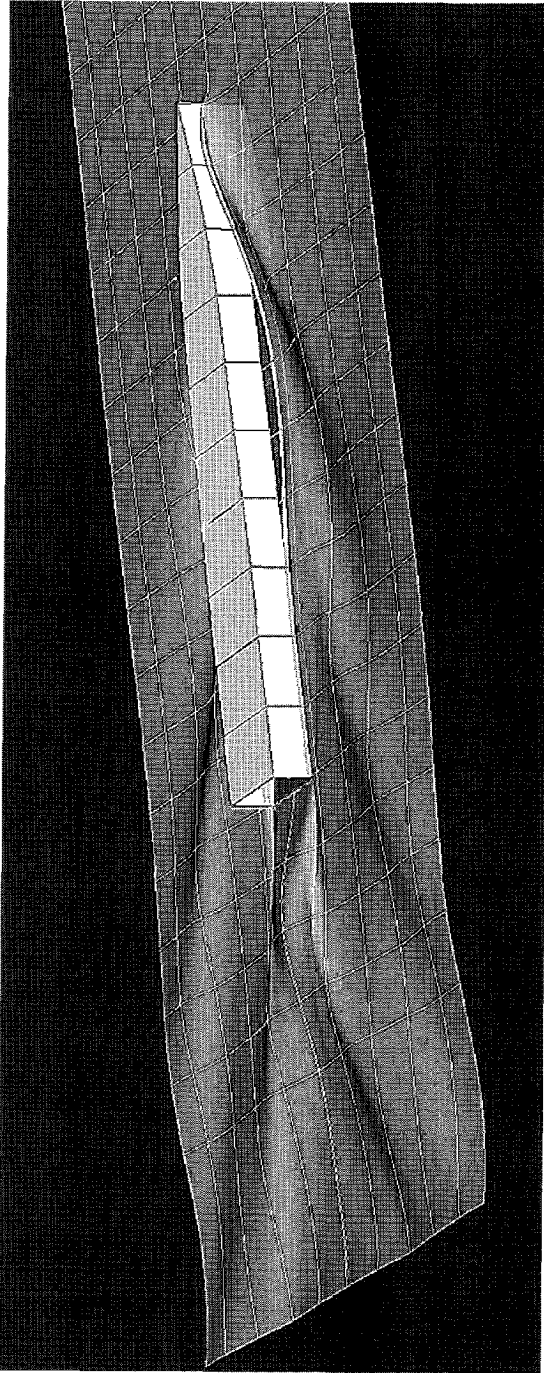
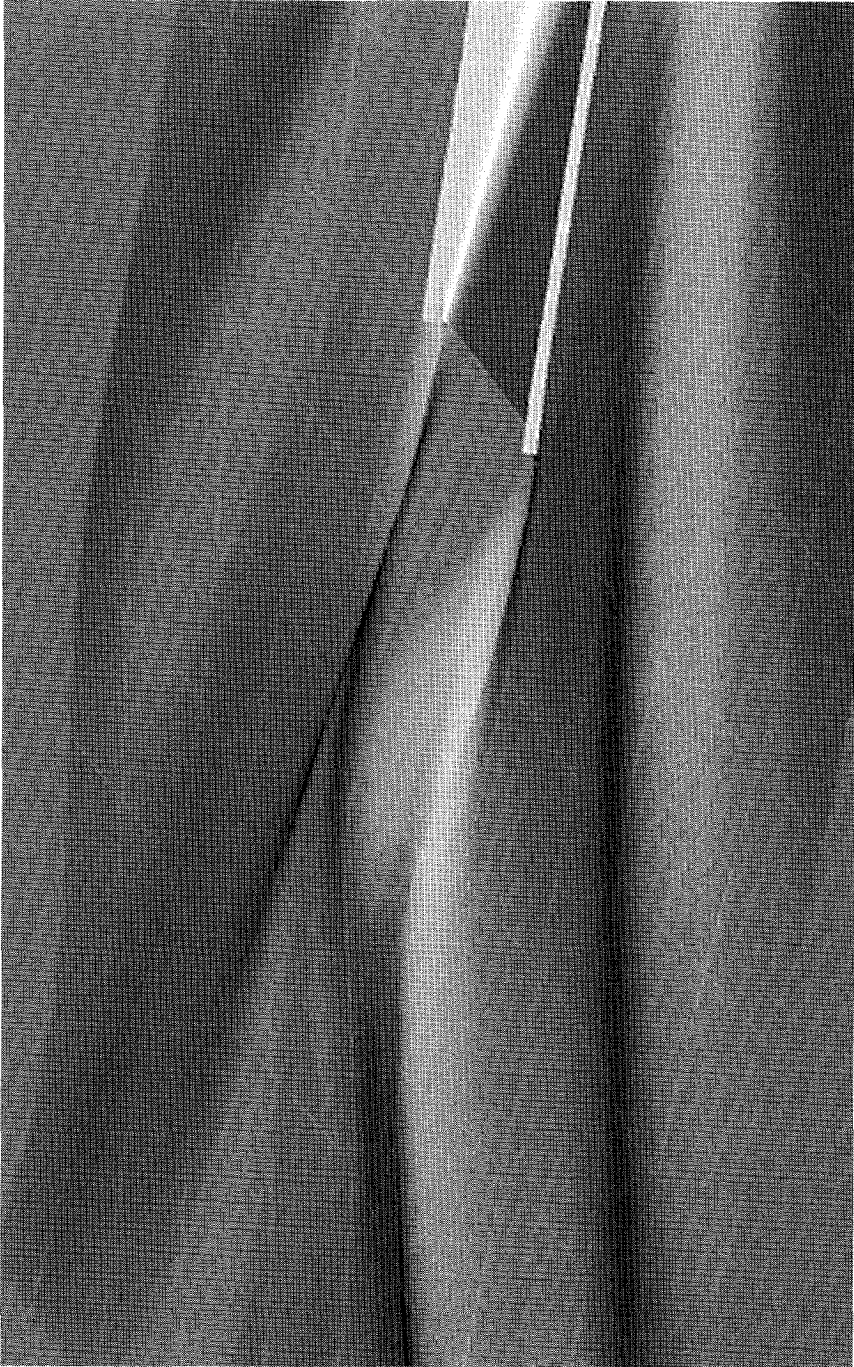Figure 8.3: Calculated wave pattern for transom stern hull. $Fn = 0.4$, $Fn_{tr} = 4.0$.

Figure 8.4: *Close-up of flow off the transom stern.* $Fn = 0.4$, $Fn_{tr} = 4.0$.
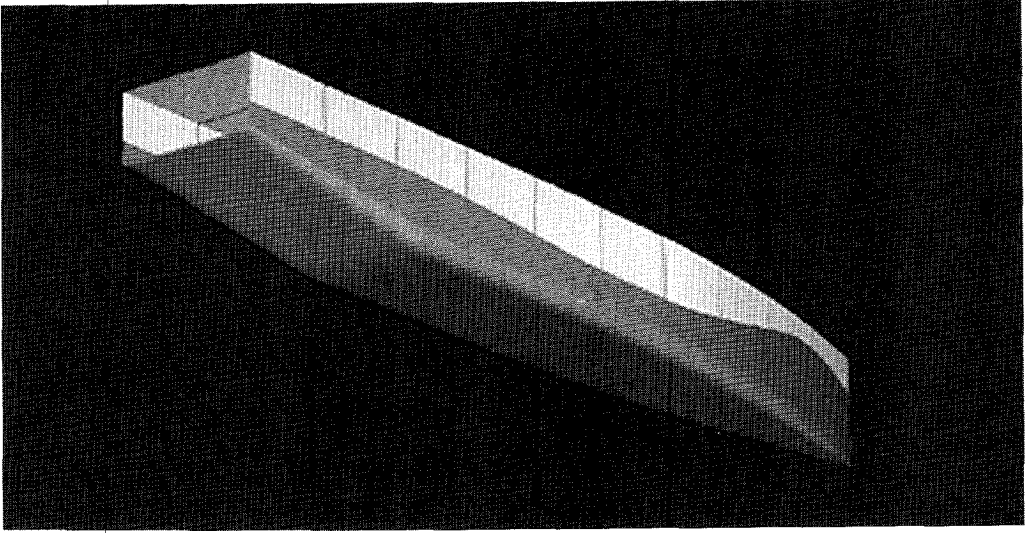
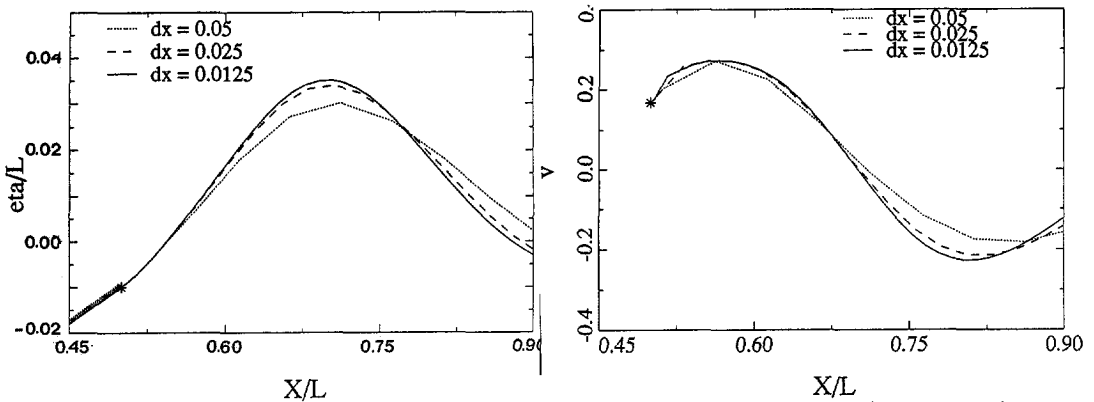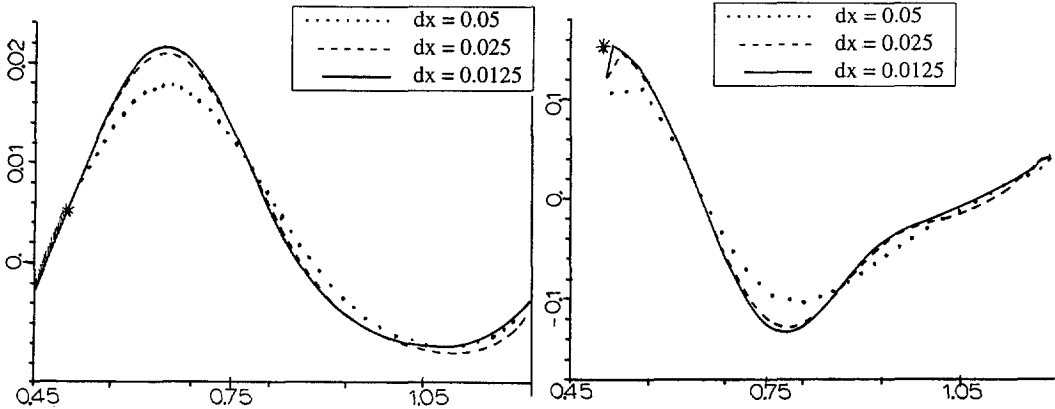Figure 8.5: *Transom stern hull form for test calculations.*

Figure 8.6: *Effect of longitudinal panel refinement on wave profile (left) and vertical velocity (right) aft of a transom stern. Fn = 0.4 , η_{tr} = −0.01 , Fn_{tr} = 4.0 . Transom edge located at X/L = 0.5 .*

It is obvious that the calculated flow is absolutely smooth, and that the free surface very precisely originates at the transom edge. This strongly suggests that the pressure at the transom edge actually vanishes as it should. Also the vertical velocity matches the theoretical value quite accurately, indicating that the desired tangential flow is obtained. The convergence of the wave profile and vertical velocity for decreasing panel size is very good, and there is hardly any difference between the two finer panellings. In particular the behaviour just aft of the transom is perfect.
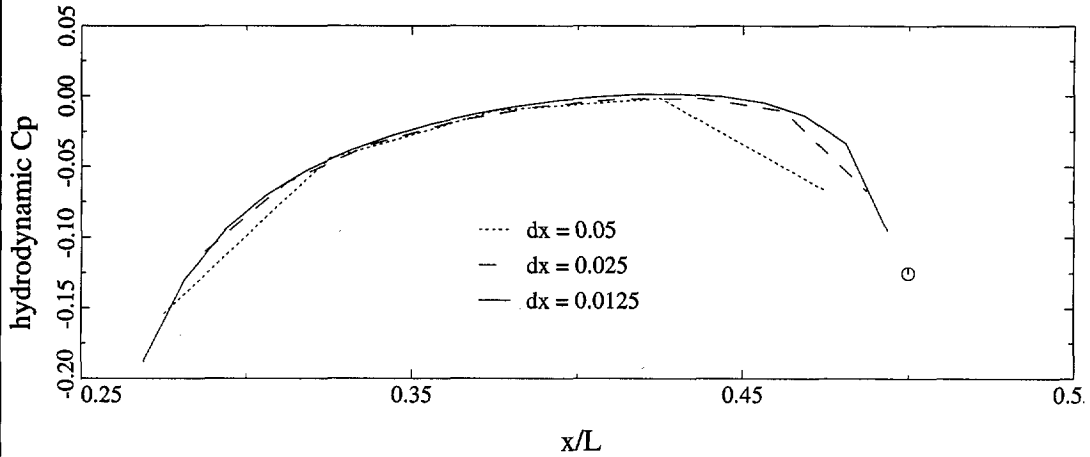
Figure 8.7: *Effect of longitudinal panel refinement on hull pressure distribution along the centre-line.* $Fn = 0.4$, $Fn_{tr} = 4.0$. *Marker indicates pressure at transom edge according to dynamic condition.*

Figure 8.8: *Effect of longitudinal panel refinement on wave profile (left) and vertical velocity (right) aft of a transom stern.* $Fn = 0.4$, $\eta_{tr} = +0.005$. *Transom edge located at $X/L = 0.5$.*

Fig. 8.7 shows the convergence of the hydrodynamic pressure distribution on the aft part of the hull upon panel size reduction. The only significant changes occur on the very last part of the hull near the transom edge, where a large and still incompletely resolved pressure gradient is found, reminiscent of the singular behaviour derived by Schmidt, eq. (8.2). But these variations of the local pressure gradient appear to have no significant effect on the wave pattern.

A similar study for the same model with reduced draft and the transom edge at $0.005L$ above the still water surface is illustrated in Fig. 8.8. We observe the downward curvature of the free surface necessary to produce a positive hydrodynamic pressure at the transom edge. The convergence of

the wave profile is again perfect, that of the vertical velocity as well except for a peculiar deviation of the value in the first collocation point. This puzzling behaviour has been carefully analysed, and the explanation has been found in the inconsistency of using hull panels on the hull surface itself in combination with raised free surface panels. At the transom edge the effect of the hull panels is sharply cut off, but that of the free surface panels increases only more or less gradually, resulting in a local deficit of the vertical velocity. However, it could be demonstrated that the effect of this deviation is quite small and restricted to the immediate vicinity of the transom edge, and is, therefore, of no concern.

As longitudinal panel refinement has very little effect on the solution, we can be confident that the exact free surface conditions are accurately satisfied in all points on the free surface (not only the collocation points) in the nonlinear solution.

8.5.2   Flow behaviour at the transom edge

Because of the possibility of a weakly singular behaviour of the solution at the transom edge, longitudinal panel refinement could in principle give convergence towards an erroneous solution, in particular one having a small residual pressure at the transom edge. As argued before, the uncertainty is in the terms of $\mathcal{O}(x^{3/2})$ or higher, which determine the streamline curvature and pressure increase or decrease at the transom edge. But the difference between the results obtained with the Schmidt- and the Taylor expression for η_x, (8.5) and (8.6), which differ precisely in these terms, was only quite local and too small to be distinguished on the scale of the plots. Subtracting the two expressions we then find that $C_2 x^{1/2}$ must have been relatively small. In other words, with the discretisations used the curvature contributions to η_x in the first collocation points appear to be negligible, and we may conclude that this detail of the modelling is not too important and is very unlikely to lead to an erroneous solution globally. At the same time it means that the main streamline curvature, which makes the pressure at the transom edge vanish, is well resolved in our calculations. Thus the method proposed may be supposed to be adequate, as the smoothness of the results already suggest.

Which flow model is more appropriate is hard to say. Fig. 8.6 suggests that $\partial v/\partial x$ might tend to infinity upon panel refinement, and might assume the square-root behaviour following from the Schmidt theory. Similar behaviour is observed for the hull pressure in Fig. 8.7.

8.5.3   Transverse refinement

In 3D cases some particular effects might occur at the edges of the transom. If the sides of an immersed transom are vertical, the free surface leaves the transom with infinite transverse slope. Physically, what probably happens is that at the sudden end of the sidewalls a condition of zero pressure is to be satisfied, which again requires that the hydrostatic pressure is cancelled by a
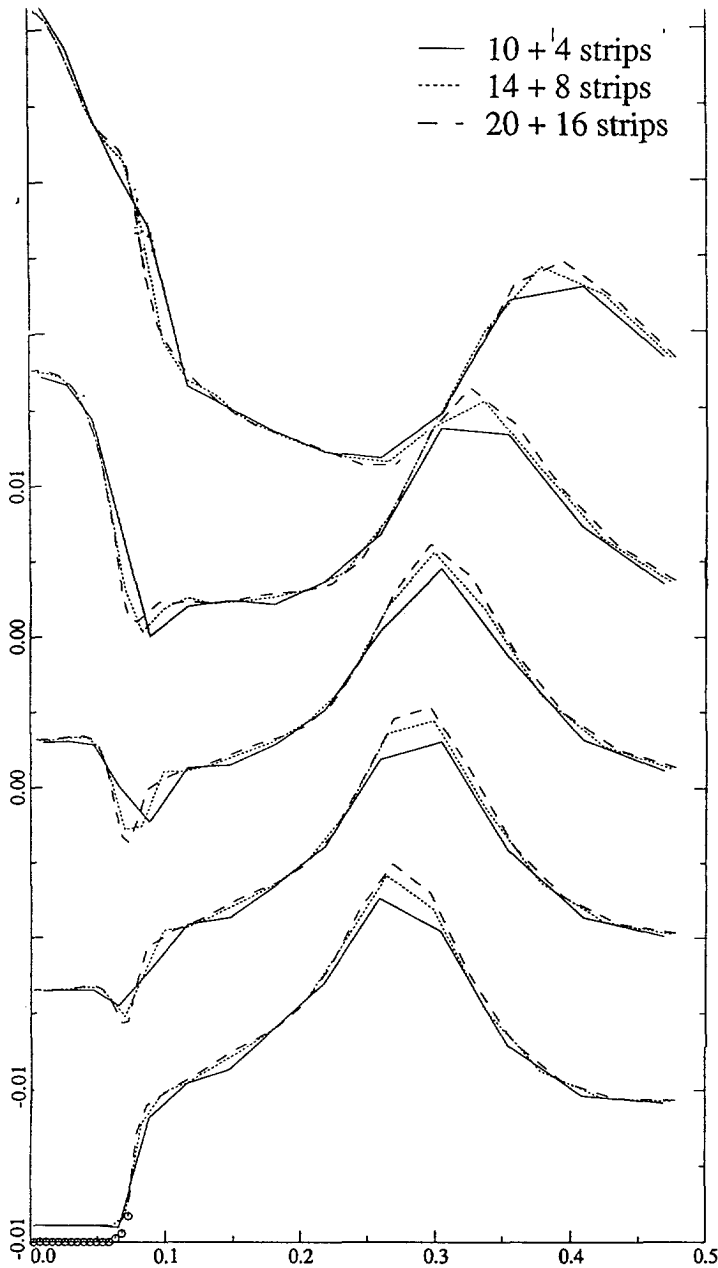
Figure 8.9: *Transverse cuts through the wave pattern aft of the transom, with transverse panel refinement.   Fn = 0.4 ,   Fn_{tr} = 4.0 . Transom at x/L = 0.5 , cuts at x/L =* 0.5063,   0.5313,   0.5562,   0.6062 *and* 0.7062 *(bottom to top).   The markers at the bottom of the figure represent the transom cross section.*

negative hydrodynamic pressure. This can be achieved by the flow curving inward in the direction of the centreline, similar to the upward curvature at the horizontal parts of the transom edge. At the deeper parts of the transom this inward curvature must be larger than near the waterline, and consequently the vertical wave slope is quickly eliminated. However, wave breaking effects may change the picture, and a sort of slight "ridge" on the free surface moving inward from the transom edge may frequently be observed.

The vertical wave faces and variable inward curvature clearly cannot be represented in our method. Transverse wave slopes are determined from finite difference schemes, and remain finite by definition. To identify the effect of this inaccuracy on the results I have carried out calculations for the same test case at $Fn_{tr} = 4.0$ with successive transverse refinement; using 4, 8 and 16 strips aft of (one half of) the transom, with 10, 14 and 20 strips next to the hull, respectively. Thus on the finest grid the panel width aft of the transom is 0.5 % of the ship length, 3 % of the beam.

The series of transverse cuts in Fig. 8.9 in the first place shows how much quicker the evolution of the flow is aft of the transom than further outside; a fact that justifies the particular attention given to transom flows in this chapter. On the finer grids, the cross section through the wave pattern directly aft of the transom accurately reproduces the shape of the transom itself (indicated by the markers). Further aft the shape of the transom is more or less inverted, the smaller immersion at the rounded corners of the transom leading to a smaller upward curvature of the streamlines and a slower rise of the free surface. Going further aft this effect gradually disappears.

The effect of transverse refinement generally is small. At the first stations aft of the transom the transverse wave slopes increase. Transverse refinement gives a more accurate description of the transom shape and therefore a more pronounced effect of the corner. But further downstream very little effect remains from the poorer resolution on the coarser grids. At $x = 0.7$, at the crest of the rooster tail, the maximum wave height predicted is about equal for all grids, and the difference between the two finer grids is quite small throughout.

Therefore we conclude that there are no indications of any major effect of insufficient resolution of the flow around the corners of the transom. Whether all the physics of the flow are fully represented by our model of course cannot be shown in this way.

8.5.4   Comparison with linearised results

It is interesting to see how the linearised and nonlinear method represent the effect of the transom depth on the predictions. The draft of the test model is varied to obtain the transom heights - 0.02 L, -0.01 L, 0., 0.008 L and 0.015 L (positive is above the still water level). Fig. 8.10 shows the wave profile on the centreline behind the transom predicted by RAPID and by the linearised code DAWSON, which uses a similar transom modelling but which misses all nonlinear effects. The nonlinear predictions have a somewhat higher and steeper stern wave; the greater the transom immersion, the stronger the nonlinearity. But, fortuitously or not, the several nonlinear
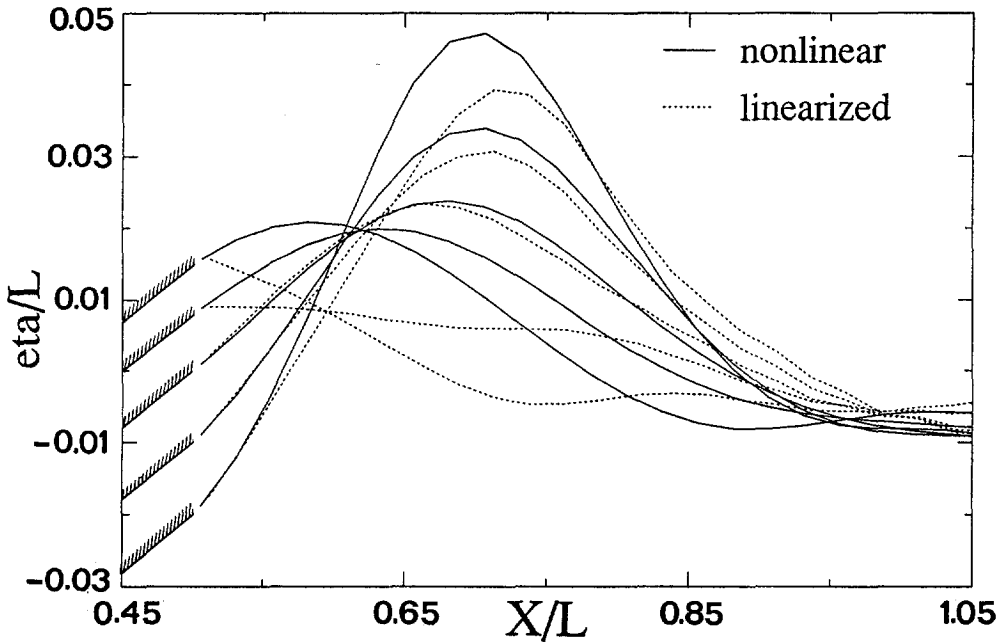
Figure 8.10: *Calculated stern wave profile for varying transom edge height, for linearised and nonlinear method. Fn = 0.4 .*

contributions, each very large for the large gradients and the large vertical velocities occurring (up to 40 % of the ship speed), appear to cancel to a substantial extent; the difference between DAWSON and RAPID is therefore relatively moderate, up to 20 % in maximum wave height in this case.

For the cases with the transom *above* the still water level however, the differences are much larger. While in RAPID the height of the rooster tail continuously changes for decreasing draft, in DAWSON the rooster tail suddenly disappears and the free surface starts with an incorrect slope as soon as the transom edge comes above the still water line. The explanation is that in a linearised method the hull must be cut off at the still water level. If the transom is above that level, the hull panelling ends at some point ahead of the transom, and no boundary condition can be imposed between that point and the transom. Because of the double-body linearisation and the symmetry with respect to the still water level, the vertical velocity on this part of the water surface then is zero, and the free surface slope aft of the transom correspondingly is quite small.

The same tendencies are found in the predicted wave resistance (Fig. 8.11). For DAWSON a contribution

$$F_{stat} = \frac{1}{2}\rho g \int \eta_{tr}^2 dz \qquad (8.7)$$

has been added, which in an ad hoc fashion accounts for the absence of hydrostatic pressure on the transom. This correction apparently has been introduced by M.S. Chang [75] in the context
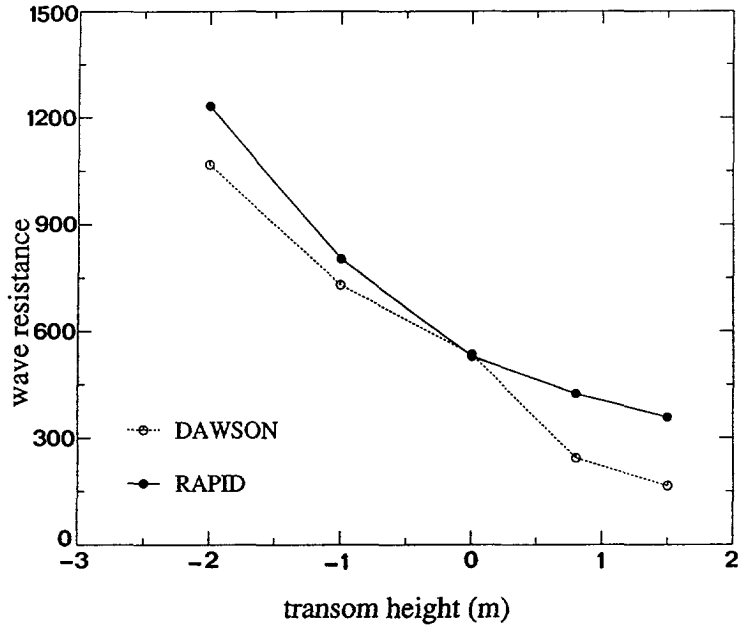
Figure 8.11: *Wave resistance against transom edge height; linear and nonlinear method. Fn =* 0.4 .

of another linearised method. Although entirely inconsistent, the correction (which here is up to 30 % of the resistance) appears to bring the resistance fairly close to the nonlinear result (which does not require such a correction because the total pressure is integrated over the actual wetted surface). At zero transom immersion the two predictions are almost equal. The cases with transom above the still water surface again show a deviation in the DAWSON results.

8.5.5   Limits of the transom flow regime

Earlier the question was raised to what extent the transitions to the other flow regimes (dead water and early detachment) are indicated by the nonlinear calculations. But obviously for increasing transom immersion the transition to a dead-water flow regime is not indicated, as neither viscous effects, nor a criterion for the inception of wave breaking are included. Consequently there is a range of transom heights for which the code erroneously predicts a smooth flow off the transom. It is interesting to see what happens if the transom immersion is further increased.

As mentioned before, Vanden-Broeck [66] found that, at least for the simple 2D case he considered, a transom flow mathematically exists only for $Fn_{tr} > 2.23$. For comparison I made calculations for a flat-bottomed finite-length *threedimensional* ship. For decreasing Fn_{tr} it becomes harder

and harder to arrive at a converged solution, and for this case no solution could be found below $Fn_{tr} = 1.77$. The first wave crest aft of the transom then had grown to 94 % of the stagnation height. A sort of limit on Fn_{tr} as a matter of fact seems to be there, and the difference with that of Vanden-Broeck most likely has to do with the threedimensionality which permits additional energy transport by diverging wave components. [2]

The other extreme situation is that of early detachment of the free surface for a transom high above the still water surface. If a transom flow is assumed, such detachment is indicated in the calculations by the pressure along the bottom of the hull falling below zero. In that case, in the calculations a regular flow type is to be assumed instead. The program logic currently prevents the RAPID code to make this switch without user intervention.

8.6   Conclusions

The following main conclusions on the modelling of the flow off transom sterns can be drawn:

- Previous methods to deal with transom flows have often been hampered by the inconsistency of imposing transom conditions in a linearised method, leading to all kinds of conceptual difficulties. The nonlinear modelling of transom flows results in a more straightforward, more complete and more reliable formulation.

- Without any "Kutta condition" imposed at the transom edge the problem is already completely posed by the hull and free surface boundary conditions. The use of trailing vorticity *inside* the flow domain to model the smooth flow off the stern is fundamentally wrong. Vorticity on the free surface is of mathematical rather than physical meaning and the present source-only formulation works equally well.

- While theoretical studies indicate a weakly singular behaviour of the flow at the transom edge, this has little effect except locally. The numerical solutions obtained are quite smooth, converge well upon grid refinement and are fairly insensitive to the assumptions on the precise behaviour. Therefore the method proposed here most likely is adequate.

- For the cases studied also the results of the linearised method appear to be quite reasonable for all *immersed* transoms, with a moderate deviation due to nonlinear effects; but transoms above the still water level, definitely the most common type of stern for cargo vessels, require a nonlinear method. Consequently the RAPID code is more generally applicable and in principle permits optimisation of the transom immersion and stern shape throughout the

---

[2]It is interesting to note that the Fn_{tr}−limit in 2D is directly related to the maximum possible energy flux out of a control volume moving with the hull, in 2D periodic waves, which is $\dot{E}_{max} = 0.0200\rho c^5/g$ per unit span (Ref. [80], Epilogue part 2); where c is the wave propagation velocity. For a 2D semi-infinite body the wave resistance is simply the hydrostatic contribution, $R_w = 1/2\rho g\eta_{tr}^2$ per unit span. The energy supplied to the flow can only be carried away by waves if $R_w.c < \dot{E}_{max}$, which immediately leads to: $Fn_{tr} > 2.236$.

practical range of true transom flows. However, care is needed since the occurrence of a dead-water flow is not indicated by the calculations.

Experimental validations of the transom flow modelling will be discussed in the next chapter.

Chapter 9

Experimental validations

The wave pattern and wave resistance predicted by the nonlinear method are compared with experimental data for a range of cases, to study the accuracy of the results in practice. Some comparisons with predictions by a linearised method are made as well.

Having established the level of numerical accuracy of the solutions, analytically in Chapter 6 and by numerical tests in Chapters 7 and 8, we shall now make comparisons with experimental data in order to assess the actual validity and usefulness of the method. At the same time some of the differences between predictions by linearised and nonlinear methods will be illustrated.

model	Fn	# hull panels	# FS strips	# panels/strip	$\lambda_0/\Delta x$	$\Delta z_1/L$
Wigley	0.316	816	24	169	50	0.0057
Series 60	0.316	896	17	203	56	0.0172
Container ship	0.236	763	18 + 4	165	28	0.0110
DTRC 5415	0.25	432	16 + 4	232	24	0.0225
DTRC 5415	0.4136	432	16 + 4	127	32	0.0281
Quapaw	0.3197	264	15	220	32	0.0351
Frigate	0.292	1108	14 + 5	120	27	0.0236
Frigate	0.3844	1108	14 + 5	120	46	0.0236
Frigate	0.4613	1108	14 + 5	88	53	0.0236

Table 9.1: *Panel numbers and sizes used in validation calculations. Numbers are for one symmetric half. Δz_1 is the width of the free surface panels adjacent to the centreline; the strip width expansion ratio is 1.1 in all cases.*
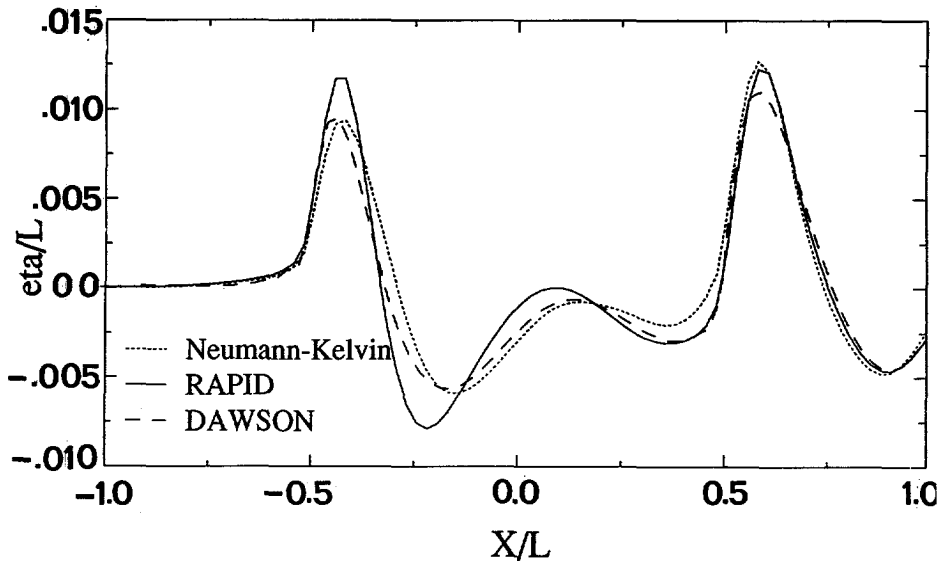
Figure 9.1: *Hull wave profile predictions, Wigley hull, Fn* = 0.316 .

The cases to be discussed, and the panel numbers used in the calculations, are listed in Table 9.1. Firstly, two standard cases will be shown that are far from discriminative but that permit comparison with results of others and with extensive experimental data. Then some practical cases are considered, three of which also were the subject of earlier comparative calculations for linearised methods. Finally a series of measurements and calculations is described, carried out specifically to validate the transom flow modelling.

9.1   Wigley hull

The predicted hull wave profile of a Wigley parabolic hull at *Fn* = 0.316 , for zero trim and sinkage, has already been shown in Fig. 7.8. It is in complete agreement with the wave profile measured in the ITTC Cooperative Experimental Program. The only exception is the height of the bow wave, which on the finest grid is about 11 % less than in the experiment. This deviation could be due to spray, which makes an experimental bow wave determination rather uncertain, but it is likely that it at least partly has to do with incomplete resolution of the singular behaviour at the bow. The effect of this appears to be quite localised though.

Fig. 9.1 illustrates that even for this unusually slender hull (*L/B* = 10) nonlinear effects are significant, linearised codes giving substantially larger deviations from the data.
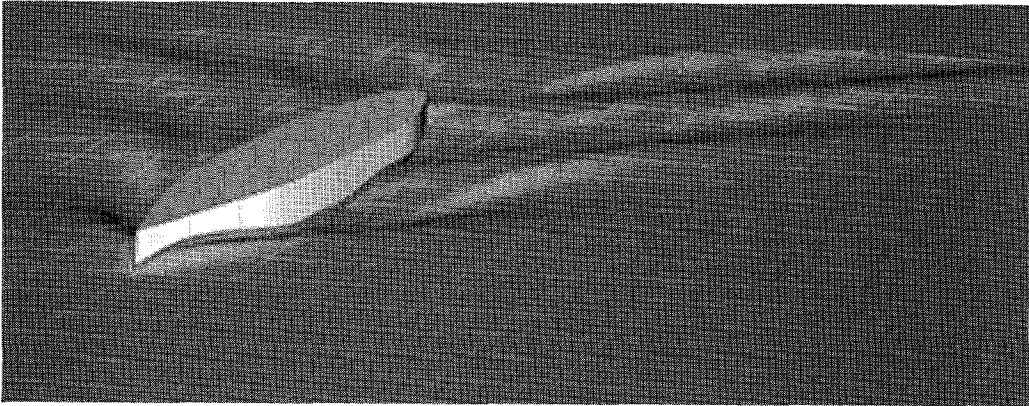
Figure 9.2: *Calculated wave pattern for Series 60 model, Fn = 0.316 .*

9.2 Series 60 Cb = 0.60 model

For this case an extensive set of longitudinal and transverse wave cuts has been measured at the Iowa Institute of Hydraulic Research [64]. The Froude number was 0.316, and the model was towed at zero trim and sinkage. In Section 7.3.4 grid refinement studies for this case have already been discussed, and below we shall consider the results on the finest grid only.

Fig. 9.3 compares calculated and measured longitudinal cuts. Overall the agreement is excellent and far better than anything published before 1993 for this case. Even many of the short-wave features are reproduced by the calculation. Remaining deviations are in the first place in the amplitude of the stern wave system, which is much lower and more irregular in the experiment. This is caused by viscous effects, which are considerable for this 3 m model. Ref. [64] shows wave pattern calculations for the same case in which the displacement effect of the boundary layer and wake has been incorporated; as a matter of fact this has an important effect on the stern wave system.

Also the downstream part of the outer cuts contains some deviations. But a closer inspection shows that these move forward rather than aft when going further away from the hull, and therefore may well be due to partial reflections at the wave absorber located at $y/L = 0.40$.

Some transverse cut comparisons have been shown in Figs 7.14 and appeared to be favourable. Fig. 9.4 compares the hull wave profiles. The maximum bow wave height is well predicted, but the high wave elevation right at the bow in the experiment is not reproduced. As this appears to have no effect in the nearby longitudinal cut, it probably has been a very thin fluid or spray sheet.
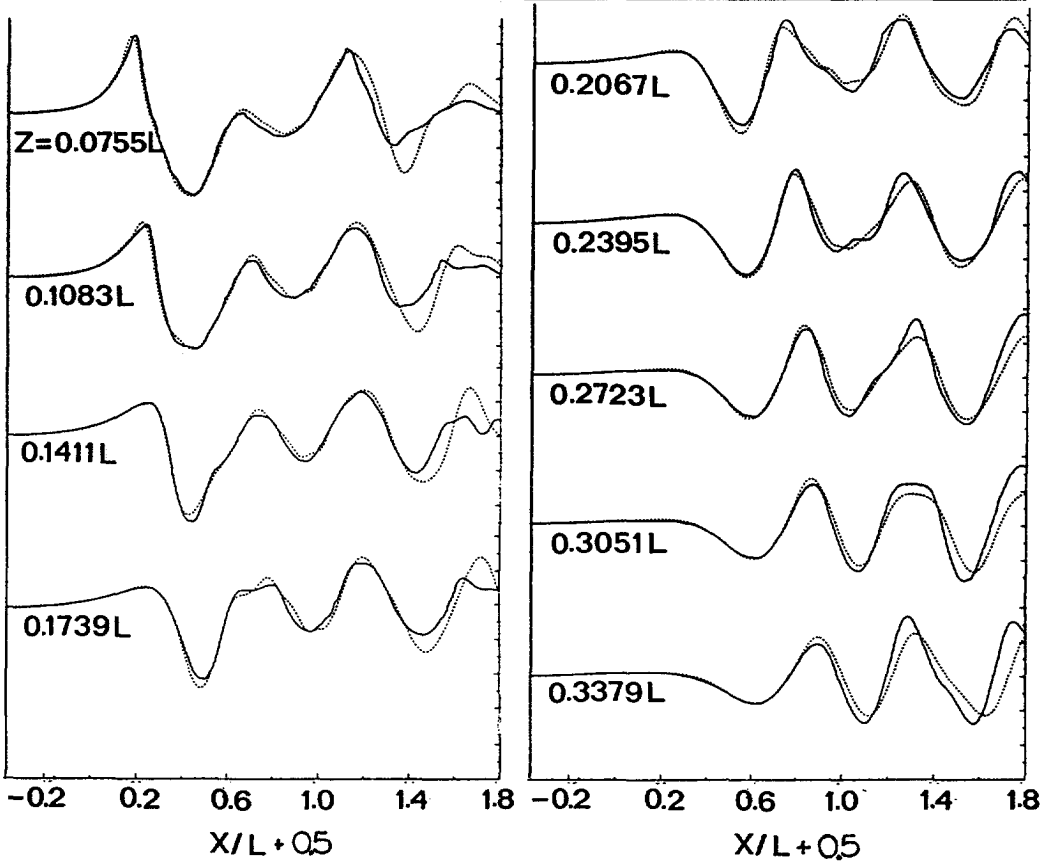
Figure 9.3: *Longitudinal wave cuts for Series 60 model, Fn = 0.316 , experimental (full line) and calculated (dotted line).*
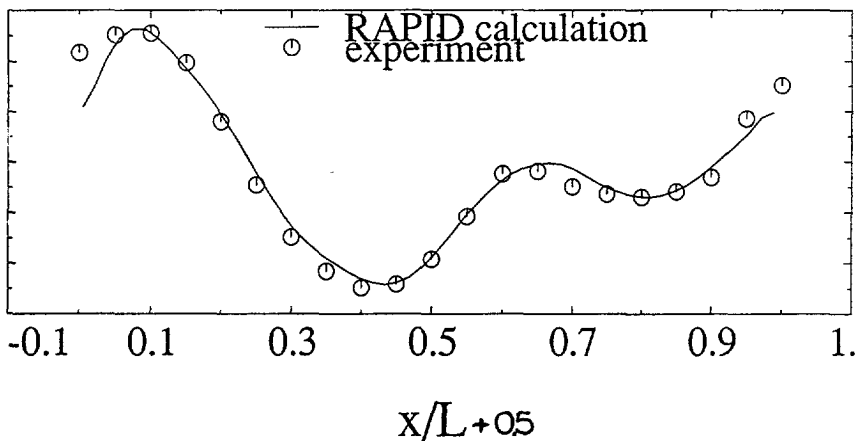

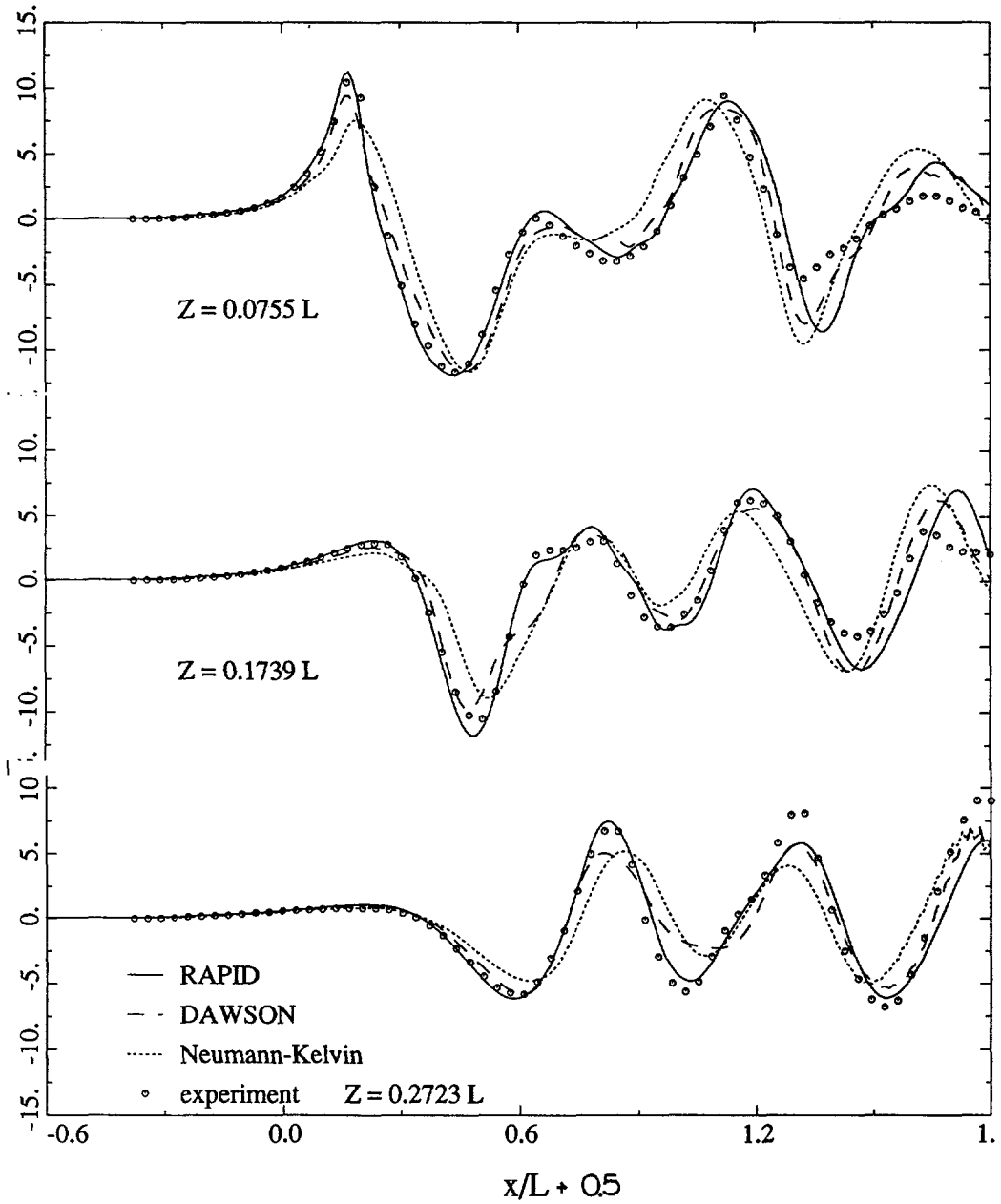Figure 9.4: *Hull wave profile, Series 60 model, Fn = 0.316 .*

Figure 9.5: *Longitudinal wave cuts for Series 60 model, Fn = 0.316 . Experimental data, linear and nonlinear predictions.*
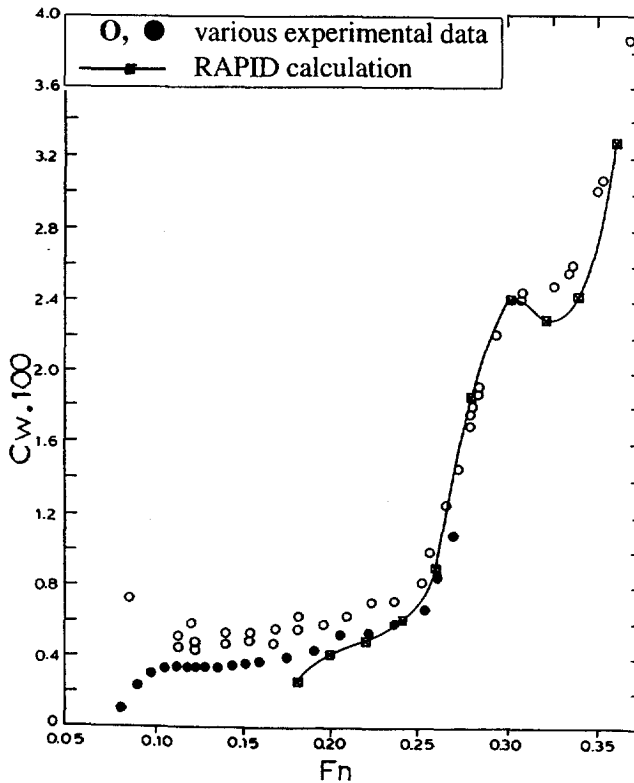
Figure 9.6: *Predicted wave resistance and experimental residual resistance coefficients for Series 60 model, free trim and sinkage.*

Fig. 9.5 shows the nonlinear and linearised predictions for some longitudinal cuts. The differences are small in this case, but the nonlinear result is consistently the best. Both linearised methods slightly underestimate most wave amplitudes; the Neumann-Kelvin result in addition has a phase lag at a distance from the hull. Only the nonlinear results seem to include all high-wavenumber contributions. The downstream part of the linear results shows some wiggles, an illustration of the instability for fine grids discussed on page 21; the nonlinear (raised-panel) results are perfectly smooth.

Fig. 9.6 compares the predicted wave resistance with some experimental data for the residual resistance (copied from [64]). While the agreement is excellent, it must be noticed that for this case experimental resistances from various tanks appeared to have a substantial scatter. Moreover, my predictions actually seem to be on the high side; no form factor has been used to estimate the viscous resistance, so the viscous form drag is included in the residual resistance data. Anyway, the shape of the resistance curve is quite accurately reproduced.
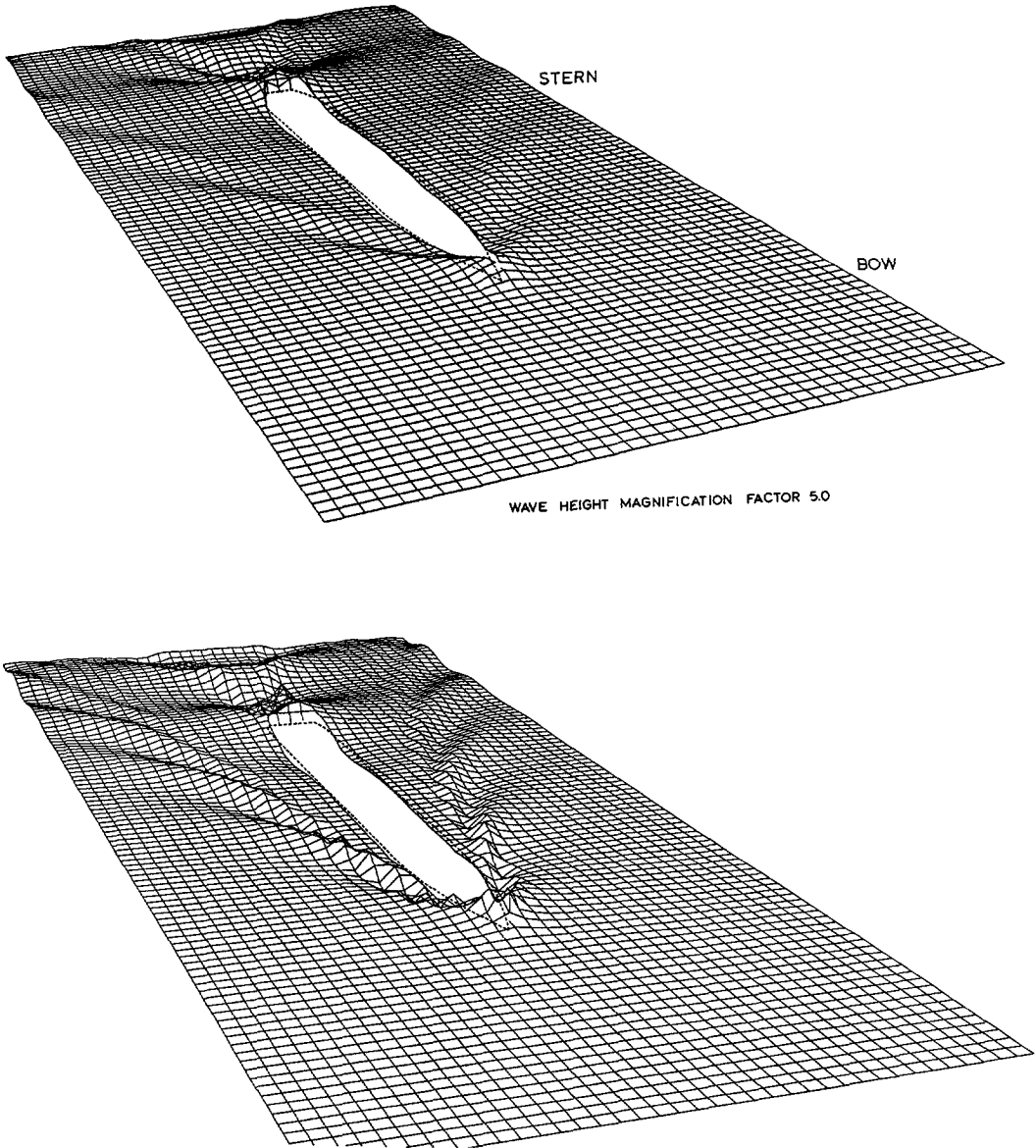
Figure 9.7: *Wave patterns of container ship, predicted by* DAWSON *(top) and* RAPID *(bottom). Wave elevations 5 times magnified.*
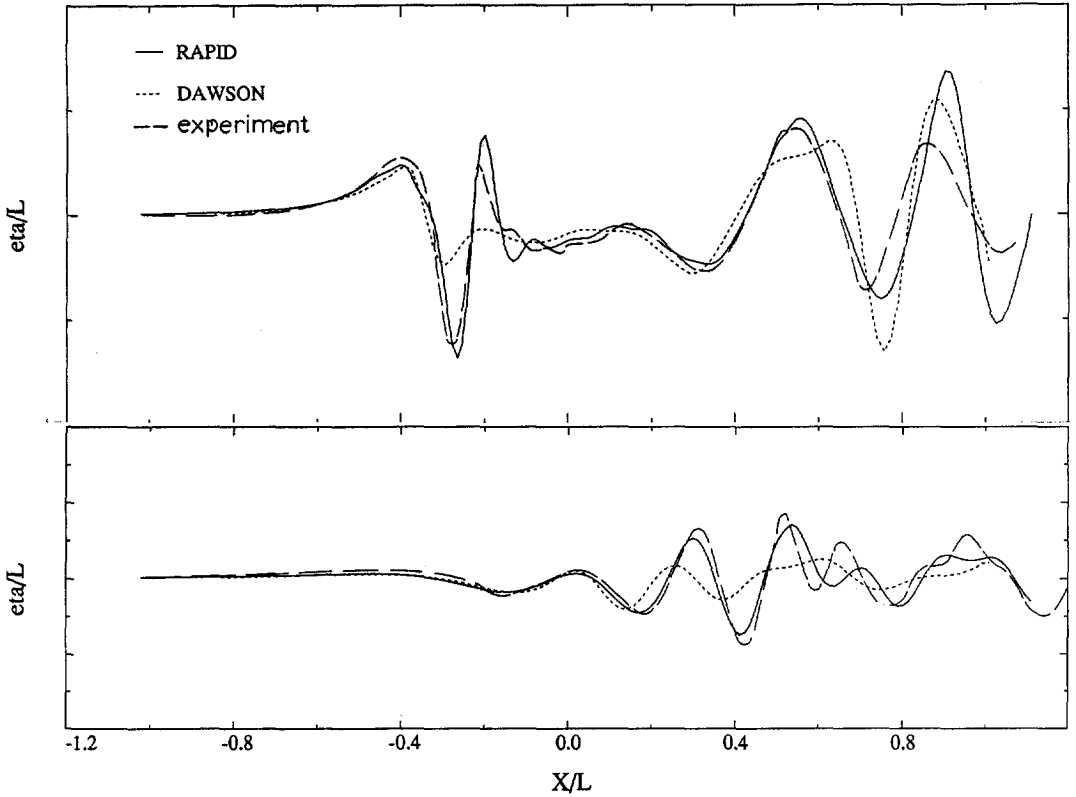
Figure 9.8: *Calculated and measured longitudinal wave cuts for container ship, at z/L = 0.1 (top) and z/L = 0.3 (bottom).*

9.3   Container ship

For this ship, one of the first applications of the RAPID code in practical ship design, drastic differences were observed between the RAPID and DAWSON predictions of the wave pattern at $Fn = 0.24$ (Fig. 9.7); in particular for the amplitude of the bow wave system at a distance from the hull. These differences were rather unexpected in view of the slenderness of the vessel ($L/B = 8.7$) and asked for experimental clarification. Longitudinal wave cut measurements have therefore been made in the MARIN towing tank. Fig. 9.8 shows the experimental results, together with the predictions by DAWSON and RAPID.[1]

---

[1]The calculations are recent ones using a newer version of the code (permitting larger panel numbers and incorporating the transom flow), and are even more accurate than those published before [76].

The conclusion is quite clear: while the linearised prediction severely underestimates the bow wave amplitude, the nonlinear result is in very close agreement with the data and represents a spectacular improvement. Remaining deviations mainly are related to small amplitude and phase errors in the shortest components, resulting in incidental increases or reductions of local wave elevations different from those in the experiment. At $z/L = 0.3$ the leading waves are in almost full agreement, indicating an excellent phase accuracy even at larger distances. The stern waves in the cut at $z/L = 0.10$ are well predicted up to $x/L = 0.7$, but the amplitude of the waves further aft, which originate from the rooster tail, is far overestimated. The cause of this is the assumption of a pure transom flow here, while in the experiment some extent of dead-water flow was present.

We thus find that the striking difference in the calculated wave patterns is entirely due to shortcomings of the *linearised* method. The magnitude of the difference, and the fact that it is entirely localised in the bow wave system, is puzzling. This is a genuine nonlinear effect and not a consequence of different numerics (e.g. the use of raised panels): The first iteration of RAPID, a Neumann-Kelvin solution in this case, displays the same shortcomings as Dawson's method. The next chapter will cast some light on this issue.

The predicted wave resistance turned out to be rather sensitive to variations of the grid and the panel elevation. Doubling the free surface panel widths or reducing α from 0.8 to 0.48 caused differences up to 7 %. The resistance was about 10 to 20 % higher than that derived from the experiments. On the other hand the prediction by DAWSON (without trim and sinkage) was about 20 % lower than the experimental value.

For the same vessel at ballast draft the top of the bulbous bow is at 1.2 m above the still water surface, which is 15 % of the stagnation height. A question of practical interest is whether at the speed desired the flow will still pass steadily and smoothly over the bulbous bow. If not, the bulbous bow looses its beneficial influence and a resistance penalty may be incurred. This question cannot be answered by calculations with a linearised method, since that imposes the free surface condition at the undisturbed water surface and thereby cuts off the hull at the still water line, prohibiting any meaningful treatment of such surface-piercing bulbous bows.

For a fully nonlinear method such a case in principle does not present any particular problem. But grid refinement studies for this case indicated that what happens directly above the bulbous bow can only be captured with a fine grid, because of the large gradients occurring. In that case the predictions correctly indicate that a thin fluid sheet passes over the bulb, as is illustrated by Fig. 9.10. The calculated bow wave pattern is shown in Fig. 9.9. In the experiment, a very deep and narrow wave trough was formed immediately downstream of the bulbous bow next to the hull, and even this feature was to some extent indicated by the calculations. In view of the excessive gradients the slightly less accurate prediction of the longitudinal cuts (Fig. 9.11), in particular for the bow wave amplitude at $z/L = 0.10$, comes as no surprise, but the principal features of the flow are well covered.
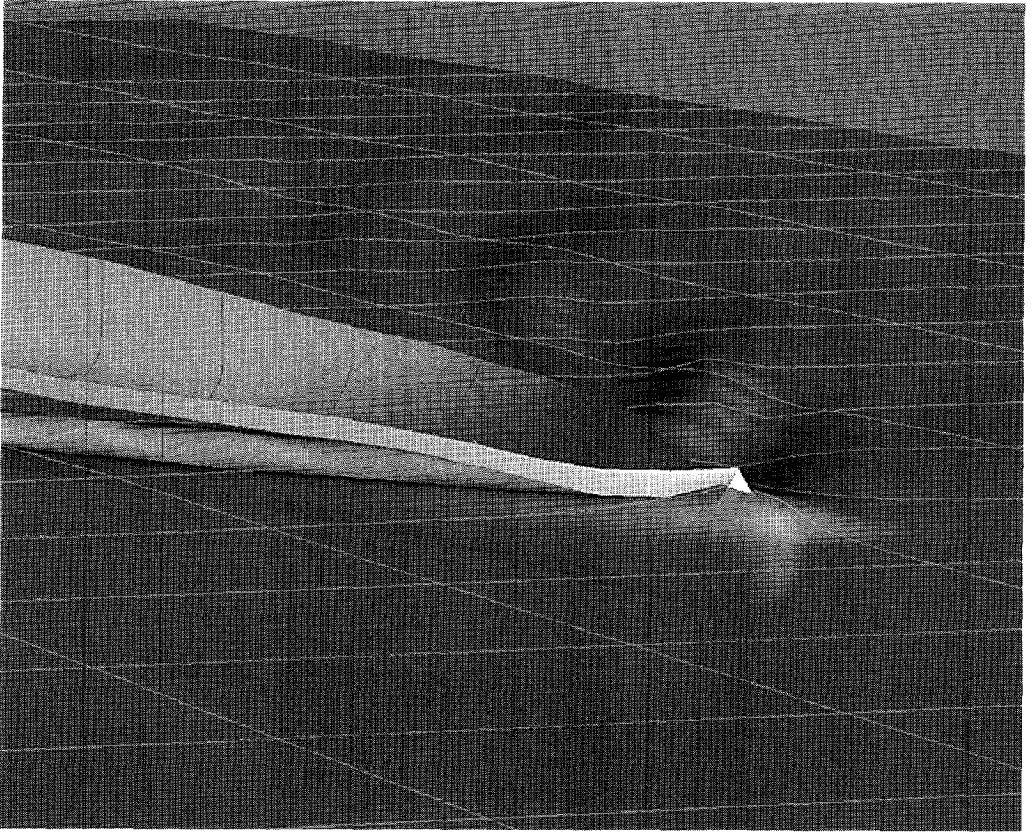
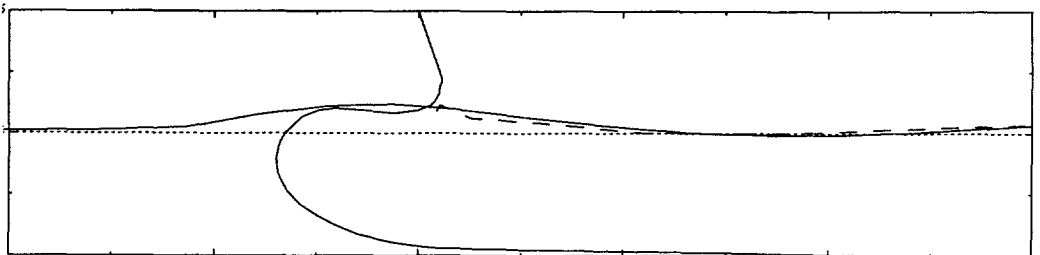Figure 9.9: *Calculated wave pattern for container ship at ballast draft.*

Figure 9.10: *Side view of bulbous bow outline and calculated wave surface, for container ship at ballast draft. Full line is wave elevation in collocation points near centreline and hull; dashed line is hull wave profile.*
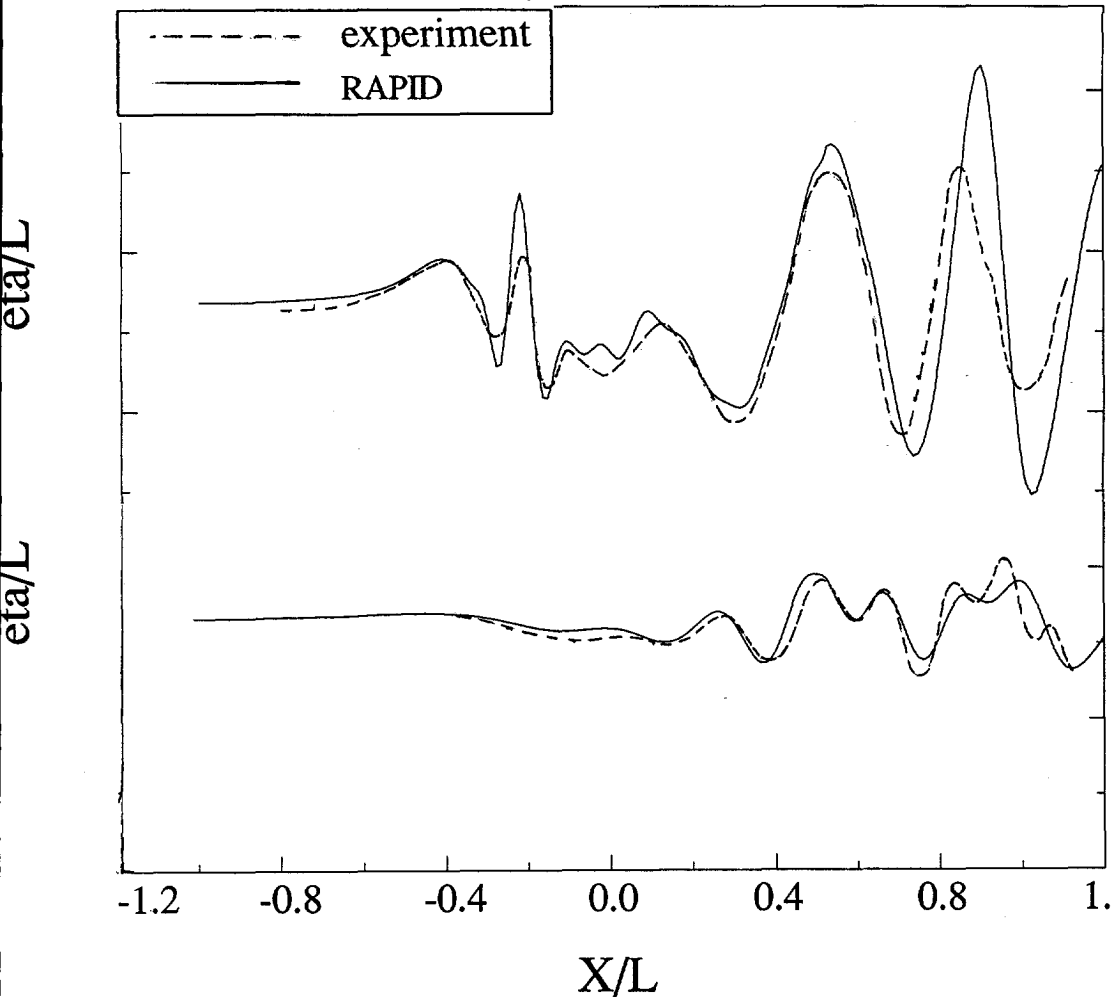
Figure 9.11: *Calculated and measured longitudinal wave cuts for container ship at ballast draft, at z/L = 0.1 (top) and z/L = 0.3 (bottom).*

9.4   DTRC model 5415

In 1988 the so-called "Wake-off" workshop [77] was organised by the David Taylor Research Center, with the purpose of judging the ability of methods then available to predict the wave pattern of ships, specifically that at somewhat larger distances from the hull. Two models were used as test cases, DTRC model 5415, a high-speed transom-stern destroyer, and the "Quapaw",

2% INTERVALS (Δη = 0.02 K₀)
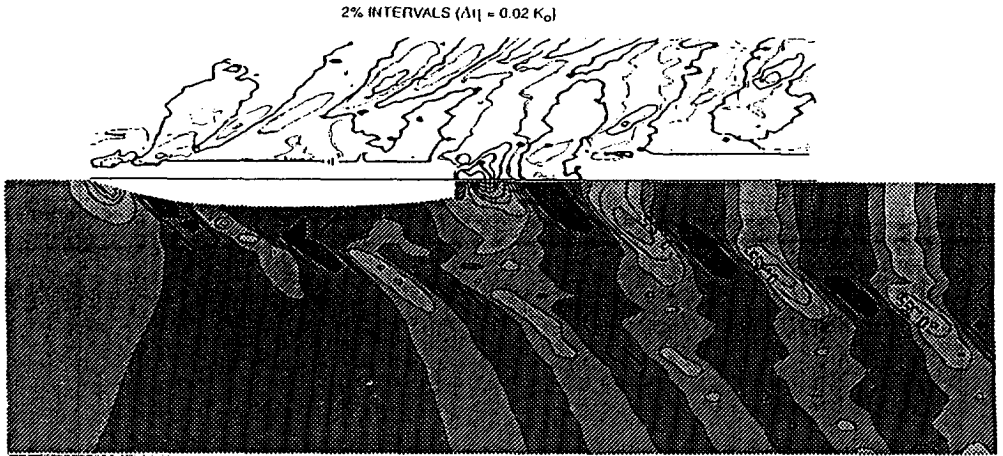
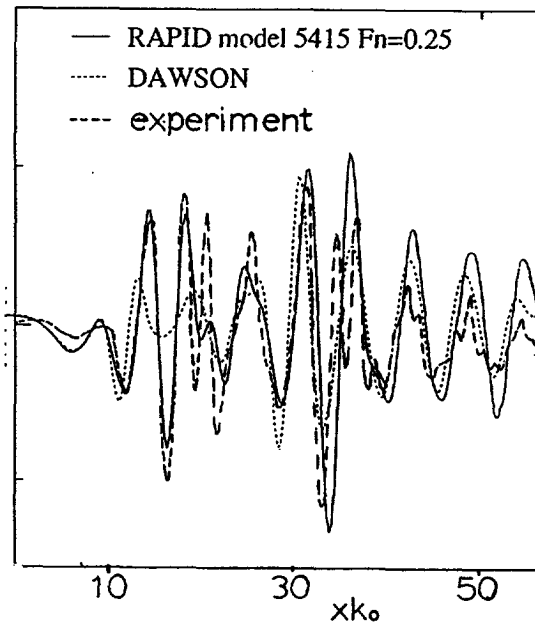Figure 9.12: *Wave pattern of DTRC Model 5415, Fn = 0.25 ; calculated (bottom) and experimental (top).*

Figure 9.13: *Calculated and experimental wave cut; DTRC Model 5415, Fn = 0.25 , z/L = 0.324 .*

a tug. The panel files for both were kindly provided to me by DTRC. These already included the experimental trim and sinkage. We shall consider DTRC model 5415 first.

Speed 18.1 knots, $Fn = 0.25$
Figure 9.12 shows the wave contours as calculated by RAPID and as measured. The interval for both is $\Delta \eta k_0 = 0.02$. Precise comparisons are fairly hard to make, but the general appearance is correct. As far as can be judged the calculated stern wave peak aft of the transom is somewhat higher and located slightly further aft than in the experiment. On the other hand the typical shape of the contours aft of the transom is very well predicted.

Fig. 9.13 compares the longitudinal cuts through the wave pattern at $y/L_{wl} = 0.324$. The bow wave system is very well predicted, except for some underestimation of the second trough. The pronounced waves around $xk_o = 20$ to 25 are not accurately predicted; the cause of this is unknown. The stern wave at $xk_0 = 30 - - - - 40$ is well predicted, both in location and in magnitude, although the shape of its second crest is not correct. Here it seems that a short component superimposed on the second crest is missed. The amplitude of the trailing wave system is too large. The cause of this is not entirely clear, but the irregularity of the experimental wave cut suggests viscous or wave breaking effects.

The longitudinal cut predicted by the linearised DAWSON code, also included in Fig. 9.13, again shows a striking difference for the amplitude of the bow wave system. The diverging waves from the bow once more are drastically underestimated and smoothed out. The stern wave system is better than that, and the trailing transverse waves are fairly well predicted although again too regularly shaped.

Overall the nonlinear predictions are significantly better than those of DAWSON and of the 9 other linearised methods considered in the workshop.

Speed 30 knots, $Fn = 0.4136$
The wave contours in Fig. 9.14 show a good prediction of the bow wave ($0.06 < \eta k_0 < 0.08$ for calculation and experiment), a generally good prediction of the wave trough alongside the hull (calculation $\eta k_0 < -0.06$, experiment $\eta k_0 \approx -0.08$), and a calculated stern wave aft of the transom with almost precisely the right location and contour shape, but a little bit too high as far as can be derived from the data ($\eta k_0 = 0.12$ instead of 0.10). The longitudinal cut at $z/L = 0.324$ (Fig. 9.15) is very good, except for some underestimation of a shorter component superimposed on the dominant system, which gives some deviations due to a modified interference. The amplitude of the trailing transverse waves is almost exactly predicted. This seems to support our suspicion that for the lower speed the deviation was due to viscous effects or wave breaking and not to an improper transom flow modelling.

The improvement compared to linearised predictions is less pronounced for this speed. The DAWSON prediction of the wave cut is very similar, except for a somewhat lower first crest and the complete absence of the short disturbances. In general all linear predictions presented at the workshop were better for $Fn = 0.4136$ than for $Fn = 0.25$, most likely because transverse wave
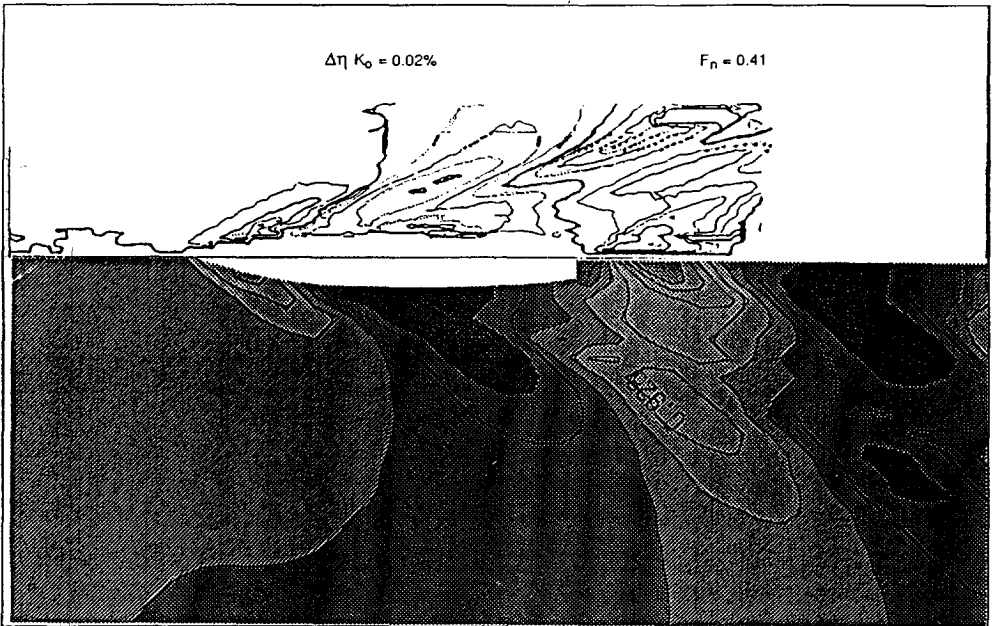
Figure 9.14: *Wave pattern of DTRC Model 5415, Fn = 0.4136 ; calculated (bottom) and experimental (top)*

components are more dominant. It has been found several times that these are less affected by nonlinearities than diverging waves.

For the experimental resistance coefficients given in the DTRC reports the reference area on which they are based is not mentioned. Supposed that this has been the wetted area, the predicted values are substantially too high as Table 9.2 shows. But the experimental data are wave *pattern* resistances, and it is known that these often are significantly lower than the residuary resistance; perhaps because any wave energy dissipated in wave breaking is not included. This might explain the relatively larger difference at the lower speed, when wave breaking probably is present behind the transom.

9.5   DTRC model "Quapaw"

Another test case of the workshop is a naval tug with a cusped stern. The data apply to $Fn = 0.3197$. The experimental wave contours were rather deficient and did not permit a meaningful comparison. Fig. 9.16 compares the measured and calculated wave cut at $z/L_{wl} = 0.373$. The prediction is

model	Fn	Cw_{RAPID}	Cw_{DAWSON}	$Cw_{exp.}$
DTRC 5415	0.25	0.00079	0.00061	0.00037
DTRC 5415	0.4136	0.00315	0.00277	0.00240
DTRC Quapaw	0.3197	0.00389	0.00340	0.00180

Table 9.2: *Calculated and experimental wave resistances for DTRC models*
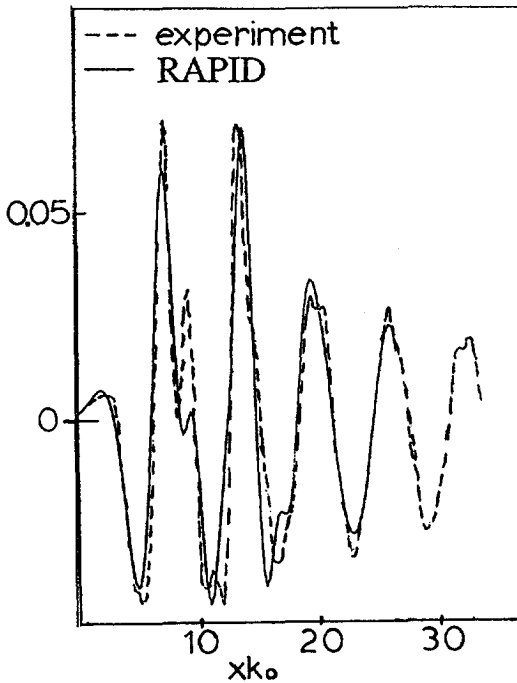
Figure 9.15: *Calculated and experimental wave cut; DTRC Model 5415, Fn = 0.4136, z/L = 0.324.*
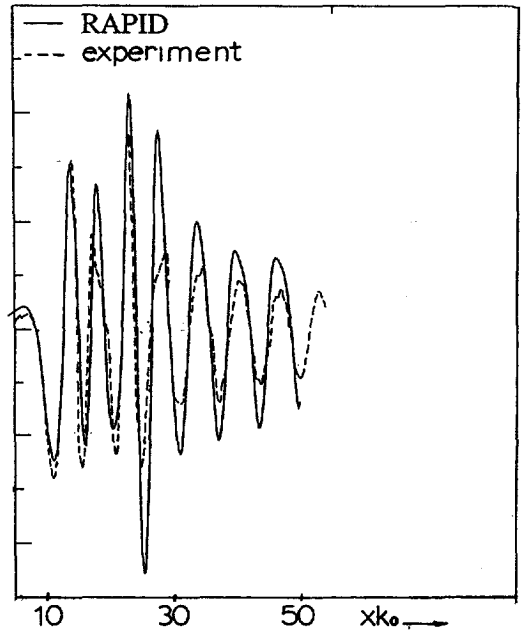
Figure 9.16: *Calculated and experimental wave cut; DTRC Model Quapaw, Fn = 0.3197.*

generally good, with only small deviations for the bow wave system. But the stern wave system ($xk_0 = 20 - - - 25$) and the trailing transverse waves are significantly overestimated. This may, at least partly, be due to viscous effects. For a cusped stern the increase of the waterline angles in the afterbody causes an increase of the boundary layer thickness. The two boundary layers from both sides of the hull then merge at the stern, forming a relatively thick wake that substantially reduces the pressure rise towards the stern. The viscous effect will thus be larger than for a transom stern, which does not lead to a similar increase of the boundary layer thickness and confluence of boundary layers.
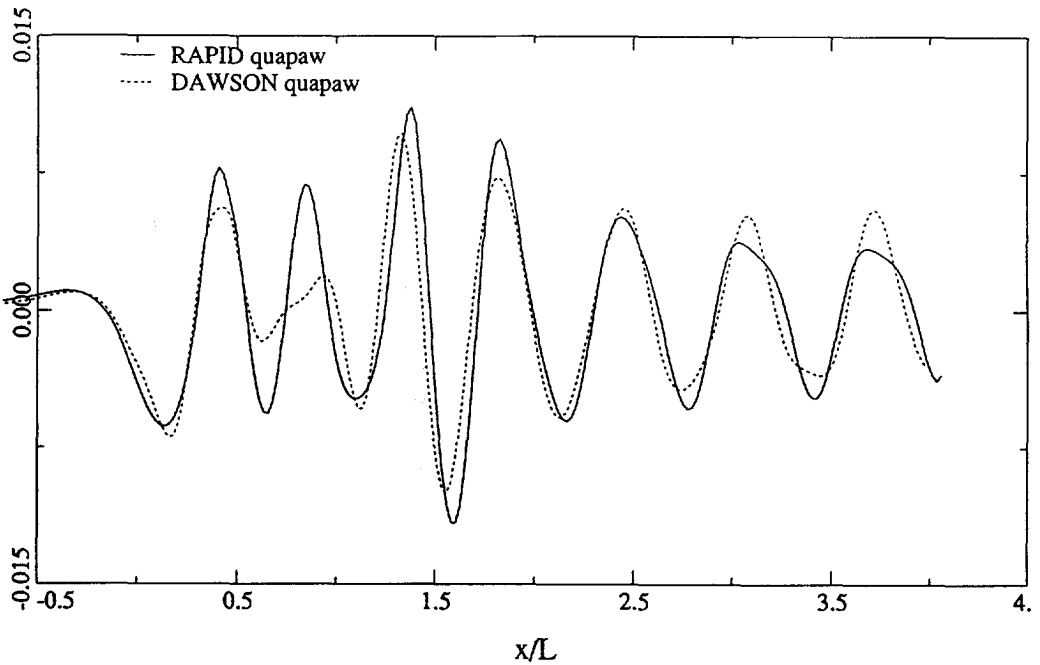
Figure 9.17: *Wave cut calculated using linearised and nonlinear method; DTRC Model Quapaw,* *Fn* = 0.3197

Fig. 9.17 compares the linearised and nonlinear predictions. Evidently nonlinear effects are only modest here.

The calculated wave resistance coefficients (Table 9.2) again are much higher than the experimental wave pattern resistance. This agrees with the overestimation of the stern wave system which here is responsible for most of the wave drag.

9.6   Frigate

In a validation project ordered by the Royal Netherlands Navy, MARIN has carried out detailed wave pattern measurements for a model of a frigate with a bow dome and a rather shallow transom stern, to some extent similar to DTRC model 5415. This project provided a unique opportunity to collect detailed experimental data on transom flows, which otherwise are generally lacking. The validation of the transom flow modelling could thus be much more detailed than in any comparable study published so far. The transom flow behaviour over a range of conditions has been observed and stern waves have been carefully measured.

A main question was whether RAPID would correctly predict the dependence of the stern wave shape on transom immersion, and the optimum immersion. Therefore we have carried out tests and calculations for the model with varying amounts of bow-down trim at constant displacement. A series of RAPID calculations preceding the tests has been made to fix the conditions to be tested. Some initial towing tests have then been performed to determine the speeds at which transitions to dead-water flow and early detachment occurred. The latter approximately matched that indicated by RAPID. At the lowest speed chosen the trim conditions selected covered the entire range of transom flows: in even keel condition the transom was only just cleared and most of the wave breaking and unsteadiness directly aft of the transom had just disappeared; and at maximum bow-down trim the transom edge was so high that the flow only just stayed attached to the hull bottom.

The trim conditions labelled A, B, and C in the discussion below refer to the trim at zero speed. In the towing tests the model was ballasted (at equal displacement) to the desired trim, and left free in dynamic sinkage and trim during the run. Trim A is the even keel condition, trim C is the maximum bow-down trim, and trim B is an intermediate position. In the calculations the equilibrium trim and sinkage have been determined and they will be compared with the data; but to separate this possible error source from others, the wave pattern comparisons below are for calculations with a trim and sinkage equal to that found in the tests.

Several longitudinal cuts have been recorded using wave probes at a fixed location in the tank, at $z/L = 0.40$, 0.20 and 0.09. The latter is just outside the hull and provides near-field data. But specific data on the flow off the transom cannot be collected using such stationary wave probes outside the path of the model. Therefore a new experimental setup has been developed. A longitudinal rail bearing a small subcarriage was mounted under the towing carriage behind the model. Fitted to the subcarriage was a servo-driven wave probe, which followed the position of the instantaneous wave surface. During a towing test the subcarriage was slowly moved along the rail, and a longitudinal wave cut at the model centreline aft of the transom could thus be recorded. The cut started at 1 to 2 % of the model length off the transom and extended about 0.5 model length aft. This system has allowed to collect most valuable and otherwise scarce data.

Fn = 0.292 , trim A

Fig. 9.18 compares the computed wave cuts with those measured. It appears that RAPID very accurately reproduces the first part of the cut at all transverse distances. The shorter wave components further aft (which also originate at the bow) are slightly distorted by insufficient resolution, but qualitatively well predicted. At larger transverse distances these short components tend to lag behind those measured and to have slightly insufficient amplitude, in qualitative agreement with the numerical dispersion and damping effect found theoretically. Shape and amplitude of the stern wave system are fairly well predicted, but the wave crest is somewhat too far aft and the subsequent wave trough is too deep.
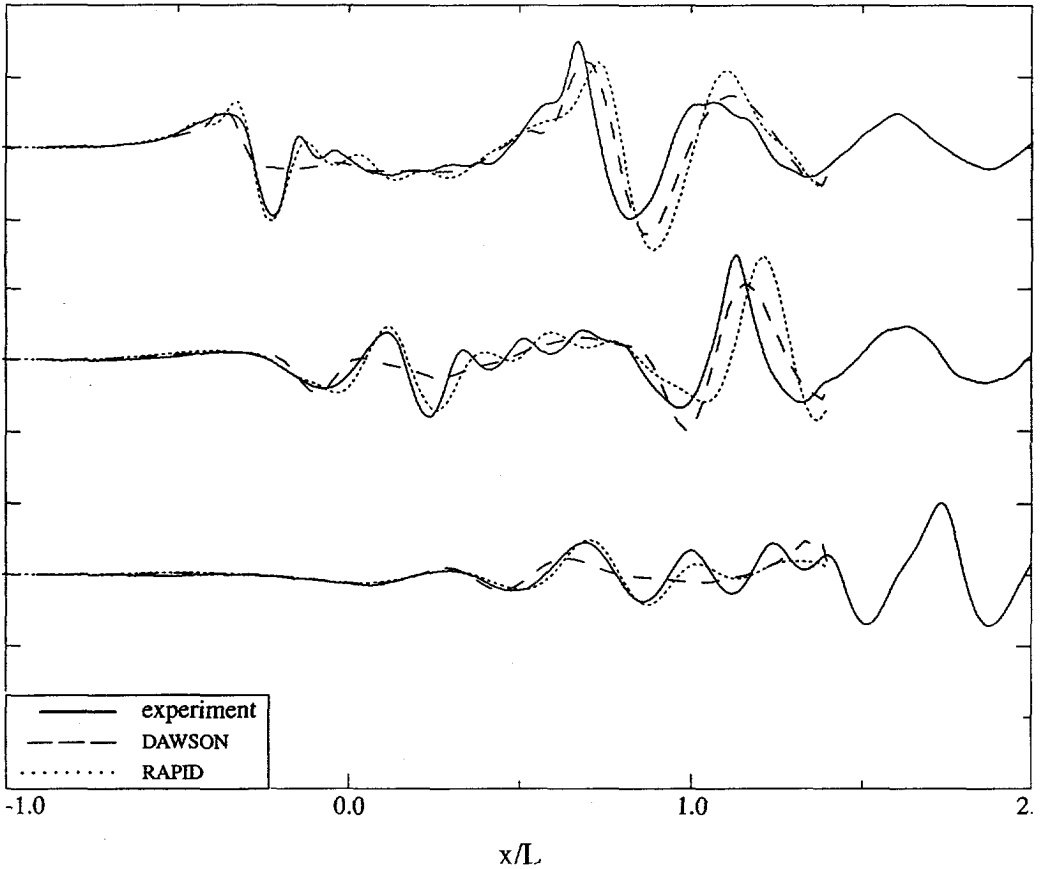
Figure 9.18: *Calculated and measured longitudinal wave cuts for frigate, Fn = 0.292 , trim A.*
z/L = 0.09, 0.20 and 0.40 .

In the same figures the DAWSON predictions (also for experimental trim and sinkage) are shown.
Again the linearised code severely underestimates the diverging waves from the bow. The
following shorter components are mostly absent. But the stern wave system is surprisingly
accurately predicted, with a smaller phase lag and better amplitude than by RAPID.

Fig. 9.19 compares the measured and computed stern wave profile at the model centreline aft of
the transom. Note that this figure only shows a detail of the wave system, and all deviations seem
to be amplified. The experimental wave crest is markedly peaked. In potential flow such a kink in
the wave surface in the symmetry plane could only occur at a stagnation point, but then the wave
height should be 3 times as large as that measured. But in the experiment the peak appeared to
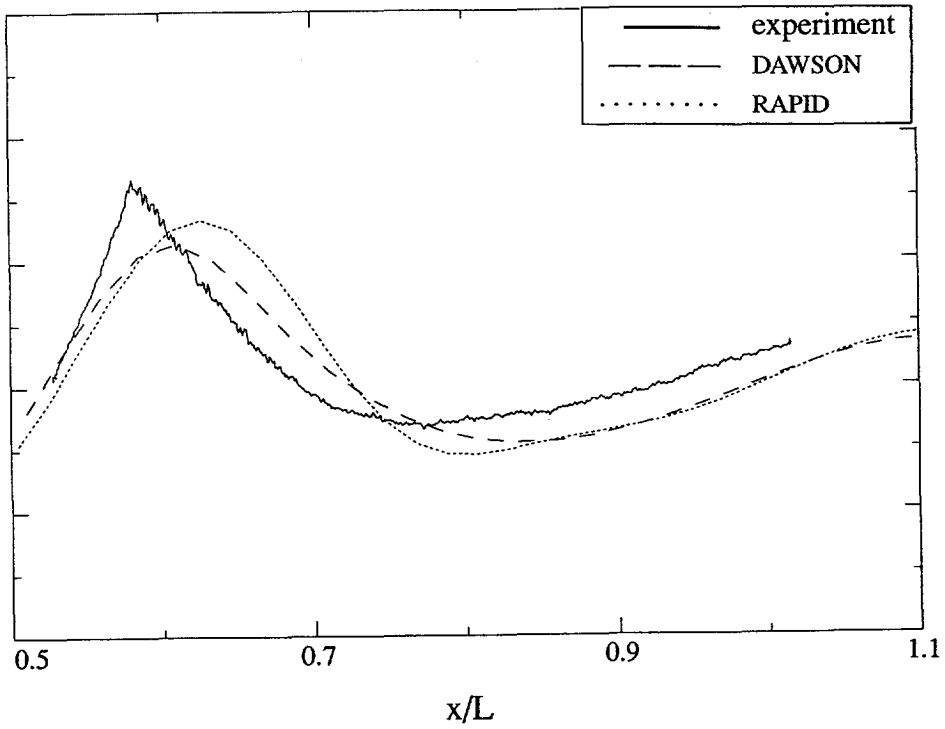occur where two converging ridges on the water surface, originating from the edges of the transom

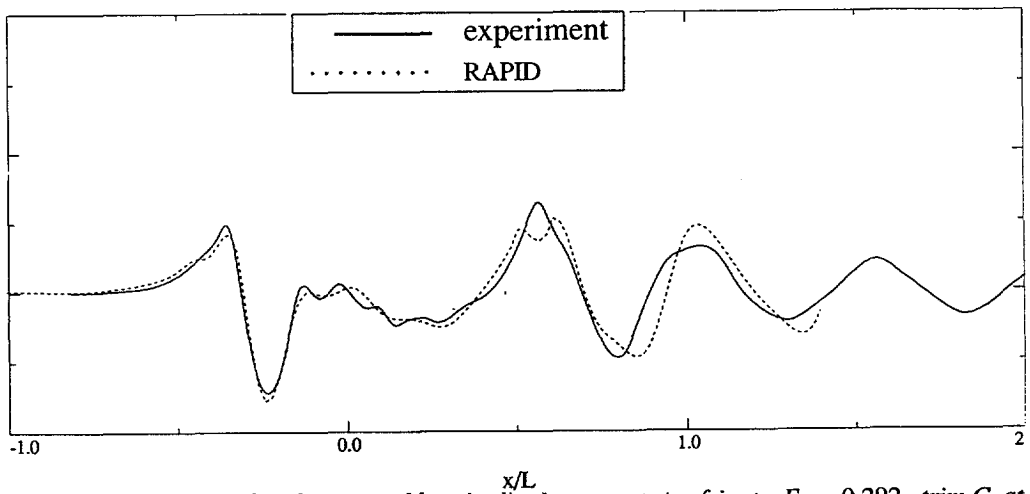Figure 9.19: *Calculated and measured longitudinal stern wave cut at the centreline. Frigate, Fn = 0.292 , trim A.*

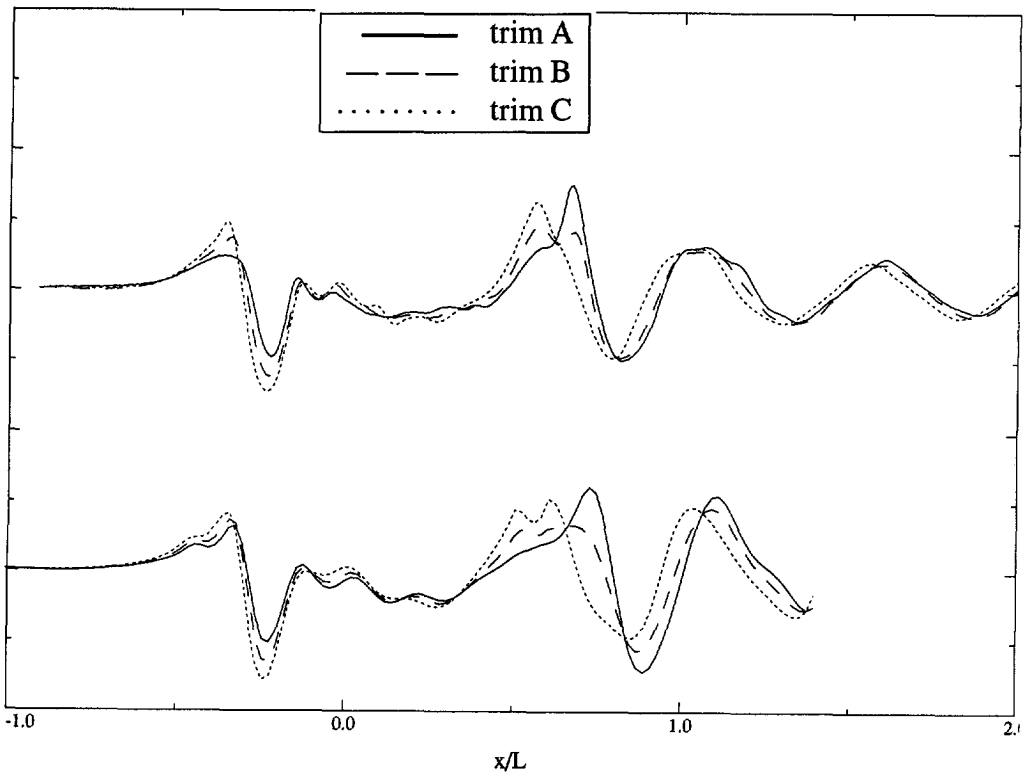Figure 9.20: *Calculated and measured longitudinal wave cuts for frigate, Fn = 0.292 , trim C, at z/L = 0.09.*

Figure 9.21: *Effect of trim on longitudinal wave cut at z/L = 0.09 ; measured (top) and calculated (bottom). Frigate at Fn = 0.292 .*

at each side, meet. At higher speeds the ridges converge less quickly and meet further aft. How this particular phenomenon should be modelled theoretically is not yet clear, but most likely it represents a form of wave breaking severely affected by surface tension. The experimental wave cut also shows the irregularity in the wave profile just behind the peak, caused by the fact that slight wave breaking was excited by the passage of the wave probe here.

Both prediction methods miss the wave peak and predict a smooth wave crest of insufficient height; for RAPID the difference is 17 %. Additionally there is an aft shift of the stern wave, which is larger for RAPID than for DAWSON. But DAWSON does not display the proper behaviour close to the transom. An improved linearised transom modelling, more similar to that in RAPID, has been developed and found to cure this deficiency in DAWSON, but to increase the phase lag. This indicates that, as far as DAWSON is doing better here than RAPID in some respects, this is due to fortuitous error cancelling.
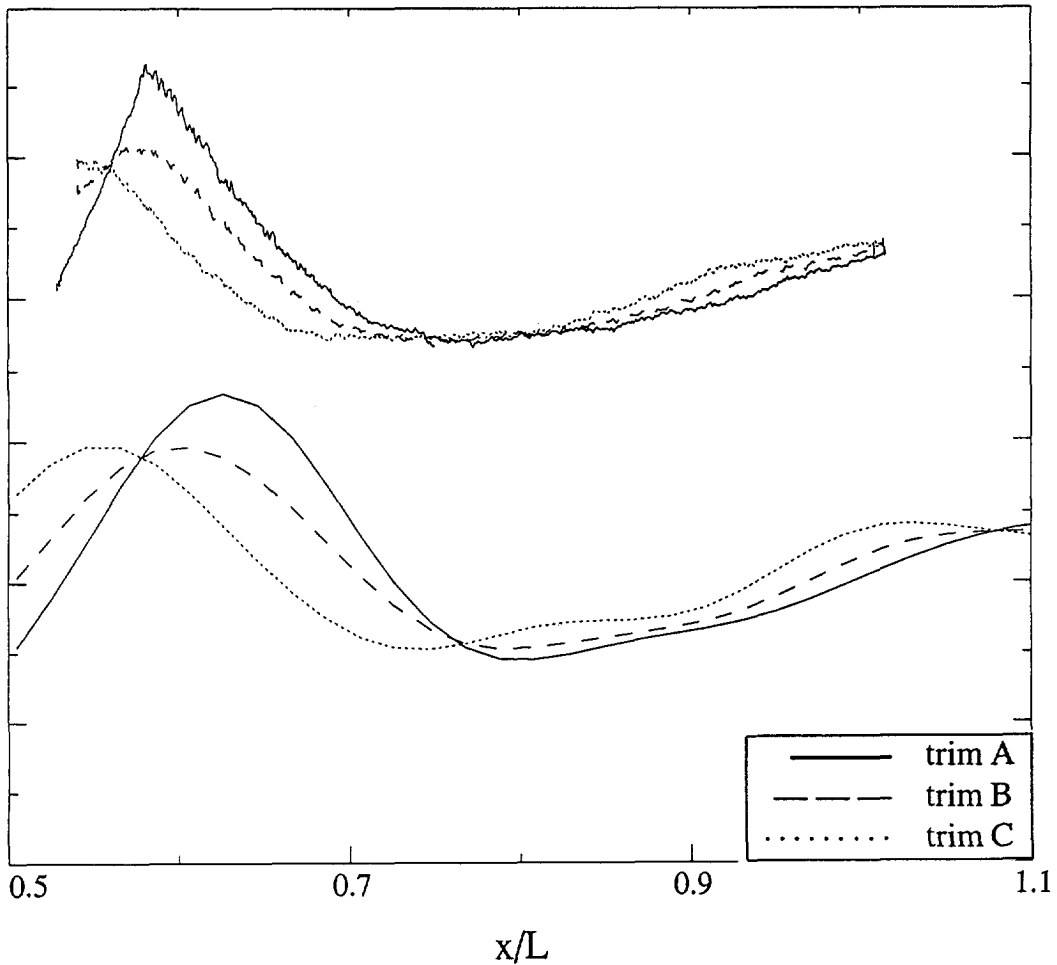
Figure 9.22: *Effect of trim on centreline stern wave cut; measured (top) and calculated (bottom). Frigate at Fn = 0.292 .*

Fn = 0.292 , effect of trim

Similar comparisons have been made for the bow-down trim conditions. Generally the agreement of calculations and experiments is significantly better than that for trim A, due to the less severe flow conditions at the stern. The RAPID prediction for trim C (Fig. 9.20) is very accurate, except for a small remaining phase lag of the stern wave. No accurate DAWSON calculation is possible for condition C since the transom edge is above the still water surface.

Figs 9.21 and 9.22 show the effect of forward trim on the wave cut at $z/L = 0.09$ and the centreline

stern wave cut, in the experiment and according to RAPID. The following features are identified:

- Bow-down trim here increases the bow wave amplitude without change in shape. This increase is very accurately predicted.

- Both in the calculations and in the experiments, when the transom is lifted the stern wave height at $z/L = 0.09$ first decreases substantially, then becomes higher again in condition C (only slightly less than in condition A). The highest crest of the stern wave system moves forward with trim. This behaviour is accurately predicted, except for a slight disagreement for the stern wave shape for trim C and the phase lag for condition A.

- With reduced transom immersion the stern wave on the centreline immediately looses its peaked appearance. Consequently the agreement of the prediction with the data improves considerably, both in amplitude and in phase. The underestimation of the stern wave height is 17 % for trim A, 9 % for trim B and zero for trim C. The predictions show at least qualitatively the correct dependence on transom height: a forward movement of the crest, a decrease of the wave height when going from A to B and no significant change from B to C. The reduction of the stern wave height from A to B is 35 % in the experiment, 28 % in the calculations.

In general we conclude that RAPID predicts the effect of forward trim on the wave system well, with only a few aspects for which the agreement is only qualitative. The linearised DAWSON method is doing well for the stern wave at trim A, but is strictly inapplicable to other trim conditions and is poor for the bow wave system.

Fn = 0.38

Fig. 9.23 compares the wave cuts at $z/L = 0.09$ for trim A at a larger speed. The bow wave height is slightly overestimated, but in general the wave cut is very well predicted by the nonlinear code. All significant wave components are reproduced, with minor errors in amplitude and phase. The stern wave height is almost correct, but again it is predicted a little bit too far aft. The subsequent wave trough is too deep, possibly because wave breaking (visible in irregularities in the measured wave cut) has affected the experimental data. Forward trim again was found to make the agreement still significantly better.

The linearised DAWSON calculation reproduces the overall shape of the pattern at trim A, in particular of the longer components. Most of the shorter components, however, are again absent. On the other hand the stern wave prediction happens to be better than that by RAPID, in particular for the phase.

Fig. 9.24 compares the centreline wave profiles for trim A and C at this speed. For trim A the calculated wave profile initially is almost identical to that of the experiment, but it has a slightly too
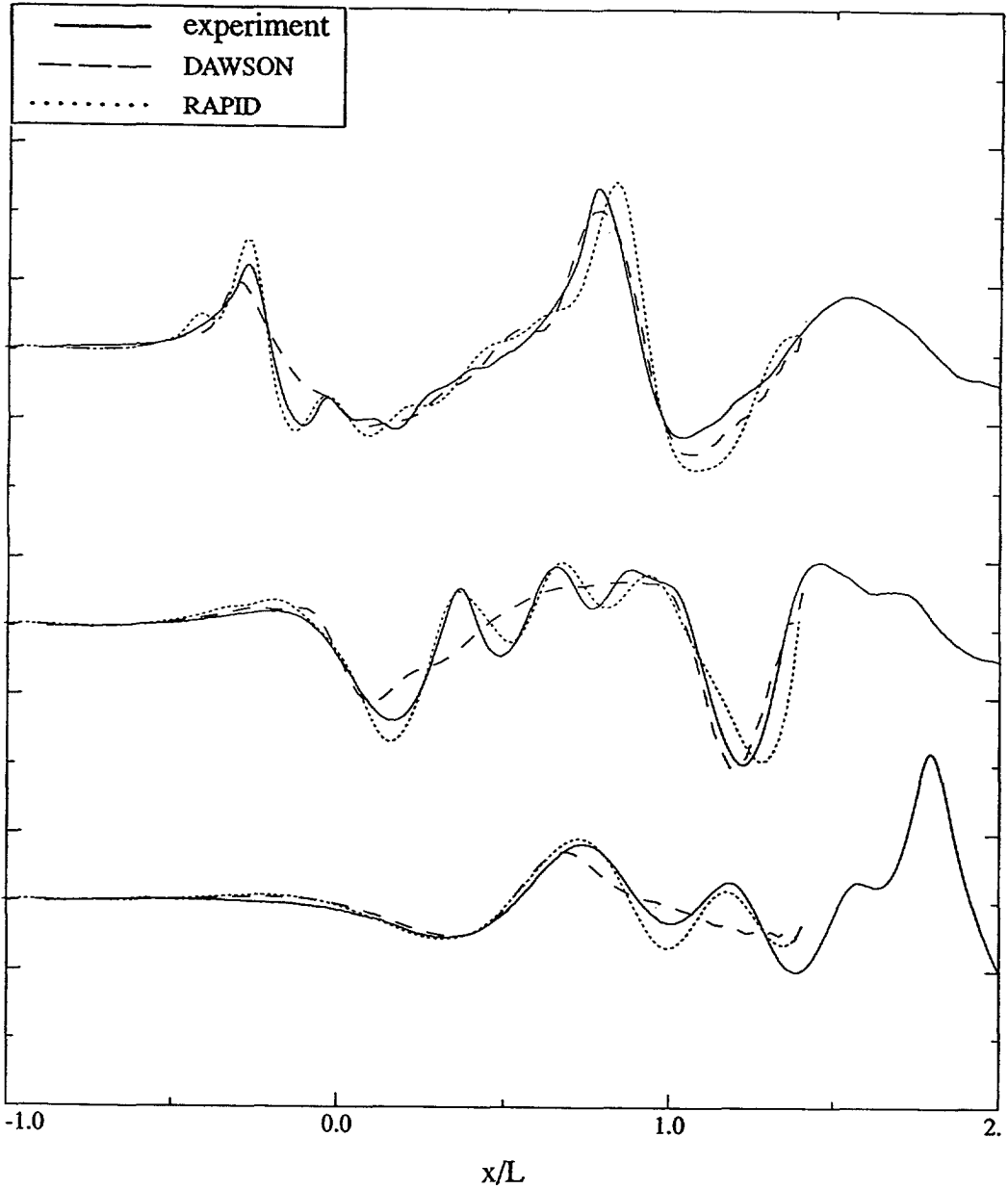
Figure 9.23: *Calculated and measured longitudinal wave cuts for frigate, Fn = 0.38   , trim A.*
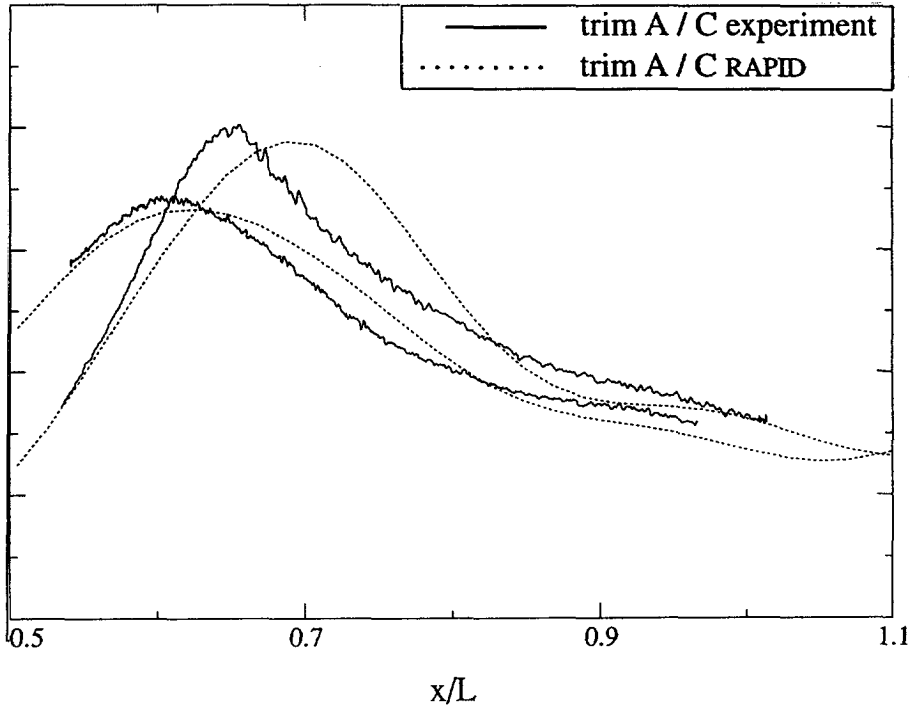*z/L = 0.09, 0.20 and 0.40 .*

Figure 9.24: *Effect of trim on centreline stern wave cut; measured and calculated. Frigate at* $Fn = 0.38$

small upward curvature and again misses the somewhat peaked appearance of the actual wave. For trim C the prediction is very good, with a negligible error in wave height and a quite small phase lag. Still the experimental wave crest is slightly more pointed than that predicted. Overall the representation of the trim effect on the stern wave is very good in the calculations. The decrease of the stern wave height with forward trim is 29 % in both the experiments and the calculations.

Validations for an even higher speed ($Fn = 0.46$) led to similar conclusions and will not be shown here in the interest of brevity.

Resistance, trim and sinkage predictions

A residuary resistance has been deduced from the experimental data using a somewhat approximate viscous resistance estimate. In RAPID the calculated wave resistance has been found as usual by pressure integration over the wetted surface. In DAWSON the pressure forces have been integrated over the hull area under the still waterline (in trimmed and sunk condition), but a correction has been applied for the absence of a hydrostatic force on the transom, as described on page 147. The addition amounted to 21 %, 21 % and 28 % of the total wave resistance for trim A at the three

speeds considered.

The relative deviations of the predicted wave resistance so obtained (Table 9.3) appear to be fairly small for both codes. Although there is a substantial difference in the diverging wave components between RAPID and the experiment on the one hand, and DAWSON on the other hand, this appears to have only a modest effect on the overall drag.

Table 9.4 shows the effect of trim on the experimental residuary resistance and the wave resistance calculated by RAPID. It has been assumed that the viscous resistance is not affected by the trim in this case. Although the magnitude of the variations is not exactly predicted, the general dependency on trim is reproduced.

The predicted trim and sinkage (in calculations with trim and sinkage free) for static trim A are compared in Fig. 9.25. The trim is in very good agreement, with a small but consistent underestimation in this case. The sinkage is underestimated by a larger amount, in particular at higher speeds.

Fn	error Cw_{RAPID}	error Cw_{DAWSON}
0.29	- 8 %	- 8 %
0.38	- 6 %	- 13 %
0.46	- 1 %	- 7 %

Table 9.3: *Relative error of predicted wave resistances compared with experimental residuary resistances, for trim condition A.*

Fn	trim cond.	resid. res. change	calculated Rw change
0.29	B	- 17 %	- 23 %
0.29	C	+ 5 %	- 4 %
0.38	C	+ 8 %	+ 2 %

Table 9.4: *Experimental and calculated dependence of wave resistance on trim condition. The changes are given as a percentage of the wave resistance in trim condition A.*
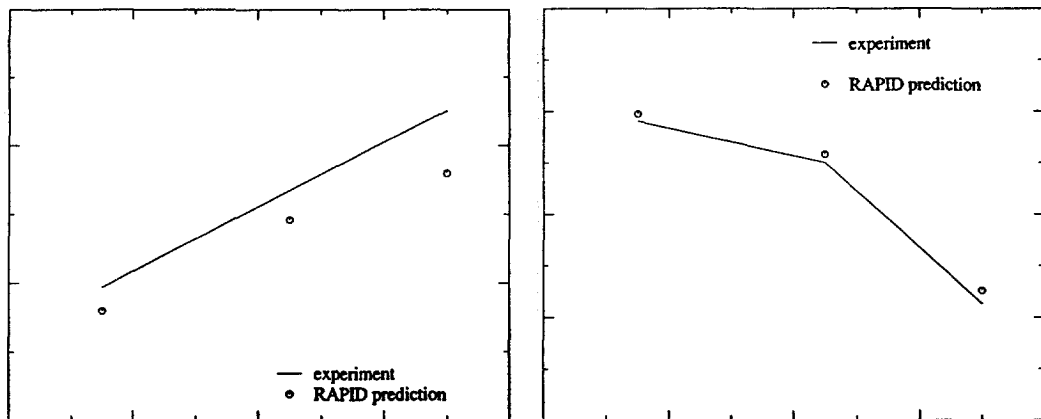
Figure 9.25: *Measured sinkage (left) and trim (right) for frigate at static trim A.*

9.7   Conclusions

From these and other validation studies several common features emerge.

- The nonlinear method is able to reproduce most of the features of the wave pattern found in the experiments. This includes the specific shape of the waves at various speeds, trim conditions and hull forms, the shorter components and complicated interferences between different components.

- For the simplest cases like the Wigley hull and Series 60, the agreement is essentially perfect, except for viscous effects at the stern (which by the way will be less on full scale). Occasionally the predicted bow wave height is just below the experimental one, most likely a consequence of the practical impossibility to capture the singular behaviour at the bow. But this deficiency is quite localised. For other cases the agreement is generally good, viscous effects and wave breaking being the principal remaining source of deviations.

- The phase of the dominant waves is always very well predicted. Some amplitude errors still may occur, but these are consistent for design variations if similar free surface panellings are used, and therefore do not prohibit optimisation. Even very short, diverging components are predicted, although often with some distortion due to numerical damping and dispersion. The latter qualitatively correspond with the analysis in Chapter 6.

- The modelling of transom flows proposed in the previous chapter is essentially validated by the study for the frigate. Nevertheless there are somewhat larger deviations just behind a transom than elsewhere. In particular the predicted stern wave is slightly too far aft and too smooth for the lowest transom Froude numbers. There are indications that viscous effects (e.g. the fact that the flow passing around the transom edge has been retarded in the hull boundary layer) or slight wave breaking play a role here. All the same the qualitative

features of the transom flow and its dependence on transom immersion are well reproduced, and a computational optimisation of the stern wave shape seems justified. A principal advantage of a nonlinear method here is its ability to deal with transoms above the still water surface.

- Obviously, the occurrence of a dead-water region abaft the transom invalidates the transom flow modelling applied, and results in an often drastic reduction of the height of the "rooster tail" and the following wave system, compared to that calculated. Whether or not such a dead-water area will occur still requires some judgement.

- Predicting the wave resistance is still difficult. While for slender ships such as the frigate, Wigley hull and Series 60 the level and trends of resistance are correct, for several other cases inaccuracies have been observed, resulting from the poorly conditioned hull pressure integration. Determination of the resistance based on the predicted wave pattern seems more promising.

- Besides the known numerical dispersion and damping some other numerical deficiencies have been observed. One is the rather common occurrence of a small dip in the wave surface just ahead of the bow wave crest at some distance from the hull (visible in the wave cuts for the frigate). Another is the fact that apparently a large bow flare or unusually fine panellings can give rise to transverse source strength oscillations that to some extent may affect wave amplitudes away from the hull. This shortcoming will be further investigated and cured in the near future.

- Even for slender ships, nonlinear effects on the wave pattern are often drastic, contrary to the former widespread belief that they are mainly important for fuller hulls forms. The main difference is in diverging bow waves, which are consistently underestimated by linearised methods. But linearised methods even so give a quite reasonable prediction of the longer, more transverse wave components near the hull, which happen to be dominant for the wave resistance.

Despite certain points of disagreement I conclude that the level of accuracy reached is far beyond that previously achieved. The nonlinear predictions often are a radical step forward compared to linearised ones. The amplitude of diverging wave components, in particular in the bow wave system; the phase of waves at a distance from the hull; and the presence of short wave components, all are considerable improvements in the realism of the predictions. The method responds correctly to trim changes and, therefore, presumably to other changes in the hull geometry as well. Contrary to linearised methods it is able to handle transoms or bulbous bows above the still water surface. All this opens the way to a more accurate and more comprehensive optimisation of ship hull form designs.
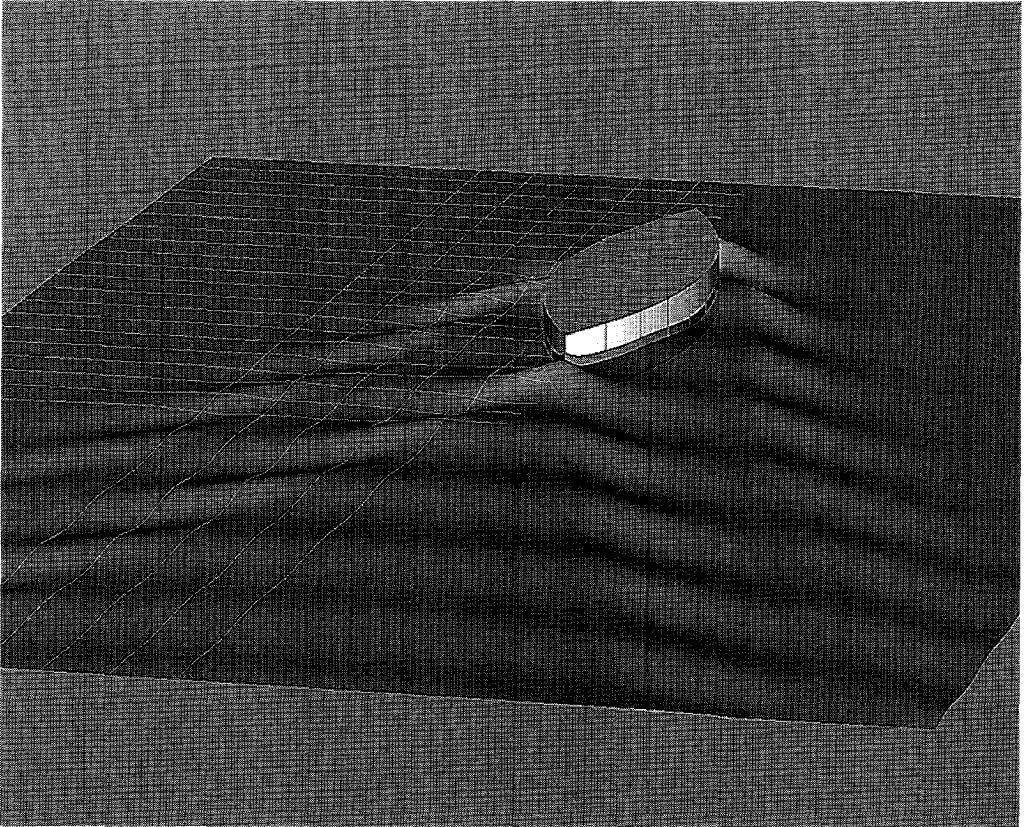
Figure 9.26: Wave pattern computed by RAPID for parabolic model with $L/B = 4$.

Chapter 10

The nature of nonlinear effects in wave pattern predictions

By using the nonlinear method now avaliable, the magnitude and nature of nonlinear effects are studied. Several of the unexpected phenomena are tentatively explained in terms of transfer and refraction effects.

10.1 Introduction

Chapter 4 described the results of a study, mainly carried out in 1989 — 1990, on the adequacy of linearised free surface conditions for the wave resistance problem. The various approaches used there to assess the errors introduced by the linearisation all were rather indirect, and the study was not conclusive in all respects. With the nonlinear method now available a much more direct assessment of the adequacy of linearised methods and the importance of nonlinearities can be made. This is what we shall do in the present chapter.

An important reason to have a closer look at the magnitude and nature of nonlinear effects is that some puzzling results have been obtained. As has already been shown in Chapter 9, *nonlinear effects are much larger, and occur in other cases, than had generally been expected. In many cases there is a surprisingly large effect of nonlinearities on the wave pattern of faster, more slender ships (ferries, containerships etc.). For full-block ships like tankers on the other hand, nonlinear effects often do not modify the general character of the wave pattern but only cause certain phase and amplitude changes. In general, diverging waves are much more affected than transverse waves.*

179

For the wave *resistance* it seems to be just the other way round: for slender ships the difference between the predictions by linear and nonlinear methods is often not really large (although there are notable exceptions), but for full hull forms the small wave pattern changes have a large effect on resistance and appear to eliminate the negative resistance values predicted by slow-ship linearised methods.

In the practical use of wave pattern calculations for optimising a hull form design, recommendations are made as to how the design can be improved, based on analysis of the calculated flow and wave pattern. This requires insight in the relation between hull form aspects and relevant flow features. Understanding of the nature of nonlinear effects, which now have been found to play an important role, is therefore desired.

The study described below tries to categorise and explain the nonlinear effects, drawing upon physical intuition rather than mathematical rigour. We only consider nonlinearities in the free surface conditions, not those in the hull conditions (viz. the effect of imposing the hull boundary condition on the actual wetted surface, and of the dynamic trim and sinkage).

10.2   Classification of nonlinear effects

A distinction can be made between different types of nonlinear effects. To illustrate this we first consider slow-ship linearised free surface conditions, which can all be written as:

$$Fn^2(\Phi_x^2\varphi'_{xx} + 2\Phi_x\Phi_z\varphi'_{xz} + \Phi_z^2\varphi'_{zz}) + \varphi'_y = RHS \qquad (10.1)$$

imposed on $y = 0$ or $y = \eta_r$. Here Φ is the double-body potential and φ' is a wave-like perturbation. Various slow-ship theories proposed differ in the form of the right hand side, which amongst other things includes wave excitation by the double-body pressure field. Note that the right hand side may contain terms in φ' as well.

In agreement with the assumption of small Fn, the left hand side has a form pertinent to *refraction of short waves by a slowly varying flow field,* in this case the double-body flow field. This can be shown by linearising with respect to a base flow $\nabla\Phi$ and neglecting all contributions from $\nabla\eta_r$. Replacing the double-body flow by a uniform flow we obtain the Kelvin free surface condition, which evidently contains no refraction effect.

In a fully nonlinear method we do not usually distinguish a non-wavy base flow and a wave-like perturbation. But if any such distinction is made,

$$\phi = \Phi_{nw} + \varphi_w , \qquad (10.2)$$

we can cast the free surface condition in the form:

$$Fn^2(\phi_x^2\varphi_{w_{xx}} + 2\phi_x\phi_z\varphi_{w_{xz}} + \phi_z^2\varphi_{w_{zz}}) + \phi_y = RHS \qquad (10.3)$$

on $y = \eta$, which is similar to (10.1). Therefore, a nonlinear solution

- includes refraction by the *actual* flow field around the hull, rather than by the double-body flow;

- includes all terms of higher order in the wave perturbation (but no order assumptions are actually made);

- imposes the free surface condition at the *actual* wave surface instead of at the still water surface. This gives rise to what we have called earlier the *"transfer effect"*.

We remark that the first two items can only be separated when there is a sufficient disparity of their length scales, i.e. for waves that are short relative to the dimensions of the hull.

We shall now try to determine the relative importance of the transfer and refraction effects for a number of cases, and see whether the above distinction, which admittedly may seem fairly artificial, increases our understanding of the physics. To study the relative importance of the transfer effect I have made a reduced, "No Transfer" version of RAPID, in which the free surface condition is imposed on the still water plane. This eliminates the transfer effect but all other nonlinear effects are present; therefore iteration remains necessary. Convergence is very fast and stable in all cases, which confirms that *it is the vertical movement of the collocation points and free surface panels, with its somewhat unpredictable effects on the residues, that is the cause of the convergence difficulties typical of many solution methods for the nonlinear wave resistance problem.*

The distinction of nonlinear effects can now be made by comparing wave patterns predicted by a Neumann-Kelvin method, found as the first iteration of RAPID (labelled "NK" in the following); Dawson's slow-ship linearised method; the nonlinear "No Transfer" method (labelled "NT"); and the full RAPID code. Which effects these methods do and do not incorporate is indicated in Table 10.1. To minimise the effect of numerical errors on the comparison, all methods have been implemented using raised panels, and the same panellings have been applied.

method	refraction	transfer	other nonlinear effects
Neumann-Kelvin	no	no	no
Dawson	double-body flow	no	some
No transfer method	yes	no	yes
RAPID	yes	yes	yes

Table 10.1: *Nonlinear effects incorporated in various methods*

These methods have first been applied to a variety of practical cases, but no clear-cut explanation was found for the difference in diverging wave amplitude in particular. Therefore a "systematic model series" has been set up, of three models with parabolic waterlines (fore and aft symmetric), rounded rectangular sections, $L/T = 20$, and length/beam ratio's of 12, 8 and 4, respectively. By increasing the beam we expect that the importance of nonlinear effects is increased. The entrance

angle is about 27° for $L/B = 4$, a usual value for e.g. fishing vessels or container feeder ships. The hull panelling comprises 60 strips of 17 panels (1020 on each symmetric half), the free surface panelling consists of 14 * 112 panels. All calculations are for $Fn = 0.25$.

10.3   Bow wave height and shape errors in linearised methods

Fig. 10.1 shows the calculated hull wave profiles for the three models. The wave heights are scaled with the beam, so a thin-ship method, in which the entire perturbation caused by the ship is proportional to the beam, would give just coincident lines. All methods considered here, even the fully nonlinear one, very nearly do so for the two more slender models. But large deviations occur when going to $L/B = 4$: Both linearised methods predict a decrease of the bow wave height and a strong reduction of the wave amplitude along the hull, while in the nonlinear method the bow wave slightly *increases* in height and waves along the hull remain significant.

The wave profiles for $L/B = 12$ are compared directly in Fig. 10.2. There is very little difference between the NK and slow-ship solution, as could be expected because the double body flow is still very nearly uniform. But there is already a significant difference of the nonlinear prediction with both linearised ones; in particular the bow wave height is already 16 % larger. A similar case was already met in Fig. 9.1. Quite remarkably the NT result is virtually identical to that of DAWSON.

For $L/B = 4$ (Fig. 10.3) the nonlinear bow wave height is 40 % larger than that according to Dawson's method, so the difference increases with the fullness of the body, but fairly slowly. The nonlinear NT method again gives almost the same bow wave height as both linearised methods. This is a recurrent feature of all cases studied and indicates that *the underestimation of the bow wave height by all linearised methods is merely a consequence of imposing the free surface condition at the still water surface and neglecting the transfer effect.* As far as I know this is a new finding that finally throws some light on this shortcoming of linearised methods that is known already for decades. It also indicates that any improvement of this feature in a linearised approach should be sought in modelling the transfer effect.

Returning to Fig. 10.1 we see that with increasing beam the crest and the backward face of the bow wave remain almost at the same longitudinal position in NK, move slightly forward in the slow-ship result, and move significantly forward in the fully nonlinear solution, making the bow wave shorter and more pointed. Method NT fully agrees with RAPID in this respect, as can be appreciated from Figs 10.2 and 10.3. This indicates that *the difference in bow wave length and position is a consequence of refraction* or other nonlinear contributions.

This is easy to explain in the case of low Fn, when the waves generated are short compared to the length scale of the velocity variations in the flow around the hull. We may then assume that the wave only feels the local velocity, not the undisturbed velocity at infinity; and that the phase speed of the waves relative to that *local* velocity is connected with the *local* wavelength by the usual dispersion relation; assumptions first phrased by Ursell [79]. Near the bow the flow is
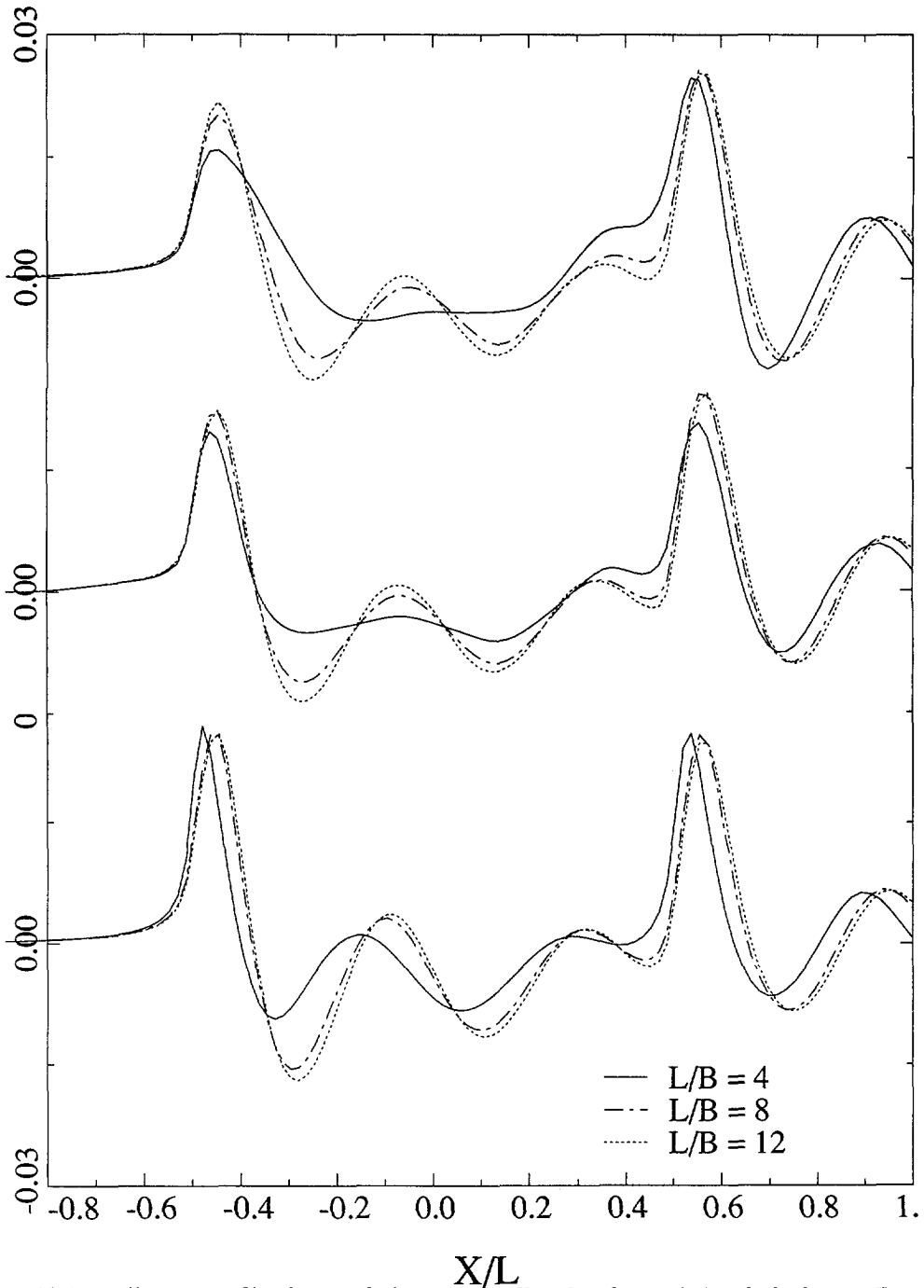
Figure 10.1: *Hull wave profiles for parabolic models. Wave heights scaled with the beam. Top: Neumann-Kelvin. Middle: Dawson. Bottom: nonlinear.*
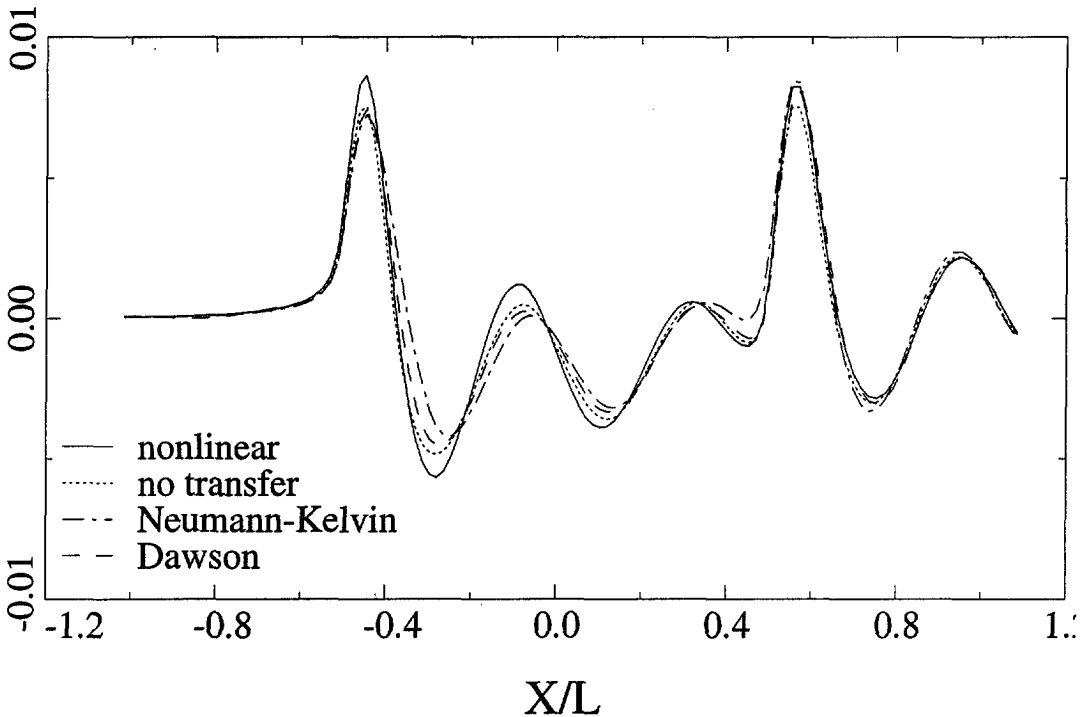
Figure 10.2: *Hull wave profiles for parabolic model with L/B = 12 .*

retarded, and a smaller wave propagation speed suffices to make the wave stationary relative to the ship. This corresponds with a smaller local wavelength. The fuller the bow, the larger the local wavelength reduction. Method NT fully includes this refractive effect and shows the proper behaviour. In the slow-ship method the refracting velocity field is represented by the double-body flow, which shows qualitatively the right features. But the flow retardation in the bow area in double body flow is smaller than that in the actual flow (the true bow wave height is generally larger than that found from the double-body flow), such that the shift and wave length reduction are somewhat too small. In the NK method the refraction effect is entirely absent, so the length of the bow wave is greater and does not respond to increasing bow fullness. Although in the case considered here we cannot assume that the waves are really short, the nonlinear effects still appear to show precisely the same trends.
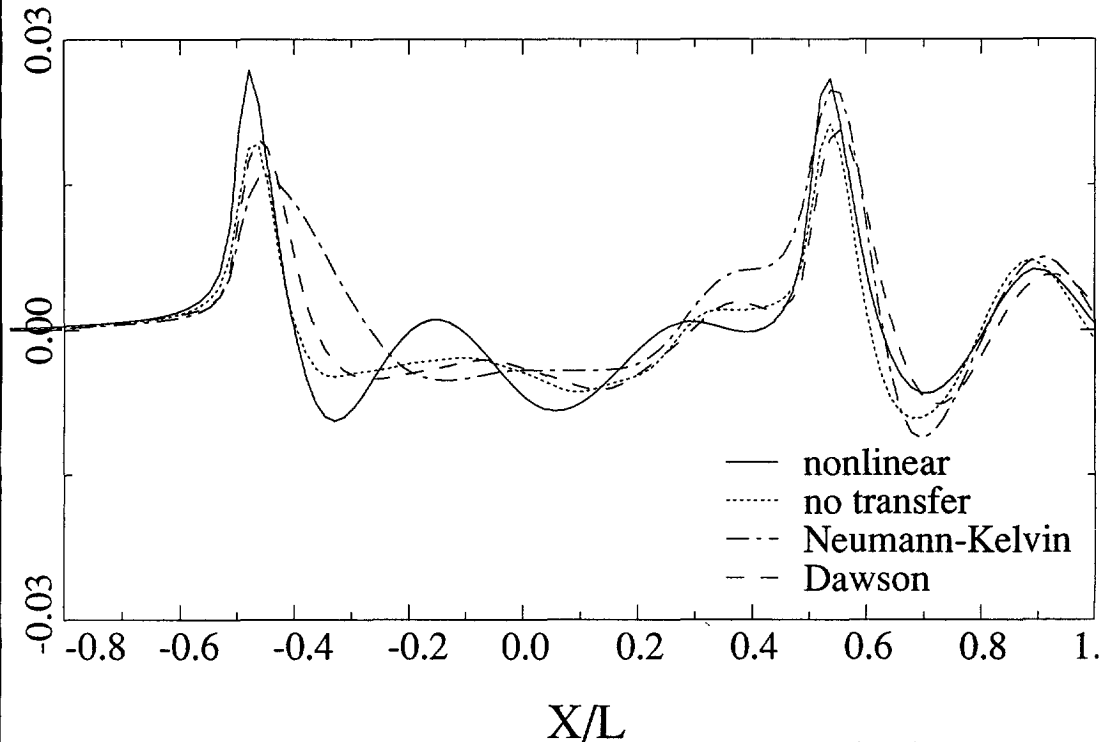
Figure 10.3: *Hull wave profiles for parabolic model with L/B = 4 .*

10.4   Diverging wave amplitude and phase errors in linearised methods

Fig. 10.4 shows longitudinal wave cuts at 0.20*L* off the centreline. Each figure compares the predictions for one length/beam ratio by the different methods. The vertical scales are proportional to the beam, so a thin-ship method would give three times the same figure. Instead, for increasing fullness the waves appear to move forward in all methods, except in the NK method: here the phases do not respond to the fullness at all; thus the waves incur a substantial phase lag for fuller vessels. At least for $L/B = 12$ and 8, method NT has the same phase as the fully nonlinear prediction, so again it is refraction that causes these phase differences; and compared to both these nonlinear methods the refraction in the slow-ship method is slightly too small. As refraction effects are cumulative, they are more pronounced at a distance from the hull.

Already for $L/B = 12$ the nonlinear method predicts a 30 % larger amplitude of the bow wave system at $z/L = 0.20$ than the slow-ship method, and this increases to 70 — 90 % for $L/B = 4$. This therefore is again an example of a drastic difference in diverging bow wave amplitude between the linear and nonlinear predictions. The NT result is somewhere in between, indicating that the
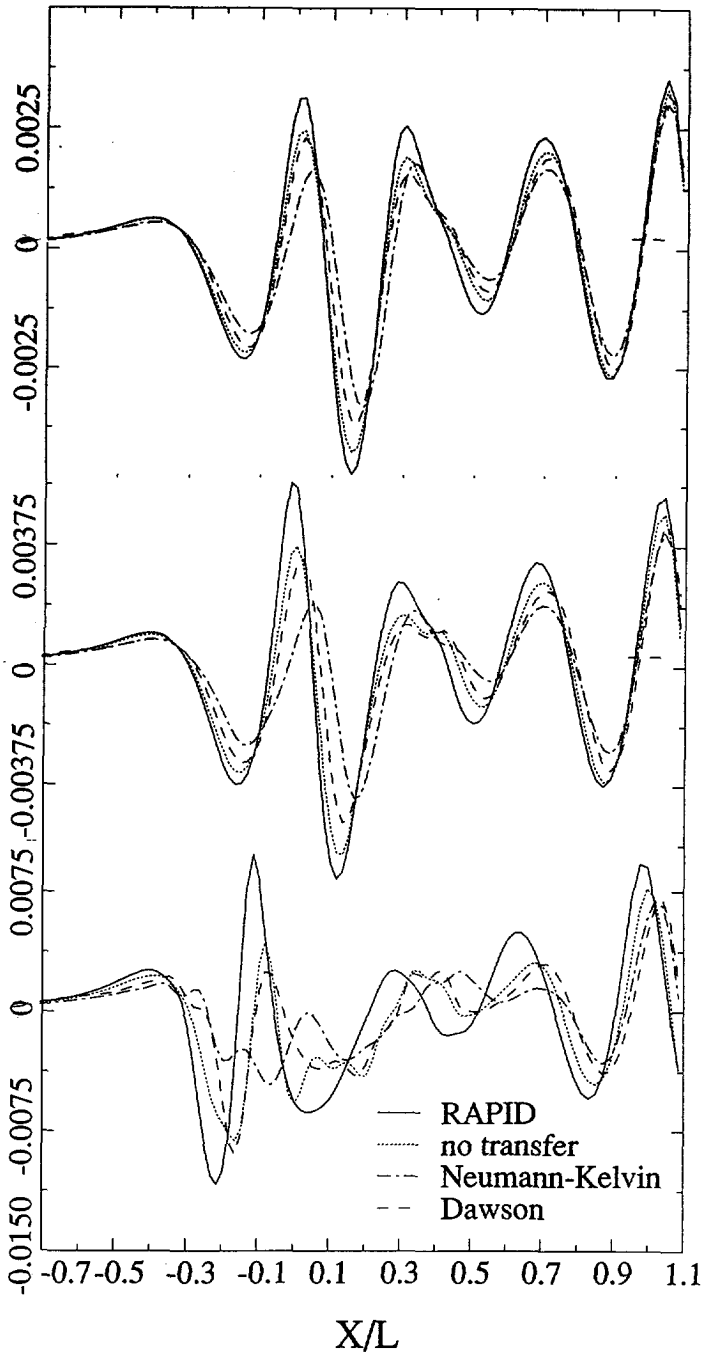
Figure 10.4: *Longitudinal wave cuts at z/L = 0.20 , for parabolic models. Top: L/B = 12 ; middle: L/B = 8 ; bottom: L/B = 4 .*
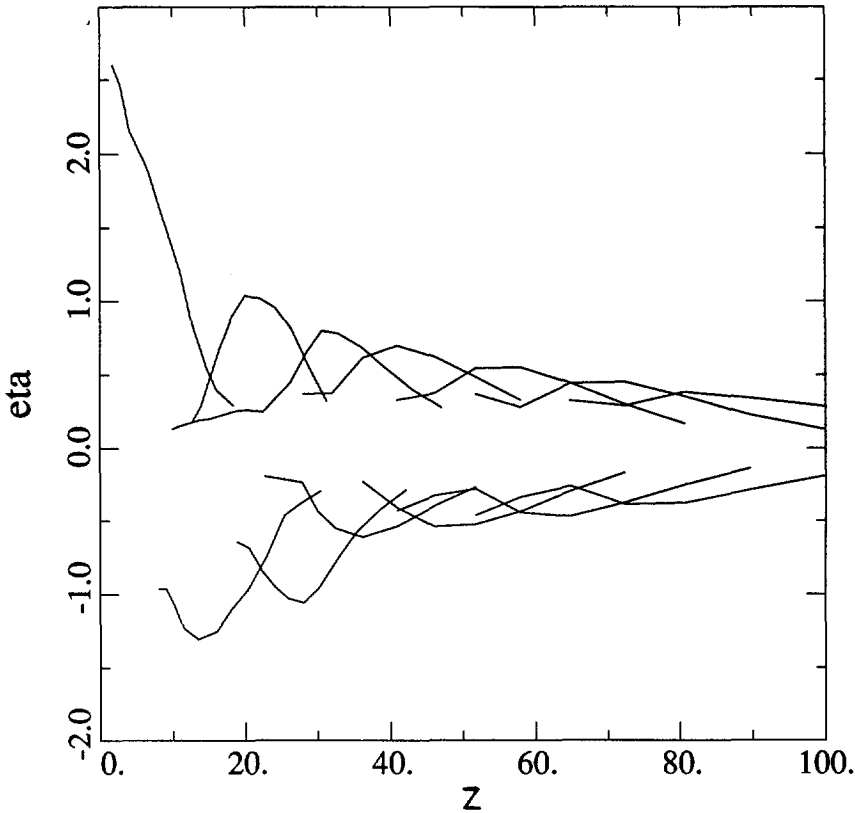
Figure 10.5: *Front view of crest and trough outlines of the bow wave system, computed by* RAPID *for parabolic model with L/B = 4 .*

difference is partly due to transfer, partly to refraction.

These wave amplitude differences at some distance away from the hull are significantly larger than the differences in bow wave height at the hull itself (which were 16 % and 40 % for *L/B* = 12 and 8, respectively), so something particular is happening to the wave amplitude between the bow and the wave cut considered. To further study this phenomenon I have made some additional calculations for the *L/B* = 4 vessel on a larger free surface domain. Fig. 9.26 and the cover photo of this book show the calculated wave pattern. Fig. 10.5 displays a number of consecutive crests and troughs of the bow wave system, projected onto a $y - z-$plane, as calculated by the nonlinear method. By drawing the envelope of these waves we can find the variation of crest-to-trough wave heights with distance (z) from the hull centreplane. Fig. 10.6 gives another representation of the wave height decay. I first have subtracted the local double-body wave heights η_r from all wave elevations, to more clearly distinguish the true wavelike part of the free surface disturbance. For all longitudinal lines of free surface collocation points the maximum and minimum values of $\eta - \eta_r$ in the bow wave system have been determined, and these are represented by markers in
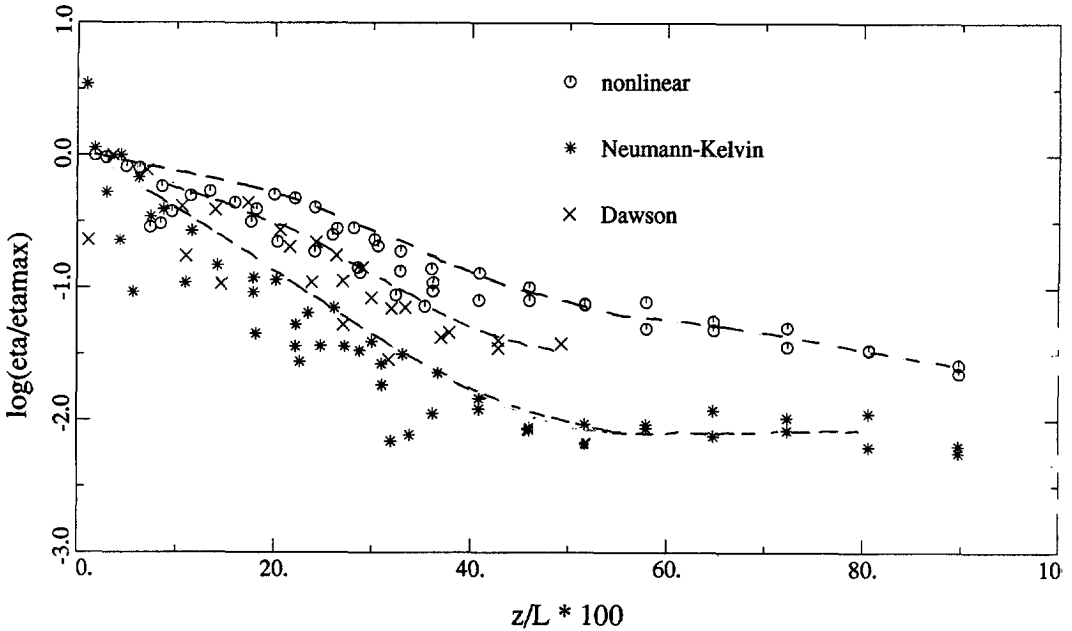
Figure 10.6: *Logarithm of normalised maximum height of bow wave system predicted by various methods, for parabolic model with L/B = 4* .

the plot. The apparent irregularity of the plot simply results from the discrete data and the finite number of crests and troughs; the figure essentially conveys the same information as Fig. 10.5. The shape of the envelope of the waves is suggested by the lines sketched in the plot. Because we want to separate the decay properties from the prediction of the wave height at the bow itself, all wave heights have been normalised by the value of $\eta - \eta_r$ at the bow predicted by the same method; and these relative wave amplitudes are plotted on a logarithmic scale.

It then appears that a large difference arises during the propagation of the waves through the ship's near field, for $z/L < 0.30$. In this area, for the NK method the relative decay is much quicker than for the fully nonlinear method; and for the slow-ship method, somewhat quicker. The result is that after the waves have travelled through this near field, the normalised wave heights for the NK method are about 50 % lower than for the fully nonlinear solution; and for the slow-ship solution they are 30 % lower. The relative differences in wave amplitudes so obtained are essentially conserved at larger distances. Here the local disturbance has died out, the wave steepness is small enough to permit linearisation, and all methods essentially become equal. Therefore the asymptotic decay rates are roughly equal for the various methods.

We can conclude that the large differences in amplitude of the bow wave system at a distance from the hull are not only a consequence of the differences in bow wave height right at the bow, but also of the difference in decay rate of the waves while they travel through the ship's near field.

Methods that predict a higher wave at the bow appear to give some further amplification (or slower decay) of the waves in the near field. While the mechanism behind this has not yet been clarified, the relative ranking of the methods suggests that again refraction is playing a role here.
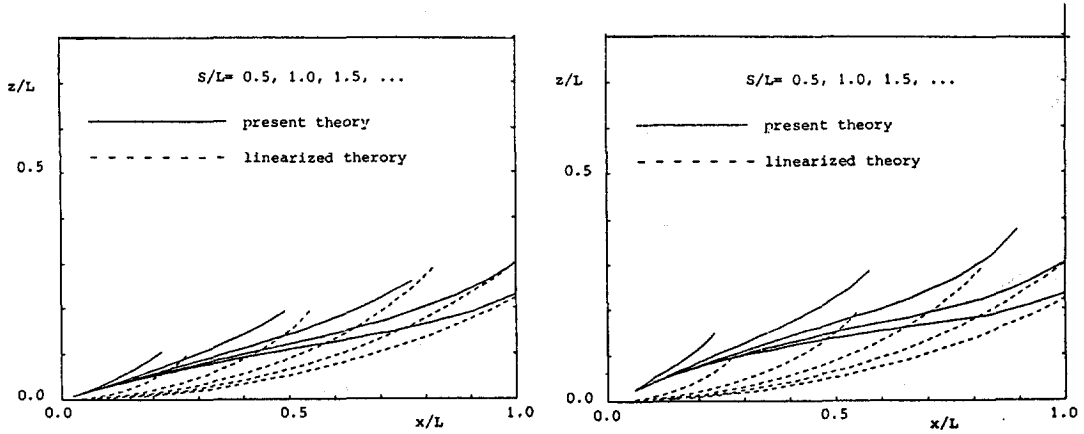

Figure 10.7: *Effect of double-body flow refraction on wavefronts for diverging bow-wave system, as calculated by Brandsma and Hermans. Circular-arc struts with bow entrance angles of 15° (left) and 22.5° (right).*
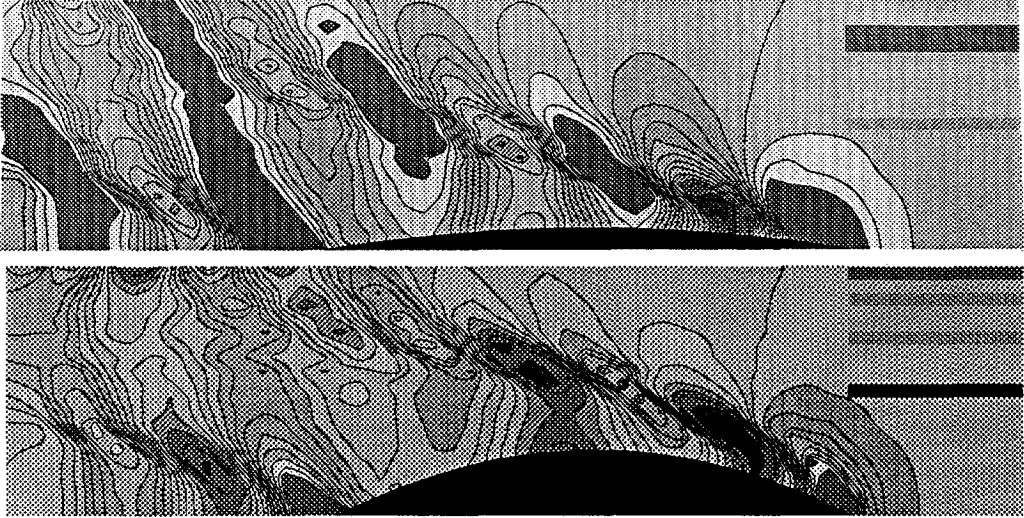

Figure 10.8: *Wave pattern of parabolic models with L/B = 12 (top) and L/B = 4 (bottom), calculated using* RAPID.

10.5   A ray theory explanation

To detect a possible cause of this phenomenon we again suppose that the waves are relatively short and propagate over a slowly varying base flow field around the hull. We may then apply ray theory. The rays represent the paths of the energy transport connected with the various wave components, and run in a direction which is the vector sum of the group velocity and the local base flow velocity. Along a ray, refraction changes the wave number vector k according to (See Ref. [80], Section 4.6):

$$\frac{dk_x}{dt} = -k_x \frac{\partial U}{\partial x} - k_z \frac{\partial W}{\partial x} \tag{10.4}$$

$$\frac{dk_z}{dt} = -k_x \frac{\partial U}{\partial z} - k_z \frac{\partial W}{\partial z}, \tag{10.5}$$

where U, W are the x and z components of the base flow velocity. In our coordinate system

$$k_x = -|k| \cos \gamma \quad , \quad k_z = |k| \sin \gamma,$$

γ being the angle of wave propagation relative to the x-axis. Near the crest of the bow wave close to the bow

$$\frac{\partial U}{\partial x} > 0, \quad \frac{\partial U}{\partial z} = \frac{\partial W}{\partial x} > 0, \quad \frac{\partial W}{\partial z} < 0.$$

It then follows that k_x may increase or decrease, and will tend to decrease in particular for larger γ (diverging waves); and k_z increases along a ray. This means that the refraction by the flow field around the bow wave increases the angle γ of diverging waves (makes the crests more "longitudinal") while they move away from the hull.

For double-body flow refraction the effect on the crest lines has been calculated by Hermans and Brandsma [81] using a numerical ray tracing method. An example is shown in Fig. 10.7. For comparison Fig. 10.8 shows wave patterns found from RAPID for the parabolic models with $L/B = 12$ and 4 . In both figures we observe that the larger refraction for the fuller hull form leads to a local outward displacement of the outmost crests and increases the divergence angle γ. The outward displacement is observed as a forward shift in the longitudinal cuts in Fig. 10.4. This good qualitative agreement suggests that the trends indicated by ray theory still hold for not-so-short waves.

Besides these changes of wave angles and locations, ray theory also indicates the corresponding variation of the wave energy per unit area, W_r , and thereby of the wave amplitude [80]:

$$dW_r/dt = -W_r \frac{\partial u_i}{\partial x_i} + \frac{W_r}{\omega_r} \cdot \frac{d\omega_r}{dt} , \tag{10.6}$$

where u_i are the components of the group velocity and ω_r is the relative wave frequency in a coordinate system moving with the local flow. The derivatives are along a ray. The first term can be regarded as the variations of the wave energy, required to conserve the wave energy flux if the group velocity varies. The second term represents energy exchange between the waves and the mean flow.

When the waves are generated at the bow they first propagate over a flow with reduced velocity; upon leaving the near vicinity of the bow they meet an increasingly opposing flow due to the increase of U and decrease of W. This results in an increase of the wave energy. The larger the flow retardation at the bow is (so, the higher the bow wave), the stronger the refraction, and thereby the larger the wave amplification. This matches our observation that the largest amplification is obtained for the fully nonlinear method (having the highest bow wave), slightly less for the slow-ship method (refraction by double-body flow, with reduced retardation), and no amplification for the NK method (which lacks any refractive effect).

The magnitude of refraction effects is demonstrated by an example given in a paper by Longuet-Higgins and Stewart [82], of waves propagating obliquely over a current of which the velocity increases in transverse direction, as shown in Fig. 10.9 copied from [82]. We translate this to the case of the flow along a ship hull, which has a longitudinal velocity $U(0)$ at the waterline, increasing to 1.0 away from the hull. We suppose that this base flow has little variation in longitudinal direction. Superimposed on this flow there are waves, with, in our case, an initial phase velocity related to their initial direction through a local dispersion relation:

$$c_0 = U_0 \sin \theta_0 \qquad (10.7)$$

where θ_0 is as defined in Figure 10.9. During the propagation of the waves over the current field with its increasing velocity, the longitudinal component of the wave number vector remains constant but the transverse component increases: waves become shorter and more diverging, as indicated in the figure. It can be derived that the wave direction satisfies:

$$\sin \theta(z) = \sin \theta(0) . \frac{U(0)^2}{U(z)^2} \qquad (10.8)$$

Simultaneously the wave amplitude changes according to [82]:

Figure 10.9: *Schematic diagram of wave refraction by a shearing current, taken from Longuet-Higgins and Stewart 1961.*

$$\frac{a}{a_0} = \sqrt{\frac{\sin 2\theta_0}{\sin 2\theta}} \qquad (10.9)$$

For assumed values of U_0 and θ_0 the amplification of the waves by the refraction can now directly be found. The refraction effect appears to be drastic. E.g. for $U(0) = 0.7$, the amplification ratio's
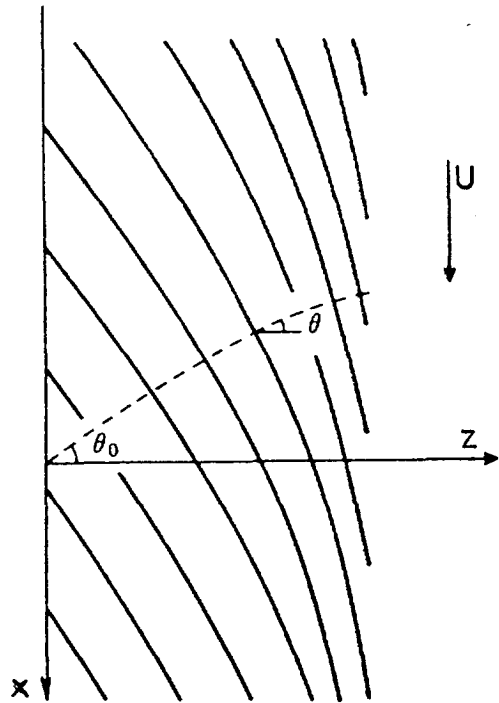
due to the increase of the base flow velocity to 1.0, are 1.06 , 1.24 and 1.35, for $\theta_0 = 60°$, $45°$ and $30°$, respectively.

This simplified example therefore displays a similar change of wave directions as we observe in ship waves; it shows that already a modest transverse variation of the refracting velocity field may have a large impact on the wave amplitude; and that the largest effect is found on the amplitude of diverging waves. It may be considered as supporting our hypothesis that the substantial differences in the decay rate of the bow wave system are caused by refraction of waves during their propagation through the near field.

Again, the use of these theories here is far from mathematically rigorous. The basic assumption that short waves propagate over a slowly varying base flow field, is obviously violated here: the variations in the base flow field, and in particular the differences in those variations between the methods, have the same length scale as the waves themselves. In any case ray theory cannot be applied to the behaviour at the bow itself, because of the possibly singular behaviour of the base flow there. The quantitative results of ray theory therefore cannot be used; but the trends it indicates appear to be in good agreement with what we see in nature and what we observe from our calculations, and they help us to understand what happens.

10.6   Conclusions

- As is well known, bow wave heights are systematically underestimated by all linearised methods. This is entirely caused by imposing the free surface condition at the still water surface and neglecting the transfer effect. The underestimation gradually increases with bow fullness.

- Linearised methods often predict a bow wave somewhat too far aft and too long. This is caused by the absence or incomplete incorporation of the refraction effect.

- Linearised methods dramatically underestimate the amplitude of diverging bow waves at a distance from the hull. The cause seems to be twofold. In the first place there is the underestimation of the bow wave height at the bow, which causes a too small initial height of the wave system. Secondly, linearised methods underestimate (or neglect) the wave amplification by refraction in the near field, by using a base flow with reduced velocity gradients or perhaps improper phasing or length scale of these gradients.

- The latter refraction effect qualitatively corresponds with a case studied in [82], which demonstrates the magnitude of the wave amplification and explains our observation of a much stronger effect on diverging rather than on transverse waves.

The present study is no more than a first attempt to understand the principal differences between linearised and nonlinear wave pattern predictions. There appears to be a rich variety of nonlinear effects in ship wave patterns, and more is to be done before their nature is fully understood.

Chapter 11

Discussion and conclusions

This chapter discusses some aspects of the method developed that leave room for further improvement. Disregarded physical aspects and remaining areas of research are identified. The main conclusions are listed, and the work completed is surveyed.

11.1   Remaining problems and restrictions

In the previous chapters, and in various applications of the method, some remaining shortcomings and possibilities for further improvement of the accuracy, efficiency or flexibility of the method have been identified. These will now be discussed.

11.1.1   Numerical aspects

First a few points regarding the numerical modelling and implementation will be considered.

The principal feature of the numerical modelling applied in the nonlinear method is probably its simplicity. Flat, constant-density source panels are used, the iterative scheme is fairly straightforward and most components of the method are basically conventional. Nevertheless, as mentioned before, the care taken in defining many details is decisive for the convergence of an iterative approach for the steady problem considered. With all the choices as made in the present method, the convergence and robustness appear to be amply sufficient for routine application.

While the numerical accuracy of the wave pattern predictions in general is quite satisfactory, we often have to use fairly large panel numbers. As a rule, free surface panel lengths are about 3 to 4

% of the transverse wave length, and total panel numbers of 5000 are not exceptional. Such panel densities have been made possible by the removal of the instability with regard to point-to-point oscillations which is typical of a more conventional implementation. With current computational facilities the panel numbers used present no problem at all. Still, alternative methods often use a much smaller number of panels; but detailed grid dependence studies for the wave pattern have almost never been published, and most likely those calculations are significantly less accurate.

To improve the numerical accuracy for a given panel density, for the hull higher-order source panels could be adopted. The resulting reduction of computational effort would be immaterial, but it could save time in case the hull panelling is generated manually from a lines drawing, as is often the case. For the free surface, however, the use of higher-order panels would be useless. Chapter 6 shows that the discretisation of the free surface source distribution in the raised-panel approach is extremely accurate, and no significant improvement is possible.

But the dominant error source for the free surface is the use of finite difference schemes, and a major improvement could perhaps be obtained by using analytical derivatives instead. This should be checked by repeating the analysis of Chapter 6 for such a formulation. At the moment that the decision was taken to use difference schemes, their influence on the accuracy was not as evident as it is now. What the use of analytical derivatives would mean for the stability and robustness is not clear however, and in view of the favourable properties of the method as it is we do not envisage such a modification at present.

The numerical tests discussed in Chapter 7, and the validations in Chapter 9, have indicated some remaining points on which the numerics ask for improvement. One is the frequent occurrence of a slight dip just ahead of the bow wave crest at some distance away from the hull, as observed in e.g. Figs 7.7, 9.21 and 9.23. Its cause is not yet known. Another, probably related, flaw is the incidental occurrence of slight short, strongly diverging waves for fine transverse discretisations and relatively large panel elevations. There may be a connection with the occasional transverse point-to-point oscillations in the free surface source strengths. The precise treatment of the hull-free surface intersection for sloping sections appears to play a large role here. Some strategies to cope with this problem have been worked out, and will be incorporated in the code soon.

What could be illuminating with respect to some of these questions is a three-dimensional version of the accuracy and stability study carried out in Chapter 6. This could indicate the effect of e.g. transverse difference schemes and transverse collocation points shifts, which otherwise will have to be found by plain numerical experimentation. Extension of the analysis now available to 3D is to be considered. On the other hand, some of the properties to be studied are strongly affected by the finite transverse extent of the domain and the treatment at the waterline, which are disregarded in the analysis.

The numerical convergence studies and validations have indicated that the prediction of the wave resistance still is to be improved. Current experience is that it has an unacceptable sensitivity to numerical parameters such as hull and free surface panelling and the panel elevation. Even so, a comparison of variations of a design, keeping these parameters equal, usually provides good

indications of resistance changes, often even quantitatively. This was not the case for slow-ship methods. But additional study is necessary and will be carried out to improve the numerical accuracy. In view of the accurate and stable prediction of the wave pattern, evaluation of the resistance from analysis of that pattern seems most promising and will soon be implemented. What remains is the fact that the wave resistance so obtained is that in inviscid flow, and full agreement with experimental residual or wave pattern resistances cannot be expected.

However, the importance of quantitatively accurate wave resistance predictions should not be overemphasised. The RAPID method is used mainly as a tool to optimise the hull form design. Here, human judgement of the desired direction of modification is still superior to any automatic optimisation approach, and this judgement requires an accurate prediction of the entire flow pattern rather than a single resistance number.

11.1.2   Viscous effects

Apart from the points mentioned above, and perhaps a few others, it seems that the problem of a non-breaking free surface potential flow around a conventional ship hull at usual speeds now is solvable with an accuracy sufficient for practical purposes. But an important question is, to what extent the *real* wave resistance problem now can be considered as solved. In other words: what is the role of physical phenomena disregarded in the mathematical model?

As is quite clearly observed in several of the validations, viscous effects often substantially influence the stern wave system. Experience tells that predicted hull wave profiles usually are accurate until quite close to the stern, and only the very last part is seriously affected by the boundary layer and wake. But this may have an appreciable effect on the stern wave generation and resistance. For the model scale Series 60 wave pattern shown in Fig. 9.3 for instance, viscous effects were the main source of deviations. For full-scale vessels the deviations will be much smaller. It could be worthwhile to attempt to incorporate some of the effect through the addition of a displacement thickness or surface transpiration velocity, but these concepts are hard to apply where viscous effects are really important.

Harder to deal with are viscous effects in the flow off a transom stern. While linearised methods do not provide any useful indication as to the best shape of the stern and position of the transom edge if that is above the still water line, with RAPID stern optimisation is possible and has been found to be quite effective. But this presumes a smooth "transom flow", not severely affected by viscous effects. If some amount of dead-water flow is present behind the transom, the inviscid flow model usually strongly overestimates the amplitude of the waves behind it. It is to be investigated whether or not in such a condition the prediction still provides at least qualitatively useful guidelines for the stern design. If not, any major step forward for such cases probably will require solution of the viscous flow strongly coupled with the free surface, which will be a major challenge.

11.1.3   Wave breaking

Another class of physical phenomena that generally occurs but is commonly disregarded, is wave breaking. The state of the art regarding prediction of wave breaking and its effects is rather unsatisfactory. The most common type of breaking in steady ship wave patterns is the so-called *spilling* breaker, a region of strongly turbulent aerated flow riding steadily on the forward face of a wave crest. This may occur amongst others in diverging bow waves, even at a distance from the hull; right at the bow and the fore shoulder for full hull forms; and behind transom sterns at low transom Froude numbers. For twodimensional cases, a simple shear-flow model of a spilling breaker has been proposed by Tulin and Cointe [83], based on physical considerations and some quantitative data from experiments by Duncan [84]. In principle it also indicates the effect of the breaking on the following wave train. For 3D waves the model may require further tuning or extension.

The other type is a *plunging* breaker. After gradual steepening and overturning of a wave crest, the tip of the wave plunges into the wave surface. This phenomenon is best known from quasi-twodimensional time-dependent flows, such as for waves approaching a beach. But a quite similar situation may occur at a sharp ship bow, where usually a thin jet of water climbs up along the hull surface and overturns. The subsequent process again involves turbulent mixing and air entrainment, and is as little studied as a spilling breaker. Therefore, while the occurrence of a plunging breaker and its development up to (almost) the moment of impact can be predicted by a potential flow model, e.g. Refs. [85, 86], the effect of the breaking on the flow and wave pattern still cannot be satisfactorily predicted.

Wave breaking being so common in ship waves and being disregarded in potential flow models, some important questions arise:

- Is a method like that treated here able to deal with flows in which wave breaking occurs in reality?

- If so, what solution is found in such cases, and is the wave breaking indicated?

- To what extent is this solution useful from the practical point of view?

It is to be kept in mind here that the behaviour of a method solving the steady problem may well be different from that of a transient method. An interesting related question is, whether the description of the free surface as a single-valued function of the horizontal coordinates limits the applicability to moderate wave slopes and thereby excludes strongly nonlinear cases with wave breaking; as was stated in [87].

Let us consider the plunging type of breaking first. For describing what happens at a sharp bow the single-valued description could in principle be restrictive. Removing that restriction could permit to model the jet rising along the hull surface, but not its further evolution and effect on the wave pattern. Present simplified methods to deal with this situation have to make ad-hoc

assumptions or stop at the point of impact of the overturning wave crest on the wave surface. As long as this has not been properly solved the inability of the present approach to precisely model the behaviour right at the bow is not a true drawback in practice.

In the present method it appears that a plunging bow wave of the type just discussed most likely is "discretised away" and no particular sign of its occurrence is found; even not if the panelling is refined, as has been shown in Chapter 7. But for vanishing panel size a singularity at the bow might prohibit convergence of the solution. There is an obvious similarity with the 2D time-dependent problem of an impulsively started wave maker. A thin upward jet arises there, too, but has been shown to have just a quite localised effect on the flow. The 3D steady case will be less singular, the jet height being bounded by the stagnation height. In view of this presumably local character the solution obtained by the present method may well be appropriate except in the immediate vicinity of the bow, as is confirmed by the many validations.

Considering spilling wave breaking now, we observe that steady wave slopes in reality are only quite moderate. According to Duncan [84], in the wave train induced by a 2D submerged hydrofoil inception of wave breaking occurs at wave slopes between 16 and 24 degrees. That perhaps the spilling breaker itself has a very large local wave slope is a different issue, as the breaking will require a different modelling anyway; but the underlying irrotational flow can well be described by the present method. In practice, for cases displaying spilling wave breakers in reality, converged, smooth and basically plausible solutions have been obtained without any problem [76]. No particular indication of the occurrence of breaking is obtained, and a separate criterion for its inception would be needed. The solution found probably is similar to the actual behaviour, but with a larger wave amplitude due to the absence of dissipation.

There are, however, more severe cases in which the potential flow solution not only is not physically realisable, but even is nonexistent. An example is the 2D transom stern flow studied by Vanden-Broeck [66]. For $Fn_{tr} < 2.23$ the transom flow is nonexistent. Current experience suggest that then also the present method fails to converge, as indicated in Section 8.5.5.

There is a possible connection with occasional convergence difficulties for certain full hull forms at relatively high speed. It happens that the convergence first looks alright and then fails or suddenly blows up. This invariably happens near the steepest wave slopes, such as at the bow wave crest at some distance from the hull. In such cases violent wave breaking is present in reality, and these might also be cases for which a potential flow solution is nonexistent or unstable, and the dissipation of wave energy by breaking is indispensable. But this hypothesis would be hard to verify.

Both to reduce such convergence problems and to increase the realism of the predictions it could be useful once to incorporate an (approximate) model for the dissipation of wave energy by a spilling breaker, such as that proposed in [83].

Summarising, while the state of the art regarding the modelling of wave breaking and its effects is rather unsatisfactory, it is fortunate that for most practical applications the relevance of wave

breaking is limited.   Apparently, wave breaking must be fairly extensive in order to have an identifiable effect on the wave pattern.   In the majority of practical cases the present method provides a useful solution.

11.2   Conclusions

While most of the conclusions have been given at the end of the previous chapters, some of the more general ones are repeated below.

- For a linearised method, the slow-ship free surface boundary condition proposed by Dawson is a fairly good choice overall, although it is strictly inconsistent.   Main deficiencies in practice are the underestimation of the bow wave height (due to the neglect of the transfer effect), the underestimation of the amplitude of diverging bow waves (due to the neglect of the transfer effect and the insufficient wave amplification by refraction in the near field), the occurrence of negative resistance predictions (caused by an energy flux through the free surface), and the impossibility to take into account hull form features above the still water level. No true improvement on these points seems to be possible without leaving the concept of linearisation.

- Nonlinear effects on ship wave patterns have been found to be much stronger than anticipated, even for slender ships; in particular for the amplitude of diverging bow waves. Transverse wave components are much less affected.

- The nonlinear potential flow model often is a radical step forward compared to linearised methods and appears to incorporate much of the physics of ship wave making. The present method has a much better accuracy than linearised methods, and a substantially extended range of application and versatility of optimisation. In many cases detailed agreement with experimental data is obtained. The principal remaining deviations are due to viscous effects on stern waves, in particular if a dead water flow is present behind a transom stern.

- Modelling transom flows in a nonlinear method is more straightforward than in a linearised method, and is equally well applicable to transoms above the still waterline. The mathematical model and implementation selected lead to numerically accurate results. Agreement with experimental data for pure transom flows is fair, but somewhat less than for other aspects of the wave making, presumably because viscous effects again are felt here.

- The use of raised source panels has proven to be practical and accurate. Even with simple constant-density panels a very good smoothness of the velocity field is thus obtained, the familiar instability for high grid wavenumbers has entirely been eliminated, and numerical dispersion at low grid wavenumbers has been reduced from first to third order in the panel size. The remaining numerical dispersion is due to the difference scheme only. Moreover, the use of raised panels here has some advantages for efficiency and robustness.

- Within certain limits the distance of the panels above the wave surface has very little influence on the flow near the hull, somewhat more for the wave pattern at a greater distance. A good convergence of the predicted wave pattern with increasing panel density is found. In many respects the dependence on such numerical parameters is less than for a Dawson-type linearised method. An exception is the numerical evaluation of the wave resistance from the hull pressure distribution, which asks for improvement.

- Further improvement is desired in the methodology to evaluate the wave resistance, and in enhancing the stability of the method with regard to transverse oscillations or nonphysical strongly diverging waves. No fundamental difficulties are expected in this respect.

11.3   Epilogue — The development in retrospect

Besides describing the development of the RAPID method this Thesis also represents an almost chronological account of the work on wave pattern calculation methods that I have done at MARIN during the last 6 years. Chapter 3 outlined the situation around 1989, when linearised codes for wave pattern prediction were available at many institutes but were used only at few. The main reason for this was the fact that the incompleteness and unreliability of their predictions made interpretation and analysis rather difficult. The development of a fully nonlinear method was still considered to be a large step at that time, and in 1989 — 1990 I first have investigated whether it would be possible to improve the accuracy of the predictions within the framework of linearised methods. This study has been described in Chapter 4 and has been published before in [88, 89, 2]. A comparison of various linearisation proposals was made, and the validity of some of them was studied in different ways. This led to the conclusion that none of the alternative linearisations seemed to be able to remove the shortcomings identified. Further progress would require the development of a solution method for the fully nonlinear wave resistance problem.

That development has then been undertaken. The study of linearised methods was helpful in emphasising the importance of nonlinear effects and by indicating which effects would be dominant, what aspects would require particular attention and what should be demanded from the numerics. Based on these insights, on available literature and on considerations of accuracy and efficiency [90], around 1990 a basic solution approach has been selected (Chapter 5).

An unconventional choice made here, although already proposed before for such free surface problems, was to use a raised-panel method, a decision motivated in Chapter 6. One of the incentives was the fact that an analytical study on numerical accuracy, performed in 1990 [59, 91], indicated that a raised-panel discretisation introduces no significant numerical dispersion, contrary to a conventional method. The accuracy analysis in Chapter 6 basically extends that earlier study, but is much more complete because it pays attention to the difference scheme and the numerical damping. Consequently it yields several novel results, providing much better insight in the performance of the method as it is and how it might be further improved.

The iterative procedure has been implemented in 1991, initially based on a stripped raised-panel version of the DAWSON code, and it immediately proved stable and convergent. Extensive further work has been done in 1991 — 1992 to implement the free surface and hull panel adaptation, for reprogramming and for numerical accuracy and sensitivity studies. The essential steps of the complete method as described in Chapter 7 were published before in [91, 92]. The growing confidence in the RAPID method permitted to use it in a first commercial project in 1992, immediately proving its value for designing surface-piercing bulbous bows [92].

In 1992-1993 the modelling of the flow off transom sterns has been studied and implemented, as described in Chapter 8 and [76]. Paying attention to the possibly singular behaviour at the transom edge I have devised a certain implementation, basically similar to (but much more complete than) the transom modelling used already for several years in DAWSON. A study of the numerical accuracy indicated its usefulness in the context of the nonlinear method.

An experimental study carried out in 1994 confirmed the validity of the transom flow modelling and provided most valuable data on transom flows. Chapter 9 discussed this study, and some of the other experimental validations performed over the years for a variety of cases. It was demonstrated that the results are generally accurate and that most of the remaining deviations can be explained in terms of viscous effects, wave breaking, or the known and quantifiable effect of discretisation errors. At the same time some minor other shortcomings could be identified that will require further study.

Besides the work reported here, much had to be done to treat all geometric aspects involved and to implement the indispensable pre- and postprocessing. In 1994 I have improved the calculation efficiency, the user-friendliness and robustness of the code. This has permitted an almost immediate introduction of the RAPID method in ship design practice, and at MARIN it is now being applied to about 80 different hull forms per year in practical design projects [93], having almost completely replaced DAWSON, the linearised method that has served us well for 9 years.

The unexpected magnitude of nonlinear effects on the wave pattern even for slender ships, a recurrent feature in many applications, was the incentive for a study on the origin of these differences in 1995 [78]. While this study, described and extended in Chapter 10, has not been conclusive in all respects, it is a first step to cast light on the cause of several of the shortcomings of linearised predictions, such as the underestimation of the bow wave height and diverging bow waves, and it proposes explanations for some observed "nonlinear effects". It illustrates how the availability of a solution method for the full nonlinear problem can give us a better understanding of the physics of ship waves.

The final write-up of all this in the present Thesis in itself has proven to be useful, requiring further extension of several of the studies mentioned and providing several new insights and ideas for improvement of the method.

Further developments connected with wave making of ships will probably rather be concerned with the solution of Reynolds-Averaged Navier-Stokes equations with free surface boundary

conditions, which is already a very active research area. The present underestimation of wave amplitudes by such methods due to numerical damping first has to be removed. In the end such methods may be able to more accurately predict stern waves, and might even predict the flow off transom sterns with some extent of dead-water flow. The latter applications may require substantial further research however. While such methods may well be able to replace inviscid methods within 5 to 10 years, I expect methods such as the present one will remain useful for a longer period as a quick, stable and accurate method to predict the major features of the wave pattern of ships.

Overall I believe that the development of the RAPID method has been a successful venture. The use of the program has already had a substantial impact on the ship hull form design practice at MARIN. The proven success of the method in day-to-day ship design practice is definitely a gratifying experience for me. With the work described here I hope to have contributed to the development of numerical ship hydrodynamics, and in particular to its role in practical ship design.

Appendix A

Derivation of higher-order terms for linearised free surface conditions

Below we shall expand both the Kelvin condition and the slow-ship free surface condition to the next higher order in ϵ. Care should be taken with the "transfer" of the boundary condition from the actual towards the undisturbed free surface. We define:

η_r : the double-body wave height in slow-ship theory;
η_0 : the linearised wave elevation, simply expressed in quantities evaluated at $y = 0$;
$\bar{\eta}$: the expression for the wave elevation to the next higher order, still evaluated at $y = 0$;
η^* : the expression for the wave elevation including transfer terms and other higher order terms.
Unless indicated otherwise all quantities are evaluated at $y = 0$.

Kelvin condition

The velocity components are expanded as follows:

$$(\nabla \varphi')_{y=\eta} = (\nabla \varphi')_{y=0} + \eta \nabla \varphi'_y + \mathcal{O}(\epsilon^3) \tag{A.1}$$

The dynamic free surface condition then yields:

$$\bar{\eta} = \eta_0 - \frac{1}{2} Fn^2 (\varphi_x'^2 + \varphi_y'^2 + \varphi_z'^2) \tag{A.2}$$

$$\eta^* = \bar{\eta} - Fn^2 \eta_0 \varphi'_{xy} + \mathcal{O}(\epsilon^3) \tag{A.3}$$

Obviously $\bar{\eta}$ is an inconsistent expression adding some but not all second order terms in the free surface condition. To second order, transfer terms should be included as in (A.3).

Entering these expressions into the kinematic free surface condition results in the following second order free surface condition:

$$\varphi'_y = \text{term1} + \text{term3} + \text{term4} + \text{term5} + \text{term6} + \mathcal{O}(\epsilon^3) \qquad (A.4)$$

where

$$\text{term1} = \eta_{0_x} = -Fn^2\varphi'_{xx}$$

$$\text{term3} = \varphi'_x\eta_{0_x} + \varphi'_z\eta_{0_z}$$

$$\text{term4} = (\bar{\eta}_x - \eta_{0_x})$$

$$\text{term5} = (\eta^*_x - \bar{\eta}_x)$$

$$\text{term6} = -\eta_0\varphi'_{yy}$$

Term 1 is the single one occurring in the Kelvin condition. Terms 5 and 6 are transfer terms; terms 3 and 4 are other higher-order contributions.

Slow-ship condition

For the slow-ship free surface boundary condition, deriving the higher-order terms immediately poses us for the choice of which basic assumptions to use: those according to Baba/Ogilvie, with order reduction by differentiation, or those according to Eggers, in which $\nabla\varphi'$ and all its derivatives are assumed to be of $\mathcal{O}(Fn^2)$. In view of the basic conformity of Dawson's method with the latter I have followed Eggers's scheme.

The neglected terms to be found are $\mathcal{O}(Fn^6)$, and we need the following expressions for the velocity components:

$$(\phi_x)_{y=\eta} = \Phi_x + \varphi'_x + \frac{1}{2}\eta_r^2\Phi_{xyy} + \eta_r\varphi'_{xy} + \mathcal{O}(Fn^6) \qquad (A.5)$$

$$(\phi_y)_{y=\eta} = \eta_r\Phi_{yy} + \varphi'_y + \eta'\Phi_{yy} + \eta_r\varphi'_{yy} + \eta'\varphi'_{yy} + \frac{1}{2}\eta_r^2\varphi'_{yyy} + \frac{1}{6}\eta_r^3\Phi_{yyyy} + \mathcal{O}(Fn^8) \qquad (A.6)$$

$$(\phi_z)_{y=\eta} = \Phi_z + \varphi'_z + \frac{1}{2}\eta_r^2\Phi_{zyy} + \eta_r\varphi'_{zy} + \mathcal{O}(Fn^6) \qquad (A.7)$$

The various expressions for the wave elevation now become:

$$\eta_r = \frac{1}{2}Fn^2(1 - \Phi_x^2 - \Phi_z^2) \qquad (A.8)$$

$$\eta_0 = \eta_r - Fn^2(\Phi_x\varphi'_x + \Phi_z\varphi'_z) \qquad (A.9)$$

$$\bar{\eta} = \eta_0 - \frac{1}{2}Fn^2(\varphi'^2_x + \varphi'^2_y + \varphi'^2_z) \qquad (A.10)$$

$$\eta^* = \bar{\eta} - \frac{1}{2}Fn^2[\eta_r^2(\Phi_x\Phi_{xyy} + \Phi_{yy}^2 + \Phi_z\Phi_{zyy}) + 2\eta_r(\Phi_x\varphi_{xy}' + \Phi_{yy}\varphi_y' + \Phi_z\varphi_{zy}')]\qquad(A.11)$$

It follows that $\eta_r = \mathcal{O}(Fn^2)$, $\eta' = \eta_0 - \eta_r = \mathcal{O}(Fn^4)$ and the other contributions are $\mathcal{O}(Fn^6)$.

The higher-order terms in the combined free surface boundary condition are found by substituting these expressions into the kinematic boundary condition. The usual linearised condition is retrieved by including all terms up to $\mathcal{O}(Fn^4)$, and may be written as:

$$\varphi_y' = \text{term1} + \text{term2} + \text{term8} + \mathcal{O}(Fn^6),\qquad(A.12)$$

where:

$$\text{term1} = \Phi_x\eta_{rx} + \Phi_z\eta_{rz} + \Phi_x\eta_x' + \Phi_z\eta_z'$$

$$\text{term2} = \varphi_x'\eta_{rx} + \varphi_z'\eta_{rz}$$

$$\text{term8} = -\Phi_{yy}(\eta_r + \eta') - \varphi_{yy}'\eta_r$$

This corresponds with expression (4.10) proposed by Eggers. In Dawson's condition term 8 is absent.

The terms dropped are $\mathcal{O}(Fn^6)$, and their leading order contributions to the right hand side of (A.12) are symbolically represented by: term3 + term4 + term5 + term6, which are defined as follows:

$$\text{term3} = \varphi_x'\eta_x' + \varphi_z'\eta_z'$$

$$\text{term4} = (\Phi_x\frac{\partial}{\partial x} + \Phi_z\frac{\partial}{\partial z})(\bar{\eta} - \eta_0)$$

$$\text{term5} = (\Phi_x\frac{\partial}{\partial x} + \Phi_z\frac{\partial}{\partial z})(\eta^* - \bar{\eta})$$

$$\text{term6} = -\eta'\varphi_{yy}' + \eta_r(\varphi_{xy}'\eta_{rx} + \varphi_{zy}'\eta_{rz}) + \frac{1}{2}\eta_r^2(\Phi_{xyy}\eta_{rx} + \Phi_{zyy}\eta_{rz} - \varphi_{yyy}') - \frac{1}{6}\eta_r^3\Phi_{yyyy}$$

Terms 5 and 6 are again higher-order transfer terms with linear and nonlinear contributions. Terms 3 and 4 are the remaining "ordinary" nonlinear contributions.

Since it is our intention to evaluate these higher-order terms numerically, a slight simplification is to be made. In particular the expressions for η^* and term 6 contain third and fourth derivative terms of the double-body potential. Computing these from a solution obtained with constant-strength source panels is inaccurate and quite susceptible to numerical oscillations that may spoil the results. Additionally it may be argued that including these higher y-derivatives of the double body flow at the still water surface in many cases will reduce the accuracy. An example is given in Fig. A.1 for a hull with strongly flared sections at the waterline. The double body has a sharp knuckle at the still waterline, which to some extent will be found in the velocity field as well. Dropping the vertical derivatives of the double-body flow components means that a base flow is used which is in better agreement with the actual flow.
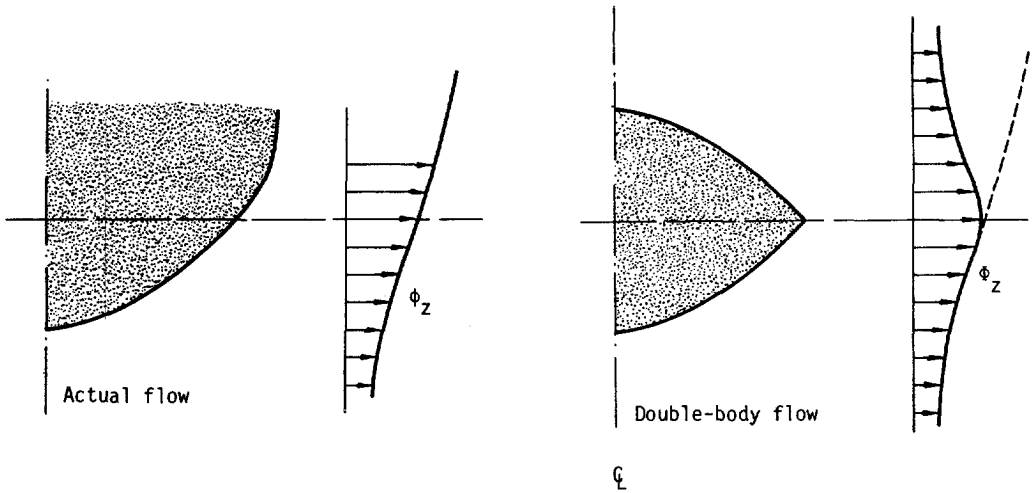
Figure A.1: *Transfer terms for double-body flow may reduce the accuracy.*

Because of this, and for mere convenience, we simplify the expressions given above for the higher-order contributions by deleting the transfer of the double-body flow, and find the following modified expressions which have been used in the actual evaluations:

$$\eta^* = \bar{\eta} - Fn^2 \eta_r (\Phi_x \varphi'_{xy} + \Phi_z \varphi'_{zy}) \tag{A.13}$$

$$\text{term6} = -\eta' \varphi'_{yy} + \eta_r (\varphi'_{xy} \eta_{rx} + \varphi'_{zy} \eta_{rz}) - \frac{1}{2} \eta_r^2 \varphi'_{yyy} \tag{A.14}$$

Bibliography

[1] Dawson, C.W., *"A Practical Computer Method for Solving Ship-Wave Problems"*, 2nd Int. Conf. Numerical Ship Hydrodynamics, Berkeley, USA, 1977

[2] Raven, H.C., *"Adequacy of Free-Surface Conditions for the Wave-Resistance Problem"*, 18th Symp. Naval Hydrodynamics, Ann Arbor, Michigan, USA, 1990.

[3] Ni, S.-Y., *"Higher-order panel methods for potential flows with linear or nonlinear free-surface boundary conditions"*, Ph.D. Thesis, Chalmers University, Göteborg, Sweden, 1987.

[4] Jensen, G., *"Berechnung der stationären Potentialströmung um ein Schiff unter Berücksichtigung der nichtlinearen Randbedingung an der Wasseroberfläche"*, Ph.D. Thesis, Univ. Hamburg, IfS Bericht 484, 1988.

[5] Campana, E., Di Mascio, A., Esposito, E., and Lalli, F., *"Domain decomposition in free-surface viscous flows"*, 6th Int. Conf. Numerical Ship Hydrodynamics, Iowa City, USA, 1993.

[6] Chen, H.C., Lin, W.-M., and Weems, K.M., *"Interactive zonal approach for ship flows including viscous and nonlinear wave effects"*, 6th Int. Conf. Numerical Ship Hydrodynamics, Iowa City, USA, 1993.

[7] Hess, J.L., and Smith, A.M.O., *"Calculation of non-lifting potential flow about arbitrary three-dimensional bodies"*, Douglas Aircraft Company, Report No. 40622, 1962.

[8] Jensen, P.S., *"On the numerical radiation condition in the steady-state ship wave problem"*, Jnl. Ship Research, Vol. 31 - 1, 1987.

[9] Bai, K.J., and Yeung, R.W., *"Numerical solutions to free-surface problems"*, 10th Symp. Naval Hydrodynamics, Cambridge, Mass., USA, 1974.

[10] Gadd, G.E., *"A method for computing the flow and surface wave pattern around full forms"*, Trans. RINA 1976, pp 207-220, London, UK, 1976.

[11] Van Beek, C.M., Piers, W.J. and Slooff, J.W., *"Panel method for the computation of the potential flow with lift and free surface effects about SWATH- and other ship configurations"*, National Aerospace Laboratory NLR, Report TR 84055 L, June 1984.

[12] Labrujère, Th. E., Loeve, W., and Slooff, J.W., *"An approximate method for the calculation of the pressure distribution on wing-body configurations at subsonic speeds"*, AGARD C.P. 71, Paper 11, 1970.

[13] Raven, H.C., *"Variations on a theme by Dawson"*, 17th Symp. Naval Hydrodynamics, Den Haag, Netherlands, 1988.

[14] Raven, H.C., *"From* HYDROPAN *to* DAWSON— *Study and revision of a wave resistance calculation method"*, Report 50600-1-RF, MARIN, Netherlands, 1986.

[15] Piers, W.J., *"Discretization schemes for the modelling of free water surface effects in first-order panel methods for hydrodynamic applications"*, National Aerospace Laboratory NLR, Report TR 83093 L, August 1983.

[16] Sclavounos, P.D., and Nakos, D.E., *"Stability analysis of panel methods for free-surface flows with forward speed"*, 17th Symp. Naval Hydrodynamics, Den Haag, Netherlands, 1988.

[17] Nakos, D.E., and Sclavounos, P.D., *"Kelvin wakes and wave resistance of cruiser- and transom stern ships"*, Jnl. Ship Research Vol. 38 - 1, 1994.

[18] Raven, H.C., *"Resistance and flow computations for 'Australia 2'; a validation study with the program* DAWSON*"*, MARIN, Netherlands, August 1987

[19] Baba, E., and Takekuma, K., *"A study on free-surface flow around bow of slowly moving full forms"*, Jnl. Soc. Naval Architects Japan, Vol. 137, 1975.

[20] Baba, E., and Hara, M., *"Numerical evaluation of a wave-resistance theory for slow ships"*, 2nd Int. Conf. Numerical Ship Hydrodynamics, Berkeley, USA, 1977.

[21] Newman, J.N., *"Linearized wave resistance theory"*, International Seminar on Wave Resistance, Tokyo / Osaka, Society of Naval Architects Japan, 1976.

[22] Ogilvie, T.F., *"Wave resistance: the low-speed limit"*, Univ. Michigan, Dept. Nav. Arch. Mar. Eng., Report No.002, Ann Arbor, USA, 1968.

[23] Eggers, K., *"Non-Kelvin dispersive waves around non-slender ships"*, Schiffstechnik, Bd. 28, 1981.

[24] Eggers, K., *"On the dispersion relation and exponential amplitude variation of wave components satisfying the slow ship differential equation on the undisturbed free surface"*, Study on local non-linear effect in ship waves, T. Inui, ed. , Tokyo 1980.

[25] Brandsma, F.J., and Hermans, A.J., *"A quasi-linear free surface condition in slow ship theory"*, Schiffstechnik, Bd. 32, 1985.

[26] Nakos, D.E., *"Ship wave patterns and motions by a three-dimensional Rankine panel method"*, Ph.D. Thesis, MIT, Cambridge, Mass., USA, 1990.

[27] Bai, K.J., and McCarthy, J.H. (ed.), *"Proceedings of the workshop on ship wave computations"*, DTNSRDC, Bethesda, Md., USA, 1979.

[28] Wehausen, J.V., and Laitone, E.V., *"Surface waves"*, in: Encyclopedia of Physics, Vol. IX, Springer Verlag, 1960, pp. 446 - 778.

[29] Eggers, K., *"A method for assessing numerical solutions to a Neumann-Kelvin problem"*, Proceedings Workshop on Ship Wave-Resistance Computations, Supplementary papers, DTNSRDC, Bethesda, Md., USA, 1979.

[30] Korving, C., and Hermans, A.J., *"The wave resistance for flow problems with a free surface"*, 2nd Int. Conf. Numerical Ship Hydrodynamics, Berkeley, USA, 1977.

[31] Oomen, A., *"Free-surface potential flow computation using a finite-element method"*, 3rd Int. Conf. Numerical Ship Hydrodynamics, Paris, France, 1981.

[32] Raven, H.C., *"Berekening van de drie-dimensionale potentiaalstroming rond een duweenheid in beperkt water"*, NSMB Report P04800-1-SR (in Dutch), Wageningen, Netherlands, Dec. 1981.

[33] Daube, O., and Dulieu, A., *"A numerical approach of the nonlinear wave resistance problem"*, 3rd Int. Conf. Numerical Ship Hydrodynamics, Paris, France, 1981.

[34] Maruo, H.R., and Ogiwara, S., *"A method of computation for steady ship waves with non-linear free surface conditions"*, 4th Int. Conf. Numerical Ship Hydrodynamics, Washington, USA, 1985.

[35] Musker, A.J., *"A panel method for predicting ship wave resistance"*, 17th Symp. on Naval Hydrodynamics, Den Haag, Netherlands, 1988.

[36] Musker, A.J., *"Stability and accuracy of a nonlinear model for the wave resistance problem"*, 5th Int. Conf. Numerical Ship Hydrodynamics, Hiroshima, Japan, 1989.

[37] Watson, S.J., Personal communication, 1995.

[38] Xia, F., *"Numerical calculations of ship flows, with special emphasis on the free-surface potential flow"*, Ph.D. Thesis, Chalmers University, Göteborg, Sweden, 1986.

[39] Kim, K.J., *"Ship flow calculations and resistance minimization"*, Ph.D. Thesis, Chalmers University, Göteborg, Sweden, 1989.

[40] Kim, Y.-H. and Lucas, T., *"Nonlinear Ship Waves"*, 18th Symp. Naval Hydrodynamics, Ann Arbor, Michigan, USA, 1990.

[41] Jensen, G., Mi, Z.-X., and Söding, H., *"Rankine source methods for numerical solutions of the steady wave resistance problem"*, 16th Symp. Naval Hydrodynamics, Berkeley, USA, 1986.

[42] Jensen, G., *"Berechnung des Wellenwiderstandes für praktische Schiffsformen"*, Jahrbuch STG, Vol. 82, 1988.

[43] Jensen, G., Bertram, V. and Söding, H., *"Ship wave-resistance computations"*, 5th Int. Conf. Numerical Ship Hydrodynamics, Hiroshima, Japan, 1989.

[44] Longuet-Higgins, M.S., and Cokelet, E.D., *"The deformation of steep surface waves on water. I. A numerical method of computation"*, Proc. Royal Society London A, Vol. 350, 1976, pp. 1-26.

[45] Coleman, R.M., and Haussling, H.J., *"Nonlinear waves behind an accelerated transom stern"*, 3rd Int. Conf. Numerical Ship Hydrodynamics, Paris, France, 1981.

[46] Coleman, R.M., *"Nonlinear flow about a three-dimensional transom stern"*, 4th Int. Conf. Numerical Ship Hydrodynamics, Washington, USA, 1985.

[47] Schultz, W.W., Cao, Y., and Beck, R.F., *"Three-dimensional nonlinear wave computation by desingularized boundary integral method"*, 5th Int. Workshop Water Waves and Floating Bodies, Manchester, UK, 1990.

[48] Cao, Y., *"Computations of nonlinear gravity waves by a desingularized boundary integral method"*, Ph.D. Thesis, Univ. Michigan, Dept. Naval Architecture and Marine Eng., Ann Arbor, USA, Report 91-3, 1991.

[49] Beck, R.F., Cao, Y., and Lee, T.-H., *"Fully nonlinear water wave computations using the desingularized method"*, 6th Int. Conf. Numerical Ship Hydrodynamics, Iowa City, USA, 1993.

[50] Nakos, D.E., Kring, D., and Sclavounos, P.D., *"Rankine panel methods for transient free-surface flows"*, 6th Int. Conf. Numerical Ship Hydrodynamics, Iowa City, 1993.

[51] Prins, H.J., *"Time-domain calculations of drift forces and moments"*, Ph.D. Thesis, Delft University of Technology, 1995.

[52] Salvesen, N., and Von Kerczek, C.H., *"Numerical solution of two-dimensional nonlinear body-wave problems"*, 1st Int. Conf. Numerical Ship Hydrodynamics, Gaithersburg, USA, 1975.

[53] Forbes, L.K., *"Progress in the calculation of nonlinear free-surface potential flows in three dimensions"*, 4th Int. Conf. Numerical Ship Hydrodynamics, Washington, USA, 1985.

[54] Korsmeyer, F.T., *"An order N algorithm for the solution of the boundary integral equations of potential flow"*, 5th Int. Workshop Water Waves and Floating Bodies, Manchester, UK, 1990.

[55] Farmer, J., Martinelli, L., and Jameson, A., *"A fast multigrid method for solving the nonlinear ship wave problem with a free surface"*, 6th Int. Conf. Numerical Ship Hydrodynamics, Iowa City, USA, 1993.

[56] Hunt, B., *"The mathematical basis and numerical principles of the boundary integral method for incompressible flow over 3-D aerodynamic configurations"*, in: Numerical Methods in Applied Fluid Dynamics, B. Hunt (ed.), Academic Press, London, 1980.

[57] Han, P.S., and Olson, M.D., *"An adaptive boundary element method"*, Int. Jnl. Num. Methods in Engineering, Vol. 24, 1987.

[58] Schultz, W.W. and Hong, S.W., *"Solution of potential problems using an overdetermined complex boundary integral method"*, Jnl. Computational Physics, Vol. 84, 1989.

[59] Raven, H.C., *"Modeling free-surface potential flows by means of elevated singularities"*, Report No. 51000 - 1 - RF, MARIN, Netherlands, 1990.

[60] Webster, W.C., *"The flow about arbitrary three-dimensional bodies"*, Jnl. Ship Research, Vol. 19-4, 1975.

[61] Strobel, K.H., and Cheng, B.H., *"Finite difference operators for the Rankine source method"*, OMAE Conference Vol. I-A, Offshore Technology, ASME, 1992.

[62] Söding, H., *"Incomplete Gauss Elimination"*, Ship Technology Research Vol. 41 - 2, 1994.

[63] Busch, S., *"Numerische Berechnung des Wellenwiderstandes eines schnellen Sportbootes"*, Diplomarbeit Univ. Duisburg, Germany, August 1990.

[64] Toda,Y., Stern, F., and Longo, J., *"Mean-flow measurements in the boundary layer and wake and wave field of a Series 60 C_b = .6 ship model for Froude numbers .16 and .316"*, IIHR Report No. 352, Iowa Institute of Hydraulic Research, Iowa City, USA, August 1991.

[65] Saunders, H.E., *"Hydrodynamics in ship design"*, Vol. I, SNAME, 1957.

[66] Vanden-Broeck, J.-M., *"Nonlinear Stern Waves"*, Jnl. Fluid Mech., Vol. 96 - 3, 19.. .

[67] Schmidt, G.H., *"Linearized stern flow of a two-dimensional shallow-draft ship"*, Jnl. Ship Research, Vol. 254, 1981.

[68] Tulin, M.P., and Hsu, C.C., *"Theory of high-speed displacement Ships with transom Sterns"*, Jnl. Ship Research, Vol. 30-3, 1986.

[69] Tulin, M.P., *"The theory of slender surfaces planing at high speeds"*, Schiffstechnik, Bd. 4, 1957.

[70] Jones, R.T., *"Wing Theory"*, Princeton University Press, Princeton, N.J., USA, 1990.

[71] Cheng, B.H., *"Computations of 3D transom stern flows"*, 5th Int. Conf. on Numerical Ship Hydrodynamics, Hiroshima, Japan, 1989.

[72] Reed, A., Telste, J., Scragg, C., *"Analysis of transom stern flows"*, 18th Symp. Naval Hydrodynamics, Ann Arbor, USA, 1990.

[73] Telste, J.G., and Reed, A.M., *"Calculation of transom stern flows"*, 6th Int. Conf. Numerical Ship Hydrodynamics, Iowa City, USA, 1993.

[74] Söding, H., Bertram, V., and Jensen, G., *"Numerische Berechnung von Absenkung und Trimm von Schiffen durch Fahrt in flachem Wasser"*, STG Jahrbuch, 1989.

[75] Chang, M.S., *"Wave resistance predictions using a singularity method"*, Proceedings of Workshop on Ship Wave-Resistance Computations, K.J. Bai and J.H. McCarthy (ed.), Bethesda, Md., USA, 1979.

[76] Raven, H.C., *"Nonlinear ship wave calculations using the* RAPID *method"*, 6th Int. Conf. on Numerical Ship Hydrodynamics, Iowa City, USA, 1993.

[77] Lindenmuth, W.T., Ratcliffe, T.J., and Reed, A.M., *"Comparative accuracy of numerical Kelvin wake code predictions — 'Wake-Off' "*, Report DTRC-91/004, David Taylor Model Basin, Sept. 1991.

[78] Raven, H.C., *"Nonlinear effects in ship wave pattern predictions"*, 10th Int. Workshop on Water Waves and Floating Bodies, Oxford, UK, 1995.

[79] Ursell, F., *"Steady wave patterns on a non-uniform steady fluid flow"*, Jnl. Fluid Mech., Vol. 9, 1960.

[80] Lighthill, J., *"Waves in fluids"*, Cambridge University Press, 1980.

[81] Hermans, A.J., and Brandsma, F.J., *"Nonlinear ship waves at low Froude number"*, Jnl. Ship Research, Vol. 33 - 3, 1989.

[82] Longuet-Higgins, M.S., and Stewart, R.W., *"The changes in amplitude of short gravity waves on steady non-uniform currents"*, Jnl. Fluid Mech., Vol. 10, 1961.

[83] Tulin, M.P., and Cointe, R., *"A theory of spilling breakers"*, 16th Symp. Naval Hydrodynamics, Berkeley, USA, 1986.

[84] Duncan, J.H., *"The breaking and non-breaking resistance of a two-dimensional hydrofoil"*, Jnl. Fluid Mechanics, Vol. 126, 1983.

[85] Longuet-Higgins, M.S., *"Advances in the calculation of steep surface waves and plunging breakers"*, 2nd Int. Conf. Numerical Ship Hydrodynamics, Berkeley, USA, 1977

[86] Broeze, J., *"Numerical modelling of nonlinear free surface waves with a 3D panel method"*, Ph.D. Thesis, Twente University, Netherlands, 1993.

[87] Jensen, G., Discussion to [92], 19th Symp. Naval Hydrodynamics, Seoul, South-Korea, 1992.

[88] Raven, H.C., *"Accuracy of free-surface conditions for the wave resistance problem"*, 4th Int. Workshop on Water Waves and Floating Bodies, Oystese, Norway, 1989.

[89] Raven, H.C., *"The negative wave resistance paradox in Dawson's method"*, 5th Int. Workshop on Water Waves and Floating Bodies, Manchester, UK, 1990.

[90] Raven, H.C., *"Solution methods for potential flow problems with nonlinear free-surface boundary conditions"*, Report 50800-1-RF, MARIN, Netherlands, January 1989.

[91] Raven, H.C., *"The* RAPID *solution of steady nonlinear free-surface problems"*, 7th Int. Workshop on Water Waves and Floating Bodies, Val de Rueil, France, 1992.

[92] Raven, H.C., *"A practical nonlinear method for calculating ship wavemaking and wave resistance"*, 19th Symp. Naval Hydrodynamics, Seoul, South-Korea, 1992.

[93] Raven, H.C., and Valkhof, H.H., *"Application of nonlinear ship wave calculations in design"*, Symp. Practical Design of Ships and Floating Structures, Seoul, Korea, 1995.

Een oplossingsmethode voor het niet-lineaire golfweerstandsprobleem

Samenvatting

Een varend schip ondervindt weerstandskrachten van verschillende aard. Een belangrijk deel is de *golfweerstand*, de weerstandskracht die samenhangt met het golfsysteem dat het schip opwekt. Hoe minder golven een schip maakt, des te minder golfweerstand, en des te lager het brandstofverbruik. Als we langs theoretische weg het door een bepaalde rompvorm opgewekte golfpatroon kunnen berekenen, kunnen we ook door een aantal zulke berekeningen te doen de rompvorm snel en doeltreffend optimaliseren.

Om het golfpatroon te berekenen moeten we een mathematisch model oplossen van een niet-viskeuze stroming rond een scheepsromp, met constante snelheid varend in stil water. De oplossing wordt bepaald door de randvoorwaarden dat de stroming om de romp heen moet gaan; dat aan het wateroppervlak de druk constant (atmosferisch) moet zijn, en dat de stroming langs het golfoppervlak gericht moet zijn. Deze laatste twee voorwaarden moeten worden opgelegd op een golvend wateroppervlak waarvan de vorm nog niet bekend is; een belangrijke complicatie. Mathematisch gezien is dit een *niet-lineair vrij oppervlak probleem.*

Tot voor enkele jaren werd dit altijd vereenvoudigd. De randvoorwaarden aan het wateroppervlak werden vervangen door een andere uitdrukking die opgelegd werd ter plaatse van het *ongestoorde* wateroppervlak. Op het Maritiem Research Instituut Nederland was een dergelijke 'gelineariseerde' methode (het programma DAWSON) al jaren met succes in gebruik. Toch bleek deze in de praktijk verschillende beperkingen en tekortkomingen te hebben. Omstreeks 1989 heb ik onderzocht wat daarvan de oorzaken waren; en steeds bleken deze in de linearisatie te liggen. Wilden we verder komen, dan zouden we het volledig niet-lineaire vrij oppervlak probleem moeten oplossen. Over de ontwikkeling van een methode daarvoor gaat dit proefschrift.

De basisaanpak is een *panelenmethode.* We definiëren het stromingsveld als de som van de ongestoorde aanstroming en de door bronpanelen geïnduceerde stromingsvelden. De sterkten van die bronnen bepalen we uit de randvoorwaarden. Het is gebruikelijk om de panelen op de romp en op het wateroppervlak te leggen. Maar om verschillende redenen heb ik gekozen voor een *raised-panel* methode, waarbij bronpanelen op enige afstand boven het wateroppervlak liggen in plaats van erop. In Hoofdstuk 6 wordt langs theoretische weg de nauwkeurigheid en stabiliteit van die aanpak onderzocht. De numerieke dispersie blijkt veel kleiner te zijn dan bij een conventionele methode (3e i.p.v. 1e orde), waardoor de fase van de voorspelde golven veel beter klopt. Bovendien is de instabiliteit voor punt-tot-punt oscillaties opgeheven, zodat we veel fijnere paneelverdelingen kunnen gebruiken. Twee belangrijke tekortkomingen van de vroegere methode zijn daarmee opgeheven.

Omdat het probleem niet-lineair is, en randvoorwaarden op een nog onbekend golfoppervlak moeten worden opgelegd, moet een stapsgewijs (iteratief) proces worden gebruikt. In elke stap leggen we een vereenvoudigde randvoorwaarde op, op het golfoppervlak dat we in de vorige

215

stap gevonden hadden. Zo vinden we een nieuwe benadering van het stromingsveld en een nieuwe golfvorm, en gaan verder met de volgende stap. Als er van stap tot stap niets meer verandert, hebben we de werkelijke oplossing gevonden. Cruciaal is de 'convergentie' van dit iteratieproces: we moeten in een redelijk aantal stappen de werkelijke oplossing vinden zonder tussentijds te ontsporen. Vroegere methoden gaven nogal wat problemen in dat opzicht. Dankzij een zorgvuldige formulering, en dankzij de raised-panel aanpak die ook een bijdrage blijkt te leveren aan de robuustheid en convergentie, kan met de nieuwe methode in de meeste gevallen de oplossing probleemloos gevonden worden.

Speciale aandacht heb ik besteed aan de afstroming van het achterschip (Hoofdstuk 8). Moderne schepen hebben meestal een 'spiegel', een afgeknotte, platte achterkant. Het wateroppervlak komt hier als het ware onder vandaan, en voor het verbeteren van het ontwerp van het achterschip willen we precies weten hoe. Over de modellering en implementatie hiervan bestond nog geen overeenstemming. Op grond van fysische overwegingen heb ik nu een bepaalde aanpak gekozen, en zowel numeriek als experimenteel gevalideerd. De resultaten blijken behoorlijk met de werkelijkheid overeen te stemmen.

Voor allerlei soorten schepen heb ik het berekende golfpatroon vergeleken met wat bij modelproeven in sleeptanks gemeten is (Hoofdstuk 9). Het blijkt dat de voorspelling kwalitatief, en meestal ook kwantitatief, erg goed is. Zelfs details van het golfsysteem worden goed weergegeven. De verbetering ten opzichte van gelineariseerde methoden is veel groter dan verwacht, een verrassend resultaat van deze ontwikkeling.

Tenslotte heb ik de aard van 'niet-lineaire effecten', die deze grote verschillen veroorzaken, onderzocht (Hoofdstuk 10). Een onderscheid is gemaakt tussen 'transfer' en 'refractie' effecten. Transfer effecten zijn vooral dichtbij de romp sterk, en verklaren het verschil in voorspelde boeggolfhoogte tussen gelineariseerde en niet-lineaire methoden. Refractie effecten werken cumulatief, en leiden dus tot grote verschillen op enige afstand van de romp. Belangrijk daarbij is dat zij kunnen leiden tot een versterking van het boeggolfsysteem in het nabije veld. Beide effecten tezamen leiden tot een zeer groot verschil in de amplitude van divergerende golven in het boeggolfsysteem.

Afgezien van wat verfijningen is de ontwikkeling van de methode nu in principe compleet. Het programma RAPID (RAised Panel Iterative Dawson) draait efficient op de CRAY supercomputer van SARA in Amsterdam, en vergt een rekentijd van 2 tot 20 minuten per geval. Het wordt in de praktijk op het MARIN intensief gebruikt voor het verbeteren van rompvormontwerpen. De algemenere toepasbaarheid, grotere nauwkeurigheid en flexibiliteit zijn daarbij belangrijke voordelen ten opzichte van vroegere gelineariseerde methoden.

Hoyte C. Raven

A solution method for the nonlinear ship wave resistance problem

Summary

A ship in steady motion in a calm sea generates a wave pattern. Associated with this is a *wave resistance* force acting on the hull, which is a significant part of the total resistance. In order to be able to minimise this wave resistance by a proper hull form design we want to predict the wave pattern generated by a given hull form at a specified speed.

The mathematical problem to be solved is that of an incompressible potential flow, subject to a Neumann boundary condition on the hull, a Neumann boundary condition on the wave surface, and a given constant (atmospheric) pressure on the wave surface. The latter free surface boundary conditions are nonlinear, and the location and shape of the wave surface is still unknown.

Until recently this problem was always linearised in perturbations of an assumed base flow, and a boundary condition was imposed on the undisturbed water surface. In particular Dawsons's slow-ship linearisation is in widespread use, but it has several shortcomings. Chapter 4 studies the origin of these and compares various alternative linearisations. Specific attention is paid to the paradoxical occurrence of negative predicted wave resistances for slow ships, which is explained in terms of a spurious energy flux through the calculated wave surface. The general conclusion from this study is that a fully nonlinear method is required to remove the shortcomings of existing methods.

The nonlinear method proposed here uses distributions of Rankine source panels on the hull and free surface. An unconventional choice made is to put the free surface panels at a small distance above the wave surface, while keeping the corresponding collocation points on the wave surface itself. This has a number of practical advantages, and improves the smoothness of the velocity field. A theoretical analysis of the numerical dispersion, damping and stability of this approach reveals that moving the source panels off the wave surface almost eliminates the numerical dispersion errors caused by the source discretisation (which is a significant first order quantity in a conventional method). The only numerical dispersion remaining is that due to the difference scheme in the free surface condition, which is of 3rd order in the panel size. Since also the susceptibility to point-to-point oscillations is removed, the raised-panel method permits to achieve a much greater numerical accuracy than a conventional method.

To solve the nonlinear free surface problem an iterative procedure is used. Each iteration solves a problem in which a linearised boundary condition is imposed on the wave surface found in the previous iteration. Convergence is generally quick and robust, requiring 10 to 20 iterations. The total CPU time amounts to 2 to 20 minutes on a CRAY C98, using up to 6000 panels per symmetric half.

Special attention is paid to the flow off an immersed transom stern, a truncated ship afterbody with a sharp lower edge. A mathematical model is selected that takes into account the possibly

217

weakly singular behaviour at the transom edge. Numerical and experimental validations confirm the usefulness of the model.

In a range of validations the wave pattern predictions have been found to be most accurate qualitatively, and often also quantitatively. The method responds correctly to changes in the hull geometry. The principal remaining deviations are due to viscous effects on stern waves. Improvement is still desired in the numerical evaluation of the resistance force, which now is too sensitive to numerical parameters; and in the stability with regard to transverse oscillations.

Nonlinear effects have been found to be far stronger than expected, in particular for slender vessels (containerships, ferries etc.) A study of the origin of these differences shows that the well-known underestimation of bow wave heights by linearised methods is entirely due to the fact that they impose the boundary condition on the still water surface rather than the true wave surface. In addition, refraction of waves by the variation of the velocity field near the ship is found to have a strong influence on the wave shape and amplitude, and this refraction is incompletely represented in linearised methods. This explains the large difference between linearised and nonlinear predictions of the amplitude of diverging bow waves.

The present nonlinear method has been implemented in the RAPID code, which now is in routine use at MARIN for practical ship hull form optimisation.

Hoyte C. Raven

Acknowledgement

Curriculum Vitae

The author was born on February 6, 1955, in Utrecht, Netherlands. After attending secondary school from 1967 to 1972 at the "Stedelijk Gymnasium" in the same town, he studied Naval Architecture at Delft University of Technology. He completed this in 1978, with a Master's thesis on the use of two-equation turbulence models for ship boundary layer calculations, for which he received an award from the "Nederlandse Vereniging van Technici op Scheepvaartgebied" (NVTS). Since 1978 Hoyte Raven is engaged at the Maritime Research Institute Netherlands (formerly, Netherlands Ship Model Basin), with as main subject the development and application of computational methods for the flow around a ship hull. After having been involved for several years in the development of viscous flow codes, since 1986 he has worked on ship wave resistance prediction methods. Initially this concerned the further development of the DAWSON code and its introduction in practical ship design. Around 1990 the development of the nonlinear RAPID method has been undertaken, which is described in the present thesis.